Eddy current canonical problems (with applications to nondestructive evaluation)

Publishers' page

Publishers' page

Publishers' page

Publishers' page

To our wives

Vasso and Zaharoula

"Engineering, electrical and mechanical, is positive in results. There is scarcely a subject that cannot be mathematically treated and the effects calculated or the results determined beforehand from the available theoretical and practical data..."

Nikola Tesla

Preface

This monograph examines a number of canonical problems in electromagnetic induction with applications to eddy current testing (ECT). ECT is a nondestructive testing (NDT) method and is used extensively in industry in order to acquire information about materials and structures. This monograph deals also with the analytical modelling of eddy current problems with the main emphasis not on specific results but methods of analysis. The contents should be of interest to scientists doing research work in various fields of electromagnetics, engineers active in ECT and graduate students. The presented techniques and configurations can be applied not only to ECT but to other applications as well, such as electrical machines, induction heating, induction geophysical prospecting and electromagnetic launching.

The problems addressed are canonical, that is the interfaces and boundaries of the various problem regions coincide with the surfaces of the particular coordinate system used. The testpiece configurations are all planar, consisting of conductive plates inside which eddy currents are induced. Thus, depending on the special symmetry of the problem we use either the Cartesian coordinate system or the cylindrical one. Furthermore, all solutions are provided for the steady state sinusoidal excitation and the source has the form of the classical cylindrical coil. The reader who seeks solutions to similar problems - we call him/her "the interested reader" throughout the book - can then apply the solution method to other coil types or superpose the harmonic solutions to acquire the response to a non-sinusoidal excitation.

With this monograph we have attempted to fill a longstanding gap in the field since to our knowledge there is nothing similar on the theory of ECT. Furthermore, we believe that it is written in a special way because

we have attempted to present the theory in a self-contained manner, with full attention to the numerical details, so that the interested reader can reproduce and extend the results. Also, we could say that it is more than a collection of solutions as it involves also a critical examination of the literature - including that not published in English. There is an important reason for writing it at this particular moment. We have noted a resurgence of interest in analytical methods due mainly to a powerful method that was introduced in the last three years. This method is the Truncated Region Eigenfunction Expansion (TREE) method and is a very promising tool that has the power to treat canonical problems that were thought, until now, to be analytically intractable.

Analytical modelling is a very rich and inexhaustible field. We believe that analytical methods are not used sufficiently by engineers although in many cases they are advantageous over pure numerical methods but above all they offer an opportunity to learn a great deal about the concepts of electromagnetic phenomena. With this monograph we want to promote analytical approaches to solving engineering problems and to encourage their development.

In Chapter 1 we provide a brief introduction to eddy current nondestructive testing and justify the need for mathematical modelling. After deriving the equations that describe the induction phenomena, we discuss the use of potentials focusing on the magnetic vector potential (MVP) and the second order vector potential (SOVP). The former is used for treating 2D (two-dimensional) problems and the latter for 3D (three-dimensional) ones. We also emphasize the value of the analytical solutions and comment on their use in combination with numerical models. The central eddy current modelling problem is then presented and the impedance change (ΔZ) formula is introduced.

In Chapter 2 we study configurations where the excitation has the form of a uniform magnetic field. In this chapter we introduce the use of the TREE method for the solution of the problem when a long surface slot (or idealized crack) enters the geometry.

In Chapter 3, using the magnetic vector potential, we present solutions for axisymmetric eddy current problems. These models, which are widely known as the Dodd and Deeds models, are extended to cover test-cases involving inhomogeneous conductors. The chapter concludes with some guidance for the efficient calculation of both electromagnetic fields and impedances.

In Chapter 4 we reformulate the models of Chapter 3 and provide al-

ternative methods, which are computationally efficient, for treating the axisymmetric geometries. This is achieved by truncating the solution domain and by replacing integral expressions with sums. We then use again the TREE method and extend the axisymmetric models to ferrite-cored probe coils and to testcases where the conductor has a cylindrical inhomogeneity.

In Chapter 5 we extend the solutions to 3D configurations involving coils of arbitrary shape above infinite planar media. The second order vector potential is used extensively in the Cartesian coordinate system and we provide general expressions for the electromagnetic field and impedance change of the coils in terms of a source coefficient that characterizes the coil. Since our primary interest is the cylindrical coil we present the various methods for calculating this source coefficient using examples from various configurations involving different orientations of this coil type.

In Chapter 6 we present alternative approaches for the solution of the problem analyzed in Chapter 5. These include again the use of Cartesian coordinates with a different definition of the second order vector potential as well as cylindrical coordinates. In both cases we derive general expressions for the coil impedance change and demonstrate the calculation of the relevant source coefficient.

In Chapter 7 we reformulate the solution of Chapter 6 in the Cartesian coordinate system and present in detail a recently published solution for the 3D configuration involving a coil above the edge of a planar conductor. This problem, which is unsolvable in the strict mathematical sense, can be treated again using the TREE method in conjunction with the second order vector potential. From the practical point of view the result is an accurate engineering solution. This solution is also extended in order to use it for a conductor with a very deep slot. Other possible extensions are also described for this important geometry.

In Chapter 8 we utilize an existing thin-skin crack model and combine it with analytical solutions from previous chapters. As a result, we develop a very useful tool for modelling surface crack inspections with eddy currents.

Finally, in the Appendix we provide some details on the rapid calculation of the magnetic field produced by an isolated cylindrical air-cored coil.

Many of the solutions presented are original but the real novelty, as already mentioned, is the presentation of the TREE method. Concerning numerical results we are mainly interested in the calculation of impedance change since this is the measured quantity that is also used for verification. A knowledge of advanced theory of electromagnetic fields as well as of

higher mathematical analysis is necessary for the reader using this book. Very often we refer to specific routines of higher programming languages such as Fortran or general mathematical packages such as Mathematica and Matlab in order to facilitate the numerical implementation of the presented solutions.

This work should not be considered as exhaustive of the subject. For example, additional books could be written addressing problems for conductors of cylindrical and spherical shapes. Moreover, we focus on the method of separation of variables throughout the text and do not cover approximate techniques.

It is certain that errors still exist in such a mathematical text even after extensive proof-reading. We welcome corrections as well as suggestions from the readers; these should be directed to `theodoul@ieee.org`.

We are deeply indebted to a number of people for their critical comments on the text. Among them are Dr J. R. Bowler and Dr N. Bowler of the Iowa State University, USA, who read parts of the manuscript, corrected errors and suggested improvements. We would like also to acknowledge the contribution of Dr Em. E. Kriezis of the Aristotle University of Thessaloniki, Greece, who assisted us with the first chapter and Mrs V. M. Kasiakogia, Greece, for help with the English text. Finally, we would like to especially thank Dr S. K. Burke of the Defence Science and Technology Organization, Australia, whose extensive proof-reading and critical comments and suggestions had a great impact on this monograph. Dr Burke has also kindly provided all the experimental results that appear in the text.

T. P. Theodoulidis and E. E. Kriezis

Contents

Chapter 1

Introduction

1.1 Eddy current testing

Eddy current testing is a nondestructive testing method. According to the ASNT Handbook (2004), all such methods "*determine the physical condition of an object without affecting that object's ability to fulfill its intended function*". These methods supply some form of energy to the inspected workpiece and then monitor the interaction between energy and workpiece by using suitable detectors (sensors). [1] In this section we attempt a brief introduction to ECT. However, the interested reader can refer to the the ASNT Handbook (2004) for more information especially to the chapters devoted to the Principles and Glossary of ECT and to the practical aspects such as the Probes and Instrumentation.

In eddy current testing the interrogating energy has the form of a time varying magnetic field and the inspected workpiece is made of a conductive material. According to the electromagnetic induction principle, varying currents are induced in the conductor and in turn produce a secondary varying magnetic field. It is the detection of this field that is of primary interest in eddy current testing since it carries information about electromagnetic and dimensional characteristics of the testpiece, including the presence of flaws. The secondary magnetic field is an indirect way of monitoring the change of eddy current flow which is actually the quantity modified by changes of the aforementioned parameters.

[1] Other common names are also used for NDT by the various communities and branches of industry. The research and academic community often refers to it as NDE which stands for nondestructive evaluation. The same acronym is used by utilities and the nuclear industry but now it stands for nondestructive examination, while NDI stands for nondestructive inspection and is used by aviation. There is also NDC for nondestructive characterization.

Eddy currents owe their name to the fact that they flow in closed loops much in the same way as eddies in water. The presence of a crack forms a barrier, as its volume is non-conductive, thus resulting in a change in the eddy current flow which in turn is reflected as a change in the secondary magnetic field. If we have the means to detect and further quantify this change we can actually detect the crack and measure its dimensions indirectly.

There are several eddy current techniques all of which rely on the same principle of electromagnetic induction. These techniques are identified according to the form of excitation applied to produce the interrogating field and the means and sensors used to detect the secondary eddy current field. Usually the excitation has a sinusoidal form of appropriate frequency, the latter being dictated by the specific application since penetration depth depends upon it. Other forms of excitation are train pulses of rectangular, triangular or other shape as well.

Regarding the sensors used, these largely depend on the specific application and this is a characteristic of the eddy current method. The usual sensor is either the air-cored or the ferrite-cored cylindrical coil, which is easily fabricated. For other applications we may need inside diameter (ID) or outside diameter (OD) coils when inspecting tubes and rods respectively and multiple coil systems arranged in differential or send-receive mode. Other types of sensors are also common, as Hall sensors for example, giant magnetoresistive (GMR) or super conducting interference quantum (SQUID) sensors.

Each NDT method is based on a different physical phenomenon and has its own advantages and disadvantages as well as its own range of applications. The usual situation is that the various methods complement one other. Consider, for example, ultrasound (UT) and radiography (RT) and compare them with eddy currents (ECT). UT can achieve penetration, and thus inspect for deeply-lying defects but it is trouble-some for surface inspections and also needs a suitable couplant. ECT, on the other hand, is contactless but is restricted to near surface areas due to the inability of the eddy currents to penetrate deeply into conductive media. Radiography achieves also deep penetration but it is potentially dangerous, requiring stringent safety procedures, and needs access to both sides of the testpiece, while ECT is completely safe and it is performed from one side of the testpiece.

The general applications of the ECT method involve flaw detection (surface and subsurface cracks, voids, corrosion, etc.), thickness measurement

(thin metallic sheet and coatings) and identification of metals and their alloys. Examples of specific applications in the chemical industries and power plants involve tube inspections of steam generators, balance of plant (BOP) heat exchangers and boilers, turbine blade inspection for cracks, wall and flaw corrosion of Aboveground Storage Tanks and weld inspection for fatigue cracks. In the metal industry the method is used for inspection of tubes (welded and seamless) and bars during the production stage and wrought products. The method also excels in the aviation industry where it is used for surface and subsurface cracks, assessment of heat damage, bolthole inspection, measurement of coatings, hidden layer corrosion and identification of Aluminum alloys. Finally it is used in the automotive industry for crack inspection of various parts, coating and hardness measurement.

The acquired information is in the form of a signal that is either static when point measurements are taken or dynamic when the probe is scanned across the inspected workpiece either manually or by mechanical means. This signal represents the impedance of the coil or the impedance change due to a specific parameter (for example a flaw). The main feature of ECT is that the acquired signals often carry information which is the simultaneous effect of a number of parameters. The effect of each parameter has to be separated and possibly cancelled out if it happens to be an irrelevant one. The output of the test is a signal that needs to be interpreted and it is this need to evaluate test data that has stimulated a number of theoretical studies for the simulation of the method.

1.2 Eddy current modelling

Over the past years we have been witnessing an evolution of model-based quantitative eddy current NDE. Steady improvements in computers and an increasing focus on accurate modelling lead the way to a thorough understanding of eddy current NDT and to the full automation of the field tests. Modelling is performed by solving Maxwell's equations. In particular, problems concerning eddy current induction are formulated by means of differential equations, which determine the magnetic field and related quantities at a certain point in terms of an existing source current density.

Eddy current NDE models can be used for coil design, test frequency selection, interpretation of inspection data and even for calculating the probability of detecting a flaw (POD). Important quantities to be calculated

are the eddy current distribution induced in the specimen undergoing inspection, as well as the resulting impedance change of the coil. Calculation and visualization of the eddy current flow pattern can be used to assess the true depth of penetration into the material and the deflection about particular defects. In this way, the coil configuration can be optimized to ensure maximum interaction with given defect types, properly taking into account frequency and material parameters. Calculation and visualization of impedance plane loci can be used for comparison with actual test signals. This provides a better understanding of the impedance variations occurring from known defects of particular size and orientation as well as from particular material and spatial features of the test component.

Although such models come in several flavors, they can be broadly classified as either analytical or numerical. It must be mentioned that the distinction is somewhat artificial since all analytical models do involve a fair amount of numerical computation and all numerical models are rooted in analytical theory. Analytical solutions, which provide closed-form expressions for the parameters of interest in eddy current testing, are the subject of this book.

The solutions from analytical methods are general and exact and since they are obtained in the form of a mathematical relationship, they can easily be used for analysis, parametric studies and calibration of test systems. An important aspect of analytical models is that closed-form expressions are easily coded, either with higher programming languages or with commercial mathematical packages, and therefore require minimal effort by the developer. When the solutions are coded, they are extremely fast compared to numerical methods, which require significantly longer computing times. Analytical solutions are also used for validation of solutions from more complex numerical methods. Since the latter produce numerical results rather than closed-form expressions, an independent method has to be used for confirming their accuracy and correctness. This can be done by analytical models, which provide an inexpensive alternative to experimental verification of numerical results.

Another description of the various solution methods can be found in Ballisti (1983), who classified them in three main classes: analytical, semi-analytical and numerical methods. Methods are called semi-analytical if they solve exactly either the partial differential equation (PDE) or the boundary conditions (BC). The BCs in the first case or the PDEs in the second are then fulfilled numerically, see Table 1.1.

Table 1.1 How methods fulfill the BCs and PDEs.

	Analytical	Semi-analytical	Numerical
PDE	exactly	exactly - approx.	approx.
BC	exactly	approx. - exactly	approx.

1.2.1 *The TREE method*

A number of complex problems in eddy current NDE have been solved recently using the truncated region eigenfunction expansion (TREE) method. As in the classical approach, the method uses separation of variables to express the electromagnetic field in the various regions of the problem in analytical form. It differs from the classical approach in truncating the solution domain to limit the range of a coordinate that would otherwise have an infinite span. As a result, the solution dependence on that coordinate is expressed as a series form, rather than as an integral. There are a number of advantages of recasting the expressions as sums rather than as integrals. For example, the numerical implementation is usually more efficient and the error control easier, but these are secondary issues. The main advantage of domain truncation is that by a careful selection of the discrete eigenvalues and the corresponding eigenfunctions, the field continuity can be satisfied at various interfaces simultaneously. In this way, the class of problems that can be treated analytically is greatly extended. The matching of the field expressions at interfaces is done either in a term by term basis or by mode matching where the testing functions are the same as the expansion ones. The latter implies that the TREE method may contain a meshless Galerkin type procedure with expansion and testing functions that are entire domain functions. At the same time, the functions satisfy the electromagnetic field equations.

This is not a numerical method though since the resultant field is an analytical solution of the governing equations. On the other hand, it is not strictly analytical because it requires the numerical inversion of a full matrix as well as the numerical computation of the discrete eigenvalues. Taking into account these facts we would avoid to classify the method according to Table 1.1 and just describe it as quasi-analytical. The TREE method is a central part of this monograph and is used in three of its chapters to provide solutions to problems that until now were thought to be analytically intractable.

1.3 Electromagnetic field equations

The eddy current nondestructive phenomena together with all electromagnetic ones, are governed by Maxwell's equations. Three of these equations that are pertinent to eddy current testing are

$$\nabla \times \mathbf{E} = -\frac{\partial \mathbf{B}}{\partial t} \tag{1.1}$$

$$\nabla \times \mathbf{H} = \mathbf{J} \tag{1.2}$$

$$\nabla \cdot \mathbf{B} = 0 \tag{1.3}$$

where $\mathbf{E}$ is the electric field intensity (V/m), $\mathbf{H}$ is the magnetic field intensity (A/m), $\mathbf{B}$ is the magnetic flux density (T) and $\mathbf{J}$ is the current density (A/m^2). Excitation frequencies are typically very low (<10 MHz) and consequently the displacement current term ($\partial \mathbf{D}/\partial t$) in (1.2) is neglected. The above equations are combined with the following constituent equations

$$\mathbf{J} = \sigma \mathbf{E} \tag{1.4}$$

$$\nabla \cdot \mathbf{J} = 0 \tag{1.5}$$

$$\mathbf{B} = \mu \mathbf{H} \tag{1.6}$$

where σ and μ are the conductivity and magnetic permeability of the medium respectively and μ is either a product $\mu_0 \mu_r$ for a linear material or, more generally, a function of $\mathbf{H}$. For the purpose of solution of the above differential equations and since $\mathbf{B}$ is divergence free, it can be expressed as

$$\mathbf{B} = \nabla \times \mathbf{A} \tag{1.7}$$

where $\mathbf{A}$ is the magnetic vector potential. Substituting (1.7) in (1.1) and using (1.2) as well as the constitutive relations (1.4), (1.6), the following result can be derived

$$\nabla \times \frac{1}{\mu} \nabla \times \mathbf{A} = \mathbf{J_s} - \sigma \frac{\partial \mathbf{A}}{\partial t} \tag{1.8}$$

where $\mathbf{J}_s$ is the applied or impressed current density. Inside a linear magnetic or nonmagnetic material, (1.8) reduces to

$$\nabla^2 \mathbf{A} = -\mu \mathbf{J}_s + \mu\sigma \frac{\partial \mathbf{A}}{\partial t} \tag{1.9}$$

where we have used the identity $\nabla \times \nabla \times \mathbf{A} = \nabla(\nabla \cdot \mathbf{A}) - \nabla^2 \mathbf{A}$ and we made the choice of a divergence free magnetic vector potential

$$\nabla \cdot \mathbf{A} = 0 \tag{1.10}$$

Eq. (1.9) governs the physical process underlying eddy current phenomena and is applicable to situations involving both sinusoidal and nonsinusoidal excitation. If the coil is excited by a sinusoidal source, then, the governing equation can be simplified, assuming steady state conditions to the following equation shown in phasor notation

$$\nabla^2 \mathbf{A} = -\mu \mathbf{J}_s + j\omega\mu\sigma \mathbf{A} \tag{1.11}$$

where $\omega = 2\pi f$ and f is the excitation frequency (Hz). A similar equation can be shown to exist for the magnetic field intensity

$$\nabla^2 \mathbf{H} = j\omega\mu\sigma \mathbf{H} \tag{1.12}$$

and we usually write $k^2 = j\omega\mu\sigma$.

1.3.1 *Second order vector potential*

The calculation of vector fields from the vector equations (1.11), (1.12) introduces considerable difficulties, which are mainly attributed to the way boundary conditions are applied and further linked to the choice of the coordinate system. A scalar field obeys either Dirichlet or Neumann boundary conditions or both. In the case of a vector field we have to specify at the boundary the values or normal gradients for all three scalar quantities constituting the vector field. This approach gives satisfactory results for a rectangular system of coordinates, as the three scalar equations obtained are very much the same as those corresponding to the scalar case. However, when considering cylindrical or spherical coordinates, additional difficulties arise, as the three component equations for the vector case cannot be separated any longer. Thus, for spherical coordinates, it is not possible to obtain three separate equations for the r, θ, φ components, respectively. Similarly, for cylindrical coordinates it is not possible to obtain separate equations for the r, φ components; however, it is still possible to obtain a separate equation for the z component.

To overcome these difficulties we can use a method which is based on the assumption that the vector field can be split into two parts. The first one, which is rotation free (irrotational), is obtained from a scalar potential by calculating its gradient and it is called longitudinal part, since the gradient coincides with the direction of greatest rate of change for the scalar potential. The second part, which is divergence free (solenoidal), is derived from a vector potential by considering its curl and it is called transverse part, as the curl of a vector is usually transverse to the direction of greatest change. The separation into a longitudinal and a transverse component provides methods for solving for the vector field. Focusing our interest on the transverse component, which is obtained from the curl of a vector potential, we can show that it can be derived from two scalars. The above requirement can be met if it is assumed that the divergence of the vector potential is zero.

Considering a vector $\mathbf{F}$ standing for a vector field that satisfies

$$\nabla^2\mathbf{F} = k^2\mathbf{F} \qquad \nabla\cdot\mathbf{F} = 0 \tag{1.13}$$

Equation (1.13) corresponds to a Helmholtz type equation, with Laplace equation being the special case ($k = 0$). A direct method for solving (1.13) for the vector field is not easy, as the Laplacian operator acts not only upon the magnitudes of the vector components, but also upon the unit vectors themselves. Only in a rectangular coordinate system do we have three separate differential equations, one for each component. As already mentioned, the way to treat the separability problem of (1.13) is to split the vector solution $\mathbf{F}$ into the longitudinal part $\mathbf{F}_l$ and the transverse part $\mathbf{F}_t$ so that $\mathbf{F} = \mathbf{F}_l + \mathbf{F}_t$. According to the physical reasoning of the preceding paragraphs, these parts are written as

$$\mathbf{F}_l = \nabla\phi \qquad \nabla\times\mathbf{F}_l = 0 \tag{1.14}$$

$$\mathbf{F}_t = \mathbf{M} + \mathbf{N} \qquad \nabla\cdot\mathbf{F}_t = 0 \tag{1.15}$$

with ϕ being the scalar potential and the transverse part having been written as the sum of two vectors $\mathbf{M}$ and $\mathbf{N}$. Morse & Feshbach (1953) have shown that these vectors have the following form in a curvilinear coordinate system which is described by the independent variables u_1, u_2, u_3 and characterized by the metric coefficients h_1, h_2, h_3.

$$\mathbf{M} = \nabla\times(\mathbf{u}_1 w\psi) = \nabla(w\psi)\times\mathbf{u}_1 \tag{1.16}$$

Table 1.2 Coordinate systems where the SOVP formulation can be used.

System	$\mathbf{u}_1$	w
Cartesian	$\mathbf{x}_0, \mathbf{y}_0, \mathbf{z}_0$	1
cylindrical	$\mathbf{z}_0$	1
elliptical	$\mathbf{z}_0$	1
parabolic	$\mathbf{z}_0$	1
spherical	$\mathbf{r}_0$	r
conic	$\mathbf{r}_0$	r

$$\mathbf{N} = \nabla \times (\mathbf{u}_1 w\chi) = \mathbf{u}_1 w\chi + \nabla \left[\frac{\partial (w\chi)}{\partial u_1} \right] \tag{1.17}$$

where ψ and χ together with ϕ in (1.14) are the three scalars that describe the vector field and w is a scalar quantity that depends on the particular coordinate system. ψ and χ satisfy the scalar Helmholtz and Laplace equations which are separable in eleven coordinate systems, see Moon (1971), and thus we treat the separability problem of (1.13) by reducing it from the solution of the vector Helmholtz or Laplace equation to the solution of the relevant scalar one. It has to be noted however, that writing the vector field in the form (1.16)-(1.17) is not possible in all eleven coordinate systems. In particular, this form can be derived only in those coordinate systems where h_1 is constant and the ratio of the other two coefficients h_2/h_3 is independent of u_1. This is possible in six out of the eleven coordinate systems. These are listed in Table 1.2 together with the relevant expression for w.

The above analysis of breaking the vector solution to the components $\mathbf{F}_l$, $\mathbf{M}$ and $\mathbf{N}$ can be made with regard to the magnetic vector potential $\mathbf{A}$, which will depend on three scalar quantities ϕ, χ, ψ. In order to decrease this number to two scalar quantities and at the same time simplify expressions, we can ignore gradient terms which include the longitudinal part and the second term in (1.17). This does not have any consequence on the calculation of the magnetic field because what remains in the definition of $\mathbf{A}$ still gives $\mathbf{B}$ since $\nabla \times (\nabla\phi) = 0$. However, we have a problem with the divergence of $\mathbf{A}$ which does not vanish as required by our original assumption. To overcome this problem we introduce a second order vector potential defined by

$$\mathbf{A} = \nabla \times \mathbf{W} \tag{1.18}$$

and write $\mathbf{W}$, with the notation used hereafter, as follows

$$\mathbf{W} = \mathbf{u}_1 w W_a + \nabla (w W_b) \times \mathbf{u}_1 \tag{1.19}$$

In this way the curl of $\mathbf{W}$ will still give $\mathbf{A}$ and in addition we ensure a solenoidal $\mathbf{A}$. On the other hand, $\mathbf{W}$ will not be solenoidal, since it misses the gradient terms but this does not matter in the derivation of the field because $\mathbf{A}$ is derived by the curl of $\mathbf{W}$ and the curl of a gradient is identically zero. The two scalar quantities W_a and W_b will satisfy the scalar Helmholtz type equation

$$\nabla^2 W_{a,b} = k^2 W_{a,b} \tag{1.20}$$

which for nonconductive media ($k = 0$) reduces to the scalar Laplace equation. The eddy current density can now be calculated from

$$\mathbf{J} = -j\omega\sigma \nabla \times \mathbf{W} \tag{1.21}$$

and the magnetic flux density from

$$\mathbf{B} = \nabla \times \nabla \times \mathbf{W} = -k^2 \left[(w W_a)\mathbf{u}_1 + \mathbf{u}_1 \times \nabla (w W_b) \right] + (\mathbf{u}_1 \cdot \nabla) \nabla (w W_a) \tag{1.22}$$

Note that in non-conductive regions, the magnetic flux density depends upon one scalar quantity namely W_a. This is expected since $\mathbf{B}$ in air is conservative and usually written as the gradient of a scalar potential.

The first appearance of $\mathbf{W}$ in the literature is attributed to Smythe (1968) and then Hannakam, among others, used it extensively to derive analytical solutions for arbitrarily shaped sources above a conductive half-space, a cylinder and a sphere. Nevertheless, the scalarization of fields was known to researchers long before and was used in others areas of electromagnetics, especially in high frequency applications involving wave propagation. Actually, the second order vector potential is just another name of the Hertz vector and the Debye potentials. A survey of the names and symbols of the potential used for scalarization of vector fields is given in Table 1.3.

1.4 Coordinate systems

Assume now an orthogonal coordinate system of curvilinear coordinates that is represented by the independent variables u_1, u_2, u_3 and characterized by the metric coefficients h_1, h_2, h_3. For a scalar function ϕ and a vector

Table 1.3 Symbols and names of the vector potential used in the scalarization of the vector field.

Researcher	Potential name	Symbols	
Smythe	Second order	W_a	W_b
Weigelt	Higher order	W_1	W_2
Hannakam	Higher order	P_1	P_2
Nethe	Higher order	P_{TE}	P_{TM}
Wait	Hertz	Π_m^* (magnetic)	Π_e^* (electric)
Weaver, Burke	Hertz	Γ (magnetic)	Π (electric)
Bowler	Hertzian	ψ'	ψ
Wait and others	Debye	π_e	π_m

function $\mathbf{A}(A_1, A_2, A_3)$ expressed with unit vectors $\mathbf{u}_1, \mathbf{u}_2, \mathbf{u}_3$ the following expressions apply for the usual operators $\nabla, \nabla\cdot, \nabla\times, \nabla^2$

$$\nabla\phi = \frac{1}{h_1}\frac{\partial\phi}{\partial u_1}\mathbf{u}_1 + \frac{1}{h_2}\frac{\partial\phi}{\partial u_2}\mathbf{u}_2 + \frac{1}{h_3}\frac{\partial\phi}{\partial u_3}\mathbf{u}_3 \tag{1.23}$$

$$\nabla\cdot\mathbf{A} = \frac{1}{h_1h_2h_3}\left[\frac{\partial}{\partial u_1}(h_2h_3A_1) + \frac{\partial}{\partial u_2}(h_3h_1A_2) + \frac{\partial}{\partial u_3}(h_1h_2A_3)\right] \tag{1.24}$$

$$\begin{aligned}\nabla\times\mathbf{A} = {} & \frac{1}{h_2h_3}\left[\frac{\partial}{\partial u_2}(h_3A_3) - \frac{\partial}{\partial u_3}(h_2A_2)\right]\mathbf{u}_1 \\ & + \frac{1}{h_3h_1}\left[\frac{\partial}{\partial u_3}(h_1A_1) - \frac{\partial}{\partial u_1}(h_3A_3)\right]\mathbf{u}_2 \\ & + \frac{1}{h_1h_2}\left[\frac{\partial}{\partial u_1}(h_2A_2) - \frac{\partial}{\partial u_2}(h_1A_1)\right]\mathbf{u}_3\end{aligned} \tag{1.25}$$

$$\nabla^2\phi = \frac{1}{h_1h_2h_3}\left[\frac{\partial}{\partial u_1}\left(\frac{h_2h_3}{h_1}\frac{\partial\phi}{\partial u_1}\right) + \frac{\partial}{\partial u_2}\left(\frac{h_3h_1}{h_2}\frac{\partial\phi}{\partial u_2}\right) + \frac{\partial}{\partial u_3}\left(\frac{h_1h_2}{h_3}\frac{\partial\phi}{\partial u_3}\right)\right] \tag{1.26}$$

where $h = h_1h_2h_3$. The lengthy general expression for $\nabla^2\mathbf{A}$ can be found in Tegopoulos (1985). We will explicitly present the above relations in the most commonly encountered coordinate systems.

(i) Rectangular coordinates:

$$u_1 = x \quad u_2 = y \quad u_3 = z \tag{1.27}$$

$$\mathbf{u}_1 = \mathbf{x}_0 \quad \mathbf{u}_2 = \mathbf{y}_0 \quad \mathbf{u}_3 = \mathbf{z}_0 \tag{1.28}$$

The infinitesimal line element is:

$$dl = \left(dx^2 + dy^2 + dz^2\right)^{1/2} \tag{1.29}$$

From (1.27) it is concluded that the coefficients h_i ; $i = 1, 2, 3$ are given by:

$$h_1 = 1 \quad h_2 = 1 \quad h_3 = 1 \tag{1.30}$$

Using (1.27), (1.28), (1.29) and (1.30), we can rewrite the operators of equations (1.23), (1.24), (1.25), (1.26) accordingly:

$$\nabla\phi = \frac{\partial\phi}{\partial x}\mathbf{x}_0 + \frac{\partial\phi}{\partial y}\mathbf{y}_0 + \frac{\partial\phi}{\partial z}\mathbf{z}_0 \tag{1.31}$$

$$\nabla \cdot \mathbf{A} = \frac{\partial A_x}{\partial x} + \frac{\partial A_y}{\partial y} + \frac{\partial A_z}{\partial z} \tag{1.32}$$

$$\nabla \times \mathbf{A} = \left(\frac{\partial A_z}{\partial y} - \frac{\partial A_y}{\partial z}\right)\mathbf{x}_0 + \left(\frac{\partial A_x}{\partial z} - \frac{\partial A_z}{\partial x}\right)\mathbf{y}_0 + \left(\frac{\partial A_y}{\partial x} - \frac{\partial A_x}{\partial y}\right)\mathbf{z}_0 \tag{1.33}$$

$$\nabla^2\phi = \frac{\partial^2\phi}{\partial x^2} + \frac{\partial^2\phi}{\partial y^2} + \frac{\partial^2\phi}{\partial z^2} \tag{1.34}$$

$$\nabla^2\mathbf{A} = \nabla^2 A_x\mathbf{x}_0 + \nabla^2 A_y\mathbf{x}_0 + \nabla^2 A_z\mathbf{z}_0 \tag{1.35}$$

Considering the definition of $\mathbf{W}$ we can choose $\mathbf{u}_1$ in (1.19) to be $\mathbf{x}_0$, $\mathbf{y}_0$ or $\mathbf{z}_0$. In case $\mathbf{u}_1 = \mathbf{z}_0$ we have

$$\mathbf{W} = W_a\mathbf{z}_0 + \mathbf{z}_0 \times \nabla W_b \tag{1.36}$$

and the components of magnetic vector potential $\mathbf{A}$ and magnetic flux density $\mathbf{B}$ are written as follows:

$$A_x = \frac{\partial W_a}{\partial y} - \frac{\partial^2 W_b}{\partial x \partial z} \tag{1.37}$$

$$A_y = -\frac{\partial W_a}{\partial x} - \frac{\partial^2 W_b}{\partial y \partial z} \tag{1.38}$$

$$A_z = \frac{\partial^2 W_b}{\partial x^2} + \frac{\partial^2 W_b}{\partial y^2} \tag{1.39}$$

$$B_x = k^2 \frac{\partial W_b}{\partial y} + \frac{\partial^2 W_a}{\partial x \partial z} \tag{1.40}$$

$$B_y = -k^2 \frac{\partial W_b}{\partial x} + \frac{\partial^2 W_a}{\partial y \partial z} \tag{1.41}$$

$$B_z = -k^2 W_a + \frac{\partial^2 W_a}{\partial z^2} \tag{1.42}$$

For a non-conductive region, the terms containing k^2 vanish and $\mathbf{B}$ can be written as

$$\mathbf{B} = \nabla \left(\frac{\partial W_a}{\partial z} \right) \tag{1.43}$$

Note that A_z does not depend on W_a and B_z does not depend on W_b. This is the reason why W_a is often referred to as transverse electric (TE) potential (and written W_{TE}) and W_b is referred to as transverse magnetic (TM) potential (and written W_{TM}).

(ii) Cylindrical coordinates:

$$u_1 = r \quad u_2 = \varphi \quad u_3 = z \tag{1.44}$$

$$\mathbf{u}_1 = \mathbf{r}_0 \quad \mathbf{u}_2 = \boldsymbol{\varphi}_0 \quad \mathbf{u}_3 = \mathbf{z}_0 \tag{1.45}$$

Cylindrical coordinates are related to rectangular coordinates through the transformation:

$$x = r\cos\varphi \quad y = r\sin\varphi \quad z = z \tag{1.46}$$

The infinitesimal line element is

$$dl = \sqrt{dr^2 + r^2 d\varphi^2 + dz^2} \tag{1.47}$$

From equation (1.47) it is concluded that the coefficients h_i ; $i = 1, 2, 3$ are given by:

$$h_1 = 1 \quad , \quad h_2 = r \quad , \quad h_3 = 1 \tag{1.48}$$

The operators of equations (1.23)-(1.26) acquire the following forms:

$$\nabla\phi = \frac{\partial \phi}{\partial r}\mathbf{r}_0 + \frac{1}{r}\frac{\partial \phi}{\partial \varphi}\boldsymbol{\varphi}_0 + \frac{\partial \phi}{\partial z}\mathbf{z}_0 \tag{1.49}$$

$$\nabla \cdot \mathbf{A} = \frac{1}{r}\frac{\partial}{\partial r}(rA_r) + \frac{1}{r}\frac{\partial A_\varphi}{\partial \varphi} + \frac{\partial A_z}{\partial z} \tag{1.50}$$

$$\begin{aligned}\nabla \times \mathbf{A} = &\frac{1}{r}\left[\frac{\partial A_z}{\partial \varphi} - \frac{\partial (rA_\varphi)}{\partial z}\right]\mathbf{r}_0 + \left(\frac{\partial A_r}{\partial z} - \frac{\partial A_z}{\partial r}\right)\boldsymbol{\varphi}_0 \\ &+ \frac{1}{r}\left[\frac{\partial}{\partial r}(rA_\varphi) - \frac{\partial A_r}{\partial \varphi}\right]\mathbf{z}_0\end{aligned} \tag{1.51}$$

$$\nabla^2 \phi = \frac{1}{r}\frac{\partial}{\partial r}\left(r\frac{\partial \phi}{\partial r}\right) + \frac{1}{r^2}\frac{\partial^2 \phi}{\partial^2 \varphi} + \frac{\partial^2 \phi}{\partial z^2} \tag{1.52}$$

$$\begin{aligned}\nabla^2 \mathbf{A} = &\left(\nabla^2 A_r - \frac{1}{r^2}A_r - \frac{2}{r^2}\frac{\partial A_\varphi}{\partial \varphi}\right)\mathbf{r}_0 \\ &+ \left(\nabla^2 A_\varphi - \frac{1}{r^2}A_\varphi + \frac{2}{r^2}\frac{\partial A_r}{\partial \varphi}\right)\boldsymbol{\varphi}_0 \\ &+ \nabla^2 A_z \mathbf{z}_0\end{aligned} \tag{1.53}$$

Considering the definition of $\mathbf{W}$ the only choice can be $\mathbf{u}_1 = \mathbf{z}_0$ so that

$$\mathbf{W} = W_a \mathbf{z}_0 + \mathbf{z}_0 \times \nabla W_b \tag{1.54}$$

and the components of magnetic vector potential $\mathbf{A}$ and magnetic flux density $\mathbf{B}$ are written as follows:

$$A_r = \frac{1}{r}\frac{\partial W_a}{\partial \varphi} - \frac{\partial^2 W_b}{\partial r \partial z} \tag{1.55}$$

$$A_\varphi = -\frac{\partial W_a}{\partial r} - \frac{1}{r}\frac{\partial^2 W_b}{\partial \varphi \partial z} \tag{1.56}$$

$$A_z = \frac{\partial^2 W_b}{\partial r^2} + \frac{1}{r}\frac{\partial W_b}{\partial r} + \frac{1}{r^2}\frac{\partial^2 W_b}{\partial \varphi^2} \tag{1.57}$$

$$B_r = \frac{k^2}{r}\frac{\partial W_b}{\partial \varphi} + \frac{\partial^2 W_a}{\partial r \partial z} \tag{1.58}$$

$$B_\varphi = -k^2 \frac{\partial W_b}{\partial r} + \frac{1}{r}\frac{\partial^2 W_a}{\partial \varphi \partial z} \tag{1.59}$$

$$B_z = -k^2 W_a + \frac{\partial^2 W_a}{\partial z^2} \tag{1.60}$$

(iii) Spherical coordinates:

$$u_1 = r \quad u_2 = \vartheta \quad u_3 = \varphi \tag{1.61}$$

$$\mathbf{u}_1 = \mathbf{r}_0 \quad \mathbf{u}_2 = \boldsymbol{\vartheta}_0 \quad \mathbf{u}_3 = \boldsymbol{\varphi}_0 \tag{1.62}$$

Spherical coordinates are related to rectangular coordinates through the transformation:

$$x = r\sin\vartheta\cos\varphi \quad y = r\sin\vartheta\sin\varphi \quad z = r\cos\vartheta \tag{1.63}$$

The infinitesimal line element is

$$dl = \sqrt{dr^2 + r^2 d\vartheta^2 + r^2\sin^2\vartheta d\varphi^2} \tag{1.64}$$

From equation (1.64) it is concluded that the coefficients h_i ; $i = 1, 2, 3$ are given by:

$$h_1 = 1 \quad , \quad h_2 = r \quad , \quad h_3 = r\sin\vartheta \tag{1.65}$$

The operators of equations (1.23)-(1.26) acquire now the following forms:

$$\nabla\phi = \frac{\partial\phi}{\partial r}\mathbf{r}_0 + \frac{1}{r}\frac{\partial\phi}{\partial\vartheta}\boldsymbol{\vartheta}_0 + \frac{1}{r\sin\vartheta}\frac{\partial\phi}{\partial\varphi}\boldsymbol{\varphi}_0 \tag{1.66}$$

$$\nabla\cdot\mathbf{A} = \frac{1}{r^2}\frac{\partial}{\partial r}(r^2 A_r) + \frac{1}{r\sin\vartheta}\frac{\partial}{\partial\vartheta}(\sin\vartheta A_\vartheta) + \frac{1}{r\sin\vartheta}\frac{\partial A_\varphi}{\partial\varphi} \tag{1.67}$$

$$\begin{aligned}\nabla\times\mathbf{A} = {} & \frac{1}{r\sin\vartheta}\left[\frac{\partial}{\partial\vartheta}(\sin\vartheta A_\varphi) - \frac{\partial A_\vartheta}{\partial\varphi}\right]\mathbf{r}_0 \\ & + \frac{1}{r}\left[\frac{1}{\sin\vartheta}\frac{\partial A_r}{\partial\varphi} - \frac{\partial}{\partial r}(rA_\varphi)\right]\boldsymbol{\vartheta}_0 \\ & + \frac{1}{r}\left[\frac{\partial}{\partial r}(rA_\vartheta) - \frac{\partial A_r}{\partial\vartheta}\right]\boldsymbol{\varphi}_0\end{aligned} \tag{1.68}$$

$$\nabla^2\phi = \frac{1}{r^2}\frac{\partial}{\partial r}\left(r^2\frac{\partial\phi}{\partial r}\right) + \frac{1}{r^2\sin\vartheta}\frac{\partial}{\partial\vartheta}\left(\sin\vartheta\frac{\partial\phi}{\partial\vartheta}\right) + \frac{1}{r^2\sin^2\vartheta}\frac{\partial^2\phi}{\partial\varphi^2} \tag{1.69}$$

$$\nabla^2\mathbf{A} = \left(\nabla^2 A_r - \frac{2}{r^2}A_r - \frac{2}{r^2}\frac{\partial A_\theta}{\partial\vartheta} - \frac{2\cot\varphi}{r^2}A_\theta - \frac{2}{r^2\sin^2\vartheta}\frac{\partial A_\varphi}{\partial\varphi}\right)\mathbf{r}_0 + \left(\nabla^2 A_\theta + \frac{2}{r^2}\frac{\partial A_r}{\partial\vartheta} - \frac{1}{r^2\sin^2\vartheta}A_\theta - \frac{2\cot\vartheta}{r^2\sin\vartheta}\frac{\partial A_\varphi}{\partial\varphi}\right)\boldsymbol{\vartheta}_0 + \left(\nabla^2 A_\varphi + \frac{2}{r^2\sin\vartheta}\frac{\partial A_r}{\partial\varphi} + \frac{2\cot\vartheta}{r^2\sin\vartheta}\frac{\partial A_\theta}{\partial\varphi} - \frac{1}{r^2\sin^2\vartheta}A_\varphi\right)\boldsymbol{\varphi}_0 \tag{1.70}$$

Considering the definition of $\mathbf{W}$ the only choice can be $\mathbf{u}_1 = \mathbf{r}_0$, so that

$$\mathbf{W} = (W_a r)\,\mathbf{r}_0 + \mathbf{r}_0 \times \nabla\,(W_b r) \tag{1.71}$$

and the components of magnetic vector potential $\mathbf{A}$ and magnetic flux density $\mathbf{B}$ are written as follows:

$$A_r = \frac{\cot\vartheta}{r}\frac{\partial W_b}{\partial\vartheta} + \frac{1}{r}\frac{\partial^2 W_b}{\partial\vartheta^2} + \frac{1}{r\sin^2\vartheta}\frac{\partial^2 W_b}{\partial\varphi^2} \tag{1.72}$$

$$A_\vartheta = \frac{1}{\sin\vartheta}\frac{\partial W_a}{\partial\varphi} - \frac{\partial^2 W_b}{\partial\vartheta\partial r} - \frac{1}{r}\frac{\partial W_b}{\partial\vartheta} \tag{1.73}$$

$$A_\varphi = -\frac{1}{r\sin\vartheta}\frac{\partial W_b}{\partial\varphi} - \frac{1}{\sin\vartheta}\frac{\partial^2 W_b}{\partial\varphi\partial r} - \frac{\partial W_a}{\partial\vartheta} \tag{1.74}$$

$$B_r = r\frac{\partial^2 W_a}{\partial r^2} + 2\frac{\partial W_a}{\partial r} - k^2 W_a r \tag{1.75}$$

$$B_\vartheta = \frac{\partial^2 W_a}{\partial\vartheta\partial r} + \frac{1}{r}\frac{\partial W_a}{\partial\vartheta} + \frac{k^2}{\sin\vartheta}\frac{\partial W_b}{\partial\varphi} \tag{1.76}$$

$$B_\varphi = \frac{1}{\sin\vartheta}\left(\frac{\partial^2 W_a}{\partial\varphi\partial r} + \frac{1}{r}\frac{\partial W_a}{\partial\varphi}\right) - k^2\frac{\partial W_b}{\partial\vartheta} \tag{1.77}$$

1.5 Boundary conditions

The field equations of the preceding sections are valid for all points in space, for which the physical properties vary continuously. However, in many instances more than one medium fills the space with the parameters μ, σ changing discontinuously across the media interfaces. In these cases the following interface conditions hold:

$$\mathbf{n} \times (\mathbf{E}_2 - \mathbf{E}_1) = 0 \tag{1.78}$$

$$\mathbf{n} \times (\mathbf{H}_2 - \mathbf{H}_1) = \mathbf{J} \tag{1.79}$$

$$(\mathbf{B}_2 - \mathbf{B}_1) \cdot \mathbf{n} = 0 \tag{1.80}$$

$$(\mathbf{D}_2 - \mathbf{D}_1) \cdot \mathbf{n} = \rho_s \tag{1.81}$$

where $\mathbf{D}$ is the electric flux density ($\mathrm{Cb/m^2}$) and ρ_s is the surface charge density. If the conductivities of the two media are finite, then the surface current density $\mathbf{J}$ vanishes and equation (1.79) simplifies to

$$\mathbf{n} \times (\mathbf{H}_2 - \mathbf{H}_1) = 0 \tag{1.82}$$

In 2D problems where we use the magnetic vector potential there is only one component and in this case the above interface conditions reduce to the continuity of this component and the discontinuity of its derivative with respect to the normal direction

$$A_1 = A_2 \qquad \frac{1}{\mu_1}\frac{\partial A_1}{\partial n} - \frac{1}{\mu_2}\frac{\partial A_2}{\partial n} = J_t \tag{1.83}$$

the second one taken with $J_t = 0$ in case the surface current vanishes. Not all interface conditions are independent since (1.80) and (1.81) can be derived from (1.82) and (1.78). In the classical eddy current analysis the independent boundary conditions at the interface of regions with different material parameters σ, μ are the continuity of the tangential components of the magnetic and electric field intensity which imply the continuity of the normal components of the current density and the magnetic flux density.

If the displacement current is neglected in a nonconductive subspace, the normal component of the conduction current density vanishes on the conductor's surface. The remaining independent boundary conditions are the continuity of the tangential component of the magnetic field intensity and the continuity of the normal component of the magnetic flux density, instead of the continuity of the tangential component of the electric field. This continuity is not used since the electric field outside the conducting regions is considered to be of no (practical) importance.

When using the SOVP formulation we base the solution on the magnetic field calculation which depends on two scalars (W_a and W_b) in conductive regions and on only one scalar (W_a) in nonconductive regions. We can easily show that in an air-conductor interface imposing the continuity of the magnetic field components does ensure a vanishing normal component for the electric field and thus of the eddy current density at the conductor

surface. For example, at an interface that has the form of a plane vertical to the z-axis, denoting with (1) the air region and with (2) the conductor region, the continuity of the tangential components of the magnetic field intensities gives

$$H_x^{(1)}\Big|_{z=c} = H_x^{(2)}\Big|_{z=c} \Rightarrow \mu_r \left.\frac{\partial^2 W_a^{(1)}}{\partial x \partial z}\right|_{z=c} = k^2 \frac{\partial W_b^{(2)}}{\partial y} + \left.\frac{\partial^2 W_a^{(2)}}{\partial x \partial z}\right|_{z=c} \tag{1.84}$$

$$H_y^{(1)}\Big|_{z=c} = H_y^{(2)}\Big|_{z=c} \Rightarrow \mu_r \left.\frac{\partial^2 W_a^{(1)}}{\partial y \partial z}\right|_{z=c} = -k^2 \frac{\partial W_b^{(2)}}{\partial x} + \left.\frac{\partial^2 W_a^{(2)}}{\partial y \partial z}\right|_{z=c} \tag{1.85}$$

Now differentiating (1.84) with respect to y and (1.85) with respect to x and then subtracting them we get

$$k^2 \left(\frac{\partial^2 W_b^{(2)}}{\partial x^2} + \frac{\partial^2 W_b^{(2)}}{\partial y^2} \right)_{z=c} = 0 \tag{1.86}$$

which is equivalent to $J_z\big|_{z=c} = 0$. Thus, in air-conductor interfaces we need only satisfy the continuity of the three components of the magnetic field.

1.6 Separation of variables

Perhaps the most powerful analytical method is the separation of variables, which is a general approach to the solution of differential equations in field theory, taking into account the particular boundary conditions of the problem. Boundary conditions are classified into three types: (a) Dirichlet boundary conditions for which the field values on the boundary are specified, (b) Neumann boundary conditions for which the normal derivatives of the field on the boundary are specified and (c) mixed boundary conditions for which field values are known on part of the boundary while normal derivatives are known for the remaining part.

From the preceding analysis concerning the second order vector potential we concluded that even in 3D problems we need to solve the scalar Laplace or Helmholtz equation. We will present here the general procedure of applying the method to the Laplace equation $\nabla^2 \phi = 0$ in the three main coordinate systems. The interested reader can find solutions for special cases as well as the general solution and special cases solution of the

Helmholtz equation in various textbooks, see for example Moon (1971).

1.6.1 *Cartesian coordinates*

We will first consider a system of Cartesian coordinates and further assume that the unknown function satisfying the Laplace equation

$$\nabla^2\phi(x,y,z) = \frac{\partial^2\phi}{\partial x^2} + \frac{\partial^2\phi}{\partial y^2} + \frac{\partial^2\phi}{\partial z^2} = 0 \tag{1.87}$$

is a product of three one-variable functions as follows:

$$\phi(x,y,z) = X(x)Y(y)Z(z) \tag{1.88}$$

Substituting equation (1.88) in (1.87) we obtain the following differential equation:

$$YZ\frac{d^2X}{dx^2} + XZ\frac{d^2Y}{dy^2} + XY\frac{d^2Z}{dz^2} = 0 \tag{1.89}$$

Dividing equation (1.89) by the product XYZ, which is not zero, yields:

$$\frac{1}{X}\frac{d^2X}{dx^2} + \frac{1}{Y}\frac{d^2Y}{dy^2} + \frac{1}{Z}\frac{d^2Z}{dz^2} = 0 \tag{1.90}$$

Each term in equation (1.90) is a function of one variable only, and therefore, each term must be equal to a constant, in order for (1.88) to be satisfied for arbitrary values of the three independent variables (x, y, z). This means that the following equations should hold:

$$\frac{1}{X}\frac{d^2X}{dx^2} = k_x^2 \tag{1.91}$$

$$\frac{1}{Y}\frac{d^2Y}{dy^2} = k_y^2 \tag{1.92}$$

$$\frac{1}{Z}\frac{d^2Z}{dz^2} = k_z^2 \tag{1.93}$$

The separation constants are linked together through the relation:

$$k_x^2 + k_y^2 + k_z^2 = 0 \tag{1.94}$$

Considering now the differential equations of (1.91), (1.92) and (1.93), we can write the general solution as

$$\begin{aligned}\phi(x,y,z) = &[A_1\sin(k_x x) + A_2\cos(k_x x)] \\ &\times [B_1\sin(k_y y) + B_2\cos(k_y y)] \times [C_1\sinh(|k_z|z) + C_2\cosh(|k_z|z)]\end{aligned} \tag{1.95}$$

where $|k_z| = \sqrt{k_x^2 + k_y^2}$. If the region of interest is infinite we have to integrate over k_x and k_y from 0 to ∞ to get the final general solution. If the solution region is finite then k_x and k_y assume discrete values and we have to sum them up to ∞ to get the final general solution. The constants $A_1, A_2, B_1, B_2, C_1, C_2$ are then determined by satisfying the boundary and interface conditions.

1.6.2 *Cylindrical coordinates*

In a system of cylindrical coordinates, the Laplace equation for the scalar function is written as:

$$\nabla^2\phi(r,\varphi,z) = \frac{1}{r}\frac{\partial}{\partial r}\left(r\frac{\partial\phi}{\partial r}\right) + \frac{1}{r^2}\frac{\partial^2\phi}{\partial\varphi^2} + \frac{\partial^2\phi}{\partial z^2} = 0 \tag{1.96}$$

The function $\phi(r,\varphi,z)$ can be written as the product of three functions, each one depending on a single coordinate variable:

$$\phi(r,\varphi,z) = R(r)F(\varphi)Z(z) \tag{1.97}$$

Equation (1.97) is substituted for in (1.96), resulting in the following differential equation:

$$FZ\frac{1}{r}\frac{d}{dr}\left(r\frac{dR}{dr}\right) + RZ\frac{1}{r^2}\frac{d^2F}{d\varphi^2} + RF\frac{d^2Z}{dz^2} = 0 \tag{1.98}$$

This is further divided by the product RFZ and multiplied by r^2 leading to:

$$\frac{r}{R}\frac{d}{dr}\left(r\frac{dR}{dr}\right) + \frac{1}{F}\frac{d^2F}{d\varphi^2} + r^2\frac{1}{Z}\frac{d^2Z}{dz^2} = 0 \tag{1.99}$$

The second term in the above equation is independent of variables (r,z) and thus, the differential equation can only hold true for all values of (r,φ,z) if this second term is equal to a constant:

$$\frac{1}{F}\frac{d^2F}{d\varphi^2} = \nu^2 \tag{1.100}$$

If the function is to be single-valued, $\phi(2\pi) = \phi(0)$, then the separation constant ν must be equal to an integer value n. This leads to the general solution of equation (1.100), which can be written according to the following two alternative forms:

$$F(\varphi) = B_1 \sin(n\varphi) + B_2 \cos(n\varphi) \tag{1.101}$$

$$F(\varphi) = B_1 e^{jn\varphi} + B_2 e^{-jn\varphi} \tag{1.102}$$

If n is not an integer, these are still the general solutions of equation (1.100). The sum of the first and third terms in equation (1.99) should equal $-\nu^2$. Considering this, and further dividing by r^2 we get:

$$\left[\frac{1}{R}\frac{1}{r}\frac{d}{dr}\left(r\frac{dR}{dr}\right) + \frac{\nu^2}{r^2}\right] + \frac{1}{Z}\frac{d^2Z}{dz^2} = 0 \tag{1.103}$$

Clearly, each term in the above equation is a function of a single variable and therefore it must be equal to a constant. Setting the first term (in brackets) equal to a constant κ we obtain the differential equation

$$\frac{d^2R}{dr^2} + \frac{1}{r}\frac{dR}{dr} + \left(\kappa^2 - \frac{\nu^2}{r^2}\right) R = 0 \tag{1.104}$$

which is immediately identified as a Bessel equation and thus admits the general solution:

$$R(r) = A_1 J_\nu(\kappa r) + A_2 Y_\nu(\kappa r) \tag{1.105}$$

Returning back to equation (1.103) the second term should equal κ^2 thus developing the differential equation for z

$$\frac{d^2Z}{dz^2} - \kappa^2 Z = 0 \tag{1.106}$$

which has the general solution

$$Z(z) = C_1 \sinh(\kappa z) + C_2 \cosh(\kappa z) \tag{1.107}$$

Combining the solutions for $R(r)$, $F(\varphi)$ and $Z(z)$, the general solution of Laplace equation is written as:

$$\begin{aligned}\phi(r,\varphi,z) = \sum_n \sum_\kappa &\left[A_{1,n} J_n(\kappa r) + A_{2,n} Y_n(\kappa r)\right] \\ &\times \left[B_{1,n} e^{jn\varphi} + B_{2,n} e^{-jn\varphi}\right] \left[C_{1,\kappa} \sinh(\kappa z) + C_{2,\kappa} \cosh(\kappa z)\right]\end{aligned} \tag{1.108}$$

Here we assumed that the solution region is finite and κ assumes discrete values, so we superposed the solutions with a sum. In case the solution region was infinite the sum over κ should be replaced by an infinite integral.

1.6.3 *Spherical coordinates*

In a system of spherical coordinates the Laplace equation for the scalar function $\phi(r, \vartheta, \varphi)$ acquires the form:

$$\nabla^2\phi(r,\vartheta,\varphi) = \frac{1}{r^2}\frac{\partial}{\partial r}\left(r^2\frac{\partial\phi}{\partial r}\right) + \frac{1}{r^2\sin\vartheta}\frac{\partial}{\partial\vartheta}\left(\sin\vartheta\frac{\partial\phi}{\partial\vartheta}\right) + \frac{1}{r^2\sin^2\vartheta}\frac{\partial^2\phi}{\partial\varphi^2} = 0 \tag{1.109}$$

As before, a product solution of the function $\phi(r, \vartheta, \varphi)$ will be assumed

$$\phi(r,\vartheta,\varphi) = R(r)\Theta(\vartheta)F(\varphi) \tag{1.110}$$

Substituting this to (1.109) and dividing by the product $R\Theta F$ we obtain:

$$\frac{\sin^2\vartheta}{R}\frac{\partial}{\partial r}\left(r^2\frac{\partial R}{\partial r}\right) + \frac{\sin\vartheta}{\Theta}\frac{\partial}{\partial\vartheta}\left(\sin\vartheta\frac{\partial\Theta}{\partial\vartheta}\right) + \frac{1}{F}\frac{\partial^2 F}{\partial\varphi^2} = 0 \tag{1.111}$$

In order to satisfy equation (1.111) one should assign to the last term a constant (separation constant), here denoted as $-n^2$ and therefore

$$\frac{\partial^2 F}{\partial\varphi^2} + n^2 F = 0 \tag{1.112}$$

The general solution of (1.112) is easily obtained as:

$$F(\varphi) = C_1\cos(n\varphi) + C_2\sin(n\varphi) \tag{1.113}$$

Replacing the last term in equation (1.111) by n^2 and further dividing by $\sin^2\vartheta$ the former equation becomes:

$$\frac{1}{R}\frac{\partial}{\partial r}\left(r^2\frac{\partial R}{\partial r}\right) + \frac{1}{\Theta\sin\vartheta}\frac{\partial}{\partial\vartheta}\left(\sin\vartheta\frac{\partial\Theta}{\partial\vartheta}\right) - \frac{n^2}{\sin^2\vartheta} = 0 \tag{1.114}$$

The first term in equation (1.114) is a function of r only, and as a consequence it must be equal to a constant, here set to $m(m+1)$. The same is also true for the remaining two terms, which are involving only the variable ϑ, and thus must equal $-m(m+1)$. All of the above are reflected in the following equations:

$$\frac{d}{dr}\left(r^2\frac{dR}{dr}\right) - m(m+1)R = 0 \tag{1.115}$$

$$\frac{d}{d\vartheta}\left(\sin\vartheta\frac{d\Theta}{d\vartheta}\right) + \left[m(m+1)\sin\vartheta - \frac{n^2}{\sin\vartheta}\right]\Theta = 0 \tag{1.116}$$

The general solution of (1.115) is:

$$R(r) = A_1 r^m + A_2 r^{-(m+1)} \tag{1.117}$$

The differential equation in (1.116) is identified as the Legendre's equation with general solution

$$\Theta(\vartheta) = B_1 P_m^n(\cos\vartheta) + B_2 Q_m^n(\cos\vartheta) \tag{1.118}$$

where P_m^n and Q_m^n are associated Legendre's functions of the first and second kind respectively. Combining the above equations we result in the following expression for the solution of Laplace equation in spherical coordinates:

$$\begin{aligned}\phi(r,\vartheta,\varphi) = \sum_{m=0}^{\infty}\sum_{n=0}^{\infty} &\left[A_{1,m}r^m + A_{2,m}r^{-(m+1)}\right] \\ &\times \left[B_{1,m}P_m^n(\cos\vartheta) + B_{2,m}Q_m^n(\cos\vartheta)\right] \\ &\times \left[C_{1,n}\cos(n\varphi) + C_{2,n}\sin(n\varphi)\right]\end{aligned} \tag{1.119}$$

1.7 The general eddy current NDE problem

Fig.1.1 shows the general eddy current problem that needs to be solved. Almost all eddy current NDE problems can be derived from this basic configuration (by considering the flaw present or absent). A probe coil induces eddy currents in a conductive workpiece that contains an inhomogeneity (flaw). The coil is driven by a harmonically varying current $Ie^{j\omega t}$ and induces eddy currents in the conductive workpiece. These eddy currents are obstructed by the flaw and the result is reflected to the coil as an impedance change. When the coil is isolated from any conductors, the impedance is Z_0 and purely imaginary since we neglect in the analysis the dc wire resistance of the coil. The presence of the workpiece affects the impedance of the coil and this is referred to as impedance change ΔZ. If in addition a flaw is present in the workpiece there is an additional change to the coil

impedance change and we refer to that as ΔZ^c. In all cases the impedance is calculated by first calculating the electromagnetic field and then by either integrating the magnetic flux density over the surface of the coil windings or by using the ΔZ formula which involves an integration over the surface of the conductor or the surface of the flaw, see Sec.1.7.1.

What makes eddy current modelling a relatively difficult task is the fact that the shape of the probe coil, conductor and flaw can be arbitrary. In

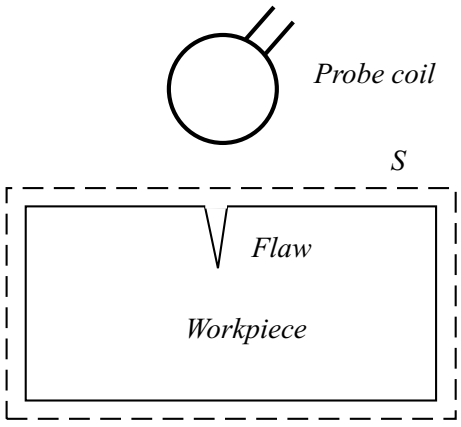

Fig. 1.1 The central eddy current NDE problem.

addition, the fact that the flaw dimensions are usually very small compared to the conductor and problem region dimensions makes the use of numerical methods, such as FEM, somewhat problematic because of the very dense grid that has to be used in the area of the flaw in order to get accurate and meaningful results. Alternative numerical methods do exist, for example integral methods such as the volume integral method (VIM), which requires the discretization of only the flaw region and solves for the electric field in the presence of the flaw. In such integral methods the following equation holds

$$\mathbf{E}_0(\mathbf{r}) = \mathbf{E}(\mathbf{r}) - (\sigma_f - \sigma_h) \int_V \mathbf{G}(\mathbf{r}, \mathbf{r}') \cdot \mathbf{E}(\mathbf{r}') dV \tag{1.120}$$

where $\mathbf{E}_0(\mathbf{r})$ is the incident electric field in the absence of the flaw at the coordinate $\mathbf{r} = (x, y, z)$, $\mathbf{E}(\mathbf{r})$ is the total electric field, σ_f is the flaw conductivity (usually zero), σ_h is the host conductivity, V is the flaw volume and $\mathbf{G}(\mathbf{r}, \mathbf{r}')$ is the electric field Green's tensor for a unit current at $\mathbf{r}'$ that

satisfies the differential equation

$$\nabla^2 \mathbf{G} = k^2 \mathbf{G} - j\omega\mu \mathbf{I}\delta\left(\mathbf{r} - \mathbf{r}'\right) \tag{1.121}$$

Thus, knowing the incident electric field in the flaw, (1.120) may be used to compute the total (incident plus "scattered") electric field in it. The scattered field is due to a distribution of electric dipoles equivalent to the presence of the flaw in the host. Of course, integral methods are not without difficulties since an analytical expression is required for the Green's tensor and this is possible in only very few canonical conductor geometries.

The question now is in which cases the analytical solutions can prove useful. First of all they can be used to solve problems where there is no flaw and the conductor has the form of an infinite plane (either layered or not) or infinite cylinder or sphere. The shape of the coil does not add much to the complexity of the solution and as will be shown in the following chapters of this monograph it can be treated easily. In cases where we have edges or canonically shaped cuts in the conductors we may be able to use the quasi-analytical TREE method. Finally when we have these conductor shapes with a flaw and we use an integral method, analytical solutions are useful for providing closed form expressions both for the incident field $\mathbf{E}_0(\mathbf{r})$ and the Green's tensor $\mathbf{G}(\mathbf{r}, \mathbf{r}')$. Thus, integral methods can benefit from analytical solutions since these can be used to calculate analytically $\mathbf{G}(\mathbf{r}, \mathbf{r}')$ in a broader class of canonical geometries.

1.7.1 *The ΔZ formula*

The general forward problem in eddy current NDE is the calculation of the impedance change of the coil produced by the inhomogeneity. The inverse problem is defined as the identification of the inhomogeneity characteristics (dimensional and material) from measurements of the coil impedance change.

The forward problem has been considerably simplified by introducing a formula that allows the calculation of the impedance change due to the flaw by knowing the electromagnetic field on the flaw surface. The analysis leading to the derivation of the so called ΔZ formula begins with the Lorentz reciprocity relation

$$\nabla \cdot \left(\mathbf{E} \times \mathbf{H}' - \mathbf{E}' \times \mathbf{H}\right) = 0 \tag{1.122}$$

where $\mathbf{E}, \mathbf{H}$ and $\mathbf{E}', \mathbf{H}'$ are any two solutions to Maxwell's equations. This equation is applicable at any point in the medium where the material prop-

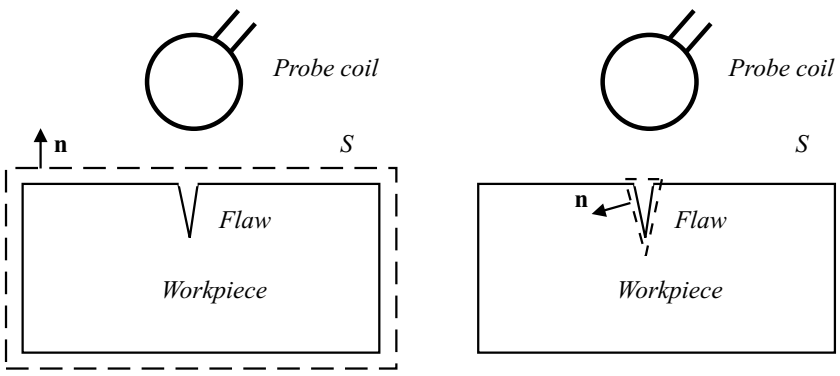

Fig. 1.2 Application of the ΔZ formula.

erties of the medium are the same for the two solutions and where no source currents are present. The solutions are also assumed to be time harmonic, with angular frequency ω. Using (1.122), Auld (1981) derived the ΔZ formula, where the change in the probe impedance due to the flaw is computed by an integration over the flaw surface

$$\Delta Z = \frac{1}{I^2} \oint_S (\mathbf{E} \times \mathbf{H}' - \mathbf{E}' \times \mathbf{H}) \cdot \mathbf{n} ds \tag{1.123}$$

where now $\mathbf{E}$, $\mathbf{H}$ are the field quantities without the flaw, $\mathbf{E}'$ and $\mathbf{H}'$ are the same quantities with the flaw and I is the coil current. It should be emphasized here that the integration surface can be any surface enclosing the flaw, the choice being determined by the requirements of the analysis. The formula can be used not only to find the impedance change from flaws but from any inhomogeneous part of the geometry, even from the conductor itself as shown in Fig.1.2 and further discussed in Chapter 5. In this case the integration surface encloses the whole conductor. For other work relative to the derivation of (1.123) and how this formula can also be used for computing mutual impedance change or for rewriting it as a volume integral, the interested reader can refer to Zaman (1982) and Auld (1999).

1.8 Impedance analysis and measurements

In ECT the usual method of presenting the information is in the form of impedance or impedance change diagrams where the resistance is put on the abscissa and the inductive reactance is put on the ordinate. Such a typical

diagram is shown in Fig.1.3 where the effects of frequency, conductivity, magnetic permeability, lift-off and a surface crack are depicted in the same diagram. The test case is a coil located above a conductive half-space and the curves show that signals that would have been acquired had the relevant parameters had changed.

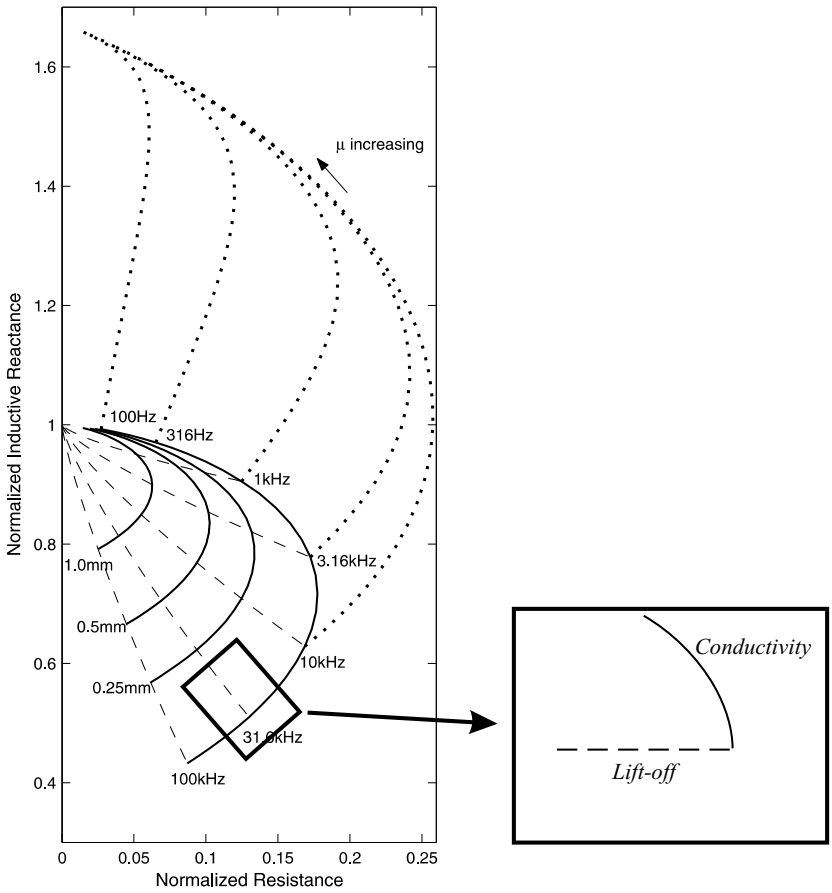

Fig. 1.3 Impedance plane diagram and a part of it as displayed by an eddyscope.

The impedance plane is also the information that an eddy current user gets during a real inspection. The eddy current instruments, also called "eddyscopes", are able to depict a portion of the impedance diagram on a vector screen, as shown in Fig.1.3. This portion can be expanded in one or

both axes, rotated, filtered, etc. However, the eddyscope does not provide an absolute measurement of the impedance change and thus it cannot be used for exact verification of theoretical results. The verification of results from either numerical or analytical computations is usually done by experimental measurements conducted in labs with special instruments like impedance analyzers and LCR bridges. Their accuracy ranges from 0.05% to 1% taking the specific frequency into account. Careful dimensioning of the coils and workpieces is needed for accurate measurements as well as careful positioning of the coils. Such a procedure was presented by Harrison (1996), where an error analysis was performed and a correction method for non-ideal coil behavior was demonstrated.

Although eddyscopes do not offer the high accuracy of impedance analyzers, there have been a number of approaches for using them as such. The procedure requires some knowledge of the electronics of the eddyscope bridge, Blitz (1981), or some initial calibration with a series of standard resistances, Lepine (1995).

Chapter 2

Uniform Field Excitation

2.1 Introduction

In this chapter, we concentrate on canonical problems where the excitation takes the form of a uniformly distributed magnetic field. The configurations examined consist of surface cracks in a semi-infinite slab of conductive material which we call a *conductive half-space* or simply *conductor*. The magnetic field is parallel to the surface of the conductor, therefore without a crack the problem is one-dimensional. At first sight it may appear to be artificial to examine the behavior of eddy currents that are constrained to be functions of one coordinate direction only. However, conclusions can be drawn from this limiting case. Eddy currents flow close to the surface of the conductor, their depth of penetration depending upon the conductivity σ, the magnetic permeability μ and the frequency of excitation f. Thus, the electromagnetic field solution will provide us with expressions that describe the dependence of eddy currents upon these parameters.

After presenting the solution for this trivial problem, we examine the much more complex problem of a crack embedded in the conductive half-space and provide expressions for the magnetic field and eddy current behavior as well as the impedance change per unit length due to the crack. If we want to study eddy current-flaw interaction, the simplest non-trivial model is probably the case of an infinitely long surface crack oriented so that the interrogating magnetic field lies parallel both to the surface of the conductor and the plane of the crack. The crack is modelled as an infinitely thin insulating layer at which the normal component of the current must vanish. In this configuration the crack produces the greatest obstacle to the eddy currents; the problem may also be treated by 2D methods. Although real probes and flaws require a 3D representation, the study of 2D problems

is valuable since independent analytical results can be found against which numerical models can be validated in appropriate limits. In addition, such solutions provide insight into the interaction between flaws and induced electromagnetic fields.

After reviewing the literature, we provide solutions not only for the ideal crack but also for cracks that have finite opening with arbitrary cross-section. For each case we calculate the spatial distribution of the magnetic field and eddy currents in the neighborhood of the crack and proceed then to give an expression for the impedance change due to the crack.

2.2 Conductive half-space

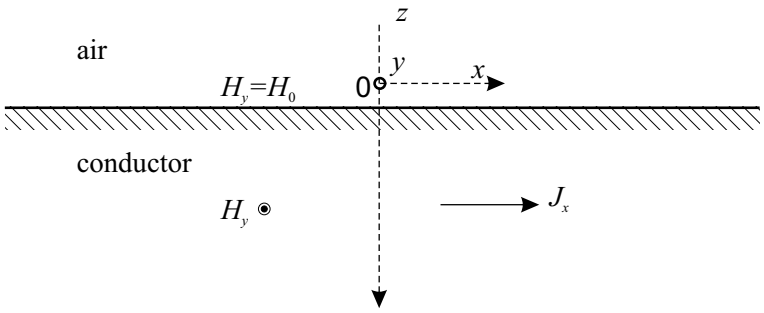

Fig. 2.1 A uniform magnetic field H_0 is applied in the air region above the conductor.

Considering the geometry of Fig.2.1 and assuming a y-directed magnetic field at the surface $H_0 \exp(j\omega t)$, it follows that the magnetic field inside the conductor is also y-directed and depends only on the depth z. Thus the problem is one-dimensional and satisfies the scalar one-dimensional Helmholtz equation:

$$\frac{\partial^2 H}{\partial z^2} = k^2 H \quad ; \quad k^2 = j\omega\mu\sigma \tag{2.1}$$

with the boundary conditions

$$H(z=0) = H_0 \tag{2.2}$$

$$H(z \to \infty) = 0 \tag{2.3}$$

The first condition specifies the applied magnetic field strength and the second is merely a statement of the fact that the field is attenuated by the conductive medium. In general, a constant magnetic field implies either that the supply is a constant current source or that the conductor carrying the eddy currents is such a small part of the system that it exerts negligible influence upon the current drawn from a constant voltage source. Alternatively, the conductor may itself form part of the winding. In fact, the one-dimensional half-space problem is a rather special case in which the magnetic field produced by the eddy currents is zero outside the plate and it is therefore particularly easy to specify the surface values of H.

The general solution to (2.1) is

$$H(z) = A\exp(kz) + B\exp(-kz) \tag{2.4}$$

and due to (2.2) and (2.3), $A = 0$, $B = H_0$ and the expression for the magnetic field finally becomes

$$H(z) = H_0\exp(-kz) \tag{2.5}$$

Since $k = (1+j)/\delta$, where $\delta = \sqrt{2/\omega\mu\sigma}$ is the standard depth of penetration (electromagnetic skin depth), it follows that (2.5) can also be written as

$$\frac{H(z)}{H_0} = \exp(-\frac{z}{\delta})\exp(-j\frac{z}{\delta}) \tag{2.6}$$

From (2.6) it is easily deduced that the attenuation of the magnetic field amplitude is exponential with depth and the variation of its phase (phase lag) is linear. Thus, at 1δ the magnetic field amplitude drops to $\exp(-1) = 36.8\%$ of its surface value and its phase lag is 1 radian, at 2δ amplitude drops to $\exp(-2) = 13.5\%$, the phase lag is 2 radians and so on. This behavior is shown in Fig.2.2 up to a depth of 5δ, at which point the field amplitude drops practically to zero. The same behavior is true for the eddy current density which is x-directed and calculated from

$$J(z) = -\frac{\partial H(z)}{\partial z} = kH_0\exp(-kz) \tag{2.7}$$

and $kH_0 = J_0$ is the surface value of the current density.

In eddy current testing, sensitivity to defects depends on eddy current density at the defect location. Although eddy currents penetrate deeper than one standard depth of penetration they decrease rapidly with depth. The signal produced by a flaw depends on both amplitude and phase of the currents obstructed. We expect that a surface flaw will give a larger signal

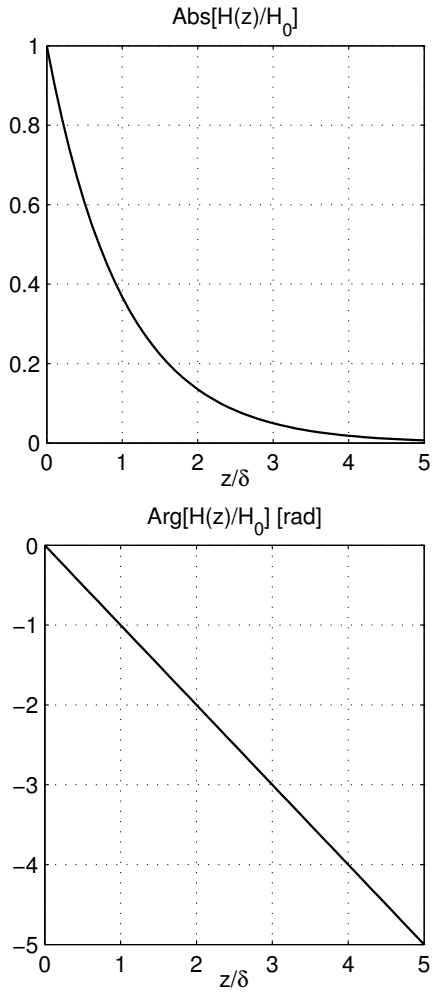

Fig. 2.2 Amplitude and phase lag variation of the magnetic field (and eddy currents) with depth.

than a subsurface one, but this depends also on its size. A small surface defect and a large internal defect can have a similar effect on the magnitude of test coil impedance. However, because of the increasing phase lag with depth, there will be a characteristic difference in the test coil impedance vector and this effect allows location and extent of a defect to be determined. This is the reason for preferring the phase as a measured quantity in eddy

current testing whenever depth information is required: there is a linear relationship between flaw depth and signal phase.

It has to be noted that the definition for the depth of penetration is valid only for the combination of a plane wave excitation (in our case the uniform magnetic field excitation) and a conductive half-space. It cannot be used for anything other than getting a very rough estimate of penetration in cases of a conductor of finite thickness or a non-uniform field produced by a real coil with finite dimensions. As we shall see in the following chapter, in these cases the effective penetration depth depends not only on the electromagnetic characteristics of the conductor but also on the coil dimensions.

2.3 Surface crack solutions

There are a number of numerical and analytical studies on the canonical problem of a long crack on the surface of a conductive half-space. We are interested in analytical or semi-analytical solutions and we categorize these as either approximate or exact. For a comprehensive review of both analytical and integral models for simulating cracks the reader can refer to Bowler (2004).

2.3.1 *Approximate solutions*

Approximate analytical solutions are limited to the low and high frequency regimes (large and small skin depth compared to the crack depth), and usually (but not always) involve elementary functions.

In the high-frequency regime, the electromagnetic skin depth (eddy current penetration) is much smaller than the depth of the crack and the current flows uniformly over the crack faces. Only near the buried edge of the crack and in the conductor corners at the crack mouth do the fields depart from this uniform behavior. Consequently, in the high-frequency regime, the solution for the fields may be found as the sum of distinct contributions from the corners, faces and edges of the crack. This constructive approach was first used by Kahn (1977) and yields good results for cracks of depth greater than about four skin depths. In a similar approach, also utilizing this effective decoupling of the corner and edge fields in the high frequency limit, Harfield (1994) presented an expression for the impedance change due to the crack in the thin skin limit which was expressed as the sum of

three terms

$$\Delta Z = Z_f + Z_e + Z_c \tag{2.8}$$

where Z_f arises from the uniform current flow over the faces of the crack, Z_e arises from the perturbation of the fields by the crack edge and Z_c from the perturbation by the corners. The final result for the total impedance change for a crack of depth greater that four skin depths in the high frequency limit is

$$\begin{aligned}\Delta Z &= \frac{1}{\sigma}\left(\frac{H_0}{I}\right)^2\left(2kc + 1 - \frac{8}{\pi}\right) \\ &= \frac{1}{\sigma}\left(\frac{H_0}{I}\right)^2\left[2(1+j)\frac{c}{\delta} + 1 - \frac{8}{\pi}\right]\end{aligned} \tag{2.9}$$

where c is the crack depth. As we shall see in the following, we usually depict ΔZ by normalizing it with the factor $(H_0/I)^2/\sigma$. The normalized ΔZ depends only on the ratio c/δ, thus for a specific conductor material the impedance change variation, with respect to crack depth and frequency, is described by a single curve.

A similar expression with additional terms that correspond to the finite gap of crack had been derived earlier by Auld (1981)

$$\begin{aligned}\Delta Z &= \frac{1}{\sigma}\left(\frac{H_0}{I}\right)^2\left[2\,(1+j)\,\frac{c}{\delta} - 1.56 - (1+j)\,\frac{\Delta u}{\delta} + 2j\frac{A_F}{\delta^2}\right] \\ &= \frac{1}{\sigma}\left(\frac{H_0}{I}\right)^2\left(2kc - 1.56 - k\Delta u + k^2 A_F\right)\end{aligned} \tag{2.10}$$

where Δu is the crack opening displacement and A_F is the crack opening cross-section area. For an ideal crack, these are both zero and (2.10) reduces to (2.9).

Seeking a more general solution which would be valid over a much wider frequency range, the problem was reformulated by Harfield (1995) by imaging in the air-conductor interface plane and use of the Wiener-Hopf method of solution. That yielded a Fredholm type integral equation of the second kind for the scattered magnetic field which was solved approximately for high frequencies and the final expression was found as a series of exponentially decreasing terms. Lower order terms account for the solutions for decoupled crack edge and corner effects, while higher order terms account for the coupling which occurs between the fields perturbed by the crack

edge and corners. Later, Harfield (1997) introduced a new theory by which approximate analytical solutions for the electromagnetic field distribution in the region of a defect can be calculated for intermediate, as well as high frequencies. The method is based on the geometrical theory of diffraction and yields solutions that agree very well with the required boundary values for cracks whose edges lie about 0.5δ (and greater) below the conductor surface.

Another approximate solution was presented by Michael *et al* (1982) for ACFM (Alternating Current Frequency Measurement) applications. Making use of the Kontorovich-Lebedev transform, they provided expressions for the electromagnetic field behavior around an inclined crack by considering again the effects of the crack corners and edge to be decoupled.

Subsequently, Harfield (1996) developed a formula valid in the low frequency regime. In this regime, the quantity kc is a small parameter and this fact can be exploited to find a field solution in the form of an ordered series using Rayleigh-Ritz perturbation theory.

$$\Delta Z = \frac{1}{\sigma}\left(\frac{H_0}{I}\right)^2\left[\frac{\pi}{2}(kc)^2 - \frac{4}{3}(kc)^3 + \ldots\right] \tag{2.11}$$

Another expression that predicted only an imaginary behavior at low frequencies and included an additional term accounting for the finite crack opening had been presented by Auld (1981).

$$\begin{aligned}\Delta Z &= \frac{1}{\sigma}\left(\frac{H_0}{I}\right)^2\left[j\pi\left(\frac{c}{\delta}\right)^2 + j2\frac{A_F}{\delta^2}\right] \\ &= \frac{1}{\sigma}\left(\frac{H_0}{I}\right)^2\left[\frac{\pi}{2}(kc)^2 + k^2 A_F\right]\end{aligned} \tag{2.12}$$

Finally, numerical results for the intermediate region, between the low and high frequency regimes were provided by Kahn (1988) by using the Boundary Integral Equation method. The method was also applied to the inclined crack and the impedance change was computed numerically as a function of the inclination angle.

2.3.2 *Exact solutions*

The problem of a long surface breaking crack in a conductive half-space does have an analytical solution for the full range of excitation frequency. Mirshekar (1982) presented such a solution in terms of expansions of higher

transcendental functions and applied it to the study of ACFM. These functions were angular and radial Mathieu functions. Overall, this is a complicated solution and the successful calculation of the electromagnetic field depends on the efficient computation of the Mathieu functions. This final expression for the magnetic field distribution will be reproduced here and extended to derive a closed-form expression for the impedance change due to the crack.

Another exact solution was presented by Theodoulidis (2004) for a long ideal crack in a conductive slab of finite thickness. Here we use the same approach to the subcase of a crack in a half-space (infinite thickness slab). Moreover, we examine the case of a surface crack with finite opening where its cross-section is symmetric but arbitrary and then proceed by giving exact expressions for the triangular, elliptical and rectangular cross-sections.

The solution is based on the TREE method where the electromagnetic field is expressed as series whose coefficients are computed by solving a linear system of equations. As already mentioned in Chapter 1, due to the required numerical inversion of a full matrix we describe the TREE method as pseudo-analytical. The method is used throughout this book to provide solutions for eddy current problems with a non-uniform excitation, see Chapters 4 and 7. Application of the method to the case examined here is similar to method used by Fawzi (1995), who provided solutions for Transverse Electric eddy current problems with rotational symmetry and focused on the short cylindrical shell coaxial with an ac line current.

2.4 Ideal surface crack

2.4.1 *Problem definition*

In this section, we define the problem of calculating the spatial distribution of magnetic fields in the neighborhood of a long surface crack in a conductor, where a uniform ac magnetic field is applied parallel to the length of the crack. The crack is assumed to be very long compared to its depth so that the eddy currents may be treated as two dimensional and it is idealized as a plane strip that does not permit the passage of a normal component of current. The material being tested is considered to be semi-infinite as shown in Fig.2.3 and the y-direction is taken parallel to the crack tip. The applied field $H_0 \exp(j\omega t)$ is uniform outside the material and everywhere parallel to the y-direction which is perpendicular to the plane of the page. As we have already seen, without the crack the problem is one-dimensional

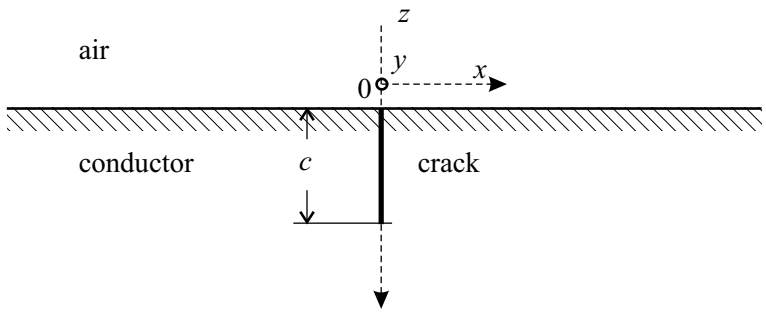

Fig. 2.3 A uniform magnetic field H_0 is applied in the air region above the conductor with a surface ideal crack.

and the magnetic field depends only on the depth z. With the addition of the ideal surface crack, as shown in Fig.2.3, the magnetic field has still only a y-component, but this now depends on both x and z and satisfies the two-dimensional Helmholtz equation:

$$\frac{\partial^2 H}{\partial x^2} + \frac{\partial^2 H}{\partial z^2} = k^2 H \quad ; \quad k^2 = j\omega\mu\sigma \tag{2.13}$$

with the following boundary conditions:

$$H(x,0) = H_0 \tag{2.14}$$

$$H(x, z \to \infty) = 0 \tag{2.15}$$

$$H(x,z)|_{x\to\pm\infty} = H_{\text{half}}(z) \tag{2.16}$$

$$H(0,z) = H_0 \quad ; \quad 0 \le z \le c \tag{2.17}$$

$$\left.\frac{\partial H(x,z)}{\partial x}\right|_{x=0} = 0 \quad ; \quad z \ge c \tag{2.18}$$

The boundary conditions (2.14), (2.15) are similar to the ones for the uncracked half-space and (2.16) means that the effect of the crack to the magnetic field is expected to vanish at large distances from the crack. The boundary condition (2.17) is equivalent to a vanishing x-eddy current component on the crack surface since

$$J_x(0,z) = -\frac{\partial H(0,z)}{\partial z} = 0 \Rightarrow H(0,z) = C \tag{2.19}$$

and the constant C is computed to H_0 by setting $z = 0$ and using (2.14). The boundary condition (2.18) means that the z-component of the eddy current density vanishes in the crack plane, below the crack.

The field is evaluated by solving an interior boundary value problem in which the total magnetic field is expressed as the sum of the unperturbed field, $H_{\text{half}}(z)$, and the perturbed field due to the crack, $H_c(x, z)$.

$$H(x, z) = H_{\text{half}}(z) + H_c(x, z) \tag{2.20}$$

The crack field satisfies also the scalar Helmholtz equation

$$\frac{\partial^2 H_c}{\partial x^2} + \frac{\partial^2 H_c}{\partial z^2} = k^2 H_c \quad ; \quad k^2 = j\omega\mu\sigma \tag{2.21}$$

and is subject to the following mixed boundary conditions:

$$H_c(x, 0) = 0 \tag{2.22}$$

$$H_c(x, z \to \infty) = 0 \tag{2.23}$$

$$H_c(x, z)|_{x \to \pm\infty} = 0 \tag{2.24}$$

$$H_c(0, z) = H_0 - H_{\text{half}}(z) = H_0 \left[1 - \exp(-kz)\right] \quad ; \quad 0 \le z \le c \tag{2.25}$$

$$\left.\frac{\partial H_c(x, z)}{\partial x}\right|_{x=0} = 0 \quad ; \quad z \ge c \tag{2.26}$$

Each boundary condition of the set (2.22)-(2.26) corresponds to the relative boundary condition of the set (2.14)-(2.18) and is produced by using (2.20). The mixed boundary conditions on the surface $x = 0$ are the main difficulty in treating this boundary value problem analytically. In the following we describe two methods to handle them.

2.4.2 *The Mirshekar-Syahkal solution.*

The Helmholtz type equation (2.21) for the crack field with mixed boundary conditions (2.22)-(2.26) can be transformed to a Mathieu type equation with uniform boundary conditions after using a suitable mapping of the problem geometry in the form of $z + jx = c\sin(u + jv)$. Application of such mappings to Helmholtz type equations is rather uncommon because

they usually result in differential equations that are difficult to handle (non-separable) but it nevertheless works in this case. The resulting differential equation for the transformed magnetic field is

$$\frac{\partial^2 \tilde{H}}{\partial u^2} + \frac{\partial^2 \tilde{H}}{\partial v^2} = k^2 c^2 \left(\cos^2 u + \sinh^2 v\right) \tilde{H} \tag{2.27}$$

After applying separation of variables, the crack magnetic field is calculated from a series involving a product of Mathieu functions

$$\tilde{H}(u,v) = \sum_{n=0}^{\infty} a_n se_{2n+1}(u,q) Fek_{2n+1}(v,-q) \tag{2.28}$$

where

$$se_{2n+1}(u,q) = \sum_{m=0}^{\infty} B_{2m+1}^{2n+1} \sin[(2m+1)u] \tag{2.29}$$

is the odd periodic (angular) Mathieu function of the first kind and

$$Fek_{2n+1}(v,-q) = (-1)^n se'_{2n+1}(0,q) se_{2n+1}\left(\tfrac{\pi}{2},q\right) k^{-1} \left(\pi B_1^{2n+1}\right)^{-2} \times \\ \times \sum_{m=0}^{\infty} B_{2m+1}^{2n+1} \left[I_m(q^{1/2}e^{-v}) K_{m+1}(q^{1/2}e^{v}) - I_{m+1}(q^{1/2}e^{-v}) K_m(q^{1/2}e^{v})\right] \tag{2.30}$$

is the even non-periodic (radial) Mathieu function of the second kind which is conveniently expressed in terms of series of modified Bessel function products in order to ensure uniform convergence. The series coefficients are calculated from

$$a_n = \frac{4}{\pi} \frac{\sum_{m=0}^{\infty} B_{2m+1}^{2n+1} \left\{ \frac{1}{2m+1} - \int_0^{\pi/2} \exp[-kc\sin(u)] \sin[(2m+1)u] du \right\}}{Fek_{2n+1}(0,-q) \sum_{m=0}^{\infty} \left(B_{2m+1}^{2n+1}\right)^2} \tag{2.31}$$

Evaluation of these Mathieu functions depends upon the characteristic value b which in turn depends upon n and the parameter q. In these equations $q = k^2c^2/4$ and is purely imaginary. Eqs (2.28)-(2.31) are the result presented by Mirshekar-Syahkal (1982). Now the impedance change due to the crack can be calculated from the integration of H_c over the transformed

solution region, which gives

$$\Delta Z = \sum_{n=0}^{\infty} a_n \left(\sum_{m=0}^{\infty} \frac{B_{2m+1}^{2n+1}}{2m+1} \right) \left(\int_0^{\infty} Fek_{2n+1}(v,-q)dv \right) \tag{2.32}$$

where the infinite integration of Fek_{2n+1} reduces to an infinite integration of Bessel functions, due to (2.30), and this integration is performed numerically. Equivalently, the impedance change can be calculated by a contour integration along a line representing the mapping of the conductor surface line and the crack line. The final result is

$$\Delta Z = \sum_{n=0}^{\infty} a_n \times \tag{2.33}$$
$$\times \left(se'_{2n+1}(0,q) \int_0^{\infty} Fek_{2n+1}(v,-q)dv + Fek'(0,-q) \sum_{m=0}^{\infty} \frac{B_{2m+1}^{2n+1}}{2m+1} \right)$$

The derivatives in (2.33) are evaluated from

$$se'_{2n+1}(0,q) = \sum_{m=0}^{\infty} B_{2m+1}^{2n+1}(2m+1) \tag{2.34}$$

and

$$Fek'_{2n+1}(0,-q) = (-1)^{n+1}\pi \left[\frac{se'_{2n+1}(0,q)}{\pi q^{1/2} B_1^{2n+1}} \right]^2 se_{2n+1}\left(\frac{\pi}{2}, q\right) \tag{2.35}$$

Obviously, the reliable calculation of the impedance change depends on the efficient calculation of the Mathieu functions and thus b and B_{2m+1}^{2n+1}. The characteristic value b and the expansion coefficients B_{2m+1}^{2n+1} are calculated following a procedure described by MacLachlan (1947). It is rather unfortunate that q is purely imaginary. We have not found any reliable calculation for Mathieu functions of complex arguments in the literature apart from Mathematica functions `MathieuS[b,q,u]` for $se_{2n+1}(u,q)$, `MathieuSPrime[b,q,u]` for $se'_{2n+1}(u,q)$ and `MathieuCharacteristicB[n,q]` for the computation of the characteristic values. Unfortunately, there is no such function for $Fek_{2n+1}(u,-q)$, so we are obliged to use its series definition and anyway compute the coefficients B_{2m+1}^{2n+1}. In principle this can be done by computing them as trigonometric coefficients of the series in (2.29) using the function evaluations of $se_{2n+1}(u,q)$ from Mathematica, but this is a rather slow process. We will

not provide any numerical results using the Mirshekar-Syakhal solution and leave this task to the interested reader.

2.4.3 *The TREE solution*

Throughout this book we use the TREE method to provide solutions to canonical eddy current problems and that is how we treat the long crack problem for the full frequency range. The main advantage of the method is its ability to handle mixed boundary conditions and the easy computer implementation, particularly with mathematical packages like Mathematica and Matlab.

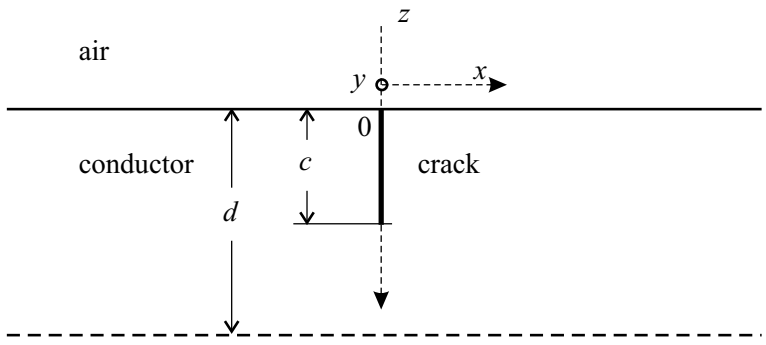

Fig. 2.4 A uniform magnetic field H_0 is applied in the air region above the conductor with the ideal crack. The solution domain is truncated at $z = d$.

In order to solve the boundary value problem described by (2.21)-(2.26) with the TREE method, we have to truncate the solution domain and we do that in the z-coordinate as shown in Fig.2.4. This is physically correct, since the exponential decay profile of the fields inside the metal is essentially unaffected by the presence of the crack, except in the region within a distance of the order of a skin depth from the crack line. As already discussed, at 5δ it is expected that the crack perturbation field vanishes, 3δ is also correct for practical purposes, while we can use 1δ for approximate solutions. Thus, playing on the safe side we can truncate the solution domain in the z coordinate by introducing an artificial boundary at a distance $d = c + 5\delta$ and replace the boundary condition (2.23) with

$$H_c(x, d) = 0 \tag{2.36}$$

After truncating the solution domain, the general solution for the crack

magnetic field has the form of a series:

$$H_c(x,z) = (A+Bz)[C\exp(kx) + D\exp(-kx)] + \sum_{n=1}^{\infty} [A_n \sin(q_n z) + B_n \cos(q_n z)]\,[C_n \exp(p_n x) + D_n \exp(-p_n x)] \tag{2.37}$$

where $p_n^2 = q_n^2 + k^2$ and q_n are the discrete eigenvalues of the problem. In view of (2.22) and (2.36), the first term should vanish. Note that the problem is symmetrical in the x-direction, therefore we can work in a semi-infinite region, for example for $x \geq 0$. Taking into account (2.22) and (2.24), the solution takes the following simplified form:

$$H_c(x,z) = \sum_{n=1}^{\infty} \sin(q_n z)\exp(-p_n x) A_n \tag{2.38}$$

Next, we consider (2.36) and derive the discrete eigenvalues that ensure a vanishing crack field at $z = d$:

$$\sin(q_n d) = 0 \Rightarrow q_n = \frac{n\pi}{d} \tag{2.39}$$

Now, we can compute the expansion coefficients A_n, by a mode matching technique where the testing functions are the same as the expanding ones. This registers TREE as a meshless Galerkin type method with entire domain (or global) basis functions. It is important to point out that the basis functions are solutions to the differential forms of the Maxwell equations and this is a major difference compared with other numerical methods. From (2.25) and (2.26) we derive:

$$\sum_{n=1}^{\infty} \sin(q_n z) A_n = H_0\,[1 - \exp(-kz)] \quad ; \quad 0 \leq z \leq c \tag{2.40}$$

$$\sum_{n=1}^{\infty} \sin(q_n z)(-p_n) A_n = 0 \quad ; \quad c \leq z \leq d \tag{2.41}$$

After truncating the series to a large N_s term, we multiply both sides of (2.40) and (2.41) with $\sin(q_m d)$ and integrate (2.40) from 0 to c and (2.41) from c to d. The result can be written in matrix form:

$$\mathbf{M}_1 \mathbf{A} = \mathbf{N}_1 \tag{2.42}$$

$$\mathbf{M}_2 \mathbf{A} = \mathbf{0} \tag{2.43}$$

where the elements of the various matrices are calculated from:

$$\begin{aligned}\mathbf{M}_{1,mn} &= \frac{\sin[c(q_m - q_n)]}{2(q_m - q_n)} - \frac{\sin[c(q_m + q_n)]}{2(q_m + q_n)} \quad m \neq n \\ &= \frac{c}{2} - \frac{\sin 2cq_m}{4q_m} \quad m = n \end{aligned} \tag{2.44}$$

$$\begin{aligned}\mathbf{M}_{2,mn} &= p_n \mathbf{M}_{1,mn} \quad m \neq n \\ &= -p_n \left(\frac{d}{2} - \mathbf{M}_{1,mn} \right) \quad m = n \end{aligned} \tag{2.45}$$

$$\begin{aligned}\mathbf{N}_{1,m} &= H_0 \frac{1 - \cos(q_m c)}{q_m} \\ &+ H_0 \frac{-q_m + \exp(-kc)\left[q_m \cos(q_m c) + k \sin(q_m c)\right]}{p_m^2} \end{aligned} \tag{2.46}$$

The total algebraic system for $\mathbf{A}$ is written as:

$$\begin{bmatrix} \mathbf{M}_1 \\ \mathbf{M}_2 \end{bmatrix} \mathbf{A} = \begin{bmatrix} \mathbf{N}_1 \\ \mathbf{0} \end{bmatrix} \tag{2.47}$$

Writing the composite matrix on the left as $\mathbf{M}$ and the composite matrix on the right as $\mathbf{N}$, the solution for $\mathbf{A}$ is:

$$\mathbf{A} = \mathbf{M}^{-1} \cdot \mathbf{N} \tag{2.48}$$

The final expression for the total magnetic field is:

$$H(x, z) = H_0 \exp(-kz) + \sum_{n=1}^{N_s} \sin(q_n z) \exp(-p_n x) A_n \tag{2.49}$$

and for the induced eddy current density:

$$\begin{aligned}\mathbf{J}(x, z) &= -\frac{\partial H}{\partial z}\mathbf{x_0} + \frac{\partial H}{\partial x}\mathbf{z_0} \\ &= \left[H_0 k \exp(-kz) - \sum_{n=1}^{N_s} \cos(q_n z) q_n \exp(-p_n x) A_n \right] \mathbf{x_0} \\ &- \left[\sum_{n=1}^{N_s} \sin(q_n z) p_n \exp(-p_n x) A_n \right] \mathbf{z_0} \end{aligned} \tag{2.50}$$

Having computed the crack magnetic field, the expression for the impedance change per-unit length is derived by integrating H_c over the half-space cross-section:

$$\Delta Z = j2\omega\mu n_t^2 \int_0^\infty \int_0^d H_c(x,z)dxdz = \frac{2k^2}{\sigma}\left(\frac{H_0}{I}\right)^2 \sum_{n=1}^{N_s} A_n \frac{2}{q_n p_n}$$
$$n = 1, 3, 5 \ldots \tag{2.51}$$

where $n_t = H_0/I$ is the turns per unit length of the energizing coil.

2.4.4 *Results*

The numerical calculations do not pose any particular problems. The most important calculation is the inversion of the non-square $\mathbf{M}$ matrix or in other words the solution of an over-determined linear system such as (2.47). This is a well-behaved system and we can use for example Matlab's $\mathbf{A} = \mathbf{M}\backslash\mathbf{N}$ command or Mathematica's `PseudoInverse[M]` routine to solve it.

Fig.2.5 shows the eddy current streamlines in a conductive half-space with an ideal surface crack 1mm deep at three frequencies that correspond to different skin depths. It is evident that with increasing frequency (decreasing skin depth and hence increasing ratio c/δ) the eddy currents concentrate near the surface and flow more closely around the crack line.

Figs 2.6, 2.7 show results for the real and imaginary part (resistive and reactive part) of ΔZ as compared to the thin skin results from (2.9). Both components are normalized to the factor $(H_0/I)^2/\sigma$. It is clearly seen that the curves coincide for a c/δ ratio above about 2. Taking into account that almost every surface eddy current inspection is performed at high frequencies, such a result means that the thin skin expressions are adequate for practical purposes.

2.5 Surface slot of arbitrary cross-section

The technique we have just used for ideal crack problems can be extended to cracks with finite opening. Consider the geometry in Fig.2.8 where we assume a surface slot which is symmetric in the x-direction and the shape of its opening is described by a function $x(z)$. As in the previous section, the total magnetic field is

$$H(x,z) = H_{\text{half}}(z) + H_c(x,z) \tag{2.52}$$

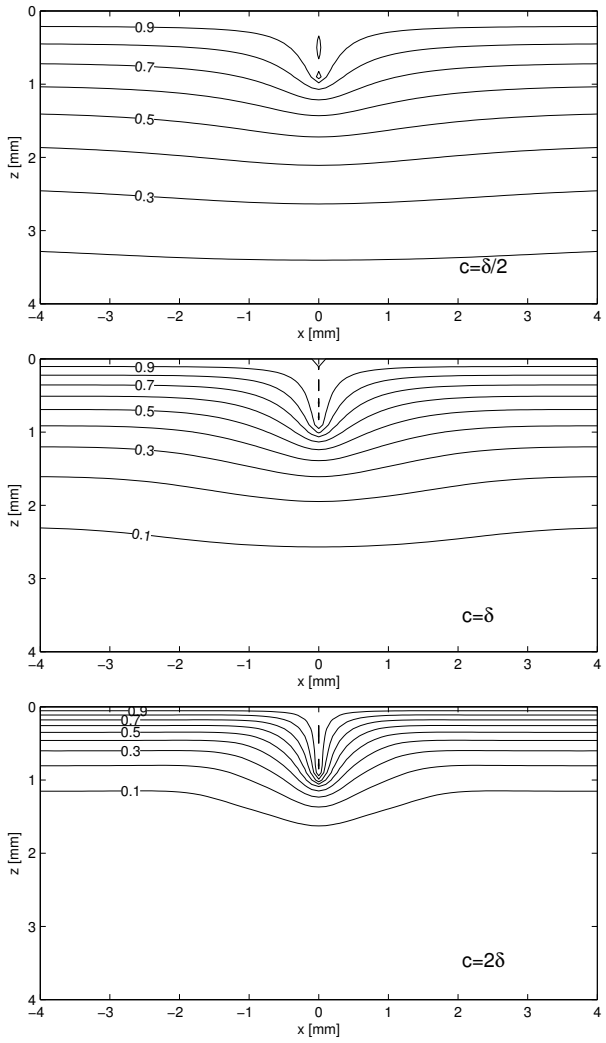

Fig. 2.5 Amplitude contours of magnetic field (streamlines of eddy currents) in a conductive half-space with a surface crack.

The function $H_c(x, z)$ again describes the contribution of the slot to the total magnetic field in the conductor and satisfies the differential equation (2.21). Let us repeat the boundary conditions that apply to this problem:

$$H_c(x, 0) = 0 \tag{2.53}$$

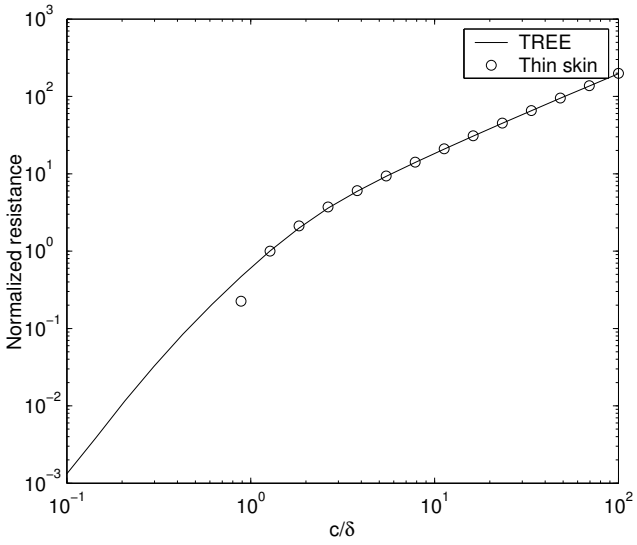

Fig. 2.6 Results for the resistive part of the impedance change due to a long surface crack

$$H_c(x,d) = 0 \tag{2.54}$$

$$H_c(x,z)\big|_{x\to\pm\infty} = 0 \tag{2.55}$$

$$H_c(x(z),z) = H_0 - H_{\text{half}}(z) = H_0\left[1-\exp(-kz)\right] \quad ; \quad 0 \le z \le c \tag{2.56}$$

$$\left.\frac{\partial H_c(x,z)}{\partial x}\right|_{x=0} = 0 \quad ; \quad z \ge c \tag{2.57}$$

Note that (2.56) is applied at the crack surface $x(z)$ and this boundary condition is equivalent to a vanishing eddy current normal to the crack surface. There is no current flowing normal to the boundary, since

$$J_n = -\frac{\partial H\left(x(z),z\right)}{\partial t} = 0 \tag{2.58}$$

where n denotes normal and t tangential direction at a point of the crack curve $x(z)$. Equivalently, we could say that eddy current streamlines are actually the equipotential lines and the crack face is just such a line.

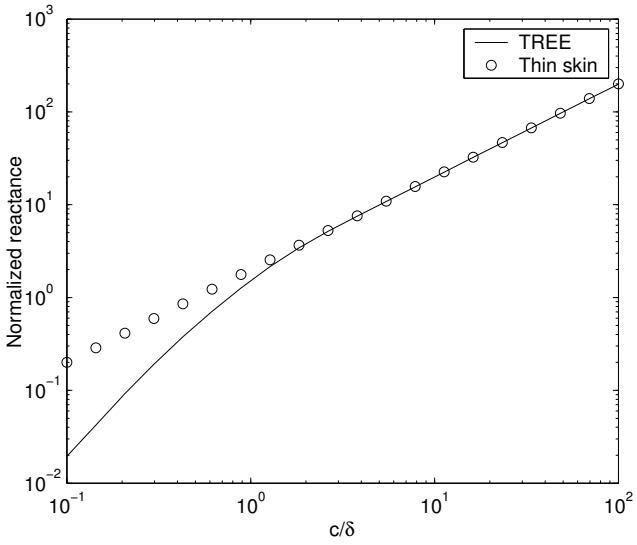

Fig. 2.7 Results for the reactive part of the impedance change due to a long surface crack

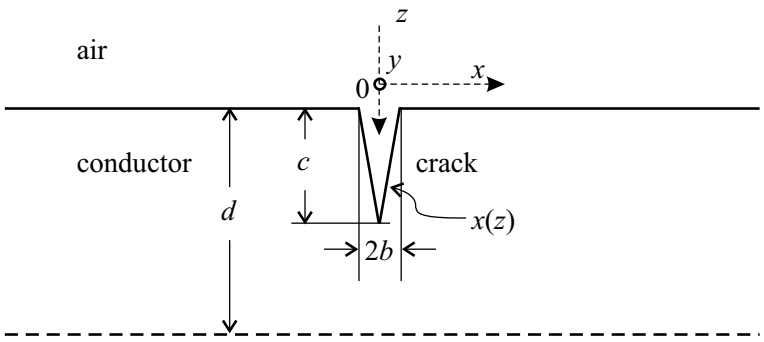

Fig. 2.8 A uniform y-directed magnetic field H_0 is applied in the air region above a conductor with a surface slot of arbitrary cross-section.

Proceeding as in the previous paragraph the general expression for the slot field is again the same

$$H_c(x,z) = \sum_{n=1}^{\infty} \sin(q_n z)\exp(-p_n x)A_n \tag{2.59}$$

Eqs (2.56) and (2.57) have to be satisfied, therefore

$$\sum_{n=1}^{\infty} \sin(q_n z) \exp[-p_n x(z)] A_n = H_0 \left[1 - \exp(-kz)\right] \quad ; \quad 0 \le z \le c \tag{2.60}$$

$$\sum_{n=1}^{\infty} \sin(q_n z)(-p_n) A_n = 0 \quad ; \quad c \le z \le d \tag{2.61}$$

The linear system is again formed as

$$\begin{bmatrix} \mathbf{M}_1 \\ \mathbf{M}_2 \end{bmatrix} \mathbf{A} = \begin{bmatrix} \mathbf{N}_1 \\ \mathbf{0} \end{bmatrix} \tag{2.62}$$

and the only different matrix is $\mathbf{M}_1$, which is now calculated from:

$$\mathbf{M}_{1,mn} = \int_{z=0}^{c} \sin(q_m z) \sin(q_n z) \exp[-p_n x(z)] dz \tag{2.63}$$

If we set $x(z) = 0$, in (2.63) we derive the same result for the case of the ideal crack examined in the previous paragraph. For a slot of elliptical cros-section shape with opening b and depth c

$$x(z) = b\sqrt{1 - \frac{z^2}{c^2}} \tag{2.64}$$

while for a triangular slot with the same opening and depth

$$x(z) = -\frac{b}{c} z + b \tag{2.65}$$

For the triangular cross-section the $\mathbf{M}_1$ matrix elements are

$$\begin{aligned} \mathbf{M}_{1,mn} = \frac{c}{2} \Bigg\{ & -\frac{4bc^2 \exp(-p_n b) p_n q_m q_n}{b^4 p_n^4 + c^4 \left(q_m^2 - q_n^2\right)^2 + 2b^2 c^2 p_n^2 \left(q_m^2 + q_n^2\right)} \\ & + \frac{b p_n \cos\left[(q_m - q_n)c\right] + c(q_m - q_n) \sin\left[(q_m - q_n)c\right]}{b^2 p_n^2 + c^2 \left(q_m - q_n\right)^2} \\ & - \frac{b p_n \cos\left[(q_m + q_n)c\right] + c(q_m + q_n) \sin\left[(q_m + q_n)c\right]}{b^2 p_n^2 + c^2 \left(q_m + q_n\right)^2} \Bigg\} \end{aligned} \tag{2.66}$$

The numerical solution proceeds in the same way as previously and the final expression for the total magnetic field is

$$H(x,z) = H_0 \exp(-kz) + \sum_{n=1}^{N_s} \sin(q_n z) \exp(-p_n x) A_n \tag{2.67}$$

The expression for the impedance change is derived after integrating the magnetic field of the slot over the conductor cross-sectional area

$$\Delta Z = j\omega\mu n_t^2 2 \left[\int_{x=x(z)}^{\infty} \int_{z=0}^{c} H_c(x(z),z) dx dz + \int_{x=0}^{\infty} \int_{z=c}^{d} H_c(z) dx dz \right] \tag{2.68}$$

which after performing the integrations gives

$$\Delta Z = \frac{2k^2}{\sigma} \left(\frac{H_0}{I} \right)^2 \sum_{n=1}^{N_s} A_n \left[\frac{c^2 \exp(-p_n b) q_n - c^2 q_n \cos(q_n c) + cbp_n \sin(q_n c)}{p_n \left(b^2 p_n^2 + c^2 q_n^2\right)} + \frac{\cos(q_n c) - \cos(q_n d)}{q_n p_n} \right] \tag{2.69}$$

2.6 Surface slot of rectangular cross-section

In the previous section we generalized the TREE approach to the surface slot of arbitrary cross-section. Unfortunately if a shape such as the rectangular one shown in Fig.2.9 (saw-cut) is to be modelled then the bottom surface of the crack, being parallel to the upper surface of the conductor, cannot be modelled. We illustrate the TREE method in this case by following a different approach.

Assume a slot with a rectangular cross-section which has an opening of $2b$. As in the previous paragraph, the total magnetic field is

$$H(x,z) = H_{half}(z) + H_c(x,z) \tag{2.70}$$

The function $H_c(x,z)$ again describes the contribution of the slot to the total magnetic field in the conductor and satisfies the differential equation (2.21). Taking into account the symmetry of the problem, the geometry is divided in two regions: The rectangular region under the slot ($0 \leq x \leq b, c \leq z \leq d$), which is denoted as Region 1 and the infinite region on the right of the slot ($x \geq b, 0 \leq z \leq d$), which in turn is denoted as Region 2.

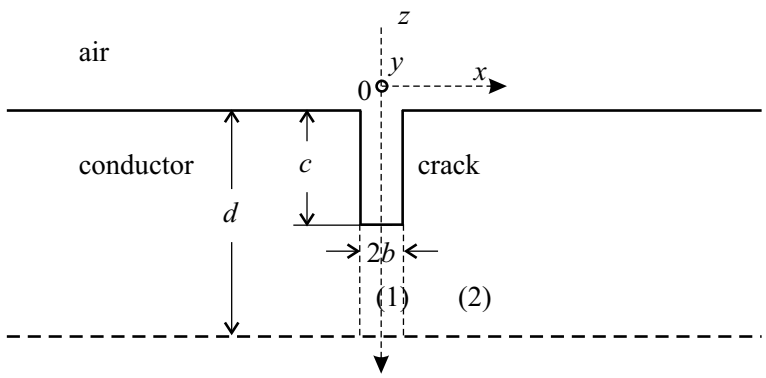

Fig. 2.9 A uniform magnetic field H_0 is applied in the air region above the conductor with a surface slot of rectangular cross-section.

The expressions for the magnetic field in the two regions that satisfy the boundary conditions are

$$H_c^{(1)}(x,z) = \sum_{n=1}^{\infty} \sin[r_n(z-c)] \cosh(s_n x) A_n^{(1)} \tag{2.71}$$

$$H_c^{(2)}(x,z) = \sum_{n=1}^{\infty} \sin(q_n z) \exp(-p_n x) A_n^{(2)} \tag{2.72}$$

where now

$$q_n = \frac{n\pi}{d} \quad p_n = \sqrt{q_n^2 + k^2} \tag{2.73}$$

$$r_n = \frac{n\pi}{d-c} \quad s_n = \sqrt{r_n^2 + k^2} \tag{2.74}$$

so that the crack magnetic field vanishes at the top and bottom of each region. The interface conditions are the continuity of the tangential magnetic and electric field components. The magnetic field continuity gives

$$\sum_{n=1}^{\infty} \sin(q_n z) \exp(-p_n b) A_n^{(2)} = H_0 \left[1 - \exp(-kz)\right]; \quad 0 \le z \le c \tag{2.75}$$

$$\sum_{n=1}^{\infty} \sin(q_n z) \exp(-p_n b) A_n^{(2)} = \sum_{n=1}^{\infty} \sin\left[r_n(z-c)\right] \cosh(s_n b) A_n^{(1)}; \quad c \le z \le d \tag{2.76}$$

while the electric field $E_z = \partial B_y/\partial x$ continuity gives for $c \leq z \leq d$

$$\sum_{n=1}^{\infty} \sin(q_n z)(-p_n) \exp(-p_n b) A_n^{(2)} = \sum_{n=1}^{\infty} \sin\left[r_n(z-c)\right] s_n \sinh(s_n b) A_n^{(1)} \tag{2.77}$$

We can see that now we have two sets of unknown coefficients $A_n^{(1)}$ and $A_n^{(2)}$ to calculate. The method we follow involves taking moments as previously. We use matrix notation for the three equations derived from the interface conditions and we rewrite them as

$$S^{\mathrm{T}}(\mathbf{q}z) \exp(-\mathbf{p}b)\mathbf{A}^{(2)} = H_0 \left[1 - \exp(-kz)\right] \quad ; \quad 0 \leq z \leq c \tag{2.78}$$

$$S^{\mathrm{T}}(\mathbf{q}z) \exp(-\mathbf{p}b)\mathbf{A}^{(2)} = S^{\mathrm{T}}[\mathbf{r}(z-c)] \cosh(\mathbf{s}b)\mathbf{A}^{(1)} \quad ; \quad c \leq z \leq d \tag{2.79}$$

$$S^{\mathrm{T}}(\mathbf{q}z)(-\mathbf{p}) \exp(-\mathbf{p}b)\mathbf{A}^{(2)} = S^{\mathrm{T}}[\mathbf{r}(z-c)]\mathbf{s} \sinh(\mathbf{s}b)\mathbf{A}^{(1)} \quad ; \quad c \leq z \leq d \tag{2.80}$$

First we multiply both sides of (2.78) with $S(\mathbf{q}z)$ and integrate from 0 to c. Then we multiply both sides of (2.79) and (2.80) with $S[\mathbf{r}(z-c)]$ and integrate from c to d. We end up with the following equations:

$$\mathbf{M}_1 \mathbf{A}^{(2)} = \mathbf{N}_1 \tag{2.81}$$

$$\mathbf{U} \exp(-\mathbf{p}b)\mathbf{A}^{(2)} = \frac{d-c}{2} \cosh(\mathbf{s}b)\mathbf{A}^{(1)} \tag{2.82}$$

$$\mathbf{U}(-\mathbf{p}) \exp(-\mathbf{p}b)\mathbf{A}^{(2)} = \frac{d-c}{2} \mathbf{s} \sinh(\mathbf{s}b)\mathbf{A}^{(1)} \tag{2.83}$$

where the elements of matrix $\mathbf{U}$ are

$$\mathbf{U}_{1,mn} = \tag{2.84}$$
$$\begin{cases} \frac{-2r_m \sin(cq_n) + (q_n + r_m)\sin[dq_n + (c-d)r_m] + (q_n - r_m)\sin[-dq_n + (c-d)r_m]}{2(q_n^2 - r_m^2)} & r_m \neq q_n \\ \frac{2(d-c)r_m \cos(cr_m) + \sin(cr_m) + \sin[(c-2d)r_m]}{4r_m} & r_m = q_n \end{cases}$$

From (2.82), (2.83) we get the expression of $\mathbf{A}^{(1)}$ in terms of $\mathbf{A}^{(2)}$ as well as a second equation for $\mathbf{A}^{(2)}$ apart from (2.81).

$$\mathbf{A}^{(1)} = \frac{2}{d-c} \cosh^{-1}(\mathbf{s}b)\mathbf{U} \exp(-\mathbf{p}b)\mathbf{A}^{(2)} \tag{2.85}$$

$$\left[-\mathbf{U}\mathbf{p} - \tanh(\mathbf{s}b)\mathbf{s}\mathbf{U}\right] \exp(-\mathbf{p}b)\mathbf{A}^{(2)} = 0 \tag{2.86}$$

Eq. (2.86) is similar to

$$\mathbf{M}_2\mathbf{A} = \mathbf{0} \tag{2.87}$$

with $\mathbf{M_2} = [-\mathbf{U}\mathbf{p} - \tanh(\mathbf{s}b)\mathbf{s}\mathbf{U}]\exp(-\mathbf{p}b)$. The linear system formed is

$$\begin{bmatrix}\mathbf{M}_1\\ \mathbf{M}_2\end{bmatrix}\mathbf{A}^{(2)} = \begin{bmatrix}\mathbf{N}_1\\ \mathbf{0}\end{bmatrix} \tag{2.88}$$

After solving the system (2.88) for the coefficients $A_n^{(2)}$ we use (2.85) to compute the coefficients $A_n^{(1)}$.

In Region 1 the final expressions for the total magnetic field are

$$H_c^{(1)}(x,z) = H_0\exp(-kz) + \sum_{n=1}^{\infty}\sin[r_n(z-c)]\cosh(s_nx)A_n^{(1)} \tag{2.89}$$

and in Region 2

$$H_c^{(2)}(x,z) = H_0\exp(-kz) + \sum_{n=1}^{\infty}\sin(q_nz)\exp(-p_nx)A_n^{(2)} \tag{2.90}$$

while for the eddy current density in Region 1

$$\begin{aligned}\mathbf{J}(x,z) &= -\frac{\partial H}{\partial z}\mathbf{x_0} + \frac{\partial H}{\partial x}\mathbf{z_0} \qquad (2.91)\\ &= \left[H_0k\exp(-kz) - \sum_{n=1}^{N_s}\cos[r_n(z-c)]r_n\cosh(s_nx)A_n^{(1)}\right]\mathbf{x_0}\\ &+ \left[\sum_{n=1}^{N_s}\sin[r_n(z-c)]s_n\sinh(s_nx)A_n^{(1)}\right]\mathbf{z_0}\end{aligned}$$

and in Region 2

$$\begin{aligned}\mathbf{J}(x,z) &= -\frac{\partial H}{\partial z}\mathbf{x_0} + \frac{\partial H}{\partial x}\mathbf{z_0} \qquad (2.92)\\ &= \left[H_0k\exp(-kz) - \sum_{n=1}^{N_s}\cos(q_nz)q_n\exp(-p_nx)A_n^{(2)}\right]\mathbf{x_0}\\ &- \left[\sum_{n=1}^{N_s}\sin(q_nz)p_n\exp(-p_nx)A_n^{(2)}\right]\mathbf{z_0}\end{aligned}$$

Finally, the expression for the impedance change is derived after integrating the magnetic field of the slot over the conductor cross-sectional area

$$\Delta Z = j\omega\mu n_t^2 2 \left[\int_{x=0}^{b} \int_{z=c}^{d} H_c^{(1)}(x,z)dxdz + \int_{x=b}^{\infty} \int_{z=0}^{d} H_c^{(2)}(x,z)dxdz \right] \quad (2.93)$$

which after performing the integrations gives

$$\Delta Z = \frac{k^2 2}{\sigma} \left(\frac{H_0}{I} \right)^2 \sum_{n=1}^{\infty} \left[A_n^{(1)} \frac{2\sinh(s_n b)}{r_n s_n} + A_n^{(2)} \frac{2\exp(-p_n b)}{q_n p_n} \right]$$
$$n = 1, 3, 5 \ldots \quad (2.94)$$

2.7 Discussion

In this chapter we have presented solutions to a number of canonical eddy current problems involving a uniform field excitation. It is true that such an excitation is not a realistic model of eddy current inspections but it nevertheless can provide some insight and qualitative conclusions into real eddy current-crack interactions and the impedance change produced by the crack. Solving these problems means that we can now visualize the eddy current flow but most importantly we can calculate the impedance change and see the effect of frequency and material characteristics as well as crack opening, depth, etc.

The important benefit gained from the study of these problems is the successful implementation of the TREE method and in this respect the uniform field+ideal crack problem has served well as a testbed for the application of new solution methods.

Chapter 3

Axisymmetric Problems

3.1 Introduction

In this chapter we present solutions to some axisymmetric eddy current problems. The excitation in these problems is provided by a cylindrical coil, i.e. a circular coil with rectangular cross-section, which is the most practical design in eddy current testing. The coil is located above a conductive half-space which can be layered or not. Again the main interest is in the calculation of the coil impedance change and the eddy currents induced in the layered conductor.

The most important contribution to this problem was made in the late sixties - early seventies by Dodd and Deeds who derived closed form integral expressions in the late sixties - early seventies for the impedance of the cylindrical coil above a layered conductive half-space as well as the impedance of a similar coil encircling a layered conductive rod. These models continue to be used extensively to this day. Among the published papers of Dodd, Deeds and co-workers, the Dodd (1968) paper is generally accepted as a cornerstone in eddy current NDE modelling. Its importance can be seen by the number of citations and by the fact that it has been widely used by the industry for designs of eddy current tests and optimization of parameter measurements such as thickness, conductivity and magnetic permeability, Dodd (1973, 1981, 1971a), and even defect detection Dodd (1971b).

During that time other researchers were also active in the study of such eddy current configurations, see for example Onoe (1968), and for a historic account of the Soviet school see Nikitin (1981). Dodd and Deeds were the first to apply a current sheet approximation, which represented the finite thickness coil with discrete windings as a continuous superposition of filamentary coils, for the coil above a conductor geometry. The derivation

of an analytical solution for this "real" coil could be validated for the first time against experimental measurements in contrast to results of other researchers that involved filamentary coils (or superposition in only one direction) where the results could not be verified. The typical agreement between theory and experiment is excellent provided of course that some general guidelines are followed, but this is the subject of a later discussion in this chapter. In the following we derive again the basic expressions of Dodd and Deeds models for the geometry depicted in Fig.3.2, following a slightly different approach. The principal motivation is to demonstrate the principle of superposition that enables us to study separately the effect of the source coil and the effect of the conductor. Thus, we use the fact that the electromagnetic field in the air-region of Fig.3.2 is the superposition of the field produced by the isolated coil and the field produced by the eddy currents induced in the conductor.

Before we examine the coil located above the planar conductor we derive expressions for the electromagnetic field with the conductor absent, i.e. for an "isolated coil" or a "coil in free-space" or an "air coil", all being valid names for a coil that is far from any other conductive object. Then, after the examination of the layered conductor we focus on the analysis of a conductive half-space. We then present the case of a layered conductor where the number of layers is infinite and the case of a conductor where the conductivity varies uniformly with depth. Finally, we discuss aspects of the numerical computing involved and refer to measurements and their agreement with theoretical results.

3.2 Isolated coil

Here we derive expressions for the isolated coil field in a different form than the one presented in the Appendix. This is done by starting with the field expression for a filamentary single-turn coil shown in Fig.3.1a and then applying the current sheet approximation principle for the finite thickness coil shown in Fig.3.1b. Due to the inherent axisymmetry of the problem geometry we use a cylindrical system where the field quantities are independent of the azimuthal coordinate φ. The circular filamentary coil is located at a height z_0, it has a radius r_0 and is described by a current density $I\delta(r - r_0)\delta(z - z_0)$ where I denotes the current magnitude. The finite thickness coil is a multi-turn coil wound with N turns and assumes the dimensions and position shown in Fig.3.1b. The coil current density has

only an azimuthal component J_φ and therefore the vector problem reduces to a scalar one.

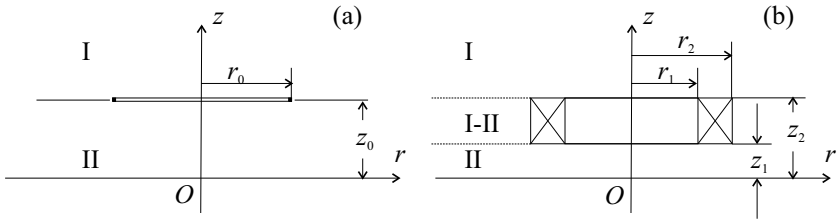

Fig. 3.1 2D axisymmetric view of (a) one-turn filamentary and (b) multi-turn cylindrical isolated coil.

3.2.1 *Filamentary coil*

The electromagnetic field of an isolated filamentary coil, which carries a constant current I, can be derived from the Biot-Savart law which states that the magnetic vector potential can be calculated from:

$$\mathbf{A} = \frac{\mu_0 I}{4\pi} \oint_l \frac{d\mathbf{l}}{|\mathbf{r} - \mathbf{r}_0|} \tag{3.1}$$

where $d\mathbf{l}$ is a vector differential line element tangential to the path of the source current, $\mathbf{r}_0$ and $\mathbf{r}$ are position vectors of the source and field point, respectively, and μ_0 is the free-space magnetic permeability. For a circular filament, the integration in (3.1) can be performed analytically and the result given in terms of elliptic integrals of the first and second kinds.

However, such a solution will not be very useful in the context of this chapter since we seek an expression with a form suitable for the application of the method of separation of variables. Such an expression can be derived by noting that the inverse of the distance vector

$$\frac{1}{R} = \frac{1}{|\mathbf{r} - \mathbf{r}_0|} = \left[(z - z_0)^2 + r^2 + r_0^2 - 2rr_0\cos(\phi - \phi_0)\right]^{-\frac{1}{2}} \tag{3.2}$$

can be written as follows, see Morse and Feshbach (1953)

$$\frac{1}{R} = \sum_{m=0}^{\infty} \varepsilon_m \cos[m(\phi - \phi_0)] \int_0^{\infty} J_m(\kappa r) J_m(\kappa r_0) e^{-\kappa|z - z_0|} d\kappa \tag{3.3}$$

where J_m denotes the Bessel function of first kind and order m, $\epsilon_m = 2-\delta_m$ and δ_m is the Kronecker symbol. In (3.2) and (3.3), (r_0, ϕ_0, z_0) are the coordinates of the source point and (r, ϕ, z) are those of the field point.

For the coil of Fig.3.1a, the line element in (3.1) is actually the azimuthal unit vector and performing the line integration which is a uniform integration due to axisymmetry, we derive the following results for the potential:

$$A^{(s)}(r,z) = \frac{\mu_0 I r_0}{2} \int_0^\infty J_1(\kappa r) J_1(\kappa r_0) e^{-\kappa|z-z_0|} d\kappa \tag{3.4}$$

This expression can be viewed as the first order inverse Hankel transform of the quantity $\mu_0 I J_1(\kappa r_0) e^{-\kappa|z-z_0|}/(2\kappa)$ since, in general, the forward and inverse Hankel transforms of order ν are defined by the pair of equations

$$F(\kappa) = \int_0^\infty f(r) J_\nu(\kappa r) r \, dr \tag{3.5}$$

and

$$f(r) = \int_0^\infty F(\kappa) J_\nu(\kappa r) \kappa \, d\kappa \tag{3.6}$$

In general, every expression for the potential or the magnetic field in similar axisymmetric configurations will be written as a Hankel transform of either zeroth or first order. This will also be true not only for the isolated coil but also for the case of a coil above a conductor.

For instructional purposes we will also show another method of deriving the result of (3.4) which is actually the approach used by Dodd and Deeds. In this method we deal with the geometry of Fig.3.1a as a boundary value problem and use the appropriate solutions for the differential equation with respect to the azimuthal component of the magnetic vector potential $\mathbf{A}$. This differential equation is the Poisson equation

$$\frac{\partial^2 A}{\partial r^2} + \frac{1}{r}\frac{\partial A}{\partial r} - \frac{A}{r^2} + \frac{\partial^2 A}{\partial z^2} = -\mu_0 I \delta(r-r_0)\delta(z-z_0) \tag{3.7}$$

The Poisson equation reduces to the Laplace equation in the two regions of the problem, above and below the filament since these regions do not include the plane $z = z_0$ and therefore the source term in (3.7) is eliminated. The

general solution to the Laplace equation has the following form:

$$A^{(s)}(r,z) = \int_0^\infty \left[A(\kappa)J_1(\kappa r) + B(\kappa)Y_1(\kappa r)\right]\left[C(\kappa)e^{\kappa z} + D(\kappa)e^{-\kappa z}\right] d\kappa \quad (3.8)$$

where Y_m denotes the Bessel function of the second kind and m order and A, B, C, D are unknown coefficients that are functions of the integration variable κ. This expression should describe the potential in both regions of the geometry, the one above the current filament which is denoted Region I and the other below the filament which is denoted Region II. Since both regions include the origin $r = 0$, we set $B(\kappa) = 0$ because the function $Y_1(x)$ has a pole there (tends to infinity). Moreover, in Region I we set $C(\kappa) = 0$ and in Region II $D(\kappa) = 0$ so that the potential remains finite. Thus, in the two regions the potential assumes the following expressions

$$A_{\mathrm{I}}^{(s)}(r,z) = \int_0^\infty J_1(\kappa r)D_{\mathrm{I}}(\kappa)e^{-\kappa z}d\kappa \quad (3.9)$$

$$A_{\mathrm{II}}^{(s)}(r,z) = \int_0^\infty J_1(\kappa r)C_{\mathrm{II}}(\kappa)e^{\kappa z}d\kappa \quad (3.10)$$

where the unknown coefficients have been merged into one in each expression. These coefficients are calculated by applying the interface conditions at the surface $z = z_0$, which are the continuity of B_z and discontinuity of H_r or equivalently

$$\left[\begin{array}{c} A_I^{(s)} = A_{II}^{(s)} \\ \frac{\partial A_I^{(s)}}{\partial z} = \frac{\partial A_{II}^{(s)}}{\partial z} - \mu_0 I\delta(r - r_0) \end{array}\right]_{z=z_0} \quad (3.11)$$

By simple inspection of the first interface condition, it is easily deduced that

$$D_{\mathrm{I}}e^{-\kappa z_0} = C_{\mathrm{II}}e^{\kappa z_0} \quad (3.12)$$

The strict mathematical derivation of (3.12), however, is performed by multiplying both sides of the first condition in (3.11) by $\int_0^\infty rJ_1(\kappa' r)dr$ and then

reversing the order of integration to get

$$\int_0^\infty \frac{D_{\mathrm{I}} e^{-\kappa z_0}}{\kappa} \left[\int_0^\infty J_1(\kappa r) J_1(\kappa' r) \kappa r \, dr \right] d\kappa$$
$$= \int_0^\infty \frac{C_{\mathrm{II}} e^{\kappa z_0}}{\kappa} \left[\int_0^\infty J_1(\kappa r) J_1(\kappa' r) \kappa r \, dr \right] d\kappa \tag{3.13}$$

Then, by using the Fourier-Bessel equation, see (3.5) and (3.6),

$$F(\kappa') = \int_0^\infty F(\kappa) \int_0^\infty J_1(\kappa r) J_1(\kappa' r) \kappa r \, dr \, d\kappa \tag{3.14}$$

we derive (3.12). The same approach can be applied to the second interface condition to get

$$\int_0^\infty D_{\mathrm{I}} e^{-\kappa z_0} \left[\int_0^\infty J_1(\kappa r) J_1(\kappa' r) \kappa r \, dr \right] d\kappa \tag{3.15}$$
$$= \int_0^\infty C_{\mathrm{II}} e^{\kappa z_0} \left[\int_0^\infty J_1(\kappa r) J_1(\kappa' r) \kappa r \, dr \right] d\kappa - \int_0^\infty \mu_0 I \delta(r - r_0) J_1(\kappa r) r \, dr$$

from which we derive the second equation between the unknown coefficients D_{I} and C_{II}

$$-D_{\mathrm{I}} e^{-\kappa z_0} = C_{\mathrm{II}} e^{\kappa z_0} - \mu_0 I r_0 J_1(\kappa r_0) \tag{3.16}$$

The solution to the system of equations (3.12) and (3.16) results in

$$D_{\mathrm{I}} = \frac{\mu_0 I}{2} r_0 J_1(\kappa r_0) e^{\kappa z_0} \tag{3.17}$$

$$C_{\mathrm{II}} = \frac{\mu_0 I}{2} r_0 J_1(\kappa r_0) e^{-\kappa z_0} \tag{3.18}$$

and hence we get again (3.4) by substituting (3.17) and (3.18) in (3.9) and (3.10) respectively.

Alternatively, in order to reach the same result, we could apply the first order Hankel transform to the differential equation (3.7) to get

$$\frac{\partial^2 \tilde{A}}{\partial z^2} = -\mu_0 I r_0 J_1(\kappa r_0) \delta(z - z_0) \tag{3.19}$$

where the tilde denotes a transformed quantity. Then, we could proceed with the solution of (3.19) in the same way as before. The transformed potential expressions in the two regions would be

$$\tilde{A}_{\mathrm{I}}^{(s)}(r,z) = D_{\mathrm{I}}(\kappa)e^{-\kappa z} \tag{3.20}$$

$$\tilde{A}_{\mathrm{II}}^{(s)}(r,z) = C_{\mathrm{II}}(\kappa)e^{\kappa z} \tag{3.21}$$

and the imposition of the interface conditions (3.11) this time for $\tilde{A}_{\mathrm{I}}^{(s)}$ and $\tilde{A}_{\mathrm{II}}^{(s)}$ would give again (3.12) and (3.16) and therefore the same results for D_{I} and C_{II}, (3.17) and (3.18) respectively. Then by taking the first order inverse Hankel transform of (3.20) and (3.21) we would get again (3.4).

This is just another way of saying the same thing and since it is only a matter of style, the interested reader can choose the way s/he prefers to work. This holds not only for the isolated coil but also for the coil above the layered conductor solution.

3.2.2 *Cylindrical coil solution*

We now approximate a multi-turn coil by the superposition of a number of filamentary coils.

$$A_{\mathrm{total}}^{(s)}(r,z) = \sum_{i=1}^{N} A_{\mathrm{filamentary}}^{(s)}(r,z,r_0,z_0) \tag{3.22}$$

In addition, if we let the current distribution in the filamentary coils approach a continuous current distribution, we can approximate a coil of finite cross-section S_C by the integral

$$A_{\mathrm{total}}^{(s)}(r,z) = \int\limits_{S_C} A^{(s)}(r,z,r_0,z_0)\, dS_C \tag{3.23}$$

where $A(r,z,r_0,z_0)$ is the potential produced by an applied current density $\iota_0(r_0,z_0)$. If the coil has a rectangular cross-section and if we assume that this current density $\iota_0(r_0,z_0)$ is constant over the dimensions of the coil, which means that the current in each loop has the same phase and amplitude, we have

$$A_{\mathrm{total}}^{(s)}(r,z) = \int\limits_{r_1}^{r_2}\int\limits_{z_1}^{z_2} A^{(s)}(r,z,r_0,z_0)\, dr_0\, dz_0 \tag{3.24}$$

After performing the two integrations we obtain the following expressions for the potentials in regions I and II, above and below the coil respectively

$$A_{\mathrm{I}}^{(s)} = \frac{\mu_0 \iota_0}{2} \int_0^\infty J_1(\kappa r) e^{-\kappa z} \frac{\chi(\kappa r_1, \kappa r_2)}{\kappa^3} (e^{\kappa z_2} - e^{\kappa z_1}) d\kappa \tag{3.25}$$

$$A_{\mathrm{II}}^{(s)} = \frac{\mu_0 \iota_0}{2} \int_0^\infty J_1(\kappa r) e^{\kappa z} \frac{\chi(\kappa r_1, \kappa r_2)}{\kappa^3} (e^{-\kappa z_1} - e^{-\kappa z_2}) d\kappa \tag{3.26}$$

where $\iota_0 = NI(r_2 - r_1)^{-1}(z_2 - z_1)^{-1}$ and the term $\chi(\kappa r_1, \kappa r_2)$ denotes a finite integral of the Bessel function that can be expressed as follows

$$\chi(x_1, x_2) = \int_{x_1}^{x_2} x J_1(x) dx = \frac{\pi}{2} x \left[J_0(x) \mathbf{H}_1(x) - J_1(x) \mathbf{H}_0(x) \right]_{x_1}^{x_2} \tag{3.27}$$

where $\mathbf{H}_n$ denotes the Struve function of order n. Later, when we comment on the computational aspects of the solution, we give some directions on computing $\chi(\kappa r_1, \kappa r_2)$ efficiently.

Going back to Fig.3.1, we have to give special treatment to region I-II, between the top and bottom of the coil, $z_1 \leq z \leq z_2$. For a point (r, z) in region I-II, we can use the equation $A_{\mathrm{I}}^{(s)}(r, z)$ for the portion of the coil from z down to z_1 and the equation $A_{\mathrm{II}}^{(s)}(r, z)$ for the portion of the coil from z up to z_2. If we substitute then $z_2 = z$ in (3.25) and $z_1 = z$ in (3.26) and add the two equations, we get

$$A_{\mathrm{I-II}}^{(s)} = \frac{\mu_0 \iota_0}{2} \int_0^\infty J_1(\kappa r) \frac{1}{\kappa^3} \chi(\kappa r_1, \kappa r_2) \left[2 - e^{\kappa(z - z_2)} - e^{-\kappa(z - z_1)} \right] d\kappa \tag{3.28}$$

Having calculated the magnetic vector potential we can easily calculate the magnetic flux density components for the isolated coil from

$$\mathbf{B} = -\frac{\partial A}{\partial z} \mathbf{r}_0 + \frac{1}{r} \frac{\partial (rA)}{\partial r} \mathbf{z}_0 \tag{3.29}$$

with the following results in the three regions of Fig.3.1b.

$$\mathbf{B}_{\mathrm{I}}^{(s)} = \frac{\mu_0 \iota_0}{2} \int_0^\infty \frac{\chi(\kappa r_1, \kappa r_2)}{\kappa^2} (e^{\kappa z_2} - e^{\kappa z_1}) e^{-\kappa z} \left[J_1(\kappa r) \mathbf{r}_0 + J_0(\kappa r) \mathbf{z}_0 \right] d\kappa \tag{3.30}$$

$$\mathbf{B}_{\mathrm{II}}^{(s)} = \frac{\mu_0 \iota_0}{2} \int_0^\infty \frac{\chi(\kappa r_1, \kappa r_2)}{\kappa^2} (e^{-\kappa z_1} - e^{-\kappa z_2}) e^{\kappa z} \left[-J_1(\kappa r)\mathbf{r}_0 + J_0(\kappa r)\mathbf{z}_0 \right] d\kappa \tag{3.31}$$

$$\mathbf{B}_{\mathrm{I-II}}^{(s)} = \frac{\mu_0 \iota_0}{2} \int_0^\infty \frac{\chi(\kappa r_1, \kappa r_2)}{\kappa^2} \left\{ \begin{array}{l} \left[e^{\kappa(z-z_2)} - e^{-\kappa(z-z_1)} \right] J_1(\kappa r)\mathbf{r}_0 \\ - \left[e^{\kappa(z-z_2)} + e^{-\kappa(z-z_1)} \right] J_0(\kappa r)\mathbf{z}_0 \end{array} \right\} d\kappa \tag{3.32}$$

and we can see that the $r-$and $z-$components are inverse Hankel transforms of first and zeroth order respectively. These expressions provide an alternative to the ones given in the Appendix for the isolated coil magnetic field. Their usefulness lies in the fact that their form is suitable for calculating the magnetic field of a coil above a half-space with the method of separation of variables. However, when it comes to computation speed, they are much slower especially if we emphasize accuracy and resort to automatic integration routines. Nevertheless, the calculations can still be accelerated, in principle, with the use of Fast Hankel Transform routines, Weider (1999).

Having calculated the potential in region I-II, we can now calculate the impedance of the coil, which is purely inductive since the dc resistance of the coil has been omitted. This is the resistance of the coil wire and since the diameter of the wire is very small, any change of the dc resistance with the frequency is assumed to be negligible. The isolated coil impedance is calculated by an integration over the coil volume, which reduces to an integration of $rA_{\mathrm{I-II}}^{(s)}$ over the rectangular cross-section, due to axisymmetry

$$Z_0 = jX_0 = j\omega L_0 = \frac{1}{I^2} \int_V \mathbf{A} \cdot \mathbf{J} dv = \frac{j2\pi\omega\iota_0}{I^2} \int_{r_1}^{r_2} \int_{z_1}^{z_2} r A_{\mathrm{I-II}}^{(s)}(r, z) dr dz \tag{3.33}$$

which gives the final result for the isolated coil impedance

$$Z_0 = \frac{j2\pi\omega\mu_0 N^2}{(r_2 - r_1)^2 (z_2 - z_1)^2} \int_0^\infty \frac{\chi^2(\kappa r_1, \kappa r_2)}{\kappa^6} \left[\kappa(z_2 - z_1) + e^{-\kappa(z_2 - z_1)} - 1 \right] d\kappa \tag{3.34}$$

As expected, Z_0 does not depend on the vertical position of the coil but rather on its width $z_2 - z_1$.

Depending on the relative width (or height) of the coil, we can identify two distinct designs. The first is the so-called "pancake" type coil when

$z_2 - z_1 \ll r_2 - r_1$ and the second the "solenoid" type coil when $z_2 - z_1 \gg r_2 - r_1$. The pancake type is primarily used as a surface coil for inspections of planar work-pieces while the solenoid type is often used as an encircling coil for outside dimension (OD) inspections of rods and tubes. In any case both of them are air-cored coils as long as no conductive or magnetic shield or core is used in conjunction with them. An examination of ferrite-cored coils and their modelling is presented in Chapter 4. Another issue is also the accuracy of the current sheet approximation and the high frequency effects. This will be discussed later in the present chapter.

3.3 Coil above a two-layer conductor

Let us now derive a solution for the electromagnetic field and the impedance of the coil when this is placed above a conductive half-space consisting of two layers, as shown in Fig.3.2. These are homogeneous layers of constant conductivity σ and relative magnetic permeability μ_r. The top layer is denoted as region 1 and the bottom layer, which extends to infinity in the z-coordinate, as region 2. The air region above the layers is region 0 and is divided to subregions I, I-II and II. The distance z_1 is called "lift-off" and it is a very important parameter in eddy current testing. It describes the degree of electromagnetic coupling of the coil with the conductor as well as the extent to which the coil impedance is affected by the induced eddy currents.

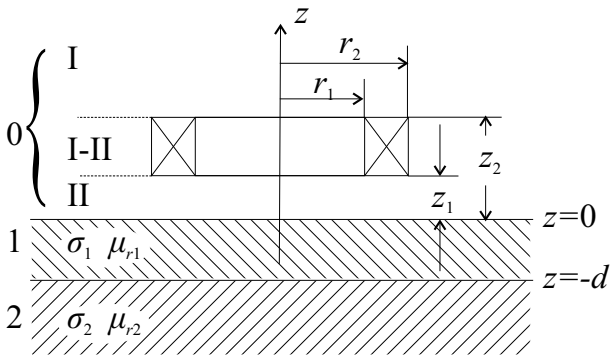

Fig. 3.2 2D axisymmetric view of a cylindrical coil above a conductive half-space consisting of two layers.

The layered conductor is a very important geometry and quite general

configuration since it can simulate a number of eddy current tests like the following:

- non-conductive coating measurement assuming $\sigma_1 = 0$
- conductive coating measurement assuming $\sigma_1 \neq 0$
- plate thickness measurement or loss of metal (corrosion) evaluation assuming $\sigma_2 = 0$
- material identification, aging and heat treatment and/or evaluation through conductivity evaluation

In all cases, the test involves the measurement of the coil impedance at one or more excitation frequencies and its association to a parameter change.

Due to the superposition principle, the total impedance of the coil is the sum of the isolated coil impedance Z_0 and the impedance change ΔZ due to the presence of the conductive layer system or equivalently the effect of eddy currents induced therein. Since we already have an expression for Z_0 we need only calculate ΔZ. The approach adopted is to consider the electromagnetic field in the air region as the sum of the field due to the coil and the field due to the eddy currents. Thus, the potential in air is $A_0 = A^{(s)} + A^{(ec)}$. The source potential $A^{(s)}$ stands for $A_{\rm I}^{(s)}$ or $A_{\rm II}^{(s)}$ or $A_{\rm I-II}^{(s)}$ as these were calculated in the previous section. The potential $A^{(ec)}$ corresponds to the one due to the eddy currents.

The potential in all regions satisfies the following Helmholtz type differential equation which stems from (1.53) for A_φ after ignoring terms that depend on the azimuthal variable φ

$$\frac{\partial^2 A}{\partial r^2} + \frac{1}{r}\frac{\partial A}{\partial r} - \frac{A}{r^2} + \frac{\partial^2 A}{\partial z^2} = k^2 A - \mu_0 I \delta(r - r_0)\delta(z - z_0) \tag{3.35}$$

where $k^2 = j\omega\mu_r\mu_0\sigma$. In the air regions where $k = 0$, (3.35) reduces to (3.7). The general solution of (3.35) has the following form:

$$A(r,z) = \int_0^\infty \left[A(\kappa)J_1(\kappa r) + B(\kappa)Y_1(\kappa r)\right]\left[C(\kappa)e^{\lambda z} + D(\kappa)e^{-\lambda z}\right] dk \tag{3.36}$$

where $\lambda = \sqrt{\kappa^2 + k^2}$. Following the discussion for the isolated coil in Sec.3.2.1, the potentials in the air subregion below the coil and in the two conductive layers assume the following expressions

$$A_0 = \int_0^\infty J_1(\kappa r)\left[C_s e^{\kappa z} + D_{ec} e^{-\kappa z}\right] d\kappa \tag{3.37}$$

$$A_1 = \int_0^\infty J_1(\kappa r)\left[C_1 e^{\lambda_1 z} + D_1 e^{-\lambda_1 z}\right] d\kappa \tag{3.38}$$

$$A_2 = \int_0^\infty J_1(\kappa r) C_2 e^{\lambda_2 z} d\kappa \tag{3.39}$$

In (3.37) the term $C_s e^{\kappa z}$ is due to the source coil, therefore C_s is a source coefficient which has a form that is easily deduced from (3.26). The term $D_{ec} e^{-\kappa z}$ is due to the eddy currents and the coefficient D_{ec} is unknown as well as coefficients C_1, D_1 and C_2. These unknown coefficients are calculated by imposing the interface conditions between the three regions 0, 1 and 2. The conditions are the continuity of the tangential components of the electric and magnetic field which can be replaced by the equivalent conditions of the continuity of the normal and tangential components of the magnetic field or just by the following conditions for the potential:

$$\left[\begin{array}{c} A_0 = A_1 \\ \frac{\partial A_0}{\partial z} = \frac{1}{\mu_{r1}} \frac{\partial A_1}{\partial z} \end{array}\right]_{z=0} \text{and} \quad \left[\begin{array}{c} A_1 = A_2 \\ \frac{1}{\mu_{r1}} \frac{\partial A_1}{\partial z} = \frac{1}{\mu_{r2}} \frac{\partial A_2}{\partial z} \end{array}\right]_{z=-d} \tag{3.40}$$

After using (3.37)-(3.39) in (3.40) we get four equations for the four unknown coefficients in the same manner as for the unknown coefficients in the analysis for the isolated coil field.

$$\begin{aligned} C_s + D_{ec} &= C_1 + D_1 \\ \kappa C_s - \kappa D_{ec} &= \lambda_1 C_1/\mu_{r1} - \lambda_1 D_1/\mu_{r1} \\ C_1 e^{-\lambda_1 d} + D_1 e^{\lambda_1 d} &= C_2 e^{-\lambda_2 d} \\ \lambda_1 C_1 e^{-\lambda_1 d}/\mu_{r1} - \lambda_1 D_1 e^{\lambda_1 d}/\mu_{r1} &= \lambda_2 C_2 e^{-\lambda_2 d}/\mu_{r2} \end{aligned} \tag{3.41}$$

The solution of the system gives the following expressions for the coeffi-

cients.

$$D_{ec} = C_s \frac{(\lambda_1\mu_{r2} + \lambda_2\mu_{r1})(\kappa\mu_{r1} - \lambda_1) + e^{-2\lambda_1 d}(\lambda_1\mu_{r2} - \lambda_2\mu_{r1})(\kappa\mu_{r1} + \lambda_1)}{(\lambda_1\mu_{r2} + \lambda_2\mu_{r1})(\kappa\mu_{r1} + \lambda_1) + e^{-2\lambda_1 d}(\lambda_1\mu_{r2} - \lambda_2\mu_{r1})(\kappa\mu_{r1} - \lambda_1)} \tag{3.42}$$

$$C_1 = C_s \frac{2\kappa\mu_{r1}(\lambda_1\mu_{r2} + \lambda_2\mu_{r1})}{(\lambda_1\mu_{r2} + \lambda_2\mu_{r1})(\kappa\mu_{r1} + \lambda_1) + e^{-2\lambda_1 d}(\lambda_1\mu_{r2} - \lambda_2\mu_{r1})(\kappa\mu_{r1} - \lambda_1)} \tag{3.43}$$

$$D_1 = C_s \frac{2\kappa\mu_{r1} e^{-2\lambda_1 d}(\lambda_1\mu_{r2} - \lambda_2\mu_{r1})}{(\lambda_1\mu_{r2} + \lambda_2\mu_{r1})(\kappa\mu_{r1} + \lambda_1) + e^{-2\lambda_1 d}(\lambda_1\mu_{r2} - \lambda_2\mu_{r1})(\kappa\mu_{r1} - \lambda_1)} \tag{3.44}$$

$$C_2 = C_s \frac{4\kappa\mu_{r1}\lambda_1\mu_{r2} e^{\lambda_2 d} e^{-\lambda_1 d}}{(\lambda_1\mu_{r2} + \lambda_2\mu_{r1})(\kappa\mu_{r1} + \lambda_1) + e^{-2\lambda_1 d}(\lambda_1\mu_{r2} - \lambda_2\mu_{r1})(\kappa\mu_{r1} - \lambda_1)} \tag{3.45}$$

Having derived the expressions for the unknown coefficients and using the result for the source coefficient C_s from (3.26) we obtain the final expressions for the potential in the various problem regions.

The eddy current density induced in the conductor layers is derived from

$$J_i = -j\omega\sigma_i A_i \qquad i = 1, 2 \tag{3.46}$$

when

$$J_1 = -\frac{j\omega\sigma_1\mu_0\iota_0}{2} \int_0^\infty J_1(\kappa r) \frac{\chi(\kappa r_1, \kappa r_2)}{\kappa^3} \left(e^{-\kappa z_1} - e^{-\kappa z_2}\right) \times \tag{3.47}$$

$$\times \frac{2\kappa\mu_{r1}\left[e^{\lambda_1 z}(\lambda_1\mu_{r2} + \lambda_2\mu_{r1}) + e^{-\lambda_1(z-2d)}(\lambda_1\mu_{r2} - \lambda_2\mu_{r1})\right]}{(\lambda_1\mu_{r2} + \lambda_2\mu_{r1})(\kappa\mu_{r1} + \lambda_1) + e^{-2\lambda_1 d}(\lambda_1\mu_{r2} - \lambda_2\mu_{r1})(\kappa\mu_{r1} - \lambda_1)} d\kappa$$

and

$$J_2 = -\frac{j\omega\sigma_2\mu_0\iota_0}{2} \int_0^\infty J_1(\kappa r) \frac{\chi(\kappa r_1, \kappa r_2)}{\kappa^3} \left(e^{-\kappa z_1} - e^{-\kappa z_2}\right) \times \tag{3.48}$$

$$\times \frac{4\kappa\mu_{r1}\lambda_1\mu_{r2} e^{\lambda_2(z+d)} e^{-\lambda_1 d}}{(\lambda_1\mu_{r2} + \lambda_2\mu_{r1})(\kappa\mu_{r1} + \lambda_1) + e^{-2\lambda_1 d}(\lambda_1\mu_{r2} - \lambda_2\mu_{r1})(\kappa\mu_{r1} - \lambda_1)} d\kappa$$

The magnetic flux density can be calculated using (3.29) and the expressions for the magnetic vector potential in the various problem regions; we leave that to the interested reader.

Finally, the impedance change due to the conductor can be calculated in a similar manner as in the case of the isolated coil impedance: we use (3.33) and this involves now the integration of $A^{(ec)}$ over the coil cross-section. This is a direct consequence of the superposition principle that we have used to represent the potential in the air region A_0 as the sum of the isolated coil potential $A^{(s)}$ and the potential due to the conductor $A^{(ec)}$. Integrating the sum over the cross-section gives the total coil impedance $Z_0 + \Delta Z$, integrating the potential $A^{(s)}$ gives the isolated coil impedance Z_0 and, finally, integrating $A^{(ec)}$ gives the impedance change ΔZ. Since we have already calculated Z_0 in (3.33), we proceed with the calculation of ΔZ

$$\begin{aligned}\Delta Z = \Delta R + j\Delta X &= \frac{j2\pi\omega\iota_0}{I^2}\int_{r_1}^{r_2}\int_{z_1}^{z_2} rA^{(ec)}(r,z)drdz \\ &= \frac{j2\pi\omega\iota_0}{I^2}\int_0^{\infty} D_{ec}\int_{r_1}^{r_2}\int_{z_1}^{z_2} J_1(\kappa r)e^{-\kappa z}rdrdz \quad (3.49)\end{aligned}$$

which gives the final result for the impedance change

$$\begin{aligned}\Delta Z = \frac{j2\pi\omega\mu_0 N^2}{(r_2-r_1)^2(z_2-z_1)^2}\int_0^{\infty}\frac{\chi^2(\kappa r_1,\kappa r_2)}{\kappa^6}\left(e^{-\kappa z_1}-e^{-\kappa z_2}\right)^2\times \quad (3.50)\\ \times\frac{(\lambda_1\mu_{r2}+\lambda_2\mu_{r1})(\kappa\mu_{r1}-\lambda_1)+e^{-2\lambda_1 d}(\lambda_1\mu_{r2}-\lambda_2\mu_{r1})(\kappa\mu_{r1}+\lambda_1)}{(\lambda_1\mu_{r2}+\lambda_2\mu_{r1})(\kappa\mu_{r1}+\lambda_1)+e^{-2\lambda_1 d}(\lambda_1\mu_{r2}-\lambda_2\mu_{r1})(\kappa\mu_{r1}-\lambda_1)}d\kappa\end{aligned}$$

Note that in the original expression in Dodd (1968) the exponential term appears as $e^{2\lambda_1 d}$ on the left terms of both nominator and denominator. Obviously this is equivalent but (3.50) avoids possible overflow problems when it comes to numerical evaluation of the integral.

3.4 Conductive halfspace

The case when the conductor is not layered but is a homogeneous half-space region of constant conductivity σ and relative magnetic permeability μ_r, as shown in Fig.3.3, can be derived from the layered conductor in a number of

ways such as setting either the conductivity of the top layer or its thickness to zero or the latter to tend to infinity or setting the conductivity and permeability of the two layers equal ($\lambda_1 = \lambda_2 = \lambda$). The expressions for the induced eddy current density and the impedance change can now be written as:

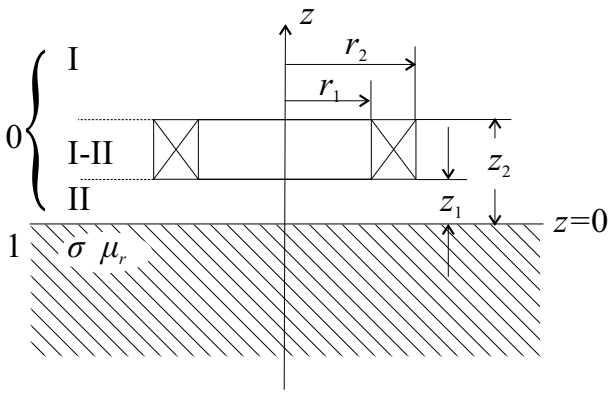

Fig. 3.3 2D axisymmetric view of a cylindrical coil above a conductive half-space

$$J = -\frac{j\omega\sigma\mu_0\iota_0}{2}\int_0^\infty J_1(\kappa r)\frac{\chi(\kappa r_1,\kappa r_2)}{\kappa^3}\left(e^{-\kappa z_1}-e^{-\kappa z_2}\right)\frac{2\kappa\mu_r e^{\lambda z}}{\kappa\mu_r+\lambda}d\kappa \quad (3.51)$$

and

$$\Delta Z = \frac{j2\pi\omega\mu_0 N^2}{(r_2-r_1)^2(z_2-z_1)^2}\int_0^\infty \frac{\chi^2(\kappa r_1,\kappa r_2)}{\kappa^6}\left(e^{-\kappa z_1}-e^{-\kappa z_2}\right)^2\frac{\kappa\mu_r-\lambda}{\kappa\mu_r+\lambda}d\kappa \quad (3.52)$$

while the magnetic flux density can be written as

$$\mathbf{B}_0 = \mathbf{B}^{(s)} + \frac{\mu_0\iota_0}{2}\int_0^\infty \frac{\chi(\kappa r_1,\kappa r_2)}{\kappa^2}(e^{-\kappa z_1}-e^{-\kappa z_2})e^{-\kappa z}\frac{\kappa\mu_r-\lambda}{\kappa\mu_r+\lambda} \left[J_1(\kappa r)\mathbf{r}_0 + J_0(\kappa r)\mathbf{z}_0\right] d\kappa \quad (3.53)$$

$$\mathbf{B}_1 = \mu_0 \iota_0 \int_0^\infty \frac{\chi(\kappa r_1, \kappa r_2)}{\kappa^2} (e^{-\kappa z_1} - e^{-\kappa z_2}) e^{\lambda z} \frac{\mu_r}{\kappa \mu_r + \lambda} \\ [-J_1(\kappa r)\lambda \mathbf{r}_0 + J_0(\kappa r)\kappa \mathbf{z}_0]\, d\kappa \tag{3.54}$$

In (3.53) $\mathbf{B}^{(s)}$ is given by (3.30)-(3.32) depending on the specific height z of the field point. The above equations enable us to draw useful conclusions from this simple configuration about eddy currents in general. For example, using (3.51) we can study the penetration depth of the induced eddy currents and hence the effective depth where eddy current testing can be used for inspections and measurements. Fig.3.4 shows eddy current contours produced at three distinct frequencies, where it is obvious that the penetration depth decreases for an increasing frequency. At the same time, the surface eddy current density is greater. This means that the higher the frequency, the larger the signal from a surface discontinuity since a larger eddy current density is obstructed. In this particular example the cylindrical probe coil has inner radius $r_1 = 2$mm, outer radius $r_2 = 4$mm, width $z_2 - z_1 = 1$mm, it is wound with 800 wire-turns and is located, at a $z_1 = 1$mm lift-off, above a conductive half-space having conductivity $\sigma = 35.4$MSiemens/m and relative magnetic permeability μ_r =1 (nonmagnetic metal).

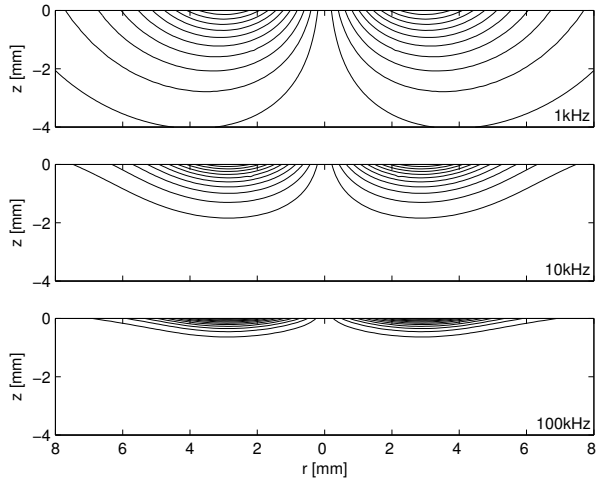

Fig. 3.4 Contours of eddy current density induced by a surface coil at various frequencies. From top to bottom, the skin depth is 2.67, 0.85 and 0.27mm

Mottl (1990) and Hoshikawa (1998) have shown that the true depth of penetration, where the actual eddy current density decreases to e^{-1} of the surface value, is considerably smaller than the standard depth of penetration δ. Also, the effective depth of penetration at which the actual current density decreases to e^{-3} of the surface value, is much smaller than the triple standard depth. The effective depth of penetration is not equal to the triple true depth of penetration 3δ, which means that the decrease of the current density is not given by the simple exponential function as in the uniform field (plane wave) case. Similar differences occur for the phase delay, where the true phase delay is smaller than the one predicted for the plane wave case. These differences will result in a lower than expected sensitivity to subsurface defect detection. It can be shown that the coil diameter D is an important parameter that largely controls penetration, see the discussion in Cecco (1985). The magnetic field in a thick material under a surface probe penetrates to a depth of about one-quarter the coil diameter $D/4$. One can decrease penetration to less than $D/4$ by raising the test frequency, but lowering the frequency will not increase penetration significantly. The only solution seems to be to increase probe diameter, but in this case sensitivity to short defects decreases as diameter is increased, because the ratio of the defect-to-inspected volume becomes smaller. Eventually we reach a point where a further increase in coil diameter would result in significant surface and subsurface defects going undetected.

Eqs (3.50) and (3.52) are also very useful in order to visualize the effect of the various parameters in eddy current testing of layered planar media. Fig.3.5 is an example of a computer generated impedance display for the surface coil which was described previously. The impedance is depicted normalized, using the inductive reactance of the isolated coil X_0 as the normalizing factor.

The solid arc-like curves represent loci produced by varying the excitation frequency. It can be seen that for nonmagnetic conductors the lower the frequency the smaller the impedance change produced by the eddy currents and hence by the conductor. In addition, the magnitude of the change depends on a logarithmic change of frequency. At higher frequencies, the impedance change tends to a constant value and in the limit $f \longrightarrow \infty$ the curve meets the vertical axis and the impedance of the coil becomes purely imaginary. For nonmagnetic conductors the resistance change is always a positive number, the total inductive reactance decreases and in general the resistance change is smaller than the reactance change. The almost straight dashed lines represent loci produced by varying the coil lift-off. The greater

the lift-off the smaller the impedance change which is seen by the smaller arc-like curves. The largest impedance change is produced for zero lift-off. The magnitude of the impedance change depends on a logarithmic variation of lift-off. The fact that the lift-off curves are almost straight lines means that the signal produced during an eddy current inspection has an almost constant phase. In fact, the lift-off curves are only straight for a limited range of liftoff, i.e. for the initial variation. The constant phase signal is true not only for a vertical movement of the coil but also for any other movement. As we will see in Chapter 5 any variation in coil orientation or position above a planar conductor produces a constant phase lift-off signal.

In this particular example the conductive half-space is made of aluminum and the solid curves represent the locus produced by varying the excitation frequency. Because conductivity and frequency always appear as a product (σf) in the normalized impedance expression, the same curve would have been produced for a constant excitation frequency and a varying conductivity. Thus, the arc-like curves represent also conductivity curves for constant frequency.

The dotted curves represent the impedance variation with varying permeability of the conductor for constant frequency and conductivity. Magnetic materials generally increase the coil reactance and thus the normalized reactance. Also, for a specific magnetic permeability for medium frequencies, normalized reactance is greater than 1 and for higher frequencies it is lower than 1. Equivalently, for medium frequencies the normalized reactance change is greater than 0 and for higher frequencies it is lower than 0.

The main purpose of such impedance displays is to demonstrate the optimum frequency for a specific test. This frequency is usually the one that produces the best phase discrimination between the loci of two parameters. We have mentioned in Chapter 1 that ECT is a multi-parametric method and often we need to separate the effects from two parameters that are both varying at the same time. Consider for example the case of lift-off and conductivity change. It can be seen from Fig.3.5 that it is better, for example, to measure in general at 10kHz than at 1kHz because the former provides a better phase discrimination between the signals of lift-off variation, conductivity variation and permeability variation. On the other hand, the 100Hz frequency is better for permeability measurements whereas 10kHz and, even worse, 100kHz would not be a good choice for discrimination between a conductivity and a permeability variation.

Another example of ECT simulation is shown in Fig.3.6 where we depict

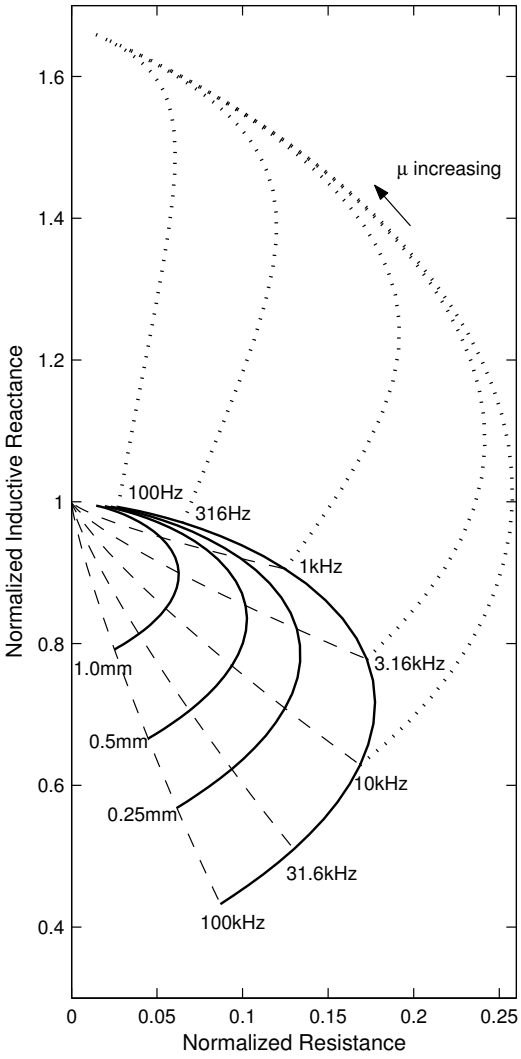

Fig. 3.5 Normalized impedance plane diagram for a coil above a conductive half-space.

the variation of the coil impedance in a two-layer conductor consisting of a brass layer with $\sigma = 14.3$MS/m (24.7%IACS) and an aluminum layer with $\sigma = 35.4$MS/m (61.0%IACS). The arc-like curves are thickness curves and represent the variation of top layer thickness. The variation is not linear and the ends of these curves lie on the points of either a brass or an aluminum

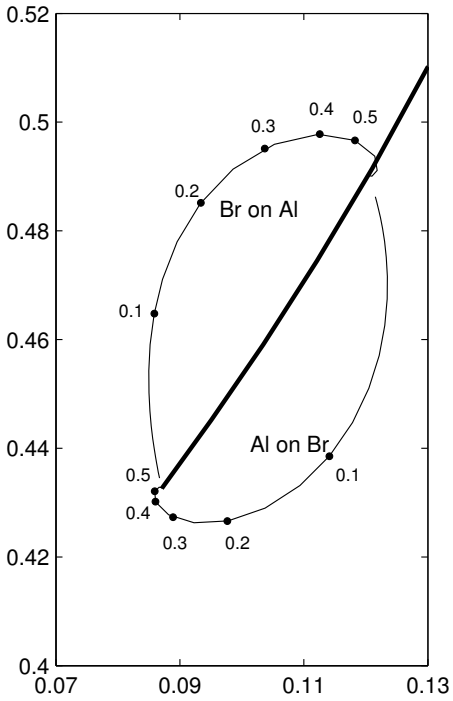

Fig. 3.6 Normalized impedance plane diagram for a coil above a two layer conductor. Numbers on the thickness curves show top-layer thickness in mm.

conductive half-space. The thicker curve represents the conductivity curve and the frequency is 100kHz. The aluminum half-space impedance point lies in a lower position in the diagram than the brass point due to its greater conductivity.

In this book we do not focus any further on the analysis of such impedance planes, but rather we provide analytical expressions and guidance to generate them easily. A number of references examine phase plane diagrams for a number of testcases including the cases of two-, three- and four-layer conductor. Using the results in this chapter, the interested reader has now the tools for repeating and generating all the fancy diagrams that appear in eddy-current textbooks, see for example Libby (1979), Hagemaier (1982), Cecco (1987), Blitz (1991), ASNT (1986, 2004).

3.5 Arbitrary number of layers

In this section we develop an expression for the impedance change of the coil when the planar conductive medium consists of an arbitrary number of layers. The geometry is shown in Fig.3.7.

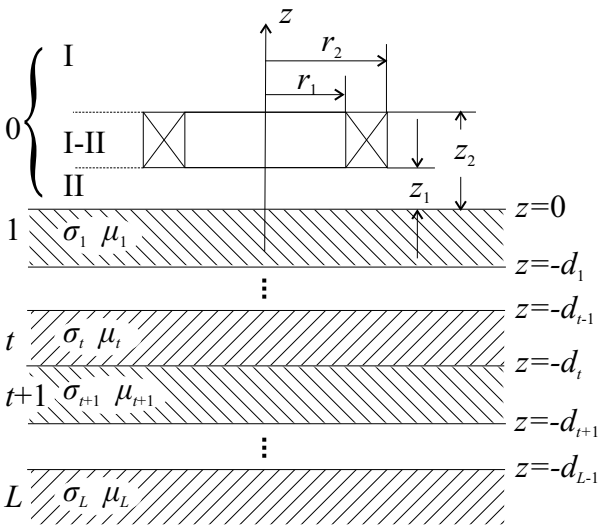

Fig. 3.7 2D axisymmetric view of a cylindrical coil above a half-space consisting of L layers.

The number of layers is L with the numbering starting from the top and with layer t having a conductivity σ_t and relative magnetic permeability μ_t. The interface between layers t and $t+1$ is located at depth $z = -d_t$. Again in the air region the potential is written as

$$A_0 = \int_0^\infty J_1(\kappa r) \left[C_s e^{\kappa z} + D_{ec} e^{-\kappa z} \right] d\kappa \tag{3.55}$$

and in each layer t the potential is

$$A_t = \int_0^\infty J_1(\kappa r) \left[C_t e^{\lambda_t z} + D_t e^{-\lambda_t z} \right] d\kappa \tag{3.56}$$

where $\lambda_t = (\kappa^2 + j\omega\mu_0\mu_t\sigma)^{1/2}$ and $D_t = 0$ in the bottom layer because this

extends to infinity.

3.5.1 *Cheng's matrix approach*

In this section, we outline a method presented by Cheng (1971), which involves three steps for the calculation of the unknown coefficients D_{ec} and C_t, D_t for $t = 1, 2, \ldots, L$:

(1) Apply the interface conditions between the layers in a progressive way from the bottom layer to the top. As already mentioned, in the bottom layer the coefficient D_L is zero in order for the potential to remain finite for $z \to \infty$. Therefore, all coefficients C_t and D_t are expressed in terms of the coefficient C_L of the bottom layer.
(2) Apply the interface conditions between the top layer and the air region. Since C_1 and D_1 are already expressed in terms of C_L from step (1), we can solve for D_{ec} and C_L.
(3) Use the previously calculated expressions in step (1) backwards to solve for the coefficients C_t and D_t.

Conditions at the interface $z = -d_t$ are

$$\left[\begin{array}{c} A_{t+1} = A_t \\ \frac{1}{\mu_{t+1}} \frac{\partial A_{t+1}}{\partial z} = \frac{1}{\mu_t} \frac{\partial A_t}{\partial z} \end{array} \right]_{z=-d_t} \tag{3.57}$$

Substitution of (3.56) in (3.57) leads to the following equation in matrix form

$$\begin{aligned} \begin{bmatrix} C_t \\ D_t \end{bmatrix} &= \begin{bmatrix} T_{11}(t,t+1)\ T_{12}(t,t+1) \\ T_{21}(t,t+1)\ T_{22}(t,t+1) \end{bmatrix} \cdot \begin{bmatrix} C_{t+1} \\ D_{t+1} \end{bmatrix} \\ &= \frac{1}{2} \begin{bmatrix} e^{(-\lambda_{t+1}+\lambda_t)d_t} \left(1 + \frac{\mu_t}{\mu_{t+1}} \frac{\lambda_{t+1}}{\lambda_t}\right) & e^{(\lambda_{t+1}+\lambda_t)d_t} \left(1 - \frac{\mu_t}{\mu_{t+1}} \frac{\lambda_{t+1}}{\lambda_t}\right) \\ e^{(-\lambda_{t+1}-\lambda_t)d_t} \left(1 - \frac{\mu_t}{\mu_{t+1}} \frac{\lambda_{t+1}}{\lambda_t}\right) & e^{(\lambda_{t+1}-\lambda_t)d_t} \left(1 + \frac{\mu_t}{\mu_{t+1}} \frac{\lambda_{t+1}}{\lambda_t}\right) \end{bmatrix} \\ &\quad \cdot \begin{bmatrix} C_{t+1} \\ D_{t+1} \end{bmatrix} \end{aligned} \tag{3.58}$$

where the elements of matrix $\mathbf{T}(t, t+1)$ depend on material characteristics of the layers and the depth of the interface. We calculate the coefficients of each layer in the following manner:

Starting from the bottom L layer and going to layer $L-1$ we derive

$$\begin{bmatrix} C_{L-1} \\ D_{L-1} \end{bmatrix} = \mathbf{T}(L-1, L) \cdot \begin{bmatrix} C_L \\ 0 \end{bmatrix} \tag{3.59}$$

The coefficients in the layer $L-2$ are obtained by

$$\begin{bmatrix} C_{L-2} \\ D_{L-2} \end{bmatrix} = \mathbf{T}(L-2, L-1) \cdot \begin{bmatrix} C_{L-1} \\ D_{L-1} \end{bmatrix}$$
$$= \mathbf{T}(L-2, L-1) \cdot \mathbf{T}(L-1, L) \cdot \begin{bmatrix} C_L \\ 0 \end{bmatrix} \tag{3.60}$$

Eventually, the coefficients for the top layer are obtained by

$$\begin{bmatrix} C_1 \\ D_1 \end{bmatrix} = \mathbf{V}(1) \cdot \begin{bmatrix} C_L \\ 0 \end{bmatrix} \tag{3.61}$$
$$= \mathbf{T}(1,2) \cdot \mathbf{T}(2,3) \cdots \mathbf{T}(L-2, L-1) \cdot \mathbf{T}(L-1, L) \cdot \begin{bmatrix} C_L \\ 0 \end{bmatrix}$$

where the matrix $\mathbf{V}$ is introduced to shorten expressions. Now we apply the usual boundary conditions across the interface $z = 0$

$$\left[\begin{array}{c} A_0 = A_1 \\ \frac{\partial A_0}{\partial z} = \frac{1}{\mu_{r1}} \frac{\partial A_1}{\partial z} \end{array} \right]_{z=0} \tag{3.62}$$

The solution of the 2×2 system that is formed from (3.62) provides the expressions for C_L and D_{ec} since C_1 and D_1 are already functions of C_L.

$$C_L = \frac{2\kappa\mu_{t+1}}{(\kappa\mu_{t+1} + \lambda_1)V_{11}(1) + (\kappa\mu_{t+1} - \lambda_1)V_{21}(1)} \, C_s \tag{3.63}$$

$$D_{ec} = \frac{(\kappa\mu_{t+1} - \lambda_1)V_{11}(1) + (\kappa\mu_{t+1} + \lambda_1)V_{21}(1)}{(\kappa\mu_{t+1} + \lambda_1)V_{11}(1) + (\kappa\mu_{t+1} - \lambda_1)V_{21}(1)} \, C_s \Rightarrow$$
$$D_{ec} = R(\kappa) \, C_s \tag{3.64}$$

If we want to proceed further with the expressions for the potential in the remaining layers, we can calculate the coefficients C_t and D_t of each layer from

$$\begin{bmatrix} C_t \\ D_t \end{bmatrix} = \mathbf{V}(t) \cdot \begin{bmatrix} C_L \\ 0 \end{bmatrix}$$
$$= \mathbf{T}(t, t+1) \cdots \mathbf{T}(L-1, L) \cdot \begin{bmatrix} C_L \\ 0 \end{bmatrix} \tag{3.65}$$

The potential in shell t takes the form

$$A_t = \int_0^\infty J_1(\kappa r) \left[V_{11}(t) C_L e^{\lambda_1 z} + V_{21}(t) C_L e^{-\lambda_1 z} \right] d\kappa \tag{3.66}$$

As in the previous paragraph, having computed the potential in all regions of the problem means that we can also calculate magnetic fields, eddy current densities and the impedance of the coil. The latter assumes the expression

$$\Delta Z = \frac{j\pi\omega\mu_0 N^2}{(r_2-r_1)^2(z_2-z_1)^2}\int_0^\infty \frac{\chi^2(\kappa r_1,\kappa r_2)}{\kappa^6}\left(e^{-\kappa z_1}-e^{-\kappa z_2}\right)^2 R(\kappa)d\kappa \tag{3.67}$$

where $R(\kappa)$ is deduced from (3.64).

3.5.2 *Alternative recursive approach*

Another method for computing the impedance change, which is essentially the same with the previous one but somewhat simpler was presented by Luquire (1970). The expression for ΔZ is written as

$$\Delta Z = \frac{j\pi\omega\mu_0 N^2}{(r_2-r_1)^2(z_2-z_1)^2}\int_0^\infty \frac{\chi^2(\kappa r_1,\kappa r_2)}{\kappa^6}\left(e^{-\kappa z_1}-e^{-\kappa z_2}\right)^2 \frac{V_1}{U_1}\,d\kappa \tag{3.68}$$

and the terms U_i, V_i are calculated from the recursive formulas

$$U_i = \left(\frac{\lambda_{i-1}}{\mu_{i-1}}-\frac{\lambda_i}{\mu_i}\right)e^{-2\lambda_i d_i}V_{i+1}+\left(\frac{\lambda_{i-1}}{\mu_{i-1}}+\frac{\lambda_i}{\mu_i}\right)U_{i+1} \tag{3.69}$$

$$V_i = \left(\frac{\lambda_{i-1}}{\mu_{i-1}}+\frac{\lambda_i}{\mu_i}\right)e^{-2\lambda_i d_i}V_{i+1}+\left(\frac{\lambda_{i-1}}{\mu_{i-1}}-\frac{\lambda_i}{\mu_i}\right)U_{i+1} \tag{3.70}$$

where i iterates from $L-1$ down to 1 and $\lambda_i = \sqrt{\kappa^2+j\omega\mu_0\mu_i\sigma_i}$. Initial values for the terms are

$$U_L = \frac{\lambda_{L-1}}{\mu_{L-1}}+\frac{\lambda_L}{\mu_L} \tag{3.71}$$

$$V_L = \frac{\lambda_{L-1}}{\mu_{L-1}}-\frac{\lambda_L}{\mu_L} \tag{3.72}$$

with the exception $(\lambda_{i-1}/\mu_{i-1})_{i=1} = \kappa$. Although a strict proof of the above formula was not provided, it does give the correct results for all special cases for which the exact expression is known, i.e. for up to four layers. The two approaches for dealing with the arbitrary number of layers are equivalent but the second one is more efficient when it comes to numerical

computation. This is due to the fact that in the first approach exponential functions with a positive argument are present and therefore round-off as well as overflow errors may occur. Note that Cheng's matrix approach requires extensive use of 2×2 matrices, although this should not be prohibitive in its implementation, especially with matrix based packages such as Matlab.

3.6 Inhomogeneous conductor

An interesting case that has received attention by researchers is the case where either a layer conductivity or permeability is a continuous function of z, i.e. the medium exhibits a 1D inhomogeneity. Continuous conductivity profiles appear in applications like the thermal processing of aerospace engineering materials in order to obtain added strength. There are two methods to compute the impedance change of a probe coil for such a case.

In the first one, the medium is subdivided in a number of parallel homogeneous layers for the approximation of a continuously varying conductivity profile. By taking a sufficiently large number of such layers of vanishing thickness and by implementing the algorithm given in the previous section, any desired degree of precision may be obtained in the computation of the electromagnetic fields and therefore the impedance of the coil. This method, although not very elegant, is very general as it can describe the effects of conductivity and permeability varying independently or together. The method is quite accurate and Uzal (1993) reports that a 1% agreement with the exact solution was achieved with 50 layers for a typical $\sigma(z)$ profile.

The alternative approach is to consider special forms of conductivity variations and try to express the solutions of the differential equations in terms of known mathematical functions. This approach for example was used again by Uzal (1993) to determine the impedance of a cylindrical coil above a nonmagnetic half-space with an arbitrary near-surface conductivity profile. The problem was formulated in terms of the solution of an ordinary differential equation involving the conductivity profile function and an exact solution was presented for the case of a near-surface profile that varies as a hyperbolic tangent with depth. Later, Theodoulidis (1995) provided expressions for a coating with a conductivity that varied as a linear, quadratic or exponential function.

For an inhomogeneous conductor the solution proceeds along the same

path as in previous paragraphs, the only difference is in the function(s) that describe the $z-$dependence of the potential when the method of separation of variables is applied. For a nonmagnetic conductor, the differential equation is

$$\frac{\partial^2 A}{\partial r^2} + \frac{1}{r}\frac{\partial A}{\partial r} + \frac{\partial^2 A}{\partial z^2} - \frac{A}{r^2} = j\omega\mu_0\sigma(z)A \tag{3.73}$$

where now the conductivity is a function of the depth $\sigma(z)$. Applying separation of variables the $R(r)$ dependence of the solution satisfies

$$\frac{d^2 R(r)}{dr^2} + \frac{1}{r}\frac{dA}{dr} + \left(\kappa^2 - \frac{1}{r^2}\right) R(r) = 0 \tag{3.74}$$

where

$$R(r) = AJ_1(\kappa r) + BY_1(\kappa r) \tag{3.75}$$

as previously and the $Z(z)$ dependence satisfies

$$\frac{d^2 Z(z)}{dz^2} = \left[\kappa^2 + j\omega\mu_0\sigma(z)\right] Z(z) \tag{3.76}$$

with the general solution

$$Z(z) = C(\kappa)F_1(f(z)) + D(\kappa)F_2(f(z)) \tag{3.77}$$

We now study the cases when there is only one layer, i.e. a conductive half-space or a two-layer conductor with only the top layer having a varying conductivity. We limit our presentation to nonmagnetic media. Needless to say, that the method can be extended to the solution of the problem when there are more layers with a varying conductivity and a different form of variation. It is also possible to solve for a varying permeability. For the later, however, the differential equation to be solved is different from (3.73), the difference lies in the $Z(z)$ dependence which now has an additional term

$$\frac{d^2 Z(z)}{dz^2} - \frac{1}{\mu(z)}\frac{d\mu}{dz}\frac{\partial Z}{\partial z} = \left[\kappa^2 + j\omega\mu_0\sigma(z)\right] Z(z) \tag{3.78}$$

Although the number of solutions that can be found in this case is even more limited, notably Kolyshkin (1991, 1997) derived solutions that involved combinations of conductivity and permeability variations of the form z^b and z^a respectively with $a+b=-2$ or $a+b=0$. However, these forms are

too restrictive and it is questionable whether they can actually represent a real situation.

3.6.1 *Inhomogeneous half-space*

When there is only one inhomogeneous layer, one of the functions in (3.77) has a pole at infinity and should therefore be excluded from the solution. If we assume that the solution which vanishes for $z \to \infty$ is F_2, then the $Z(z)$ dependence takes the form

$$Z(z) = C(\kappa)F_1(f(z)) \tag{3.79}$$

and the potential in the half-space is written as

$$A_1 = \int_0^\infty J_1(\kappa r)C_1F_1(f(z))d\kappa \tag{3.80}$$

In the region between the coil and the inhomogeneous conductor the expression is

$$A_0 = \int_0^\infty J_1(\kappa r)\left[C_s e^{\kappa z} + D_{ec}e^{-\kappa z}\right]d\kappa \tag{3.81}$$

Imposition now of the interface conditions (3.11) at $z = 0$ and solution of the resulting system for the unknown coefficients gives

$$D_{ec} = \frac{\kappa F_1 - F_1'}{\kappa F_1 + F_1'}C_s = R_{ec}(\kappa)C_s \tag{3.82}$$

and

$$C_1 = \frac{2\kappa}{\kappa F_1 + F_1'}C_s = R_1(\kappa)C_s \tag{3.83}$$

where

$$F_1 = \left[F_1(f(z))\right]_{z=0} \tag{3.84}$$

$$F_1' = \left[F_1(f(z))\right]'_{z=0} \tag{3.85}$$

and the dash denotes differentiation with respect to z. Again from (3.49), the impedance change can be written as

$$\Delta Z = \frac{j\omega\pi\mu_0 N^2}{(r_2 - r_1)^2 (z_2 - z_1)^2} \int_0^\infty \frac{\chi^2(\kappa r_1, \kappa r_2)}{\kappa^6} \left(e^{-\kappa z_1} - e^{-\kappa z_2}\right)^2 R_{ec}(\kappa)\, d\kappa \tag{3.86}$$

and the eddy current density as

$$J = -j\omega\sigma(z) \int_0^\infty J_1(\kappa r) R_1(\kappa) C_s F_1(z) d\kappa \tag{3.87}$$

The case examined by Uzal (1993) involves a conductivity profile of the form

$$\sigma(z) = \sigma_2 + \frac{\sigma_1 - \sigma_2}{2} \left(1 + \tanh \frac{z + c}{a}\right) \tag{3.88}$$

where σ_1, σ_2, a and c are constants. Assigning λ_i to $(\kappa^2 + j\omega\mu_0\sigma_i)^{1/2}$ the solution for the $Z(z)$ dependence that vanishes for $z \to \infty$ is

$$F_1(z) = y^\mu (1 - y)^\nu F(\mu + \nu, \mu + \nu + 1, 2\mu + 1; y) \tag{3.89}$$

where

$$\begin{aligned} y &= \left[1 + e^{-(z+c)/a}\right]^{-1} \\ \mu &= a\lambda_2 \\ \nu &= a\lambda_1 \end{aligned} \tag{3.90}$$

and F denotes the hypergeometric function. The tanh profile is particularly useful since it allows one to roughly model many profiles in which the conductivity varies monotonically. Later, Uzal (1994) used this profile to fit experimental impedance measurements made on nonmagnetic layered metal plates. Although the description of actual conductivity profiles is restricted to three parameters using the tanh profile, it was preferred to a numerical solution since it offered a convenient way to regularize the otherwise ill-posed inverse problem.

3.6.2 *Inhomogeneous coating*

When the conductor consists of two layers, of which the top one has a varying conductivity and the bottom one has a constant conductivity, the

expressions for the magnetic vector potential in these two layers are

$$A_1 = \int_0^\infty J_1(\kappa r)\left[C_1 F_1(f(z)) + D_1 F_2(f(z))\right] d\kappa \tag{3.91}$$

$$A_2 = \int_0^\infty J_1(\kappa r) C_2 e^{\lambda_2 z} d\kappa \tag{3.92}$$

In the top layer the expression follows from the general solution of (3.77) and in the air region between the coil and the inhomogeneous conductor the expression is the same as in (3.81). Following the application of the interface conditions between the regions, we can calculate the unknown coefficients and present expressions for the eddy current density as well as the impedance change. The unknown coefficient D_{ec} is now

$$\begin{aligned} D_{ec} &= \frac{\kappa\left[(LS - MR) + \lambda\,(MP - LQ)\right] - (NS - OR) - \lambda\,(OP - NQ)}{\kappa\left[(LS - MR) + \lambda\,(MP - LQ)\right] + (NS - OR) + \lambda\,(OP - NQ)}\, C_s \\ &= R(\kappa)\, C_s \end{aligned} \tag{3.93}$$

where the various symbols in (3.93) stand for

$$L = \left[F_1(f(z))\right]_{z=0} \tag{3.94}$$

$$M = \left[F_2(f(z))\right]_{z=0} \tag{3.95}$$

$$N = \left[F_1(f(z))\right]'_{z=0} \tag{3.96}$$

$$O = \left[F_2(f(z))\right]'_{z=0} \tag{3.97}$$

$$P = \left[F_1(f(z))\right]_{z=-d} \tag{3.98}$$

$$Q = \left[F_2(f(z))\right]_{z=-d} \tag{3.99}$$

$$R = \left[F_1(f(z))\right]'_{z=-d} \tag{3.100}$$

$$S = \left[F_2(f(z))\right]'_{z=-d} \tag{3.101}$$

Again from (3.49), the impedance change can be written as

$$\Delta Z = \frac{j\omega\pi\mu_0 N^2}{(r_2-r_1)^2(z_2-z_1)^2}\int_0^\infty \frac{\chi^2(\kappa r_1,\kappa r_2)}{\kappa^6}\left(e^{-\kappa z_1}-e^{-\kappa z_2}\right)^2 R(\kappa)\,d\kappa \tag{3.102}$$

Likewise, we can calculate the coefficients C_1, D_1 and C_2 and using (3.46) we can derive expressions for the eddy current density in the top and bottom layers.

As a simple check for (3.93) we put $F_1(z) = e^z$ and $F_2(z) = e^{-z}$ and we regain (3.42) for a nonmagnetic conductor when $\mu_{r1} = \mu_{r2} = 1$. The cases examined by Theodoulidis (1994) were the linear, the quadratic and the exponential profile. For the linear case, which is the simplest of the three, the conductivity variation is given by

$$\sigma(z) = k_1 + k_2 z \tag{3.103}$$

where k_1, k_2 are constants. Eq. (3.76) then has the solution

$$Z(z) = C\ Ai(\zeta) + D\ Bi(\zeta) \tag{3.104}$$

where Ai, Bi are Airy functions and

$$\zeta = \frac{\kappa^2 + pk_1 + pk_2 z}{(pk_2)^{2/3}} \quad ; \quad p = j\omega\mu_0 \tag{3.105}$$

Another solution to (3.76) can be found in the literature, see Mullin (1953) who analyzed a problem related to the solution of the wave equation near the extremum of the potential. The conductivity profile, which is quite a general variation that can deal with most conductivity profiles, is

$$\sigma(z) = k_0 + k_2 z^2 + k_3 z^3 + k_4 z^4 + k_5 z^5 + k_6 z^6 \tag{3.106}$$

where k_i are constants. In this case the solution is rather complex as it is given in terms of parabolic cylinder functions following a series of variable transformations.

Finally, Ton Tran-Cong (1984) provided exact solutions for some profiles of varying conductivity and permeability and also introduced perturbation methods by deriving solutions for the following profiles

$$\sigma(z) = \sigma_o(z) + \delta\sigma_1(z)$$
$$\mu(z) = \mu_o(z) + \delta\mu_1(z)$$

where δ is much smaller than unity, provided that solutions for $\sigma_o(z)$ and $\mu_o(z)$ are known.

3.7 Other solutions

There are also other approaches for computing ΔZ that involve either numerical or experimental evaluation of the terms present in the expression for ΔZ. Looking back at the expressions derived so far, for the impedance change for an axisymmetric coil, we can write them in the following form

$$\Delta Z = \frac{j4\omega}{\mu_0} \int_0^\infty C_s^2 R(\kappa) d\kappa \tag{3.107}$$

which is valid for axisymmetric coils with any cross-section shape and not only for the rectangular cross-section. The integrand is the product of two terms. The term $R(\kappa)$ depends only on the properties of the conductor and the operating frequency. The source term C_s, however, depends on the properties of the isolated coil and is considered an unknown quantity. The coefficient C_s is also present in the expression for B_z produced by the isolated coil

$$B_z = \frac{1}{r}\frac{\partial(rA)}{\partial r} = \int_0^\infty C_s \kappa e^{\kappa z} J_0(\kappa r) d\kappa \tag{3.108}$$

Putting $z = 0$ we note that C_s is actually the zero order Hankel transform of $B_z(r, z = 0)$

$$C_s = \tilde{B}_z = \int_0^\infty B_z(r, z = 0) J_0(\kappa r) r d\kappa \tag{3.109}$$

Thus, we can compute the needed source term from the Hankel transform of the $z-$component of the isolated coil magnetic flux density at $z = 0$. In principle, this term can also be computed numerically and such an approach will be presented in a relevant 3D problem in Chapter 5. The magnetic flux density values can be calculated numerically from the Biot-Savart law as we discussed in the Appendix.

Alternatively, it has been shown how experimental measurements of the coil magnetic field can be used to calculate C_s and hence coil impedance.

For details on this approach and the way to overcome the numerical problems that arise, see Burke (1992). This source term can also be determined from the impedance change spectrum due to a known specimen. For details on this approach, see Harrison (2001).

The fact that only the isolated coil magnetic field is needed to calculate every electromagnetic field quantity and impedance in the presence of a conductor system is quite general and true also for 3D configurations. In the axisymmetric 2D configuration, this is not of any particular help since the standard way to integrate the quantity $J_1(\kappa r)\exp(-\kappa z)$ over the coil cross-section is rather straightforward. However, in a 3D configuration this indirect approach is very important since it avoids an integration over the source volume that is cumbersome and often impossible.

3.8 Computational remarks

The solutions presented here together with the ones that can be derived for cylindrical conductors, Dodd (1969, 1974), are often (incorrectly) called integral solutions. In our opinion, this is misleading as they are just analytical solutions expressed as integrals and the only numerical part is the evaluation of the infinite range integrals. Strictly speaking, integral solutions involve an unknown kernel function which is embedded in an integral and thus require a much different and laborious approach.

Some researchers have tried to simplify the expression for ΔZ either by expanding the integrand to a number of terms that could further be treated analytically see Zaman (1980), Hajian (1982), Coffey (2001) or by fitting the results so that the impedance change produced by a specific coil could be described by a polynomial expression for a range of the involved parameters, Sandovskii (1974, 1977). Such treatment is supposed to give a better insight into the expressions and at the same time facilitate their numerical implementation, but nowadays these approaches are not necessary since modern computational tools have simplified considerably the task of computing efficiently the full integral expressions.

3.8.1 *Numerical calculations*

The solutions presented in this chapter involve the numerical computation of Bessel functions, an infinite range (improper) integral and the finite integral $\chi(x_1, x_2)$.

3.8.1.1 *Bessel functions*

Bessel functions in this chapter are all of integer order and real argument, but even in the general case of real order and complex argument their computation is straightforward and a number of routines are available for this purpose. A publicly available Fortran package for computation of Bessel functions is AMOS and it can be found in the netlib repository at *www.netlib.org*. The commercially available IMSL Fortran library also contains routines based on AMOS. Other packages that compute Bessel functions are Mathematica and Matlab and the routines are respectively `BesselJ[n,x]` and `besselj(n,x)` for order n and argument x. All these computations are performed to machine precision. However, we can resort to polynomial approximations of $J_0(x)$ and $J_1(x)$, see Abramowitz (1970) and Luke (1962), if we seek a simple expression of adequate accuracy.

3.8.1.2 *Finite integral*

Various approaches have been suggested so far for the efficient computation of the integral $\chi(x_1, x_2)$ defined by (3.27). The first approach is to perform a numerical integration but this method is not very accurate. If we use Mathematica and try to perform an analytical integration we get another expression

$$\int^z xJ_1(x)dx = \frac{1}{6}z^3 {}_pF_q[\{\frac{3}{2}\}, \{2, \frac{5}{2}\}, -\frac{z^2}{4}] \tag{3.110}$$

where ${}_pF_q(a; b; z)$ is the hypergeometric function, which in turn can be computed with the relevant Mathematica routine. Another approach is to write the integral as

$$\int^z xJ_1(x)dx = -xJ_0(x) + \int^z J_0(x)dx \tag{3.111}$$

and using the expansion of the integral on the right side in Chebychev polynomials, MacLeod (1996). The relevant Fortran subroutine available in the netlib repository performs the computation to computer machine accuracy. The same package can be used for computation of Struve functions, therefore making possible the computation of the χ integral through its expression in (3.27). Alernatively the integral of $J_0(x)$ can be computed

with the very fast converging series, Abramowitz (1970)

$$\int^{z} J_0(x)dx = 2\sum_{k=0}^{\infty} J_{2k+1}(z) \tag{3.112}$$

All these computations can be performed to machine precision. Again as in the case of Bessel functions computation, we can resort to polynomial approximations of χ, see Abramowitz (1970) and Luke (1962), if we seek a simple expression of adequate accuracy.

3.8.1.3 *Infinite range integral*

The problem that arises is that the infinite integration range has to be truncated and the optimum length of the truncation interval is not known beforehand. Although we can apply "rules of thumb" such as the truncation at $\kappa = 10/r_2$, it is preferable to utilize sophisticated techniques of numerical analysis for computing infinite range integrals. One such technique is the used of Gauss-Laguerre quadratures, Hower (1984). A more efficient technique using Gauss-Konrod quadratures has been utilized in the package QUADPACK. The Fortran code for this package can be found in the netlib repository and the routine that handles such integrals is `DQAGI` (double precision version). An automatic routine means that it can handle the infinite range integrals automatically, that is without specifying a truncation limit but rather providing a desirable relative accuracy error in the calculations. Usually, a relative accuracy of 1e-4 or even 1e-3 gives very adequate results. Another package that relies on QUADPACK is the IMSL Fortran library, which uses a version of `DQAGI`, now called `DQDAGI`. The disadvantage when using an automatic integration routine is that the integral needs to be computed twice: first we compute its real and then its imaginary part and so the computation time is doubled. It is important to keep an eye open for numerical overflows since the routine occasionally attempts to compute the integrand at an extremely large value of the integration variable.

In conclusion, since any other computation is performed to machine precision, the computation error in impedance and electromagnetic field calculations is the relative error reported by the routine that handles the infinite range integration. Nevertheless, in Chapter 4 we present a reformulation of the models in this chapter that does not require the computation of the infinite integral.

3.8.2 *Experimental verification*

In deriving the formulae of this chapter it was assumed that the coil current is uniformly distributed over the cross-section. In other words, the shape occupied by insulating material is assumed to be negligible and the winding spacing even. This corresponds to the ideal condition of a wire of square (or rectangular) cross-section, the turns being kept from electrical contact by insulation of negligible thickness. However, due to the unavoidable embedding of the wires as the coil is wound, even for the round, insulated wire that is commonly used, the current sheet approximation is quite satisfactory and is expected that normalization minimizes its effect even more. Correction formulae to account for discrete windings are given for the inductance of an isolated coil in Dodd (1968) and Grover (1973).

The most serious sources of error arise from high frequency effects. As the frequency increases, the current density ceases to be uniformly distributed over the cross-section of the wire and concentrates on the surface. As a result, the resistance of the coil increases whereas its inductance decreases. The current is capacitively coupled between the turns in the coil, tending to flow across the loops of wire rather than through them. Fortunately, there is a technique for compensating high frequency effects that occur not only due to the inherent coil capacitance but also due to the impedance of connecting circuits, leads, etc. The technique is described by Harrison (1996) and it can be used for frequencies up to about half the resonance frequency of the coil. This correction procedure should be an integral part of experimental measurements performed at laboratory conditions usually with an impedance analyzer or a high precision LCR bridge. If the high-frequency effects have been compensated for there is no reason for discrepancy between theory and experiment for well-characterized coils and workpieces and at least for configurations such as the ones presented in this chapter the expected agreement is of the order of 1-2%. The discrepancy between theory and experiment is slightly higher for very low frequencies but this is attributed to limitations of the impedance analyzer measuring circuits. In this case, the absolute measurement error is usually provided. It should also be noted that a useful practice is the presentation of experimental results as normalized quantities (resistance and reactance) since small systematic errors cancel out and moreover the normalized quantity is independent of the number of turns that is sometimes difficult to know exactly.

Consider Table 3.1 for a typical setup: a small air-cored coil and an

Table 3.1 Coil and conductor data for comparing theoretical and experimental results.

Coil	C9	Conductor	
r_1 [mm]	3.015	σ [MS/m]	16.5
r_2 [mm]	5.46	μ_r	1
z_1 [mm]	1.32		
$z_2 - z_1$ [mm]	2.94		
N	900		
L_0 [mH]	6.03		
R_0 [Ohm]	104		
f_R [kHz]	587		

Table 3.2 Experimental results for coil C9. Courtesy of S.K. Burke, DSTO, Australia.

f [kHz]	ΔR [Ohm]	ΔL [mH]	$\Delta R/X_0$	$\Delta X/X_0$
1	1.569±0.01	-0.262 ±0.001	0.04141	-0.04345
10	16.72±0.1	-0.7518±0.001	0.04413	-0.12468
100	77.21±1	-1.029 ±0.001	0.02038	-0.17065

Table 3.3 Theoretical results and relative difference with experimental ones.

f [kHz]	$\Delta R/X_0$ (ϵ_R)	$\Delta X/X_0$ (ϵ_X)
1	0.04267 (3.04%)	-0.04252 (2.14%)
10	0.04428 (0.34%)	-0.1238 (0.71%)
100	0.02015 (1.13%)	-0.1701 (0.32%)

aluminium alloy plate. The resonance frequency f_R is measured to 587 kHz, therefore reliable measurements can be done up to about 250 kHz. R_0 stands for the dc resistance of the coil wire, which is subtracted from all measurements.

Table 3.2 shows experimental results for the coil resistance change and inductance change as well as for the normalized resistance change and reactance change at three typical excitation frequencies. Table 3.3 shows theoretical results derived from (3.52) for ΔZ and from (3.34) for Z_0, with an automatic integration routine with relative accuracy 0.1%. The values in parentheses are the relative difference between experimental and theoretical

results defined as follows

$$\varepsilon_R = \left| \frac{(\Delta R/X_0)^{\text{meas.}} - (\Delta R/X_0)^{\text{theory}}}{(\Delta R/X_0)^{\text{meas.}}} \right| \times 100\% \tag{3.113}$$

$$\varepsilon_X = \left| \frac{(\Delta X/X_0)^{\text{meas.}} - (\Delta X/X_0)^{\text{theory}}}{(\Delta X/X_0)^{\text{meas.}}} \right| \times 100\% \tag{3.114}$$

Chapter 4

Application of the TREE method to Axisymmetric Problems

4.1 Introduction

In this chapter we reformulate the axisymmetric problems presented in Chapter 3 and extend them to more complex configurations. The method used to achieve this is again the TREE method which involves the truncation of the the solution region in one of the coordinate dimensions. Truncation of the region leads to an approximation of the unbounded domain solution but the errors introduced can be made as small as desired by increasing the width of the region.

Reformulating the boundary value problem as a finite domain problem means that the general solution after the application of the method of variables separation is in the form of a sum rather than in the form of an integral. The summation terms are eigenfunction expansion solutions of the differential equation describing the problem. Replacing integral expressions with sums has a number of numerical advantages but the most important characteristic is that it is possible to derive closed-form expressions for geometries that until now were thought to be analytically intractable.

The use of eigenfunction expansions in eddy current problems is not common in contrast to higher frequency problems. Similar techniques are used in waveguide problems in the study of wave propagation. The waveguide configuration is inherently finite since the waveguide walls constitute the artificial boundary of the geometry. In eddy current problems, however, we have to impose this boundary explicitly. This is physically consistent because at eddy current frequencies (up to a few MHz) the electromagnetic field does not extend to great distances from the excitation coil. Finally, by using region truncation we can satisfy interface conditions at two coordinate directions and also satisfy mixed boundary conditions in a single

direction. This can be done on a series term-by-term basis or through a set of simultaneous matrix equation that can be readily solved. It is actually this capability that extends the class of problems that can be solved analytically. We are now in a position not only to solve for infinitely long planes and cylinders but also to introduce cuts, edges or canonical inhomogeneities. However, the method is not purely analytical: one has to invert a full matrix and also to use a numerical method to find the eigenvalues of the problem. This was the reason for characterizing it as quasi-analytical in Chapter 1.

The axisymmetric geometries of the Dodd and Deeds models are described in the cylindrical radial and axial coordinates r and z. The reformulation requires truncation of the solution region in one of them and in the problems studied in this chapter the truncation takes place in the r coordinate. Other axisymmetric configurations require the truncation to be performed in the z coordinate. The first geometry studied with the TREE approach is the basic geometry of the familiar rectangular cross-section coil above a conductive half-space. The analytical integral expression of the previous chapter will be particularly useful in estimating the extent of the truncation required and the number of series terms for an accurate approximation. Next, the geometry will be extended to include a coil with a ferrite core in the form of a cylinder made of purely magnetic material. Finally, the TREE method will be used to model the case of the conductive half-space with an axisymmetric cylindrical inhomogeneity.

It is tempting to use the superposition principle in all cases: calculate the total electromagnetic field by superposing the field from the isolated coil and the field from the conductive half-space just like the procedure followed in the previous chapter. However, this is possible for the air-cored coil but not possible for the ferrite-cored coil because the presence of the half-space changes the magnetization of the ferrite and thus the isolated coil field is affected. What we do then instead of calculating the two fields separately and adding them is to solve for the total field from the beginning and then identify the parts of the field originating from the coil and the eddy currents. This is done initially for a filamentary coil and then for the finite thickness coil. We follow this approach also for the air-cored coil, although it is not necessary, because we treat the problems of this chapter in a uniform way. Following the solution for each case examined, we discuss the numerical aspects of the solution and provide guidance towards a successful calculation.

4.2 Isolated coil

Here we derive alternative expressions for the electromagnetic field of an isolated coil. Referring back to Fig.3.1 we add an artificial boundary in the form of a cylinder at $r = h$ where the magnetic vector potential vanishes and thus we have Fig.4.1. This is equivalent to a vanishing radial component of the magnetic flux density since $B_r = -\partial A/\partial z$.

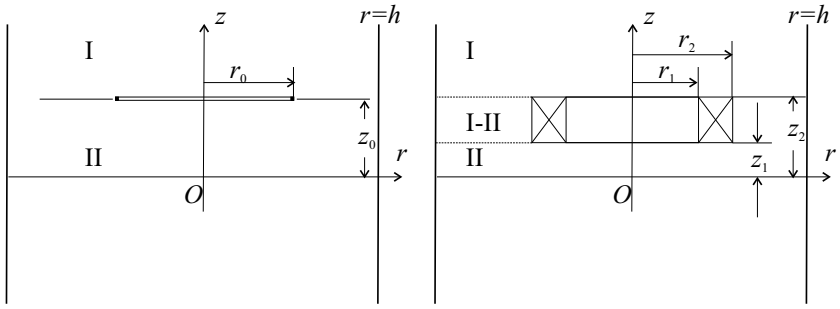

Fig. 4.1 2D axisymmetric view of (a) one-turn filamentary and (b) multi-turn cylindrical isolated coil. The solution domain is truncated at $r = h$.

Following a similar method as in Sec.3.2 the magnetic vector potential can again be calculated from

$$\mathbf{A} = \frac{\mu_0 I}{4\pi} \oint_l \frac{d\mathbf{l}}{|\mathbf{r} - \mathbf{r}_0|} \tag{4.1}$$

where now the reciprocal of the distance between a source point (r_0, φ_0, z_0) and a field point (r, φ, z), which is actually the Green's function for a space bounded externally by a cylinder at $r = h$, can be written as follows, see Gray (1931)

$$\frac{1}{R} = \frac{2}{h^2} \sum_{m=0}^{\infty} (2 - \delta_m) \cos[m(\varphi - \varphi_0)] \sum_{i=1}^{\infty} e^{-\kappa_i |z - z_0|} \frac{J_m(\kappa_i r) J_m(\kappa_i r_0)}{\kappa_i \left[J'_m(\kappa_i h)\right]^2} \tag{4.2}$$

where κ_i is a positive root of the Bessel function $J_m(\kappa_i h)$. After performing the line integration, which is uniform integration due to axisymmetry, we derive the following result for the potential:

$$A^{(s)}(r, z) = \frac{\mu_0 I}{h^2} \sum_{i=1}^{\infty} e^{-\kappa_i |z - z_0|} \frac{J_1(\kappa_i r) J_1(\kappa_i r_0) r_0}{\kappa_i \left[J_0(\kappa_i h)\right]^2} \tag{4.3}$$

where we have taken into account that $J'_m(x) = J_{m-1}(x) + (m/x)J_m(x) = J_{m-1}(x)$ for $x = \kappa_i h$.

We can now approximate a multi-turn coil by superposition. The final expressions for the magnetic vector potential and flux density in the three regions of Fig.4.1b are as follows:

$$A_{\rm I}^{(s)} = \mu_0 \iota_0 \sum_{i=1}^{\infty} J_1(\kappa_i r) e^{-\kappa_i z} \frac{\chi(\kappa_i r_1, \kappa_i r_2)}{\left[(\kappa_i h) J_0(\kappa_i h)\right]^2 \kappa_i^2} (e^{\kappa_i z_2} - e^{\kappa_i z_1}) \tag{4.4}$$

$$A_{\rm II}^{(s)} = \mu_0 \iota_0 \sum_{i=1}^{\infty} J_1(\kappa_i r) e^{\kappa_i z} \frac{\chi(\kappa_i r_1, \kappa_i r_2)}{\left[(\kappa_i h) J_0(\kappa_i h)\right]^2 \kappa_i^2} (e^{-\kappa_i z_2} - e^{-\kappa_i z_1}) \tag{4.5}$$

$$A_{\rm I-II}^{(s)} = \mu_0 \iota_0 \sum_{i=1}^{\infty} J_1(\kappa_i r) \frac{\chi(\kappa_i r_1, \kappa_i r_2)}{\left[(\kappa_i h) J_0(\kappa_i h)\right]^2 \kappa_i^2} \left[2 - e^{\kappa_i (z - z_2)} - e^{-\kappa_i (z - z_1)}\right] \tag{4.6}$$

$$\mathbf{B}_{\rm I}^{(s)} = \mu_0 \iota_0 \sum_{i=1}^{\infty} e^{-\kappa_i z} \frac{\chi(\kappa_i r_1, \kappa_i r_2)}{\left[(\kappa_i h) J_0(\kappa_i h)\right]^2 \kappa_i} (e^{\kappa_i z_2} - e^{\kappa_i z_1}) \left[J_1(\kappa_i r)\mathbf{r}_0 + J_0(\kappa_i r)\mathbf{z}_0\right] \tag{4.7}$$

$$\mathbf{B}_{\rm II}^{(s)} = \mu_0 \iota_0 \sum_{i=1}^{\infty} e^{\kappa_i z} \frac{\chi(\kappa_i r_1, \kappa_i r_2)}{\left[(\kappa_i h) J_0(\kappa_i h)\right]^2 \kappa_i} (e^{-\kappa_i z_2} - e^{-\kappa_i z_1}) \left[J_1(\kappa_i r)\mathbf{r}_0 + J_0(\kappa_i r)\mathbf{z}_0\right] \tag{4.8}$$

$$\mathbf{B}_{\rm I-II}^{(s)} = \mu_0 \iota_0 \sum_{i=1}^{\infty} \frac{\chi(\kappa_i r_1, \kappa_i r_2)}{\left[(\kappa_i h) J_0(\kappa_i h)\right]^2 \kappa_i} \left\{ \begin{array}{l} \left[e^{\kappa_i (z - z_2)} - e^{-\kappa_i (z - z_1)}\right] J_1(\kappa_i r)\mathbf{r}_0 \\ - \left[e^{\kappa_i (z - z_2)} + e^{-\kappa_i (z - z_1)}\right] J_0(\kappa_i r)\mathbf{z}_0 \end{array} \right\} \tag{4.9}$$

where again $\iota_0 = NI(r_2 - r_1)^{-1}(z_2 - z_1)^{-1} = nI$, with n denoting the wire-turns density and $\chi(\kappa_i r_1, \kappa_i r_2)$ is defined in (3.27). These expressions provide an alternative to the ones given in Chapter 3 for the isolated coil field. Having calculated the potential in region I-II, we can calculate the impedance of the coil, which is purely inductive:

$$Z_0 = j4\pi\omega\mu_0 n^2 \sum_{i=1}^{\infty} \frac{\chi^2(\kappa_i r_1, \kappa_i r_2)}{\left[(\kappa_i h) J_0(\kappa_i h)\right]^2 \kappa^5} \left[\kappa_i (z_2 - z_1) + e^{-\kappa_i (z_2 - z_1)} - 1\right] \tag{4.10}$$

Again this impedance expression provides an alternative to the one given in Chapter 3. Useful conclusions can be drawn on the suitability of the series for both magnetic field and impedance calculation by comparing expressions (4.7)-(4.10) to (3.30)-(3.34) and experimenting with the selection of h and the number of terms required in the sums so that a sound approximation is achieved. This is done later for a coil above a conductive half-space; let us only note that the larger the region width h, the more terms are required in the series but at the same time the better the calculation accuracy. Nevertheless, the use of the series expressions are computationally superior to the integral expressions because many terms can be pre-computed and kept in computer memory during calculations.

4.3 Coil above a conductive half-space

We can now proceed with deriving a TREE series solution for the electromagnetic field and the impedance of the coil when this is placed above a conductive half-space. As already mentioned, we can follow the superposition method: the total impedance of the coil is the sum of the isolated coil impedance and the impedance due to the presence of the half-space since the electromagnetic field in the air region is the sum of the field due to the coil and the field due to the eddy currents. However, in this problem we adopt an equivalent approach where we solve directly for the total field. In order to work in this way we first solve for the filamentary coil above the half-space and then extend the solution to the finite thickness rectangular cross-section coil.

4.3.1 *Filamentary coil*

The configuration to be analyzed is shown in Fig.4.2, where we can identify three distinct truncated regions ($0 \leq r \leq h$). The filamentary coil is part of the interface surface $z = z_0$ between regions 1 and 2, while the surface $z = 0$ constitutes the interface between the conductive and non-conductive area. In all these regions the magnetic vector potential satisfies either the Laplace or Helmholtz equation depending on the conductivity of the region

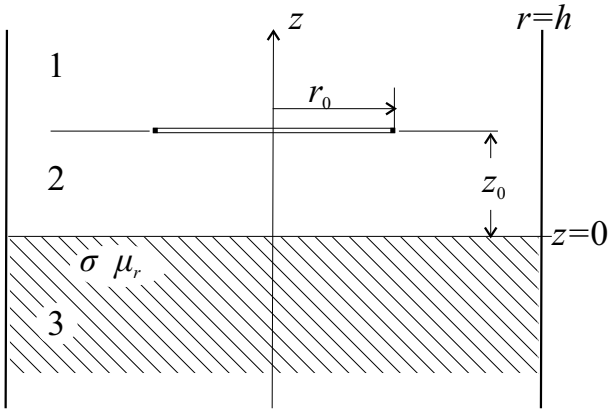

Fig. 4.2 2D axisymmetric view of a filamentary coil above a conductive half-space. The solution domain is truncated at $r = h$.

and the general form of the solution is written as a series:

$$A(r,z) = \left[A_0 r + \frac{B_0}{r}\right][C_0 + D_0 z] + \sum_{i=1}^{\infty} [A_i J_1(\kappa_i r) + B_i Y_1(\kappa_i r)][C_i e^{\lambda_i z} + D_i e^{-\lambda_i z}] \tag{4.11}$$

where $\lambda_i = \sqrt{\kappa_i^2 + j\omega\mu_0\mu_r\sigma}$. Now not only the unknown coefficients A_i, B_i, C_i, D_i but also the discrete eigenvalues κ_i are to be determined from the boundary and interface conditions. Although the complete solution is the infinite sum of (4.11), in practice only a finite number of summation terms N_s is needed for a good approximation of the solution.

Truncation of the problem region means that the cylindrical surface $r = h$ has become the outer boundary so we have to impose a boundary condition there. This can either be a homogeneous Dirichlet condition as in the case of the isolated coil, or a homogeneous Neumann condition. Setting $A_\varphi(h,z) = 0$ is equivalent to a vanishing electric field $E_\varphi(h,z) = 0$ and a vanishing normal component of magnetic field $B_r(h,z) = 0$, which is generally denoted as $\mathbf{n} \cdot \mathbf{H} = 0$ where $\mathbf{n}$ is the unit vector normal to the boundary, here $\mathbf{r}_0$. Because such a boundary is similar to a region of infinite conductivity $\sigma \to \infty$ in the area $r > h$ it is referred to as an electric boundary and because it does not let the magnetic field cross it, it is also referred to as a magnetic insulation boundary. The homogeneous Neumann condition $\mathbf{n} \times \mathbf{H} = 0$ is equivalent to $B_z(h,z) = 0$ or $(1/r)[\partial(rA)/\partial r]_{r=h} = 0$.

Again, because such a boundary is similar to a region of infinite permeability $\mu \to \infty$ in the area $r > h$ it is also referred to as a magnetic boundary and because it does not let the electric field cross it, it is referred to as an electric insulation boundary.

In the following analysis we use the Dirichlet boundary condition. There is no great difference in the resulting expressions if we use the Neumann boundary condition. Numerical results will be provided by using both so we will be able to compare their numerical efficiency.

Using the Dirichlet condition, the requirement that the potential remains finite at $z \to \pm\infty$ and vanishes at $r = 0$ and $r = h$ yields the trivial solution $A_0 = B_0 = C_0 = D_0 = 0$ for the coefficients of the first term in all regions. With regard to the coefficients of the remaining terms, due to the divergence of Y_1 at the origin we set $B_i = 0$. Considering that the potential must vanish on the outer boundary, i.e. $A(h, z) = 0$, we can satisfy this condition on a term-by-term basis and therefore the eigenvalues κ_i are the roots of the equation:

$$J_1(\kappa_i h) = 0 \tag{4.12}$$

The general expressions in the three regions of the problem are written as:

$$A_1(r, z) = \sum_{i=1}^{\infty} J_1(\kappa_i r) e^{-\kappa_i z} D_i^{(1)} \tag{4.13}$$

$$A_2(r, z) = \sum_{i=1}^{\infty} J_1(\kappa_i r) \left(e^{\kappa_i z} C_i^{(2)} + e^{-\kappa_i z} D_i^{(2)} \right) \tag{4.14}$$

$$A_3(r, z) = \sum_{i=1}^{\infty} J_1(\kappa_i r) e^{\lambda_i z} C_i^{(3)} \tag{4.15}$$

We next apply the usual interface conditions to calculate the unknown expansion coefficients C_i and D_i. From the continuity of B_z and H_r at the two interfaces $z = z_0$ and $z = 0$ we get

$$A_1(r, z_0) = A_2(r, z_0) \tag{4.16}$$

$$\left.\frac{\partial A_1(r, z)}{\partial z}\right|_{z=z_0} - \left.\frac{\partial A_2(r, z)}{\partial z}\right|_{z=z_0} = -\mu_0 I \delta(r - r_0) \tag{4.17}$$

$$A_2(r, 0) = A_3(r, 0) \tag{4.18}$$

$$\left.\frac{\partial A_2(r,z)}{\partial z}\right|_{z=0} = \frac{1}{\mu_r}\left.\frac{\partial A_3(r,z)}{\partial z}\right|_{z=0} \tag{4.19}$$

which yield the following equations:

$$\sum_{i=1}^{\infty} J_1(\kappa_i r) e^{-\kappa_i z_0} D_i^{(1)} = \sum_{i=1}^{\infty} J_1(\kappa_i r)\left(e^{\kappa_i z_0} C_i^{(2)} + e^{-\kappa_i z_0} D_i^{(2)}\right) \tag{4.20}$$

$$\begin{aligned}\sum_{i=1}^{\infty} J_1(\kappa_i r)(-\kappa_i) e^{-\kappa_i z_0} D_i^{(1)} - \sum_{i=1}^{\infty} J_1(\kappa_i r)\kappa_i\left(e^{\kappa_i z_0} C_i^{(2)} - e^{-\kappa_i z_0} D_i^{(2)}\right)\\ = -\mu_0 I\delta(r-r_0)\end{aligned} \tag{4.21}$$

$$\sum_{i=1}^{\infty} J_1(\kappa_i r)[C_i^{(2)} + D_i^{(2)}] = \sum_{i=1}^{\infty} J_1(\kappa_i r) C_i^{(3)} \tag{4.22}$$

$$\sum_{i=1}^{\infty} J_1(\kappa_i r)\kappa_i[C_i^{(2)} - D_i^{(2)}] = \frac{1}{\mu_r}\sum_{i=1}^{\infty} J_1(\kappa_i r)\lambda_i C_i^{(3)} \tag{4.23}$$

If we multiply each side of the above equations with $J_1(\kappa_i r)r$, integrate from 0 to h and use the orthogonality property of the Bessel function:

$$\begin{aligned}\int_{r=0}^{h} J_1(\kappa_i r) J_1(\kappa_j r) r\, dr &= \delta_{ij}\frac{[hJ_2(\kappa_i h)]^2}{2}\\ &= \delta_{ij}\frac{h^2}{2}\left[\frac{2}{\kappa_i h}J_1(\kappa_i h) - J_0(\kappa_i h)\right]^2\\ &= \delta_{ij}\frac{[hJ_0(\kappa_i h)]^2}{2}\end{aligned} \tag{4.24}$$

where δ_{ij} is the Kronecker symbol, we get

$$e^{-\kappa_i z_0} D_i^{(1)} = e^{\kappa_i z_0} C_i^{(2)} + e^{-\kappa_i z_0} D_i^{(2)} \tag{4.25}$$

$$\begin{aligned}\frac{[hJ_0(q_i h)]^2}{2}\left[(-\kappa_i) e^{-\kappa_i z_0} D_i^{(1)} - \kappa_i\left(e^{\kappa_i z_0} C_i^{(2)} - e^{-\kappa_i z_0} D_i^{(2)}\right)\right]\\ = -\mu_0 I r_0 J_1(\kappa_i r_0)\end{aligned} \tag{4.26}$$

$$C_i^{(2)} + D_i^{(2)} = C_i^{(3)} \tag{4.27}$$

$$\kappa_i[C_i^{(2)} - D_i^{(2)}] = \frac{1}{\mu_r}\lambda_i C_i^{(3)} \tag{4.28}$$

We then solve the 4×4 system formed by equations (4.25)-(4.28) for the unknown coefficients

$$C_i^{(2)} = \mu_0 I e^{-\kappa_i z_0} \frac{r_0 J_1(\kappa_i r_0)}{\kappa_i [h J_0(\kappa_i h)]^2} \tag{4.29}$$

$$D_i^{(2)} = \frac{\kappa_i \mu_r - \lambda_i}{\kappa_i \mu_r + \lambda_i} C_i^{(2)} \tag{4.30}$$

$$C_i^{(3)} = \frac{2\kappa_i \mu_r}{\kappa_i \mu_r + \lambda_i} C_i^{(2)} \tag{4.31}$$

$$D_i^{(1)} = \left(e^{2\kappa_i z_0} + \frac{\kappa_i \mu_r - \lambda_i}{\kappa_i \mu_r + \lambda_i} \right) C_i^{(2)} \tag{4.32}$$

Note that $C_i^{(2)}$ is a source coefficient and all other coefficients can be written in terms of it. The final expressions for the magnetic vector potential in the three regions are derived by substituting (4.29)-(4.32) to (4.13)-(4.15).

4.3.2 *Finite thickness coil*

We use superposition in (4.13)-(4.15) and calculate the magnetic vector potential for the cylindrical finite thickness coil, shown in Fig.4.3. Since we continue from the filamentary coil analysis, we retain the original assumption of a Dirichlet condition for A at $r = h$. The magnetic vector potential in regions 1, 2, 3 is then given by:

$$A^{(1)} = \mu_0 \iota_0 \sum_{i=1}^{\infty} J_1(\kappa_i r) e^{-\kappa_i z} \times \tag{4.33}$$
$$\times \left[\left(e^{\kappa_i z_2} - e^{\kappa_i z_1} \right) + \left(e^{-\kappa_i z_1} - e^{-\kappa_i z_2} \right) \frac{\kappa_i \mu_r - \lambda_i}{\kappa_i \mu_r + \lambda_i} \right] \frac{\chi(\kappa_i r_1, \kappa_i r_1)}{\kappa_i^4 \left[h J_0 \left(\kappa_i h \right) \right]^2}$$

$$A^{(2)} = \mu_0 \iota_0 \sum_{i=1}^{\infty} J_1(\kappa_i r) \left(e^{\kappa_i z} + e^{-\kappa_i z} \frac{\kappa_i \mu_r - \lambda_i}{\kappa_i \mu_r + \lambda_i} \right) \times \tag{4.34}$$
$$\times \left(e^{-\kappa_i z_1} - e^{-\kappa_i z_2} \right) \frac{\chi(\kappa_i r_1, \kappa_i r_1)}{\kappa_i^4 \left[h J_0 \left(\kappa_i h \right) \right]^2}$$

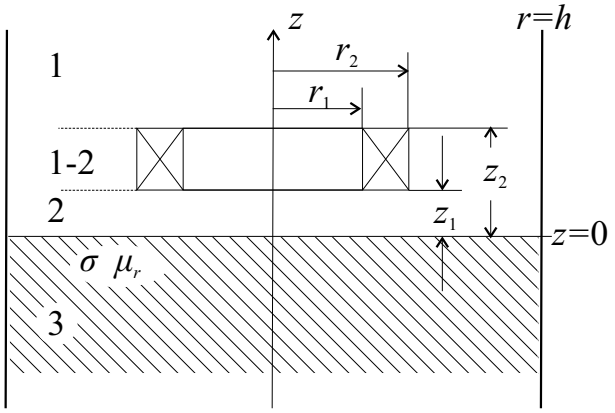

Fig. 4.3 2D axisymmetric view of a cylindrical coil above a conductive half-space. The solution domain is truncated at $r = h$.

$$A^{(3)} = 2\mu_0\mu_r\iota_0 \sum_{i=1}^{\infty} J_1(\kappa_i r) e^{\lambda_i z} \frac{(e^{-\kappa_i z_1} - e^{-\kappa_i z_2})}{\kappa_i\mu_r + \lambda_i} \frac{\chi(\kappa_i r_1, \kappa_i r_1)}{\kappa_i^3 \left[hJ_0\left(\kappa_i h\right)\right]^2} \tag{4.35}$$

where again $\iota_0 = NI(r_2 - r_1)^{-1}(z_2 - z_1)^{-1} = nI$, with n denoting the wire-turns density and $\chi(\kappa_i r_1, \kappa_i r_2)$ is defined in (3.27). Following the procedure of the previous section, the potential in region 1-2 is calculated as follows

$$A^{(1-2)} = \mu_0\iota_0 \sum_{i=1}^{\infty} J_1(\kappa_i r) \frac{\chi(\kappa_i r_1, \kappa_i r_1)}{\kappa_i^4 \left[hJ_0\left(\kappa_i h\right)\right]^2} \times \tag{4.36}$$
$$\times \left[2 - e^{-\kappa_i(z-z_1)} - e^{\kappa_i(z-z_2)} + \left[e^{-\kappa_i(z-z_1)} - e^{\kappa_i(z-z_2)}\right] \frac{\kappa_i\mu_r - \lambda_i}{\kappa_i\mu_r + \lambda_i}\right]$$

and the coil impedance is calculated by integrating $rA^{(1-2)}$ over the coil cross-section. The final result can again be written as the sum of the impedance in air Z_0 and the impedance change ΔZ produced by the eddy currents induced in the conductive half-space. The final expressions for Z_0 and ΔZ are as follows:

$$Z_0 = \frac{j\omega 2\pi\mu_0 N^2}{(r_2 - r_1)^2(z_2 - z_1)^2} \sum_{i=1}^{\infty} \chi^2(\kappa_i r_1, \kappa_i r_2) \frac{2[\kappa_i(z_2 - z_1) - 1 + e^{\kappa_i(z_1 - z_2)}]}{\left[hJ_0(\kappa_i h)\right]^2 \kappa_i^7} \tag{4.37}$$

$$\Delta Z = \frac{j\omega 2\pi\mu_0 N^2}{(r_2 - r_1)^2(z_2 - z_1)^2} \sum_{i=1}^{\infty} \chi^2(\kappa_i r_1, \kappa_i r_2) \frac{(e^{-\kappa_i z_1} - e^{-\kappa_i z_2})^2}{\left[hJ_0(\kappa_i h)\right]^2 \kappa_i^7} \frac{\kappa_i\mu_r - \lambda_i}{\kappa_i\mu_r + \lambda_i} \tag{4.38}$$

Compare these expressions with the ones written in integral form in Chapter 3 and repeated here:

$$Z_0 = \frac{j\omega 2\pi\mu_0 N^2}{(r_2-r_1)^2(z_2-z_1)^2}\int_0^\infty \frac{\chi^2(\kappa r_1,\kappa r_2)}{\kappa^6}\left\{\kappa(z_2-z_1)+e^{-\kappa(z_2-z_1)}-1\right\}d\kappa \tag{4.39}$$

$$\Delta Z = \frac{j\omega\pi\mu_0 N^2}{(r_2-r_1)^2(z_2-z_1)^2}\int_0^\infty \chi^2(\kappa r_1,\kappa r_2)\frac{\left(e^{-\kappa z_1}-e^{-\kappa z_2}\right)^2}{\kappa^6}\frac{\kappa\mu_r-\lambda}{\kappa\mu_r+\lambda}d\kappa \tag{4.40}$$

Note than in (4.39)-(4.40) κ is a continuous integration variable. Finally, the eddy current density and the magnetic flux density in the conductive half-space are given by

$$J = -j\omega\sigma A^{(3)}(r,z) \quad ; \quad z \le 0 \tag{4.41}$$

$$\mathbf{B}^{(3)} = 2\mu_0\mu_r\iota_0\sum_{i=1}^{\infty}\left[-\lambda_i J_1(\kappa_i r)\mathbf{r}_0 + J_0(\kappa_i r)\kappa_i\mathbf{z}_0\right]e^{\lambda_i z}\frac{\left(e^{-\kappa_i z_1}-e^{-\kappa_i z_2}\right)}{\kappa_i\mu_r+\lambda_i}\times$$
$$\times\ \frac{\chi(\kappa_i r_1,\kappa_i r_1)}{\kappa_i^3\left[hJ_0\left(\kappa_i h\right)\right]^2} \quad ; \quad z \le 0 \tag{4.42}$$

and the interested reader can easily derive the expressions for $\mathbf{B}^{(1)}$, $\mathbf{B}^{(2)}$ and $\mathbf{B}^{(1-2)}$.

4.3.2.1 *The Neumann condition*

If we had used the Neumann condition at the boundary

$$B_z(h,z) = 0 \Rightarrow (1/r)[\partial(rA)/\partial r]_{r=h} = 0 \tag{4.43}$$

then the eigenvalues κ_i would have to be calculated from

$$J_0(\kappa_i h) = 0 \tag{4.44}$$

and the only other change in the above expressions would be the replacement of the term $J_0(\kappa_i h)$ by $J_1(\kappa_i h)$.

Table 4.1 Coil and half-space parameters used in the comparisons.

Coil		Half-space	
r_1	5 mm	σ	35.4 MS/m
r_2	10 mm	μ_r	1
$z_2 - z_1$	2 mm		
z_1	1 mm		
N	1000		

Table 4.2 Percentage (%) difference between results from sum and integral expression for Z_0.

N_s	50	100	150	200
h	Dirichlet			
$5r_2$	0.32	0.28	0.28	0.27
$10r_2$	0.41	8.43(-2)	4.66(-2)	4.02(-2)
$15r_2$	0.62	0.11	6.13(-2)	3.08(-2)
	Neumann			
$5r_2$	-1.98(-2)	-6.50(-2)	-6.91(-2)	7.02(-2)
$10r_2$	0.38	4.33(-2)	3.99(-3)	2.45(-3)
$15r_2$	0.64	0.10	4.97(-2)	1.84(-2)

4.3.3 *Comparison with the integral expressions*

We are now in a position to compare the efficiency of the series and integral approaches to calculate both electromagnetic field quantities and coil impedance using the coil data of Table 4.1.

The percentage differences shown in the following Tables are defined as

$$100[(\Delta R^{(s)} - \Delta R^{(i)}]/\Delta R^{(i)} + j100[(\Delta X^{(s)} - \Delta X^{(i)}]/\Delta X^{(i)} \qquad (4.45)$$

where $\Delta R^{(s)} + j\Delta X^{(s)}$ and $\Delta R^{(i)} + j\Delta X^{(i)}$ are impedance changes computed using sum and integral approaches, respectively. The notation $5.62(-4)$ means $5.62 \cdot 10^{-4}$. Generally the Neumann condition is superior for relatively small truncated regions ($5r_2$) owing to the fact that this condition is a physically more accurate representation of the actual field behavior. The agreement between the integral and sum expressions is better than the relative accuracy set for the integral expression calculations, which was 0.1%. This makes the sum approach a very good alternative compared with the integral expressions for computing Z_0 and ΔZ.

The eddy current density and magnetic field intensity results are also in excellent agreement. Only very small differences are observed at large

Table 4.3 Percentage difference (%) between results from sum and integral expression for ΔZ.

f[kHz]	N_s	$h = 5r_2$	N_s	$h = 10r_2$	N_s	$h = 15r_2$
		Dirichlet				
1	28	2.51(-2)+j1.20	69	6.57(-4)+j0.15	58	5.62(-4)+j4.44(-2)
10	39	1.05(-2)+j0.73	69	3.86(-4)+j9.05(-2)	117	6.31(-5)+j2.67(-2)
100	48	7.95(-3)+j0.63	109	2.91(-4)+j7.89(-2)	118	2.40(-4)+j2.33(-2)
		Neumann				
1	35	-1.40(-2)-j0.31	45	-4.92(-5)-j3.86(-2)	85	-8.03(-5)-j1.15(-2)
10	43	-5.79(-3)-j0.19	45	6.74(-3)-j2.30(-2)	104	4.28(-5)-j7.08(-3)
100	55	-4.29(-3)-j0.16	79	7.70(-5)-j2.04(-2)	104	4.84(-4)-j6.00(-3)

distances from the coil and these are exaggerated by being presented in logarithmic diagrams in Figs 4.4, 4.5 and 4.6. The diagrams show the exact integral expression results together with the sum solution when $h = 5r_2$ and $h = 10r_2$. As expected, choosing a larger truncation region gives better agreement especially at larger distances from the coil.

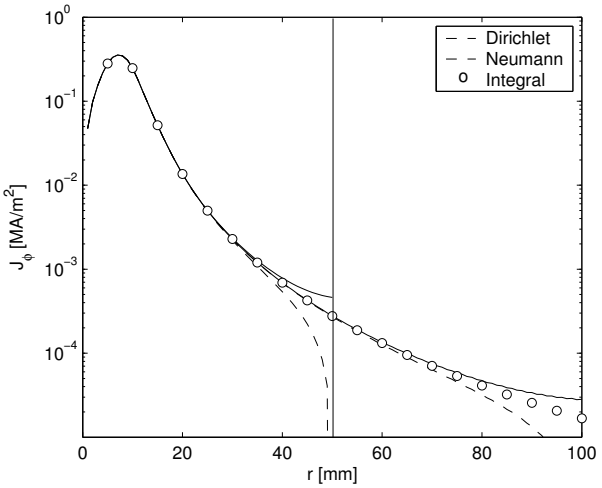

Fig. 4.4 Comparison of integral and series calculation of the variation of eddy current magnitude with radial distance on the conductor surface.

The replacement of the integral solution with a series solution has a number of advantages in terms of computation speed and accuracy control and in terms of simplicity in the model's computer implementation. For example, when we compute a frequency scan of the impedance change, every term in (4.38) except λ_i can be computed just once since it is independent

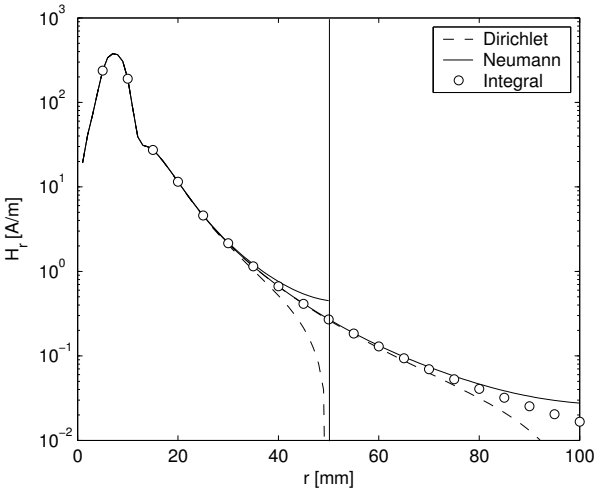

Fig. 4.5 Comparison of integral and series calculation of the variation of magnetic field intensity magnitude (r-component) with radial distance on the conductor surface.

of f. In fact, the number of frequencies where a computation is requested is a measure of how many times the sum expression is faster than the integral one.

4.4 Ferrite cored coils

The way to decrease a probes's magnetic reluctance is to wind it either on or inside ferrite cores, the latter also reduces the leakage field from the test area. Common designs for ferrite cores are shown in Fig.4.7, which due to their ferrite cross-sectional shape are called the I-, C- and E-core (or M-core). Other names are cylindrical core for the I-core and cup-core for the E-core. The I-core has the same field distribution as the air core but higher flux, while the C- and E-cores give both much higher flux density and shield the flux into the test area. Especially when inspecting ferromagnetic material, there is very little leakage field from the C- and E-cores.

Flux concentration and shielding effects from stray fields can also be obtained by surrounding the probe with a high conductivity (copper) shell but in this case, a relatively large part of the magnetic field energy is absorbed in the shield via eddy currents.

The permeability of the ferrite cores is assumed to be the initial perme-

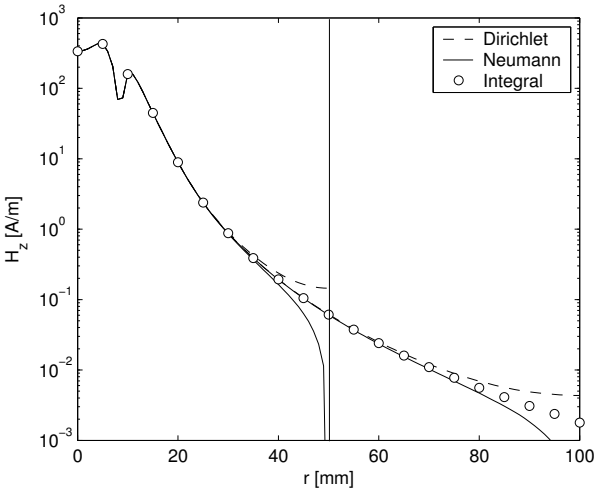

Fig. 4.6 Comparison of integral and series calculation of the variation of magnetic field intensity magnitude (z-component) with radial distance on the conductor surface.

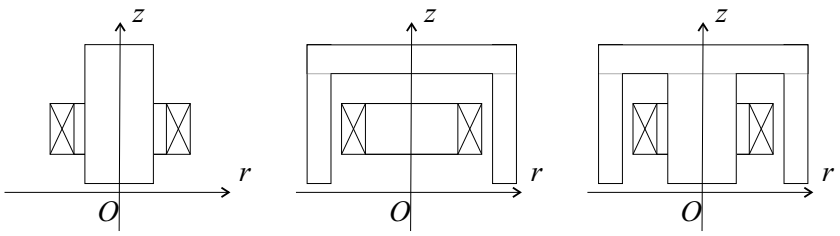

Fig. 4.7 2D axisymmetric view of coils with I-, C- and E-ferrite cores.

ability since in ECT the excitation is weak and the eddy current problem is treated as a linear one. The relative permeability is usually provided by the manufacturer and its high value usually lies in the range above 500.

We will examine here the cases of the I-core of infinite and finite height. The reader can refer to Theodoulidis (2002a) for the same type of core in the limiting case of infinite permeability and Theodoulidis (2002b) for the case of an I-core with finite height. With the theory developed the reader could also attempt to analyze the other two designs of C- and E- ferrite cores.

4.4.1 *Filamentary coil with cylindrical core*

Consider first the geometry of Fig.4.8, where a filamentary coil encircles a semi-infinite cylindrical ferrite core which has a finite value of permeability μ_c. The coil+core system is located above a half-space with conductivity σ and relative magnetic permeability μ_r. The various regions are formed by considering three interfaces: the plane $z = z_0$ where the current filament lies, the plane $z = 0$ which coincides with the bottom surface of the ferrite core and the plane $z = -l$ which is the conductor surface. The difference with Fig.4.3, where the core was absent, is that now regions 1 and 2 consist of two subregions: the *air* and the *core* one.

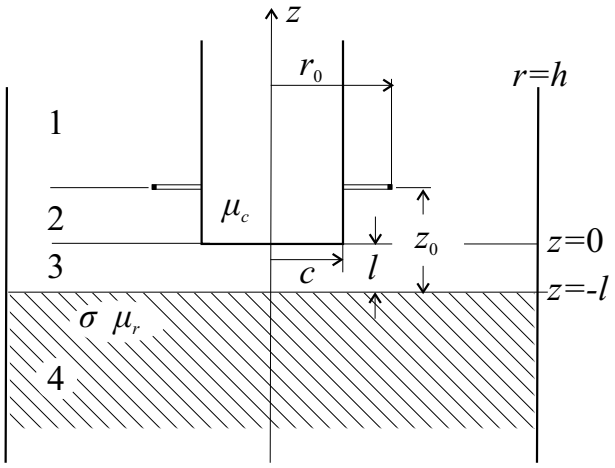

Fig. 4.8 2D axisymmetric view of filamentary coil with cylindrical core. The solution domain is truncated at $r = h$.

While for the other two regions 3 and 4 we can assume the same expressions for the magnetic vector potential as in the previous paragraph, further adjustments have to be made for regions 1 and 2. The radial dependence in the expressions for A_φ for these two sub-regions can be written as follows:

$$A_{\text{core}} = A_c J_1(q_i r) \quad 0 \leq r \leq c \tag{4.46}$$

$$A_{\text{air}} = A_a J_1(q_i r) + B_a Y_1(q_i r) \quad c \leq r \leq h \tag{4.47}$$

where q_i are now the corresponding discrete eigenvalues. Note that the coefficient of the Y_1 Bessel function in (4.47) does not vanish since it does not include the origin $r = 0$. Next, we match the two expressions on the

interface on a term by term basis and, hence, we need only the radial dependence since they have the same axial z-dependence. The continuity of B_r and H_z on the interface $r = c$ gives

$$A_c J_1(q_i c) = A_a J_1(q_i c) + B_a Y_1(q_i c) \tag{4.48}$$

$$A_c \frac{q_i J_0(q_i c)}{\mu_c} = A_a q_i J_0(q_i c) - B_a q_i Y_0(q_i c) \tag{4.49}$$

which yields the following expressions for A_a and B_a in terms of A_c

$$A_a = \frac{\pi q_i c}{2}\left[J_1(q_i c)Y_0(q_i c) - \frac{J_0(q_i c)Y_1(q_i c)}{\mu_c}\right] A_c = A_{ac}(q_i c)A_c \tag{4.50}$$

$$B_a = -\frac{\pi q_i c}{2}\left[J_1(q_i c)J_0(q_i c) - \frac{J_0(q_i c)J_1(q_i c)}{\mu_c}\right] A_c = -B_{ac}(q_i c)A_c \tag{4.51}$$

Since at the boundary $A_\varphi(h, z) = 0$ must also hold (we again work with a Dirichlet condition), the following equation is formed:

$$[A_a J_1(q_i r) + B_a Y_1(q_i r)]_{r=h} = 0 \Rightarrow A_{ac}(q_i c)J_1(q_i h) - B_{ac}(q_i c)Y_1(q_i h) = 0 \tag{4.52}$$

The eigenvalues q_i are the real positive roots of (4.52). Thus, the expressions for A_φ in all regions can be written in the following convenient form

$$A_1(r, z) = \sum_{i=1}^{\infty} \begin{matrix} J_1(q_i r) \\ R_1(q_i r) \end{matrix} \frac{e^{-q_i z} C_{1i}}{q_i} \quad \begin{matrix} 0 \le r \le c \\ c \le r \le h \end{matrix} \tag{4.53}$$

$$A_2(r, z) = \sum_{i=1}^{\infty} \begin{matrix} J_1(q_i r) \\ R_1(q_i r) \end{matrix} \frac{(e^{-q_i z} C_{2i} - e^{q_i z} B_{2i})}{q_i} \quad \begin{matrix} 0 \le r \le c \\ c \le r \le h \end{matrix} \tag{4.54}$$

$$A_3(r, z) = \sum_{i=1}^{\infty} J_1(\kappa_i r) \frac{(e^{-\kappa_i z} C_{3i} - e^{\kappa_i z} B_{3i})}{\kappa_i} \tag{4.55}$$

$$A_4(r, z) = -\sum_{i=1}^{\infty} J_1(\kappa_i r) \frac{e^{\lambda_i z}}{\lambda_i} B_{4i} \tag{4.56}$$

where we have used a couple of modifications for convenience: we have divided with the corresponding eigenvalue which we are allowed to do and

we have used the notation

$$R_n(q_i r) = A_{ac}(q_i c) J_n(q_i r) - B_{ac}(q_i c) Y_n(q_i r) \tag{4.57}$$

to simplify the expressions. The series (4.53)-(4.56) are truncated since only a finite number of terms is required in the numerical calculations and they are written using matrix notation. For an explanation of this notation consider for example the expression for A_4

$$A_4(r,z) = \left[J_1(\kappa_1 r)\ J_1(\kappa_2 r) \cdots \right] \cdot \begin{bmatrix} \lambda_1^{-1} & 0 & \cdots \\ 0 & \lambda_2^{-1} & \cdots \\ \vdots & \vdots & \ddots \end{bmatrix} \cdot \begin{bmatrix} e^{-\lambda_1 z} & 0 & \cdots \\ 0 & e^{-\lambda_2 z} & \cdots \\ \vdots & \vdots & \ddots \end{bmatrix} \cdot \begin{bmatrix} B_{41} \\ B_{42} \\ \vdots \end{bmatrix} \tag{4.58}$$

If we denote N_s the number of terms used, then the dimensions of vectors in (4.58) are also N_s and the dimensions of the square matrices are $N_s \times N_s$. Later we will discuss convergence and therefore the number of required terms. The matrix expressions for all regions are:

$$A_1(r,z) = \begin{matrix} J_1(\mathbf{q^T} r) \\ R_1(\mathbf{q^T} r) \end{matrix} \mathbf{q}^{-1} e^{-\mathbf{q}z} \mathbf{C}_1 \begin{matrix} 0 \le r \le c \\ c \le r \le h \end{matrix} \tag{4.59}$$

$$A_2(r,z) = \begin{matrix} J_1(\mathbf{q^T} r) \\ R_1(\mathbf{q^T} r) \end{matrix} \mathbf{q}^{-1} (e^{-\mathbf{q}z} \mathbf{C}_2 - e^{\mathbf{q}z} \mathbf{B}_2) \begin{matrix} 0 \le r \le c \\ c \le r \le h \end{matrix} \tag{4.60}$$

$$A_3(r,z) = J_1(\boldsymbol{\kappa}^{\mathbf{T}} r) \boldsymbol{\kappa}^{-1} (e^{-\boldsymbol{\kappa} z} \mathbf{C}_3 - e^{\boldsymbol{\kappa} z} \mathbf{B}_3) \tag{4.61}$$

$$A_4(r,z) = -J_1(\boldsymbol{\kappa}^{\mathbf{T}} r) \boldsymbol{\lambda}^{-1} e^{\boldsymbol{\lambda} z} \mathbf{B}_4 \tag{4.62}$$

where $J_1(\boldsymbol{\kappa}^{\mathbf{T}} r)$, $J_1(\mathbf{q}^{\mathbf{T}} \mathbf{r})$, $R_1(\mathbf{q}^{\mathbf{T}} \mathbf{r})$ are row vectors (denoted by the superscript $\mathbf{T}$), $\boldsymbol{\kappa}$, $\mathbf{q}$, $\boldsymbol{\lambda}$, $e^{\pm \boldsymbol{\kappa} \mathbf{z}}$, $e^{\pm \mathbf{q} \mathbf{z}}$, $e^{\boldsymbol{\lambda} \mathbf{z}}$ are diagonal matrices and $\mathbf{C}_i$, $\mathbf{B}_i$ are unknown column vector coefficients.

We will now describe the formation of the system of equations for the calculation of the unknown vector coefficients. This is performed through the application of interface conditions between the four regions of Fig.4.8:

- Interface $z = z_0$

From the continuity of B_z the following equation is formed:

$$J_0(\mathbf{q^T}r)e^{-\mathbf{q}z_0}\mathbf{C}_1 = J_0(\mathbf{q^T}r)(e^{-\mathbf{q}z_0}\mathbf{C}_2 - e^{\mathbf{q}z_0}\mathbf{B}_2); 0 \leq r \leq c \tag{4.63}$$

$$R_0(\mathbf{q^T}r)e^{-\mathbf{q}z_0}\mathbf{C}_1 = R_0(\mathbf{q^T}r)(e^{-\mathbf{q}z_0}\mathbf{C}_2 - e^{\mathbf{q}z_0}\mathbf{B}_3); c \leq r \leq h \tag{4.64}$$

If both sides of (4.63) are multiplied by $rJ_0(\mathbf{qr})$ and both sides of (4.64) are multiplied by $rR_0(\mathbf{qr})$ and then added and integrated from $r = 0$ to $r = h$ we take a matrix equation with both sides multiplied by the same matrix. If this matrix is dropped we have

$$e^{-\mathbf{q}z_0}\mathbf{C}_1 = e^{-\mathbf{q}z_0}\mathbf{C}_2 - e^{\mathbf{q}z_0}\mathbf{B}_2 \tag{4.65}$$

From the continuity of H_r inside the core and the discontinuity outside the core the following equations are formed:

$$\frac{1}{\mu_c}J_1(\mathbf{q^T}r)e^{-\mathbf{q}z_0}\mathbf{C}_1 = \frac{1}{\mu_c}J_1(\mathbf{q^T}r)(e^{-\mathbf{q}z_0}\mathbf{C}_2 + e^{\mathbf{q}z_0}\mathbf{B}_2); 0 \leq r \leq c \tag{4.66}$$

$$R_1(\mathbf{q^T}r)e^{-\mathbf{q}z_0}\mathbf{C}_1 = R_1(\mathbf{q^T}r)(e^{-\mathbf{q}z_0}\mathbf{C}_2 + e^{\mathbf{q}z_0}\mathbf{B}_2) + \mu_0 I\delta(r - r_0); c \leq r \leq h \tag{4.67}$$

If both sides of (4.66) are multiplied by $rJ_1(\mathbf{qr})$ and both sides of (4.67) are multiplied by $rR_1(\mathbf{qr})$ and then added and integrated from $r = 0$ to $r = h$ we find:

$$e^{-\mathbf{q}z_0}\mathbf{C}_1 = e^{-\mathbf{q}z_0}\mathbf{C}_2 + e^{\mathbf{q}z_0}\mathbf{B}_2 + \mu_0 I\mathbf{D}^{-1}r_0R_1(\mathbf{q}r) \tag{4.68}$$

- Interface $z = 0$

From the continuity of B_z the following equations are formed:

$$J_0(\mathbf{q^T}r)(\mathbf{C}_2 - \mathbf{B}_2) = J_0(\boldsymbol{\kappa}^{\mathbf{T}}r)(\mathbf{C}_3 - \mathbf{B}_3); 0 \leq r \leq c \tag{4.69}$$

$$R_0(\mathbf{q^T}r)(\mathbf{C}_2 - \mathbf{B}_2) = J_0(\boldsymbol{\kappa}^{\mathbf{T}}r)(\mathbf{C}_3 - \mathbf{B}_3); c \leq r \leq h \tag{4.70}$$

If both sides of (4.69) and (4.70) are multiplied by $rJ_0(\boldsymbol{\kappa}r)$ and then added and integrated from $r = 0$ to $r = h$ we find:

$$\mathbf{T}(\mathbf{C}_2 - \mathbf{B}_2) = \mathbf{E}(\mathbf{C}_3 - \mathbf{B}_3) \tag{4.71}$$

From the continuity of H_r the following equations are formed:

$$\frac{1}{\mu_c}J_1(\mathbf{q^T}r)(\mathbf{C}_2 + \mathbf{B}_2) = J_1(\boldsymbol{\kappa}^{\mathbf{T}}r)(\mathbf{C}_3 + \mathbf{B}_3); 0 \leq r \leq c \tag{4.72}$$

$$R_1(\mathbf{q}^{\mathbf{T}}r)(\mathbf{C}_2+\mathbf{B}_2)=J_1(\boldsymbol{\kappa}^{\mathbf{T}}r)(\mathbf{C}_3+\mathbf{B}_3);c\leq r\leq h \tag{4.73}$$

If both sides of (4.72) and (4.73) are multiplied by $rJ_1(\boldsymbol{\kappa}r)$ and then added and integrated from $r=0$ to $r=h$ we find:

$$\mathbf{U}(\mathbf{C}_2+\mathbf{B}_2)=\mathbf{E}(\mathbf{C}_3+\mathbf{B}_3) \tag{4.74}$$

- Interface $z=-l$

From the continuity of B_z and H_r the following equations are formed:

$$J_0(\boldsymbol{\kappa}^{\mathbf{T}}r)(e^{\boldsymbol{\kappa}l}\mathbf{C}_3-e^{-\boldsymbol{\kappa}l}\mathbf{B}_3)=-J_0(\boldsymbol{\kappa}^{\mathbf{T}}r)\boldsymbol{\kappa}\boldsymbol{\lambda}^{-1}e^{-\boldsymbol{\lambda}l}\mathbf{B}_4 \tag{4.75}$$

$$J_1(\boldsymbol{\kappa}^{\mathbf{T}}r)(e^{\boldsymbol{\kappa}l_1}\mathbf{C}_3+e^{-\boldsymbol{\kappa}l}\mathbf{B}_3)=\frac{1}{\mu_r}J_1(\boldsymbol{\kappa}^{\mathbf{T}}r)e^{-\boldsymbol{\lambda}l}\mathbf{B}_4 \tag{4.76}$$

If both sides of (4.75) and (4.76) are multiplied by $rJ_0(\boldsymbol{\kappa}r)$ and $rJ_1(\boldsymbol{\kappa}r)$ respectively and integrated from $r=0$ to $r=h$ we take matrix equations with both sides multiplied by the same matrix. If this matrix is dropped we have:

$$e^{\boldsymbol{\kappa}l}\mathbf{C}_3-e^{-\boldsymbol{\kappa}l}\mathbf{B}_3=-\boldsymbol{\kappa}\boldsymbol{\lambda}^{-1}e^{-\boldsymbol{\lambda}l}\mathbf{B}_4 \tag{4.77}$$

$$e^{\boldsymbol{\kappa}l}\mathbf{C}_3+e^{-\boldsymbol{\kappa}l}\mathbf{B}_3=\frac{1}{\mu_r}e^{-\boldsymbol{\lambda}l}\mathbf{B}_4 \tag{4.78}$$

In order to give a closed form expression for the elements of the matrices created so far, the following property of Bessel integrals has been extensively used

$$\begin{aligned}\int^{z}(k^2-l^2)\,t\,\Xi_n(kt)\Psi_n(lt)dt &= z[k\,\Xi_{n+1}(kz)\Psi_n(lz)-l\,\Xi_n(kz)\Psi_{n+1}(lz)]\\ &= -z[k\,\Xi_{n-1}(kz)\Psi_n(lz)-l\,\Xi_n(kz)\Psi_{n-1}(lz)]\end{aligned} \tag{4.79}$$

where Ξ_n, Ψ_n are any two Bessel (circular cylinder) functions or linear

combinations of them. The matrices **D**, **E**, **T**, **U** elements are defined by:

$$\begin{aligned}\mathbf{D}_{ij} &= \frac{1}{\mu_c}\int_{r=0}^{c} J_1(q_i r)J_1(q_j r)rdr + \int_{r=c}^{h} R_1(q_i r)R_1(q_j r)rdr \qquad (4.80)\\ &= 0 \quad i \neq j\\ &= \frac{h^2}{2}R_0^2(q_i h) + \frac{c^2}{2}\left(1-\frac{1}{\mu_c}\right)\left[\frac{J_0^2(q_i c)}{\mu_c} - J_1^2(q_i c)\right] \quad i = j\end{aligned}$$

$$\begin{aligned}\mathbf{E}_{ij} &= \int_{r=0}^{h} J_1(\kappa_i r)J_1(\kappa_j r)rdr = 0 \quad i \neq j \qquad (4.81)\\ &= \frac{h^2}{2}J_0^2(\kappa_i h) \quad i = j\end{aligned}$$

$$\begin{aligned}\mathbf{T}_{ij} &= \int_{r=0}^{c} J_0(\kappa_i r)J_0(q_j r)rdr + \int_{r=c}^{h} J_0(\kappa_i r)R_0(q_j r)rdr \qquad (4.82)\\ &= \frac{c}{\kappa_i^2 - q_j^2}\kappa_i J_1(\kappa_i c)J_0(q_j c)\left(1-\frac{1}{\mu_c}\right) \quad \kappa_i \neq q_j\\ &= \frac{h^2}{2}J_0(\kappa_i h)R_0(\kappa_i h) + \frac{c^2}{2}J_0^2(\kappa_i c)\left(1-\frac{1}{\mu_c}\right) \quad \kappa_i = q_j\end{aligned}$$

$$\begin{aligned}\mathbf{U}_{ij} &= \frac{1}{\mu_c}\int_{r=0}^{c} J_1(\kappa_i r)J_1(q_j r)rdr + \int_{r=c}^{h} J_1(\kappa_i r)R_1(q_j r)rdr \qquad (4.83)\\ &= \frac{c}{\kappa_i^2 - q_j^2}\kappa_i J_0(\kappa_i c)J_1(q_j c)\left(1-\frac{1}{\mu_c}\right) \quad \kappa_i \neq q_j\\ &= \frac{h^2}{2}J_0(\kappa_i h)R_0(\kappa_i h) - \frac{c^2}{2}J_1(\kappa_i c)R_1(\kappa_i c)\left(1-\frac{1}{\mu_c}\right) \quad \kappa_i = q_j\end{aligned}$$

Eqs (4.65), (4.68), (4.71), (4.74), (4.77), (4.78) form a 6×6 system of equations for the unknown coefficients. Its solution is:

$$\mathbf{C}_1 = (\mathbf{N}\mathbf{M}^{-1} - e^{2\mathbf{q}z_0})\mathbf{B}_2 \qquad (4.84)$$

$$\mathbf{C}_2 = \mathbf{N}\mathbf{M}^{-1}\mathbf{B}_2 \qquad (4.85)$$

$$\mathbf{B}_2 = -\frac{\mu_0 I}{2} e^{-\mathbf{q}z_0} \mathbf{D}^{-1} r_0 R_1(\mathbf{q}r_0) \tag{4.86}$$

$$\mathbf{C}_3 = e^{-\boldsymbol{\kappa} l}(\mathbf{I} - \mu_r \boldsymbol{\kappa}\boldsymbol{\lambda}^{-1}) e^{-\boldsymbol{\lambda} l} \mathbf{M}^{-1} \mathbf{B}_2 \tag{4.87}$$

$$\mathbf{B}_3 = e^{\boldsymbol{\kappa} l}(\mathbf{I} + \mu_r \boldsymbol{\kappa}\boldsymbol{\lambda}^{-1}) e^{-\boldsymbol{\lambda} l} \mathbf{M}^{-1} \mathbf{B}_2 \tag{4.88}$$

$$\mathbf{B}_4 = 2\mu_r \mathbf{M}^{-1} \mathbf{B}_2 \tag{4.89}$$

where

$$\mathbf{N} = \left[(\mathbf{U}^{-1} + \mathbf{T}^{-1}) e^{-\boldsymbol{\kappa} l}(\mathbf{I} - \mu_r \boldsymbol{\kappa}\boldsymbol{\lambda}^{-1}) + (\mathbf{U}^{-1} - \mathbf{T}^{-1}) e^{\boldsymbol{\kappa} l}(\mathbf{I} + \mu_r \boldsymbol{\kappa}\boldsymbol{\lambda}^{-1})\right] \cdot \cdot \frac{1}{2} e^{-\boldsymbol{\lambda} l} \mathbf{E} \tag{4.90}$$

$$\mathbf{M} = \left[(\mathbf{U}^{-1} - \mathbf{T}^{-1}) e^{-\boldsymbol{\kappa} l}(\mathbf{I} - \mu_r \boldsymbol{\kappa}\boldsymbol{\lambda}^{-1}) + (\mathbf{U}^{-1} + \mathbf{T}^{-1}) e^{\boldsymbol{\kappa} l}(\mathbf{I} + \mu_r \boldsymbol{\kappa}\boldsymbol{\lambda}^{-1})\right] \cdot \cdot \frac{1}{2} e^{-\boldsymbol{\lambda} l} \mathbf{E} \tag{4.91}$$

and $\mathbf{I}$ denotes the $N_s \times N_s$ unit matrix.

4.4.2 *Finite thickness coil with cylindrical core*

Now we can apply superposition as in the previous chapter to calculate the magnetic vector potential in the various regions for the coil of rectangular cross-section shown in Fig.4.9. Using an integration of the form

$$\int_{r_1}^{r_2} \int_{z_1}^{z_2} A(r, z, r_0, z_0) dr_0 dz_0 \tag{4.92}$$

the following expressions are derived:

$$\begin{aligned} A_1(r,z) = & -\frac{\mu_0 \iota_0}{2} \begin{matrix} J_1(\mathbf{q}^{\mathbf{T}} r) \\ R_1(\mathbf{q}^{\mathbf{T}} r) \end{matrix} \\ & \cdot \ \mathbf{q}^{-1} e^{-\mathbf{q}z} [(\mathbf{N}\mathbf{M}^{-1}(e^{-\mathbf{q}z_1} - e^{-\mathbf{q}z_2}) - (e^{\mathbf{q}z_2} - e^{\mathbf{q}z_1})] \\ & \cdot \ \mathbf{q}^{-3} \mathbf{D}^{-1} \chi_R(\mathbf{q}r_1, \mathbf{q}r_2) \quad \begin{matrix} 0 \le r \le c \\ c \le r \le h \end{matrix} \end{aligned} \tag{4.93}$$

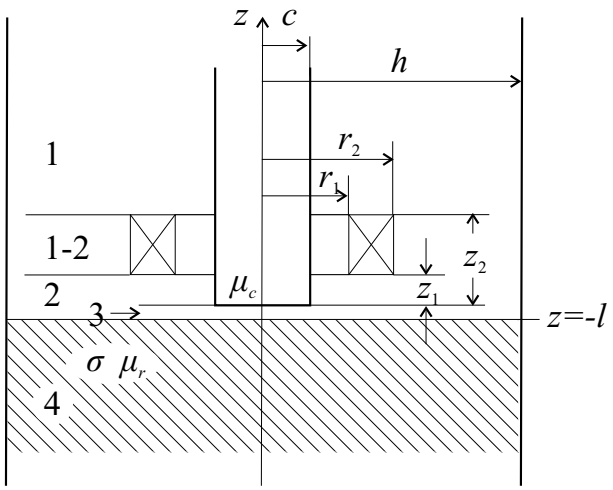

Fig. 4.9 2D axisymmetric view of finite thickness coil with I-ferrite core. The solution domain is truncated at $r = h$.

$$A_2(r,z) = -\frac{\mu_0 \iota_0}{2} \begin{matrix} J_1(\mathbf{q^T} r) \\ R_1(\mathbf{q^T} r) \end{matrix} \mathbf{q}^{-1} e^{-\mathbf{q}z} (\mathbf{N}\mathbf{M}^{-1} - e^{\mathbf{q}z})(e^{-\mathbf{q}z_1} - e^{-\mathbf{q}z_2}) \cdot \mathbf{q}^{-3}\mathbf{D}^{-1}\chi_R(\mathbf{q}r_1, \mathbf{q}r_2) \quad \begin{matrix} 0 \le r \le c \\ c \le r \le h \end{matrix} \tag{4.94}$$

$$A_3\ (\ r,z) = -\frac{\mu_0 \iota_0}{2} J_1(\boldsymbol{\kappa}^{\mathbf{T}} r)\boldsymbol{\kappa}^{-1} \cdot [e^{-\boldsymbol{\kappa}(z+l)}(\mathbf{I} - \mu_r \boldsymbol{\kappa}\boldsymbol{\lambda}^{-1}) - e^{\boldsymbol{\kappa}(z+l)}(\mathbf{I} + \mu_r \boldsymbol{\kappa}\boldsymbol{\lambda}^{-1})] e^{-\boldsymbol{\lambda}l}\mathbf{M}^{-1}(e^{-\mathbf{q}z_1} - e^{-\mathbf{q}z_2}) \cdot \mathbf{q}^{-3}\mathbf{D}^{-1}\chi_R(\mathbf{q}r_1, \mathbf{q}r_2) \tag{4.95}$$

$$A_4(r,z) = \mu_0 \mu_r \iota_0 J_1(\boldsymbol{\kappa}^{\mathbf{T}} r)\boldsymbol{\lambda}^{-1} \cdot e^{\boldsymbol{\lambda}z}\mathbf{M}^{-1}(e^{-\mathbf{q}z_1} - e^{-\mathbf{q}z_2})\mathbf{q}^{-3}\mathbf{D}^{-1}\chi_R(\mathbf{q}r_1, \mathbf{q}r_2) \tag{4.96}$$

where $\iota_0 = NI/[(r_2 - r - 1)(z_2 - z_1)] = nI$ is the coil current density and $\chi_R(x_1, x_2) = \int_{x_1}^{x_2} xR_1(x)dx$. The potential A_{1-2} in the region between z_1 and z_2 is computed again by replacing z_2 with $= z$ in (4.93) and z_1 with z

in (4.94) and adding them:

$$A_{1-2}(r,z) = \frac{\mu_0 \iota_0}{2} \begin{matrix} J_1(\mathbf{q^T} r) \\ R_1(\mathbf{q^T} r) \end{matrix} \mathbf{q}^{-1} \cdot [2\mathbf{I} - e^{-\mathbf{q}(z-z_1)} - e^{\mathbf{q}(z-z_2)} - e^{-\mathbf{q}z}\mathbf{N}\mathbf{M}^{-1}(e^{-\mathbf{q}z_1} - e^{-\mathbf{q}z_2})] \cdot \mathbf{q}^{-3}\mathbf{D}^{-1}\chi_R(\mathbf{q}r_1, \mathbf{q}r_2) \quad \begin{matrix} 0 \le r \le c \\ c \le r \le h \end{matrix} \tag{4.97}$$

Once the magnetic vector potential has been determined, all electromagnetic field quantities can also be computed. The eddy current density in the conductive half-space can easily be calculated from

$$J_\varphi(r,z) = -j\omega\sigma A_4(r,z) \tag{4.98}$$

and the magnetic flux density in the conductor is calculated from

$$\mathbf{B}_4(r,z) = -\mu_0\mu_r\iota_0[\mathbf{r}_0 J_1(-\boldsymbol{\kappa}^{\mathbf{T}} r) + \mathbf{z}_0 J_0(\boldsymbol{\kappa}^{\mathbf{T}} r)\boldsymbol{\kappa}\boldsymbol{\lambda}^{-1}] \cdot e^{\boldsymbol{\lambda}z}\mathbf{M}^{-1}(e^{-\mathbf{q}z_1} - e^{-\mathbf{q}z_2})\mathbf{q}^{-3}\mathbf{D}^{-1}\chi_R(\mathbf{q}r_1, \mathbf{q}r_2) \tag{4.99}$$

Finally, the impedance of the coil is computed by integrating rA_{1-2} over the cross-section of the coil

$$Z = \frac{j2\pi\omega i_0}{I^2} \int_{r_1}^{r_2} \int_{z_1}^{z_2} rA_{1-2}(r,z)\,dr_0\,dz_0 \tag{4.100}$$

The final expression is:

$$Z = j\omega\mu_0\pi n^2 \chi_R(\mathbf{q^T}r_1, \mathbf{q^T}r_2)\mathbf{q}^{-4} \cdot [2(z_2 - z_1)\mathbf{q} - (e^{-\mathbf{q}z_1} - e^{-\mathbf{q}z_2})\mathbf{N}\mathbf{M}^{-1}(e^{-\mathbf{q}z_1} - e^{-\mathbf{q}z_2}) - 2e^{\mathbf{q}z_1}(e^{-\mathbf{q}z_1} - e^{-\mathbf{q}z_2})]\,\mathbf{q}^{-3}\mathbf{D}^{-1}\chi_R(\mathbf{q}r_1, \mathbf{q}r_2) \tag{4.101}$$

The impedance and the inductance of the coil in the absence of the conductive half-space can also be computed from (4.101) by setting $\sigma = 0$. The only change in the above expression is that the product $\mathbf{NM^{-1}}$ is reduced to $(\mathbf{I} - \mathbf{D}^{-1}\mathbf{T}\mathbf{E}^{-1}\mathbf{U})(\mathbf{I} + \mathbf{D}^{-1}\mathbf{T}\mathbf{E}^{-1}\mathbf{U})^{-1}$ and therefore only a single inversion of a full matrix (represented by the second parenthesis) is required. In contrast, the general calculation of (4.101) requires three full matrix inversions, namely $\mathbf{T}$, $\mathbf{U}$ and $\mathbf{M}$.

4.4.3 *Limiting cases and numerical aspects*

Eq.(4.101) is a useful tool in the design and performance optimization of the ferrite-cored probe. Such studies were done until now either experimentally, Popov (1974) and Capobianco (1990), or by using numerical methods such as FEM, Sabbagh (1987) or VIM, Buvat (2002). The numerical methods are quite flexible and for the purposes of 2D axisymmetric NDE models more than adequate. However, they are time consuming especially in cases where a large number of impedance calculations is required and the modification of parameters is a cumbersome job.

In the above equations we notice that three matrix inversions are required. The situation is somewhat simplified, needing only two matrix inversions in the limiting case of an infinite core permeability. In this case the matrices $\mathbf{D}$, $\mathbf{E}$, $\mathbf{T}$, $\mathbf{U}$ are calculated again from (4.80)-(4.83) in the limit of $\mu_r \to \infty$ and matrices $\mathbf{N}$, $\mathbf{M}$ from

$$\mathbf{N} = (\mathbf{U}^{-1}\mathbf{E}+\mathbf{D}^{-1}\mathbf{T})e^{-\boldsymbol{\kappa} l}(\mathbf{I}-\mu_r\boldsymbol{\kappa}\boldsymbol{\lambda}^{-1})+(\mathbf{U}^{-1}\mathbf{E}-\mathbf{D}^{-1}\mathbf{T})e^{\boldsymbol{\kappa} l}(\mathbf{I}+\mu_r\boldsymbol{\kappa}\boldsymbol{\lambda}^{-1}) \tag{4.102}$$

$$\mathbf{M} = (\mathbf{U}^{-1}\mathbf{E}-\mathbf{D}^{-1}\mathbf{T})e^{-\boldsymbol{\kappa} l}(\mathbf{I}-\mu_r\boldsymbol{\kappa}\boldsymbol{\lambda}^{-1})+(\mathbf{U}^{-1}\mathbf{E}+\mathbf{D}^{-1}\mathbf{T})e^{\boldsymbol{\kappa} l}(\mathbf{I}+\mu_r\boldsymbol{\kappa}\boldsymbol{\lambda}^{-1}) \tag{4.103}$$

It is also easy to show how the above expressions reduce to the ones for an air-cored coil. By putting $\mu_c = 1$, the matrices $\mathbf{D}$, $\mathbf{T}$, $\mathbf{U}$ reduce to $\mathbf{E}$ and also the eigenvalues q_i reduce to κ_i. After some manipulation, the matrix product in (4.101) becomes

$$\mathbf{N}\mathbf{M}^{-1} = (\boldsymbol{\lambda} - \boldsymbol{\kappa}\mu_r)(\boldsymbol{\lambda} + \boldsymbol{\kappa}\mu_r) \tag{4.104}$$

and the expression of Z reduces to the matrix form of the superposition of (4.37) and (4.38).

The additional numerical aspect of the solution is the calculation of the eigenvalues q_i, i.e. the real roots of (4.52). We have a choice between several methods including the bisection and the Newton-Raphson method, Press (2001). The roots can also be computed numerically with Mathematica with the following code, after importing the relevant package `<< NumericalMath‘BesselZeros‘` and defining `Aac` and `Bac`

```
k=BesselJZeros[1,Ns]/h;
FindRoot[Aac BesselJ[1,q h]-Bac BesselY[1,q h]==0,q,k]
```

The first code line can be used for computing the eigenvalues κ_i needed in all cases examined throughout this chapter. Another aspect of the solution

is its convergence and the number of the required sum terms N_s. We have observed that convergence is not worse than the case of the air-cored coil and fewer terms are needed for the ferrite-cored coil than those in Tables 4.2 and 4.3. We can use the number of terms N_s for the air-cored coils as a number that guarantees convergence to an accurate result. The difficulty when using the TREE method is that if we want to calculate for example for N_s and $N_s + 1$ terms in order to check convergence we have to solve the problem twice. This is not required for the air-cored coil because in that case we can just add the extra term.

4.4.4 *Cylindrical core of finite height*

The approximation in the previous paragraph, of a real core with a semi-infinite cylinder, is a rather crude one, but it was selected because it was the simplest configuration to solve with the TREE method. The interested reader can refer to Theodoulidis (2002b) for the analysis in the case of a core with finite length as shown in Fig.4.10. The core has a finite height z_c and,

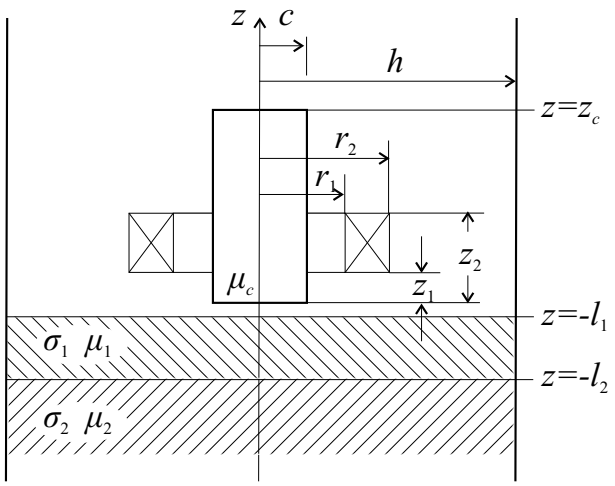

Fig. 4.10 2D axisymmetric view of finite thickness coil with I-ferrite core of finite height above a layered conductor. The solution domain is truncated at $r = h$.

in addition, the conductor configuration is more general since it comprises two layers with conductivity σ_i and relative magnetic permeability μ_i. The solution method is similar with the addition of an extra interface at the top of the core, which is treated in the same way with the interface at the

core bottom. We present the final expression for the impedance of the coil following the notation used in the previous paragraph

$$\begin{aligned} Z = {} & j\omega\mu_0\pi n^2 \chi_R(\mathbf{q^T}r_1, \mathbf{q^T}r_2)\mathbf{q}^{-4} \\ & \cdot \{2(z_2 - z_1)\mathbf{q} + e^{-\mathbf{q}z_2}e^{\mathbf{q}z_1} - e^{\mathbf{q}z_2}e^{-\mathbf{q}z_1} \\ & -[(e^{-\mathbf{q}z_1} - e^{-\mathbf{q}z_2})\mathbf{F} - (e^{\mathbf{q}z_2} - e^{\mathbf{q}z_1})\mathbf{G}]\mathbf{W}\}\ \mathbf{q}^{-3}\mathbf{D}^{-1}\chi_R(\mathbf{q}r_1, \mathbf{q}r_2) \end{aligned} \tag{4.105}$$

where

$$\begin{aligned} \mathbf{W} = {} & \left[(\mathbf{T} + \mathbf{U})e^{\mathbf{q}z_c}\mathbf{G} - (\mathbf{T} - \mathbf{U})e^{-\mathbf{q}z_c}\mathbf{F}\right]^{-1} \\ & \cdot \left[(\mathbf{T} + \mathbf{U})e^{\mathbf{q}z_c}(e^{-\mathbf{q}z_1} - e^{-\mathbf{q}z_2}) - (\mathbf{T} - \mathbf{U})e^{-\mathbf{q}z_c}(e^{\mathbf{q}z_2} - e^{\mathbf{q}z_1})\right] \end{aligned} \tag{4.106}$$

and

$$\begin{matrix} \mathbf{F} \\ \mathbf{G} \end{matrix} = \frac{1}{2}\left[(\mathbf{U}^{-1} \pm \mathbf{T}^{-1})\mathbf{E}\mathbf{F}_1 + (\mathbf{U}^{-1} \mp \mathbf{T}^{-1})\mathbf{E}\mathbf{G}_1\right] \tag{4.107}$$

$$\begin{matrix} \mathbf{F}_1 \\ \mathbf{G}_1 \end{matrix} = \frac{1}{2}e^{\mp\boldsymbol{\kappa}l_1}\left[(\mathbf{I} \pm \mu_1\boldsymbol{\kappa}\boldsymbol{\lambda}_1^{-1})e^{\boldsymbol{\lambda}_1 l_1}\mathbf{F}_2 + (\mathbf{I} \mp \mu_1\boldsymbol{\kappa}\boldsymbol{\lambda}_1^{-1})e^{-\boldsymbol{\lambda}_1 l_1}\mathbf{G}_2\right] \tag{4.108}$$

$$\begin{matrix} \mathbf{F}_2 \\ \mathbf{G}_2 \end{matrix} = \frac{1}{2}e^{\mp\boldsymbol{\lambda}_1 l_2}(\mathbf{I} \mp \mu_2\boldsymbol{\lambda}_1\boldsymbol{\lambda}_2^{-1})e^{-\boldsymbol{\lambda}_2 l_2} \tag{4.109}$$

The matrices $\mathbf{D}$, $\mathbf{E}$, $\mathbf{T}$, $\mathbf{U}$ are defined as in (4.80)-(4.83) and the function $\chi(x_1, x_2)$ as in (3.27). Note that these expressions correct some sign errors in the original expressions in Theodoulidis (2000b).

The impedance of both the isolated probe and the probe above a conductor should converge to a limit when increasing the core permeability μ_c. For such high permeability values the core can be modelled as an area of infinite μ_c and therefore only its surface needs to be considered. For infinite μ_c, all magnetic flux lines enter the core in a perpendicular manner and, thus, the core enters the calculations with a boundary condition that the magnetic field at its surface does not have a tangential component. Such an approximation can be justified not only by theoretical analysis but also by experimental measurements, see for example Capobianco (1990), where it was shown that for $\mu_c > 800$, permeability changes had no significant (measurable) effect on the impedance (when inspecting both cracked or un-cracked conductors).

In the following we will give some theoretical results derived by varying parameters such as the core permeability and the excitation frequency. The coil+core as well as conductor data are shown in Table 4.4. Consider for

Table 4.4 Coil and half-space parameters used for Figs 4.11 and 4.12.

Coil		Half-space	
r_1	4 mm	$\sigma_1 = \sigma_2$	35.4 MS/m
r_2	6 mm	$\mu_1 = \mu_2$	1
$z_2 - z_1$	4 mm	l_1	1 mm
z_1	0 mm	l_2	1 mm
N	800	h	$10r_2$
c	4 mm		

example Fig.4.11, which shows the inductance of the coil for increasing μ_c. The behavior of L_0 shows that for μ_c above 1000 there is no difference in the results. This observation justifies our expectation. The diagram shows also the dependence of L_0 with core height z_c for constant coil height $z_2 - z_1$. The inductance increases when the ferrite core height increases, rapidly in the beginning and then tends to a constant value for a semi-infinite core.

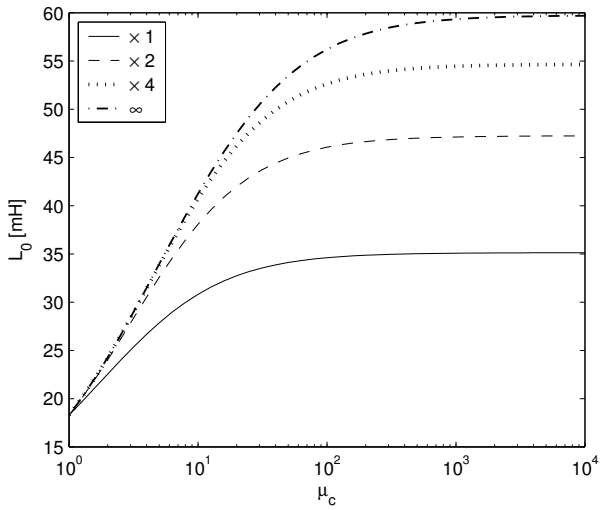

Fig. 4.11 Variation of the isolated ferrite-cored coil inductance with the relative magnetic permeability. The different curves are produced for z_c equal to the depicted number times the coil height $z_2 - z_1$.

Fig.4.12 shows the variation of the normalized impedance for the same coil with an air core and with a ferrite core of $\mu_c = 1000$ and height $z_c = 2(z_2 - z_1)$. The frequency curves are produced by varying f from 100Hz to 1MHz. The ferrite core impedance change is more pronounced due to the

better electromagnetic coupling with the conductor. Note that in Fig.4.12 the impedance is normalized and for the ferrite-cored coil it is divided by a larger number since $L_0 = 20.3$mH while for the air-cored $L_0 = 5.85$mH. Thus, in absolute terms the impedance change is even greater. This larger signal of the ferrite-cored coils (due to the concentration of the field) is the reason for their superiority over air-cored probes in specific applications and for their widespread use.

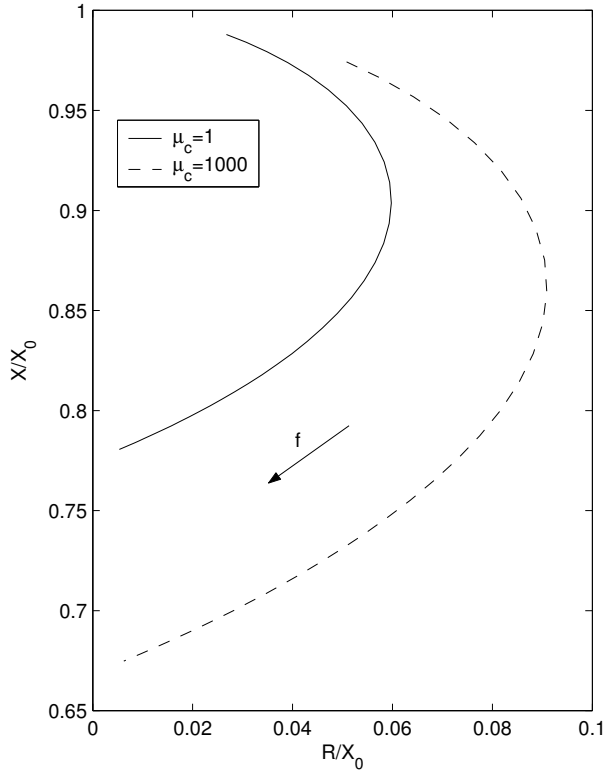

Fig. 4.12 Impedance plane diagram showing variation of normalized Z with frequency for an air-cored and a ferrite-cored coil above a conductive half-space. X_0 stands for each coil's isolated reactance.

4.5 Coil above half-space with cylindrical inhomogeneity

We have just demonstrated the ability of the TREE method to solve canonical problems such as the ferrite-cored coil, that until now evaded analytical treatment. We now proceed to apply the method to solve another axisymmetric configuration of great interest, shown in Fig.4.13.

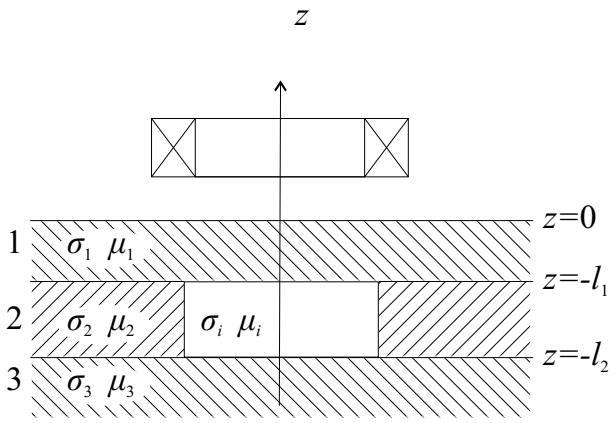

Fig. 4.13 2D axisymmetric view of the general problem of a cylindrical inhomogeneity in a layered conductor system.

The configuration simulates a layered conductive half-space with a cylindrical inhomogeneity in it. Each layer can have a different conductivity and permeability and so does the inhomogeneity. By choosing these parameters we can simulate a number of different configurations. For example, if $\sigma_3 = \sigma_i = 0$ we can simulate the case of subsurface corrosion or if $\sigma_1 = \sigma_3 = \sigma_i = 0$ we can simulate the case of a plate with a through wall cylindrical hole. In principle, all of these configurations can be treated with the TREE method, but here we will limit our study to the axisymmetric eddy current problem of a coil over a half-space with an infinitely deep hole. This configuration is shown in Fig.4.15 and it is generated from Fig.4.13 by setting $l_1 = 0$ and $l_2 \to \infty$. Following similar steps all other interesting configurations generated by Fig.4.13 can be studied by the interested reader.

As we will see, the basic difference in the use of the TREE method between the problem of Fig.4.13 and the ferrite-cored coil problem is that now the eigenvalues in region 2, which includes the inhomogeneity, are complex and this adds an extra numerical aspect in the problem since we

have to use an efficient method of computing roots of a complex equation.

4.6 Half-space with cylindrical hole

The "cylindrical hole in a conductor" problem can be seen as a highly idealized model of eddy current inspection of fastener holes in aircraft structures. First, we solve it for a filamentary coil and then we apply superposition to solve for the rectangular cross-section coil.

4.6.1 *Filamentary coil*

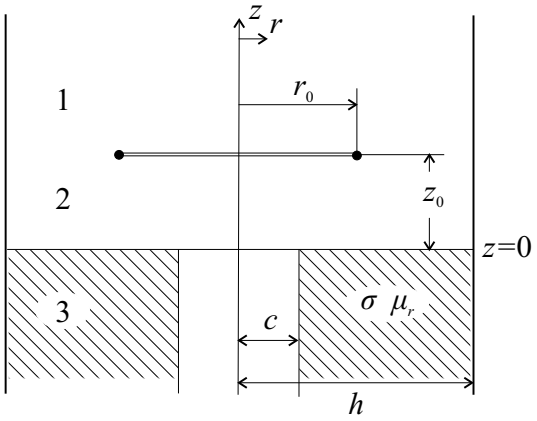

Fig. 4.14 2D axisymmetric view of a cylindrical coil above a conductive half-space. The solution domain is truncated at $r = h$.

The geometry involving the filamentary coil is the same as in Fig.4.2 with only the addition of the cylindrical hole with radius c. As in the analysis of the ferrite-cored coil, the problem is in region 3 where we have to construct appropriate eigenfunction expansions in order to match the expressions for the potential in the hole and in the conductor at the vertical boundary $r = c$. After expanding the magnetic vector potential A_φ in a series of appropriate eigenfunctions, a homogeneous Dirichlet condition is imposed on the outer boundary $r = h$. First we consider a filamentary source coil and assume a harmonic current excitation of the form $Ie^{j\omega t}$. Taking into account all the remarks made in the solution of the ferrite-cored coil problem, the expressions for A_φ in regions 1 and 2 of Fig.4.14

can be written as

$$A_1(r,z) = \sum_{i=1}^{\infty} J_1(\kappa_i r) e^{-\kappa_i z} D_i^{(1)} \tag{4.110}$$

$$A_2(r,z) = \sum_{i=1}^{\infty} J_1(\kappa_i r) \left(e^{\kappa_i z} C_i^{(2)} + e^{-\kappa_i z} D_i^{(2)} \right) \tag{4.111}$$

where κ_i are the eigenvalues computed again from

$$J_1(\kappa_i h) = 0 \tag{4.112}$$

In region 3, separation of variables implies that a solution is sought in the form of a product of two functions, which are conveniently written for a conductive region as:

$$R(r) = A(q) J_1(qr) + B(q) Y_1(qr) \tag{4.113}$$

$$Z(z) = C(q) e^{pz} + D(q) e^{-pz} \tag{4.114}$$

where the eigenvalues are q and $p = \sqrt{q^2 + j\omega\mu_0\mu_r\sigma}$. In order to construct a solution for the nonconductive region, one can either replace p in the exponential function arguments of (4.114) with q or replace q in the Bessel function arguments of (4.113) with p. In either case the Laplace equation for the magnetic vector potential in air is satisfied. The latter option is non-conventional but it has been adopted for the non-conductive region of the hole, allowing the $z-$dependence of the solution for the nonconductive region to conform to that used for the conductive region. We can of course generalize this in the case of a hole filled with conductive material by replacing q in the Bessel function arguments of (4.113) with $\sqrt{q^2 + j\omega\mu_0\mu_r\Delta\sigma}$ where $\Delta\sigma = \sigma_{\text{con}} - \sigma_{\text{hole}}$ with σ_{con} and σ_{hole} standing for the conductor and hole conductivities respectively. Note that for $\sigma_{\text{hole}} = 0$, it reduces to q being replaced by p, as already discussed. In any case, with this eigenfunction arrangement both differential equations in the hole and conductor regions (Laplace and Helmholtz respectively) are satisfied and most importantly, this is done with expansions that have the same z-dependence. Although we could discuss the general case of a hole filled with conductive material, here we focus on the special case of $\sigma_{\text{hole}} = 0$, leaving again the general case for the interested reader. The expressions for the two subregions are

then written as:

$$A_3^{\text{hole}}(r,z) = \sum_{i=1}^{\infty} J_1(p_i r) e^{p_i z} C_i^{(3-\text{h})} \tag{4.115}$$

$$A_3^{\text{con}}(r,z) = \sum_{i=1}^{\infty} \left[C_i^{(3-\text{c})} J_1(q_i r) + D_i^{(3-\text{c})} Y_1(q_i r) \right] e^{p_i z} \tag{4.116}$$

where $C_i^{(3-\text{h})}$, $C_i^{(3-\text{c})}$ and $D_i^{(3-\text{c})}$ are unknown expansion coefficients. Now, in order to satisfy the homogeneous Dirichlet boundary condition $A_3^{\text{con}}(h,z) = 0$ in a term-by-term basis we set the term in parenthesis in (4.116) to zero

$$C_i^{(3-\text{c})} J_1(q_i h) + D_i^{(3-\text{c})} Y_1(q_i h) = 0 \tag{4.117}$$

which means that the radial dependence of A_3^{con} can be rewritten as

$$\left[Y_1(q_i h) J_1(q_i r) - J_1(q_i h) Y_1(q_i r) \right] C_i^{(3)} \tag{4.118}$$

By satisfying also the continuity of B_r (or A_φ) at the hole surface (interface $r = c$) we can rearrange these equations, so that

$$A_3^{\text{hole}}(r,z) = \sum_{i=1}^{\infty} \left[Y_1(q_i h) J_1(q_i c) - J_1(q_i h) Y_1(q_i c) \right] J_1(p_i r) e^{p_i z} C_i^{(3)} \tag{4.119}$$

$$A_3^{\text{con}}(r,z) = \sum_{i=1}^{\infty} J_1(p_i c) \left[Y_1(q_i h) J_1(q_i r) - J_1(q_i h) Y_1(q_i r) \right] e^{p_i z} C_i^{(3)} \tag{4.120}$$

and the unknown coefficients have been merged to a single coefficient $C_i^{(3)}$. Using the notation

$$R_n(q_i r) = Y_1(q_i h) J_n(q_i r) - J_1(q_i h) Y_n(q_i r) \tag{4.121}$$

(4.119) and (4.120) can be written as follows

$$A_3^{\text{hole}}(r,z) = \sum_{i=1}^{\infty} R_1(q_i c) J_1(p_i r) e^{p_i z} C_i^{(3)} \tag{4.122}$$

$$A_3^{\text{con}}(r,z) = \sum_{i=1}^{\infty} J_1(p_i c) R_1(q_i r) e^{p_i z} C_i^{(3)} \tag{4.123}$$

The expressions in the two subregions of region 3 have now been written with a common z-dependence and since they involve only one unknown coefficient they are treated as one region. After truncating all the above expressions after N_s terms they can be rewritten using matrix notation as

$$A_1(r,z) = J_1(\boldsymbol{\kappa}^{\mathbf{T}} r) e^{-\boldsymbol{\kappa} z} \mathbf{D}^{(1)} \tag{4.124}$$

In (4.124) $J_1(\boldsymbol{\kappa}^{\mathbf{T}} r)$ is a $1 \times N_s$ vector, $e^{-\boldsymbol{\kappa} z}$ is a $N_s \times N_s$ matrix and $\mathbf{D}^{(1)}$ is a $N_s \times 1$ vector of unknown coefficients. Similarly, for the remaining regions

$$A_2(r,z) = J_1(\boldsymbol{\kappa}^{\mathbf{T}} r) \left[e^{\boldsymbol{\kappa} z} \mathbf{C}^{(2)} + e^{-\boldsymbol{\kappa} z} \mathbf{D}^{(2)} \right] \tag{4.125}$$

and

$$\begin{aligned} A_3(r,z) &= J_1(\mathbf{p}^{\mathbf{T}} r) R_1(\mathbf{q}c) e^{\mathbf{p} z} \mathbf{C}^{(3)} \quad 0 \le r \le c \\ &= R_1(\mathbf{q}^{\mathbf{T}} r) J_1(\mathbf{p}c) e^{\mathbf{p} z} \mathbf{C}^{(3)} \quad c \le r \le h \end{aligned} \tag{4.126}$$

The above equations involve the unknown eigenvalues q_i, p_i. These are derived by enforcing the remaining interface condition in the radial direction, which is the continuity of the tangential magnetic field H_z at $r = c$. Thus, the complex eigenvalues of the problem p_i and q_i are computed from the roots of the equation:

$$p_i R_1(q_i c) J_0(p_i c) = \frac{1}{\mu_r} q_i J_1(p_i c) R_0(q_i c) \tag{4.127}$$

The unknown vector coefficients and, hence, A_φ in all three regions of Fig.4.14, are computed from the interface conditions in the axial direction (continuity of B_z and H_r or equivalently of A_φ and $\partial A_\varphi / \partial z$ using the orthogonality properties of the Bessel functions:

- Interface $z = z_0$

From the continuity of A_φ:

$$J_1(\boldsymbol{\kappa}^{\mathbf{T}} r) e^{-\boldsymbol{\kappa} z_0} \mathbf{D}^{(1)} = J_1(\boldsymbol{\kappa}^{\mathbf{T}} r) \left(e^{\boldsymbol{\kappa} z_0} \mathbf{C}^{(2)} + e^{-\boldsymbol{\kappa} z_0} \mathbf{D}^{(2)} \right) \tag{4.128}$$

If both sides of (4.128) are multiplied by $r J_1(\mathbf{qr})$ and then integrated from $r = 0$ to $r = h$ we take:

$$e^{-\boldsymbol{\kappa} z_0} \mathbf{D}^{(1)} = e^{\boldsymbol{\kappa} z_0} \mathbf{C}^{(2)} + e^{-\boldsymbol{\kappa} z_0} \mathbf{D}^{(2)} \tag{4.129}$$

From the discontinuity of $\partial A_\varphi/\partial z$:

$$J_1(\boldsymbol{\kappa}^{\mathbf{T}}r)(-\boldsymbol{\kappa})e^{-\boldsymbol{\kappa}z_0}\mathbf{D}^{(1)} = J_1(\boldsymbol{\kappa}^{\mathbf{T}}r)\boldsymbol{\kappa}\left(e^{\boldsymbol{\kappa}z_0}\mathbf{C}^{(2)} - e^{-\boldsymbol{\kappa}z_0}\mathbf{D}^{(2)}\right) - \mu_0 I\delta(r-r_0) \tag{4.130}$$

If both sides of (4.130) are multiplied by $rJ_1(\boldsymbol{\kappa}r)$ and then integrated from $r = 0$ to $r = h$ we take:

$$-\mathbf{E}\boldsymbol{\kappa}e^{-\boldsymbol{\kappa}z_0}\mathbf{D}^{(1)} = \mathbf{E}\boldsymbol{\kappa}\left(e^{\boldsymbol{\kappa}z_0}\mathbf{C}^{(2)} - e^{-\boldsymbol{\kappa}z_0}\mathbf{D}^{(2)}\right) - \mu_0 I r_0 J_1(\boldsymbol{\kappa}r_0) \tag{4.131}$$

- Interface $z = 0$

From the continuity of A_φ:

$$J_1(\boldsymbol{\kappa}^{\mathbf{T}}r)\left(\mathbf{C}^{(2)} + \mathbf{D}^{(2)}\right) = J_1(\mathbf{p}^{\mathbf{T}}r)R_1(\mathbf{q}c)\mathbf{C}^{(3)}; 0 \le r \le c \tag{4.132}$$

$$J_1(\boldsymbol{\kappa}^{\mathbf{T}}r)\left(\mathbf{C}^{(2)} + \mathbf{D}^{(2)}\right) = R_1(\mathbf{q}^{\mathbf{T}}r)J_1(\mathbf{p}c)\mathbf{C}^{(3)}; c \le r \le h \tag{4.133}$$

If both sides of (4.132) and (4.133) are multiplied by $rJ_1(\boldsymbol{\kappa}r)$ and then added and integrated from $r = 0$ to $r = h$ we take:

$$\mathbf{E}\left(\mathbf{C}^{(2)} + \mathbf{D}^{(2)}\right) = \mathbf{U}\mathbf{C}^{(3)} \tag{4.134}$$

From the continuity of $\partial A_\varphi/\partial z$:

$$J_1(\boldsymbol{\kappa}^{\mathbf{T}}r)\boldsymbol{\kappa}\left(\mathbf{C}^{(2)} - \mathbf{D}^{(2)}\right) = J_1(\mathbf{p}^{\mathbf{T}}r)R_1(\mathbf{q}c)\mathbf{p}\mathbf{C}^{(3)}; 0 \le r \le c \tag{4.135}$$

$$J_1(\boldsymbol{\kappa}^{\mathbf{T}}r)\boldsymbol{\kappa}\left(\mathbf{C}^{(2)} - \mathbf{D}^{(2)}\right) = \frac{1}{\mu_r}R_1(\mathbf{q}^{\mathbf{T}}r)J_1(\mathbf{p}c)\mathbf{p}\mathbf{C}_3; c \le r \le h \tag{4.136}$$

If both sides of (4.135) and (4.136) are multiplied by $rJ_1(\boldsymbol{\kappa}r)$ and then added and integrated from $r = 0$ to $r = h$ we take:

$$\mathbf{E}\boldsymbol{\kappa}\left(\mathbf{C}^{(2)} - \mathbf{D}^{(2)}\right) = \mathbf{V}\mathbf{p}\mathbf{C}^{(3)} \tag{4.137}$$

The $\mathbf{E}$ matrix elements are calculated from

$$\mathbf{E}_{ij} = \int_{r=0}^{h} J_1(\kappa_i r)J_1(\kappa_j r)rdr = 0 \quad i \neq j \tag{4.138}$$

$$= \frac{h^2}{2}J_0^2(\kappa_i h) \quad i = j$$

and matrices **U V** elements are defined from

$$\mathbf{U}_{ij} = R_1(q_j c) \int_0^c J_1(\kappa_i r) J_1(p_j r) r dr + J_1(p_j c) \int_c^h J_1(\kappa_i r) R_1(q_j r) r dr \tag{4.139}$$

$$\mathbf{V}_{ij} = R_1(q_j c) \int_0^c J_1(\kappa_i r) J_1(p_j r) r dr + \frac{1}{\mu_r} J_1(p_j c) \int_c^h J_1(\kappa_i r) R_1(q_j r) r dr \tag{4.140}$$

The first integral in these definitions is calculated from

$$\frac{c}{p_j^2 - \kappa_i^2} \left[\kappa_i J_0(\kappa_i c) J_1(p_j c) - p_j J_1(\kappa_i c) J_0(p_j c)\right] R_1(q_j c) \tag{4.141}$$

while the second from

$$-\frac{c}{q_j^2 - \kappa_i^2} \left[\kappa_i J_0(\kappa_i c) R_1(q_j c) - q_j J_1(\kappa_i c) R_0(q_j c)\right] J_1(p_j c) \tag{4.142}$$

and we have used (4.79) and the fact that $J_1(\kappa_i h) = 0$ and $R_1(q_j h) = 0$. In case of $\mu_r = 1$, $\mathbf{U} = \mathbf{V}$ and after taking into account the eigenvalues equation (4.127) we have

$$\begin{aligned} \mathbf{U}_{ij} &= \left(\frac{c}{p_j^2 - \kappa_i^2} - \frac{c}{q_j^2 - \kappa_i^2} \right) \left[\kappa_i J_0(\kappa_i c) J_1(p_j c) - p_j J_1(\kappa_i c) J_0(p_j c)\right] R_1(q_j c) \\ &= \frac{-ck^2}{\left(p_j^2 - \kappa_i^2\right)\left(q_j^2 - \kappa_i^2\right)} \left[\kappa_i J_0(\kappa_i c) J_1(p_j c) - p_j J_1(\kappa_i c) J_0(p_j c)\right] R_1(q_j c) \end{aligned} \tag{4.143}$$

The solution to the matrix system of equations (4.129), (4.131), (4.134), (4.137) is

$$\mathbf{D}^{(1)} = \left(e^{2\boldsymbol{\kappa} z_0} + \mathbf{W}\right) \mathbf{C}^{(2)} \tag{4.144}$$

$$\mathbf{C}^{(2)} = \frac{1}{2} \mu_0 I r_0 e^{-\boldsymbol{\kappa} z_0} \boldsymbol{\kappa}^{-1} \mathbf{E}^{-1} J_1(\boldsymbol{\kappa} r_0) \tag{4.145}$$

$$\mathbf{D}^{(2)} = \mathbf{W} \mathbf{C}^{(2)} \tag{4.146}$$

$$\mathbf{C}^{(3)} = 2\left(\mathbf{U} + \boldsymbol{\kappa}^{-1}\mathbf{Vp}\right)^{-1}\mathbf{E}\mathbf{C}^{(2)} \tag{4.147}$$

where

$$\mathbf{W} = \mathbf{E}^{-1}\left(\mathbf{U} - \boldsymbol{\kappa}^{-1}\mathbf{Vp}\right)\left(\mathbf{U} + \boldsymbol{\kappa}^{-1}\mathbf{Vp}\right)^{-1}\mathbf{E} \tag{4.148}$$

and we can identify $\mathbf{C}^{(2)}$ as a source coefficient in terms of which all other coefficients are written. The expressions for the magnetic vector potential in the three regions of Fig.4.14 are derived by substituting (4.144)-(4.147) to (4.124)-(4.126).

4.6.2 *Finite thickness coil*

Computation of A_φ for the rectangular cross-section coil of Fig.4.15, is performed by applying superposition.

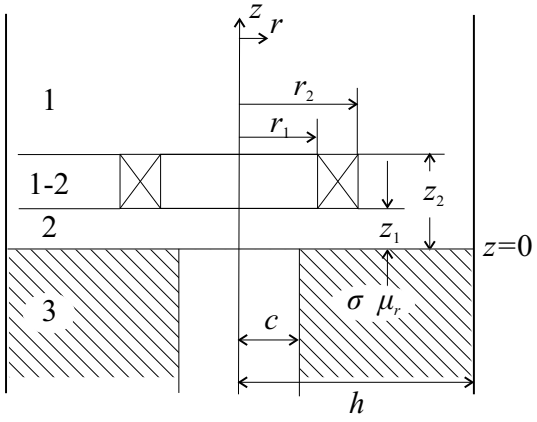

Fig. 4.15 2D axisymmetric view of a cylindrical coil above a hole in a conductive half-space. The solution domain is truncated at $r = h$.

The final expressions in the problem regions are

$$A_1 = \frac{\mu_0 \iota_0}{2} J_1\left(\boldsymbol{\kappa}^{\mathbf{T}} r\right)\mathbf{E}^{-1} e^{-\boldsymbol{\kappa} z}\left[\left(e^{\boldsymbol{\kappa} z_2} - e^{\boldsymbol{\kappa} z_1}\right) + \mathbf{W}\left(e^{-\boldsymbol{\kappa} z_1} - e^{-\boldsymbol{\kappa} z_2}\right)\right] \boldsymbol{\kappa}^{-4}\chi\left(\boldsymbol{\kappa} r_1, \boldsymbol{\kappa} r_2\right) \tag{4.149}$$

$$A_2 = \frac{\mu_0 \iota_0}{2} J_1\left(\boldsymbol{\kappa}^{\mathbf{T}} r\right)\mathbf{E}^{-1}\left(e^{\boldsymbol{\kappa} z} + e^{-\boldsymbol{\kappa} z}\mathbf{W}\right)\left(e^{-\boldsymbol{\kappa} z_1} - e^{-\boldsymbol{\kappa} z_2}\right)\boldsymbol{\kappa}^{-4}\chi\left(\boldsymbol{\kappa} r_1, \boldsymbol{\kappa} r_2\right) \tag{4.150}$$

$$
\begin{aligned}
A_3 &= \mu_0 \iota_0 J_1\left(\mathbf{p}^{\mathbf{T}} r\right) R_1\left(\mathbf{q}^{\mathbf{T}} c\right) e^{\mathbf{p}z} \\
&\quad \cdot \left(\mathbf{U} + \boldsymbol{\kappa}^{-1}\mathbf{V}\mathbf{p}\right)^{-1}\left(e^{-\boldsymbol{\kappa}z_1} - e^{-\boldsymbol{\kappa}z_2}\right)\boldsymbol{\kappa}^{-4}\chi\left(\boldsymbol{\kappa}r_1, \boldsymbol{\kappa}r_2\right) \quad 0 \le r \le c \\
&= \mu_0 \iota_0 R_1\left(\mathbf{q}^{\mathbf{T}} r\right) J_1\left(\mathbf{p}^{\mathbf{T}} c\right) e^{\mathbf{p}z} \\
&\quad \cdot \left(\mathbf{U} + \boldsymbol{\kappa}^{-1}\mathbf{V}\mathbf{p}\right)^{-1}\left(e^{-\boldsymbol{\kappa}z_1} - e^{-\boldsymbol{\kappa}z_2}\right)\boldsymbol{\kappa}^{-4}\chi\left(\boldsymbol{\kappa}r_1, \boldsymbol{\kappa}r_2\right) \quad c \le r \le h
\end{aligned} \tag{4.151}
$$

where again $\iota_0 = NI/[(r_2 - r_1)(z_2 - z_1)]$ and $\chi(x_1, x_2)$ is defined in (3.27). The expression for $A_{1-2}(r, z)$ is

$$
\begin{aligned}
A_{1-2} &= \frac{\mu_0 \iota_0}{2} J_1\left(\boldsymbol{\kappa}^{\mathbf{T}} r\right) \mathbf{E}^{-1} \\
&\quad \cdot \left[2\mathbf{I} - e^{-\boldsymbol{\kappa}(z - z_1)} - e^{\boldsymbol{\kappa}(z - z_2)} + e^{-\boldsymbol{\kappa}z}\mathbf{W}\left(e^{-\boldsymbol{\kappa}z_1} - e^{-\boldsymbol{\kappa}z_2}\right)\right] \\
&\quad \cdot \boldsymbol{\kappa}^{-4}\chi\left(\boldsymbol{\kappa}r_1, \boldsymbol{\kappa}r_2\right)
\end{aligned} \tag{4.152}
$$

and any electromagnetic field quantity can now be determined. The eddy current density is calculated from $J_\phi = -j\omega\sigma A_3$ $(c \le r \le h)$ as

$$
\begin{aligned}
J_\phi = -j\omega\sigma\mu_0\iota_0 R_1\left(\mathbf{q}^{\mathbf{T}} r\right) J_1\left(\mathbf{p}^{\mathbf{T}} c\right) e^{\mathbf{p}z} \left(\boldsymbol{\kappa}\mathbf{U} + \mathbf{V}\mathbf{p}\right)^{-1}\left(e^{-\boldsymbol{\kappa}z_1} - e^{-\boldsymbol{\kappa}z_2}\right) \\
\boldsymbol{\kappa}^{-3}\chi\left(\boldsymbol{\kappa}r_1, \boldsymbol{\kappa}r_2\right)
\end{aligned} \tag{4.153}
$$

The coil impedance is calculated from the integration of (rA_{1-2}) over the coil cross-section. Since we already have an expression for the isolated coil impedance (4.37), we need not integrate A_{1-2} but only the part of A_{1-2} that is due to the conductor with the hole. This will actually provide the expression for the impedance change due to the conductor with the hole. The result then is

$$
\begin{aligned}
\Delta Z &= \frac{j\omega\mu_0\pi N^2}{\left(r_2 - r_1\right)^2\left(z_2 - z_1\right)^2}\chi\left(\boldsymbol{\kappa}^{\mathbf{T}} r_1, \boldsymbol{\kappa}^{\mathbf{T}} r_2\right)\boldsymbol{\kappa}^{-3}\mathbf{E}^{-1} \\
&\quad \cdot \left(e^{-\boldsymbol{\kappa}z_1} - e^{-\boldsymbol{\kappa}z_2}\right)\mathbf{W}\left(e^{-\boldsymbol{\kappa}z_1} - e^{-\boldsymbol{\kappa}z_2}\right)\boldsymbol{\kappa}^{-4}\chi\left(\boldsymbol{\kappa}r_1, \boldsymbol{\kappa}r_2\right)
\end{aligned} \tag{4.154}
$$

and it can also be written in the compact form

$$
\Delta Z = \frac{j\omega 2\pi\mu_0 N^2}{(r_2 - r_1)^2(z_2 - z_1)^2 h^2}\mathbf{C}^{\mathbf{T}} J_0(\boldsymbol{\kappa}h)^{-2}\left(\boldsymbol{\kappa}\mathbf{U} - \mathbf{V}\mathbf{p}\right)\left(\boldsymbol{\kappa}\mathbf{U} - \mathbf{V}\mathbf{p}\right)^{-1}\boldsymbol{\kappa}\mathbf{C} \tag{4.155}
$$

where

$$
\mathbf{C} = (e^{-\boldsymbol{\kappa}z_1} - e^{-\boldsymbol{\kappa}z_2})\boldsymbol{\kappa}^{-4}\chi(\boldsymbol{\kappa}r_1, \boldsymbol{\kappa}r_2) \tag{4.156}
$$

As a test of the final expression, we can check whether for $c \to 0$, i.e. when the hole vanishes, the expression for the impedance change reduces to (4.38), which gives the impedance change due to the conductive half-space. Indeed, in this case $\mathbf{q} = \boldsymbol{\kappa}$, all matrices are diagonalized $\mathbf{U} = \mathbf{E}$, $\mathbf{V} = \mathbf{E}/\mu_{\mathbf{r}}$ and (4.155) is eventually simplified to the matrix form of (4.38).

4.6.3 *Numerical results*

4.6.3.1 *Computation of complex eigenvalues*

In contrast to the ferrite-cored coil problem the eigenvalues are now all complex. This adds another numerical aspect in the solution, in fact the most important one. The correct and exact computation of eigenvalues q_i or equivalently p_i is the step that ensures a meaningful and thus valid solution. What we actually need is an efficient method of finding complex roots of (4.127).

We have based our search on p_i eigenvalues and tried a number of automatic root finding routines. Among them was the Mathematica routine `FindRoot[ ]` with initial guesses $p_i = \sqrt{\kappa_i^2 + j\omega\mu_0\mu_r\sigma}$ (for $c = 0$) and $p_i = \kappa_i$ (for $c = h$) as follows:

```
                                        oms=ωμ0μrσ;
                                    q[p_]:=p p-I oms;
                                k=BesselJZeros[1,Ns]/h;
                               J[n_,r_]:=BesselJ[n,pr];
                    R[n_,r_]:=BesselY[1,qh] BesselJ[n,qr]
                            -BesselJ[1,qh] BesselY[n,qr];
g1=FindRoot[p R[1,c] J[0,c]-q J[1,c] R[0,c]/mr==0,q,k]
    g2=FindRoot[p R[1,c] J[0,c]-q J[1,c] R[0,c]/mr==0,
                                    {q,Sqrt[k k+I oms]}]
                                     Union[p/.g1,p/.g2];
```

The final eigenvalues set is derived by merging the results from these two computations. This procedure should be accompanied by additional criteria for discarding roots with negative signs, zero roots, etc. While this approach is generally acceptable, we have observed a difficulty in reliably computing eigenvalues at higher frequencies and for magnetic materials ($\mu_r \gg 1$). A more robust calculation method can be adopted that involves an iteration

scheme as follows.

We start by considering the case of $c = 0$ when the starting value for each eigenvalue p_i is $\sqrt{\kappa_i^2 + j\omega\mu_0\mu_r\sigma}$ (the eigenvalue for the half-space without the hole). We then increase the hole radius step by step in small increments Δc until it acquires the value for which the calculations are performed. In each step we use the Newton-Raphson iteration scheme to compute the eigenvalue for that particular c until p_i^{m+1} differs from p_i^m by a specified, very small amount. The iterative change in the eigenvalue is written

$$p_i^{m+1} = p_i^m - \frac{f(p_i)^m}{\left.\frac{df(p_i)}{dp_i}\right|^m}, \tag{4.157}$$

where

$$f(p_i) = p_i R_1(q_i c) J_0(p_i c) - \frac{1}{\mu_r} q_i J_1(p_i c) R_0(q_i c) \tag{4.158}$$

and m is the iteration number. Next, c is incremented by Δc, and the starting eigenvalue for the new hole radius width, $c + \Delta c$, is the one that was computed for c in the previous step. With this method an accurate computation of eigenvalues is performed. The same procedure should be repeated by considering initially the case $c = h$ and using the starting eigenvalue $p_i = \kappa_i$. Then we should decrease c step-by-step and apply the Newton-Raphson iteration scheme in each step, until c acquires again the value for which the calculations are performed.

These calculations, which we call hereafter "incrementing" and "decrementing" provide two different sets of eigenvalues. Both of these sets are necessary, so the final set is formed by merging them. This technique can also be used in conjunction with the `FindRoot[ ]` routine in each step, but this may affect calculation speed.

The step-by-step incrementing technique can be used not only on a dimensional parameter such as the hole radius, but also to other parameters as well. In another eigenvalue equation resulting in a similar application described in the Cartesian coordinate system, Weigelt (1990) increments conductivity step-by-step or permeability for a magnetic material. More on the incrementing-decrementing technique as well as on the TREE method can be found in Albach (1981), Hannakam (1982), Flitz (1990), Nethe (1991), Theodoulidis (2005) and in Chapter 7 where we apply the method to the 3D edge problem.

In the following we verify theoretical results against numerical results from a 2D-FEM package, for the coil and conductor data shown in Table

Table 4.5 Coil and half-space parameters used for Fig.4.16.

Coil		Half-space	
r_1	4 mm	σ	18.72 MS/m
r_2	6 mm	μ_r	1
$z_2 - z_1$	1 mm	c	5 mm
z_1	0.2 mm	h	$10r_2$
N	200		

4.5. The theoretical calculations using (4.155) and the FEM results are compared in Fig.4.16 which shows the resistive and reactive parts of the impedance change as a function of frequency. The impedance change is due to the conductor with the hole and the results are normalized to the isolated coil reactance X_0, following the usual practice in eddy current NDE. The conductor is made of an Aluminum alloy and the terms we used in the calculations were $N_s = 50$. Concerning convergence we could repeat here the facts as in the case of the ferrite-cored coil solution. Note that the TREE method does not provide meaningful results (not shown in the Figures) above about 50 kHz because `FindRoot[ ]` has problems in automatically computing roots for higher frequencies. The solution would be the use of the incrementing-decrementing technique with a very small step Δc. Incorrect eigenvalues produce ill-conditioned matrices, therefore the required inversion $(\boldsymbol{\kappa}\mathbf{U} - \mathbf{V}\mathbf{p})^{-1}$ will be numerically inaccurate, thus producing wrong results.

Results for the plate without the hole are also depicted for comparison. Excellent agreement is observed between the FEM and TREE results. Usually results from a numerical method (like FEM) are verified with results from a closed-form analytical solution. In this case, however, we have the opposite situation: results from an analytical calculation (or quasi-analytical according to the discussion in Chapter 1) are verified by a numerical method (FEM). Although the higher authority in verifying theoretical results are carefully prepared experimental measurements, FEM provides a reasonably accurate verification tool in 2D problems where it is now well-established. The situation is different in 3D NDE problems, however, where numerical methods have a long way to go and their accuracy has still to be proved.

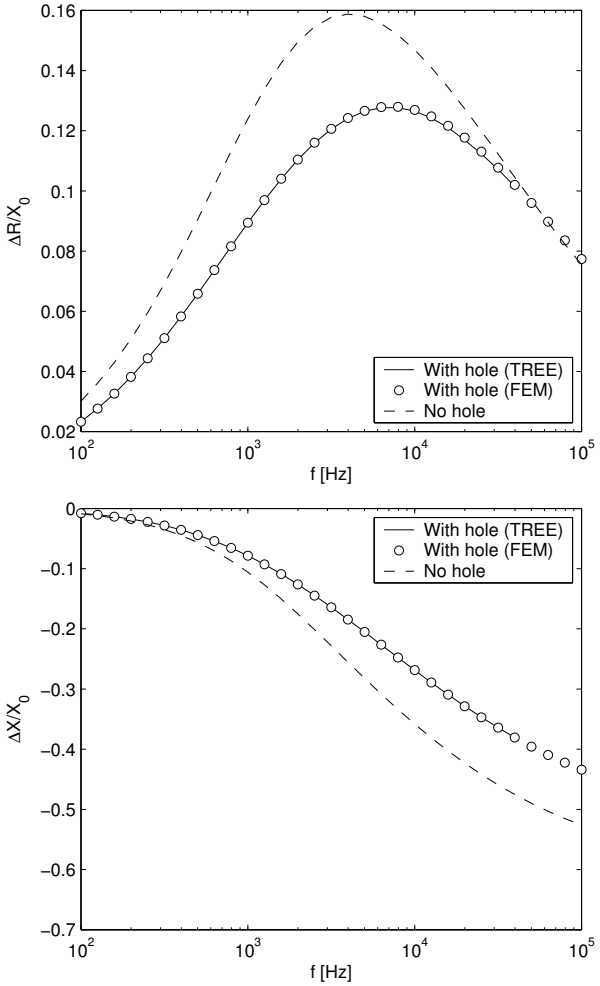

Fig. 4.16 Frequency variation of normalized impedance change (resistive and reactive parts) for a coil above a cylindrical hole in a conductive half space.

4.6.4 *Discussion*

The above analysis covers the case where the coil is located above the conductor. But the coil can also assume another axisymmetric position. If it is of an appropriate size it can be positioned inside the hole or a part of it inside and a part of it outside the hole. Although this interesting case can also be solved with the method presented in this chapter, it would be

better if the truncation took place in the axial direction rather that in the radial one. In this case, however, different eigenfunction expansions would be needed and the configuration would be more connected to "the coil in a cylindrical conductor" configuration of the Dodd and Deeds models, see Theodoulidis (2004). For examples of truncation in the z-direction involving a coil encircling a finite length solid cylinder or a layered one, see Bowler (2005) and Sun (2005).

As for other conductor configurations, it is needless to say that with the same technique we can study a lot of different geometries starting from the general one in Fig.4.13. We leave all these extensions to the interested reader, but for an extension of the model to a hole in a plate see Theodoulidis (2004b).

Chapter 5

3D Configurations

5.1 Introduction

In this chapter we provide analytical expressions for the coil impedance in planar geometries when the configuration is 3D, that is, when all three components of the electric and magnetic field are present. The planar conductor has again the form of a conductive half-space, as in previous chapters, and the 3D nature of the problem is manifest by the orientation or the shape of the exciting coil.

In order to characterize a problem as 2D or 3D we have to take also into account the particular coordinate system that we use to describe the problem geometry. Consider for example Fig.5.1 where the cylindrical coil is positioned with its axis perpendicular to the conductor surface and with its axis tilted through an angle φ. Using a Cartesian coordinate system in

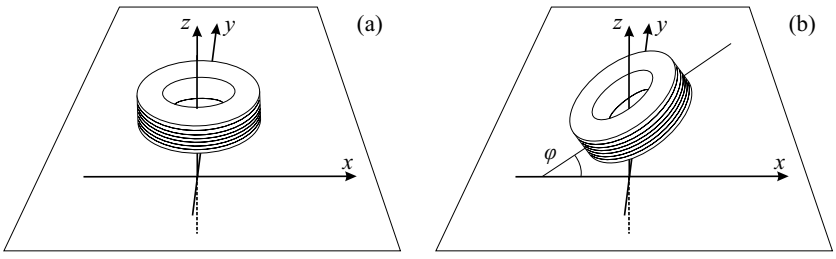

Fig. 5.1 (a) 2D axisymmetric and (b) 3D arrangements of the cylindrical coil above a planar conductor.

both cases, all three components of the magnetic field are present and, as we will see, only two components of the eddy current density are present in the conductor if it extends infinitely in the x and y directions. Therefore,

in both cases the problem is 3D but in the first case we can make use of a cylindrical coordinate system and in this case it is 2D as we have already seen, so that we can use only one scalar quantity (the φ-component of the magnetic vector potential) to describe the problem. We do not have the luxury of using any suitable coordinate system in the second case, so we have to use more than one scalar quantity to describe the problem. If we use the Magnetic Vector Potential $\mathbf{A}$ we need three scalar quantities, which is the number of its components but since these are interconnected ($\mathbf{A}$ solenoidal), we should be able to reduce this number to two by imposing explicitly $\nabla \cdot \mathbf{A} = 0$. We can avoid such extra workload, however, by using the Second Order Vector Potential $\mathbf{W}$ where the solenoidal MVP is implicit in the formulation, see the discussion in Chapter 1. The 3D vector problem will eventually reduce to a scalar one and its solution will depend on the calculation of a source term that relates to the coil free-space magnetic field. The aim of this chapter is to present various techniques for an efficient calculation of this source term. The focus will be again on the cylindrical coil but the presented techniques can be used for other coil designs as well.

Before proceeding with the solution of the general 3D problem using the SOVP formulation let us have a look at previous studies on the subject. A significant amount of work concerns models of coils that have shapes other than the classical cylindrical coil or positions that cancel axisymmetry. A general treatment of the problem was presented by Weaver (1970) who used Hertz potentials to provide general expressions for the electromagnetic field. Later Hannakam (1972) provided solutions for a filamentary coil of arbitrary shape by using the SOVP formulation. As already presented in Chapter 1 the Hertz potential approach is equivalent to the SOVP approach. Based on Hannakam's work, Kriezis (1979) evaluated the eddy current density from a filamentary vertical circular coil while other researchers like Beissner (1986) and Bowler (1987) favored the use of Green's dyadic functions to solve the problem. Bowler presented also analytical expressions for the eddy current density of a vertically oriented cylindrical coil over the conductive half-space, thus extending the results of Kriezis to a real eddy current probe coil. Beissner (1984) and Tsaknakis (1985) presented formulas for the eddy current distribution from cylindrically symmetric sources inclined at an arbitrary angle with respect to the surface normal. Upon the use of the Cartesian coordinate system, the general solution for a nonsymmetric source is in the form of a two-dimensional Fourier integral. Numerical computations for the nonsymmetric case are therefore more demanding than the application of the Dodd and Deeds formulas to axisymmetric situations,

where the integrals are one-dimensional. A semi-analytical model was presented by Juillard (2000) for the same problem where the coil is divided in a number of elements called Point Current Sources. Beissner (1990) presented a general method of treating arbitrarily shaped coils located in a plane parallel to the conductive half-space by considering the equivalence of the isolated coil scalar potential at a point in space and the solid angle subtended by the coil at that point. Similar methods for computing the magnetic field, based on the Fourier Transform, were presented by Panas (1991) and Sadeghi (2001), who solved the problem of an elliptical loop and a rectangular coil in an inclined position, respectively. An important conclusion of all these studies is that the eddy currents induced in the conductor flow parallel to its surface, irrespective of the shape and position of the inducing coil. This important conclusion will be discussed in detail later.

All of these analytical solutions concern the electromagnetic field with emphasis on the induced eddy current density. Calculation of the impedance change of the coil, on the other hand, requires an extra step: after evaluating the 3D electromagnetic field we have to apply the general expression of the impedance change of a coil. This impedance change expression, derived by Auld (1981) and called ΔZ formula, was presented in Chapter 1. Auld showed through the use of Lorentz reciprocity theorem that the change in the impedance of an eddy current probe in the presence of a flaw can be expressed in terms of an integral evaluated over any closed surface S containing the flaw. In order to find the impedance change of a coil with arbitrary shape and orientation, due to the presence of the conductive half-space, we make use of the ΔZ formula by considering the half-space as a very large "flaw". Following this approach, which was proposed by Auld (1983, 1984, 1999) and solving analytically for the 3D electromagnetic field, Burke (1986, 1990) presented solutions for the perpendicular coil above an isotropic and a uniaxially anisotropic conductive half-space. The same approach was followed by Theodoulidis (2002) for evaluating the impedance of a rectangular coil located above a conductive half-space.

The focus in this chapter is on the cylindrical coil and each solution technique is presented by considering the various positions it can take. Apart from the classical cylindrical coil, analytical expressions for the electromagnetic field and therefore for the source coefficient can be found in the literature for other coils as well. Extensions to the cylindrical coil have been presented by Ditchburn (2003) who provided expressions for the thin

spiral coil (fabricated with printed circuit board technology) and by Burke (2004) who studied various parallel and perpendicular coil arrangements in order to model the mutual impedance between the coils.

The eddy current distribution generated by the circular coil has an axial symmetry and no eddy current density at the center. Besides, not having eddy current at the center, the circular coil may suffer a loss of spatial resolution of measurement. Also, due to the axial symmetry the circular coil cannot detect the anisotropic properties of the target material. Nevertheless, it can be made to exhibit directional properties by using it in a perpendicular position, with its axis parallel to the conductor surface, see Burke (1990) who used such an arrangement to detect the anisotropy direction of a uniaxially anisotropic plate. However, the perpendicular coil design has a low degree of electromagnetic coupling with the inspected conductor, thus producing weak impedance change signals. In order to overcome the lack of directional properties and at the same time ensure good electromagnetic coupling we can resort to alternative coil designs.

The filamentary elliptical loop has been studied by Panas (1991), Theodoulidis (1994) and Bavall (2002). The first two studies presented solutions in the Cartesian coordinate system, while in the third one the coil was modelled in the elliptical cylinder coordinate system giving a closed form expression for the impedance in terms of Mathieu's functions. The rectangular (orthogonal) filamentary coil was studied by Grimberg (2000) while the rectangular coil of finite thickness was analyzed by Theodoulidis (2002) who provided analytical expressions for the source term for both the parallel and the perpendicular position of the coil. McKirdy (1996) presented a solution for the filamentary D-coil while Bowler (2004) solved the case of a racetrack coil with finite thickness by considering it as the superposition of two semi-circles (D-coils) and two straight segments. Finally, an analytical solution exists for the rectangular coil with rounded corners Zhou (1994). Other coil designs such as the double-D coil, Bae (2000) and the mesh-type coil, Mukhopadhyay (2002), can also be studied with the solution technique of this chapter.

5.2 Solution of the general problem in the Cartesian coordinate system

The general 3D induction problem is shown in Fig.5.2. A source coil of arbitrary shape lies above a conductive half space and the electromagnetic

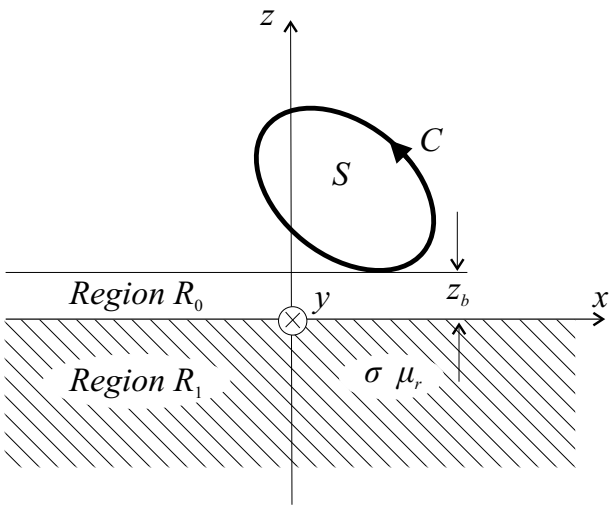

Fig. 5.2 General 3D coil arrangement above a planar conductor.

field quantities to be calculated are the magnetic field, eddy current density induced in the half-space and the impedance of the coil. The excitation current has a sinusoidal form $Ie^{j\omega t}$ where $\omega = 2\pi f$ and f is the excitation frequency. The half-space is assumed to have a constant conductivity σ and magnetic permeability $\mu = \mu_r\mu_0$ where μ_r is the relative magnetic permeability and μ_0 is the vacuum permeability. Introducing a Cartesian coordinate system in which the plane $z = 0$ is the interface, two regions of interest are created and denoted accordingly:

- air region between the bottom of the coil and the interface, $R_0 : 0 \leq z < z_b$
- conductive half-space region, $R_1 : z \leq 0$

We will now solve this 3D problem by using the SOVP formulation. Choosing a z-preferred direction, the potential is defined as

$$\mathbf{W} = W_a\mathbf{z}_0 + \mathbf{z}_0 \times \nabla W_b \tag{5.1}$$

where $\mathbf{z}_0$ is the unit vector in the z-direction while W_a is the transverse electric (TE) and W_b the transverse magnetic (TM) potential both of which satisfy the 3D scalar Laplace and Helmholtz equations in the air and con-

ductor regions respectively

$$\frac{\partial^2 W_{a,b}}{\partial x^2} + \frac{\partial^2 W_{a,b}}{\partial y^2} + \frac{\partial^2 W_{a,b}}{\partial z^2} = k^2 W_{a,b} \quad ; \quad k^2 = j\omega\mu_r\mu_0\sigma \tag{5.2}$$

As we have already pointed out in Chapter 1, we have a freedom to choose the unit vector in (5.1). This is not only a matter of preference but also a matter of convenience as we will see later. Here we derive the general solution by using the normal to the surface unit vector $\mathbf{z}_0$ whereas in Chapter 6 we present the solution with one of the tangential to the surface unit vectors $\mathbf{x}_0$ or $\mathbf{y}_0$. With the specific choice of unit vector, the equations connecting the components of $\mathbf{A}$ and $\mathbf{B}$ to W_a and W_b have been derived in Chapter 1 and are rewritten here for convenience.

$$A_x = \frac{\partial W_a}{\partial y} - \frac{\partial^2 W_b}{\partial x \partial z} \tag{5.3}$$

$$A_y = -\frac{\partial W_a}{\partial x} - \frac{\partial^2 W_b}{\partial y \partial z} \tag{5.4}$$

$$A_z = \frac{\partial^2 W_b}{\partial x^2} + \frac{\partial^2 W_b}{\partial y^2} \tag{5.5}$$

$$B_x = k^2 \frac{\partial W_b}{\partial y} + \frac{\partial^2 W_a}{\partial x \partial z} \tag{5.6}$$

$$B_y = -k^2 \frac{\partial W_b}{\partial x} + \frac{\partial^2 W_a}{\partial y \partial z} \tag{5.7}$$

$$B_z = -k^2 W_a + \frac{\partial^2 W_a}{\partial z^2} \tag{5.8}$$

For a non-conductive region, the terms containing k^2 vanish and $\mathbf{B}$ can be written as the gradient of a scalar quantity

$$\mathbf{B} = \nabla \left(\frac{\partial W_a}{\partial z} \right) \tag{5.9}$$

In this section we derive the eddy currents and the magnetic flux density in terms of TE and TM potentials and in the next section we give an expression for the impedance change of the coil due to the induced current in the conductor. All of these calculations are performed in the quasi-static limit without defining the TM potential in air or the conservative part of the electric field in air, by using the continuity of the normal magnetic flux density and tangential magnetic field at conductor-air interfaces, see the discussion in Chapter 1.

The magnetic field in region R_0, can be described by $W_a^{(0)}$, which in turn can be expressed as the sum of two potentials: the primary potential $W_a^{(s)}$ due to the excitation current of the coil in free-space and the secondary potential $W_a^{(ec)}$ which originates from the eddy currents induced within the conductive half-space.

$$W_a^{(0)} = W_a^{(s)} + W_a^{(ec)} \tag{5.10}$$

Upon using the 2D Fourier transform on (5.2) with respect to the x and y coordinates we get the differential equation in 2D Fourier space

$$\frac{\partial^2 \tilde{W}_{a,b}}{\partial z^2} = \lambda^2 \tilde{W}_{a,b} \tag{5.11}$$

where $\lambda^2 = \kappa^2 + k^2$, $\kappa^2 = u^2 + v^2$. The tilde denotes Fourier transformation and we have defined the forward and inverse 2D transforms as

$$\tilde{W}_{a,b}(u,v,z) = \int_{-\infty}^{\infty}\int_{-\infty}^{\infty} W_{a,b}(x,y,z) e^{-jux} e^{-jvy} dxdy \tag{5.12}$$

$$W_{a,b}(x,y,z) = \frac{1}{4\pi^2}\int_{-\infty}^{\infty}\int_{-\infty}^{\infty} \tilde{W}_{a,b}(u,v,z) e^{jux} e^{jvy} dudv \tag{5.13}$$

Now the general solution to (5.11) is

$$\tilde{W}_{a,b}(z) = C(u,v)\mathrm{e}^{\lambda z} + D(u,v)\mathrm{e}^{-\lambda z} \tag{5.14}$$

From (5.14) we deduce the following expressions for the potentials in R_0 and R_1 according to the conductivity of the region and and the fact that they must remain finite

$$\tilde{W}_a^{(s)}(z) = C^{(s)}\mathrm{e}^{\kappa z} \tag{5.15}$$

$$\tilde{W}_a^{(ec)}(z) = D^{(ec)}\mathrm{e}^{-\kappa z} \tag{5.16}$$

$$\tilde{W}_a^{(1)}(z) = C_a^{(1)}\mathrm{e}^{\lambda z} \tag{5.17}$$

$$\tilde{W}_b^{(1)}(z) = C_b^{(1)}\mathrm{e}^{\lambda z} \tag{5.18}$$

Eqs (5.15)-(5.18) are valid for any source coil, the characteristics of which are described through the coefficient $C^{(s)}$. Assuming that $C^{(s)}$ is a known quantity, we will express the other coefficients in terms of it. Thus, the

whole electromagnetic field problem reduces to the calculation of this coefficient. In fact, most of this chapter is devoted to the presentation of techniques for calculating $C^{(s)}$.

We can now apply the interface conditions at $z = 0$ in order to calculate the unknown coefficients. These interface conditions are the continuity of the tangential electric and magnetic field components but as we have already seen in Chapter 1, in an air-conductor interface these can be replaced by the three continuity equations of the magnetic field, namely the tangential components of $\mathbf{H}$ and the normal component of $\mathbf{B}$.

The transformed magnetic field components are written in terms of the transformed potentials from (5.6)-(5.8) as:

$$\tilde{B}_x = k^2 jv\tilde{W}_b + ju\frac{\partial \tilde{W}_a}{\partial z} \tag{5.19}$$

$$\tilde{B}_y = -k^2 ju\tilde{W}_b + jv\frac{\partial \tilde{W}_a}{\partial z} \tag{5.20}$$

$$\tilde{B}_z = -k^2\tilde{W}_a + \frac{\partial^2 \tilde{W}_a}{\partial z^2} \tag{5.21}$$

and so the interface conditions become

$$\tilde{H}_x^{(0)} = \tilde{H}_x^{(1)} \Rightarrow \frac{1}{\mu_0} ju\frac{\partial\left(\tilde{W}_a^{(s)} + \tilde{W}_a^{(ec)}\right)}{\partial z} = \frac{1}{\mu_0\mu_r}\left(k^2 jv\tilde{W}_b^{(1)} + ju\frac{\partial \tilde{W}_a^{(1)}}{\partial z}\right) \tag{5.22}$$

$$\tilde{H}_y^{(0)} = \tilde{H}_y^{(1)} \Rightarrow \frac{1}{\mu_0} jv\frac{\partial\left(\tilde{W}_a^{(s)} + \tilde{W}_a^{(ec)}\right)}{\partial z} = \frac{1}{\mu_0\mu_r}\left(-k^2 ju\tilde{W}_b^{(1)} + jv\frac{\partial \tilde{W}_a^{(1)}}{\partial z}\right) \tag{5.23}$$

$$\tilde{B}_z^{(0)} = \tilde{B}_z^{(1)} \Rightarrow \frac{\partial^2\left(\tilde{W}_a^{(s)} + \tilde{W}_a^{(ec)}\right)}{\partial z^2} = -k^2\tilde{W}_a^{(1)} + \frac{\partial^2 \tilde{W}_a^{(1)}}{\partial z^2} \tag{5.24}$$

These equations yield the following linear system of equations for the unknown coefficients

$$ju\kappa\mu_r\left(C^{(s)} - D^{(ec)}\right) = k^2 jvC_b^{(1)} + ju\lambda C_a^{(1)} \tag{5.25}$$

$$jv\kappa\mu_r\left(C^{(s)} - D^{(ec)}\right) = -k^2 juC_b^{(1)} + jv\lambda C_a^{(1)} \tag{5.26}$$

$$\kappa^2 \left(C^{(s)} + D^{(ec)} \right) = \left(-k^2 + \lambda^2 \right) C_a^{(1)} \\ = \kappa^2 C_a^{(1)} \tag{5.27}$$

We have three independent equations and three unknowns. The solution of the system in terms of $C^{(s)}$ is

$$D^{(ec)} = \frac{\kappa\mu_r - \lambda}{\kappa\mu_r + \lambda} C^{(s)} = R(u,v) C^{(s)} \tag{5.28}$$

$$C_a^{(1)} = \frac{2\kappa\mu_r}{\kappa\mu_r + \lambda} C^{(s)} \tag{5.29}$$

$$C_b^{(1)} = 0 \tag{5.30}$$

The term $R(u,v)$ is essentially a reflection coefficient which determines the relationship of the eddy current secondary field to the incident free-space source field. We have derived a similar form of reflection coefficient in the previous chapter where we dealt with axisymmetric geometries and extended it to cases where the conductive half-space is layered. The same extension, in the context of the present chapter, is discussed in a following section. Now substituting (5.28)-(5.30) in (5.15)-(5.18) and inverse-transforming we derive the final expressions for the potential in the two regions of interest

$$W_a^{(0)}(x,y,z) = \frac{1}{4\pi^2} \int_{-\infty}^{\infty} \int_{-\infty}^{\infty} \left(e^{\kappa z} + \frac{\kappa\mu_r - \lambda}{\kappa\mu_r + \lambda} e^{-\kappa z} \right) C^{(s)} e^{jux} e^{jvy} du dv \tag{5.31}$$

$$W_a^{(1)}(x,y,z) = \frac{1}{4\pi^2} \int_{-\infty}^{\infty} \int_{-\infty}^{\infty} \frac{2\kappa\mu_r}{\kappa\mu_r + \lambda} e^{\lambda z} C^{(s)} e^{jux} e^{jvy} du dv \tag{5.32}$$

$$W_b^{(1)}(x,y,z) = 0 \tag{5.33}$$

The left term in the parenthesis of (5.31) corresponds to the part of $W_a^{(0)}$ due to the source $W_a^{(s)}$ and the right term to the part due to the eddy currents $W_a^{(ec)}$. Eq. (5.30) and therefore (5.33) imply that the transverse magnetic potential is zero inside the half-space conductor. This has two consequences: (i) we can describe the problem in terms of the transverse electric potential only and (ii) due to (5.5) the z-component of the electric

field and thus the z-component of the eddy current density is zero throughout the conductor volume. The latter result is independent of the source coil shape or position and the practical meaning of not being able to induce a vertical eddy current component is that we cannot use the eddy current inspection method to detect laminations. These are planar discontinuities with negligible width parallel to the surface of the conductor. Due to their orientation they do not obstruct eddy currents and therefore they do not produce any impedance change.

5.2.1 *Eddy currents and magnetic field*

Knowledge of the potential W_a means that we can calculate the electromagnetic field in regions R_0 and R_1. More specifically, we can calculate the electric field and eddy currents in the conductor region R_1 and the magnetic field in both regions R_0 and R_1. Regarding the electric field in air region R_0, we do not know its part owing to the W_b potential but in the context of eddy current testing this is not required since it does not contribute to the coil impedance, which is the quantity of interest.

Using $\mathbf{A} = \nabla \times \mathbf{W}$ and $\mathbf{J} = -j\omega\sigma\mathbf{A}$ the eddy current density is written in terms of the source term $C^{(s)}$ as follows

$$\mathbf{J} = \frac{-j\omega\sigma}{4\pi^2} \int_{-\infty}^{\infty} \int_{-\infty}^{\infty} C^{(s)} \frac{2\kappa\mu_r}{\kappa\mu_r + \lambda} \left(jv\mathbf{x}_0 - ju\mathbf{y}_0\right) e^{\lambda z} e^{jux} e^{jvy} du dv \qquad (5.34)$$

We have already mentioned that the vertical component of the eddy current density vanishes throughout the planar conductor volume. We should mention, however, that as it was shown by Burke (1990) the presence of horizontal uniaxial anisotropy (met in composite materials) has a dramatic effect on the nature of the induced currents. While the normal component of the induced current density J_z is always zero for an isotropic plate, J_z is nonzero for an anisotropic one. The degree to which the z-directed eddy currents affect measurements depends on material parameters, fiber layup of the composite material, measurement frequency as well as coil orientation, Treece (1991).

In terms of the source coefficient $C^{(s)}$ the magnetic field is written as

follows inside ($z \leq 0$)

$$\mathbf{B}^{(1)} = \frac{1}{4\pi^2} \int_{-\infty}^{\infty} \int_{-\infty}^{\infty} C^{(s)}(u,v) \frac{2\kappa\mu_r\lambda}{(\kappa\mu_r + \lambda)} \left(ju\mathbf{x}_0 + jv\mathbf{y}_0 + \lambda\mathbf{z}_0\right) e^{\lambda z} e^{jux} e^{jvy} du dv \tag{5.35}$$

and outside $0 \leq z \leq z_b$ of the planar conductor

$$\mathbf{B}^{(0)} = \frac{1}{4\pi^2} \int_{-\infty}^{\infty} \int_{-\infty}^{\infty} C^{(s)}(u,v)\kappa \left\{ \left[e^{\kappa z} - \frac{\kappa\mu_r - \lambda}{\kappa\mu_r + \lambda} e^{-\kappa z} \right] \left(ju\mathbf{x}_0 + jv\mathbf{y}_0\right) + \left[e^{\kappa z} + \frac{\kappa\mu_r - \lambda}{\kappa\mu_r + \lambda} e^{-\kappa z} \right] \kappa\mathbf{z}_0 \right\} e^{jux} e^{jvy} du dv \tag{5.36}$$

5.2.2 *The ΔZ formula*

The change in coil impedance due to the induction of eddy currents in the conductor ΔZ is the difference between the coil impedance measured when the coil is located above the conductor system Z and the impedance Z_0 measured when the coil is in isolation. This change can be conveniently obtained using the result from Auld (1981), which relates ΔZ to a surface integral involving the electric and magnetic fields. This formula, which was devised for the general case of an inhomogeneity embedded in a host conductor as shown in Fig.5.3, has the following form

$$\Delta Z = \frac{1}{\mu_0 I^2} \oint_{S_F} d\mathbf{s} \cdot \left(\mathbf{E} \times \mathbf{B}^{(F)} - \mathbf{E}^{(F)} \times \mathbf{B} \right) \tag{5.37}$$

where S_F is a surface enclosing the flaw and $d\mathbf{s}$ is a surface element directed along the outward normal to S_F. The difference with the version presented in Chapter 1 is that here we use $\mathbf{B}$ instead of $\mathbf{H}$. Now $\mathbf{E}^{(F)}$ and $\mathbf{B}^{(F)}$ are the electric and magnetic fields in the presence of the flaw while $\mathbf{E}$ and $\mathbf{B}$ are the fields with the flaw absent. This general formula can be utilized in another way for calculating the impedance change due to the half-space itself, as shown in Fig.5.4, and written in the following form

$$\Delta Z = \frac{1}{\mu_0 I^2} \oint_{S_C} d\mathbf{s} \cdot \left(\mathbf{E}^{(s)} \times \mathbf{B}^{(0)} - \mathbf{E}^{(0)} \times \mathbf{B}^{(s)} \right) \tag{5.38}$$

In this case, the surface S_C is an arbitrary closed surface enclosing the conductor system but excluding the coil and $d\mathbf{s}$ is a surface element

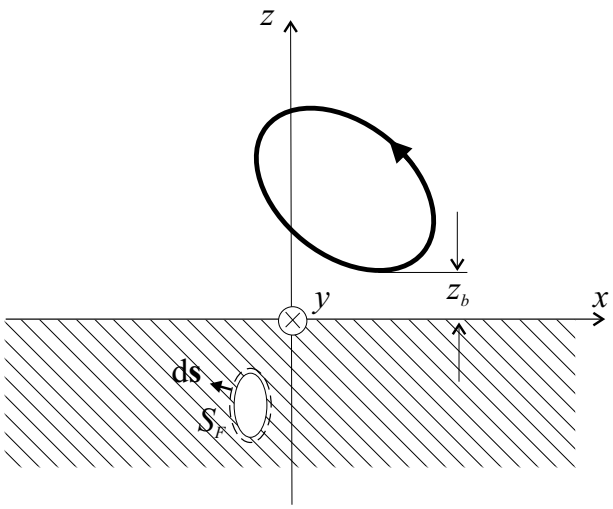

Fig. 5.3 Sketch showing application of the ΔZ formula to the general 3D planar problem.

directed along the outward normal to S_C. $\mathbf{E}^{(0)}$ and $\mathbf{B}^{(0)}$ are the electric and magnetic fields in the presence of the conductor system while $\mathbf{E}^{(s)}$ and $\mathbf{B}^{(s)}$ are the fields which would prevail if the conductors were absent. Using the vector identity $\nabla \times (U\mathbf{A}) = \nabla U \times \mathbf{A} + U\,(\nabla \times \mathbf{A})$, the first term in the parenthesis of (5.38) becomes

$$\begin{aligned}\mathbf{E}^{(s)} \times \mathbf{B}^{(0)} = -\nabla \frac{\partial W_a^{(0)}}{\partial z} \times \mathbf{E}^{(s)} &= -\nabla \times \frac{\partial W_a^{(0)}}{\partial z}\mathbf{E}^{(s)} + \frac{\partial W_a^{(0)}}{\partial z}\nabla \times \mathbf{E}^{(s)} \\ &= -\nabla \times \frac{\partial W_a^{(0)}}{\partial z}\mathbf{E}^{(s)} - j\omega \frac{\partial W_a^{(0)}}{\partial z}\mathbf{B}^{(s)}\end{aligned} \tag{5.39}$$

where we have also used Faraday's law $\nabla \times \mathbf{E} = -j\omega\mathbf{B}$ for the curl of $\mathbf{E}^{(s)}$. Likewise, the second term in the parenthesis of (5.38) becomes

$$\mathbf{E}^{(0)} \times \mathbf{B}^{(s)} = \ldots = -\nabla \times \frac{\partial W_a^{(s)}}{\partial z}\mathbf{E}^{(0)} - j\omega \frac{\partial W_a^{(s)}}{\partial z}\mathbf{B}^{(0)} \tag{5.40}$$

Now using Gauss's theorem, the integrals of the first terms in (5.39) and (5.40) are converted to volume integrals of the divergence of a curl of a vector and therefore they are identically zero.

For the half-space conductor system it is convenient to choose S_C as the top surface $z = 0^+$ of the conductive half-space closed at infinity by

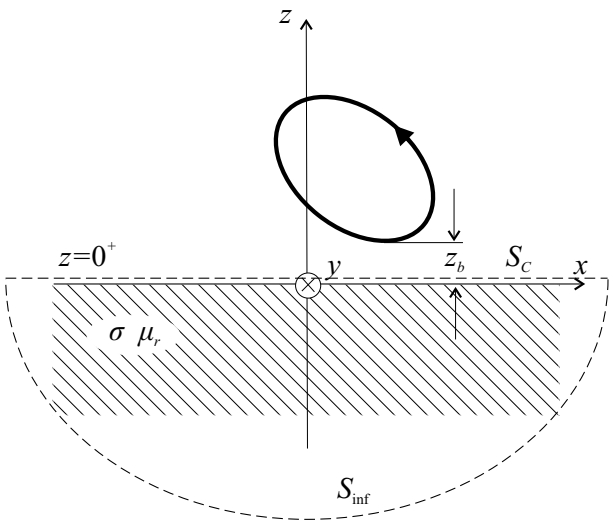

Fig. 5.4 Sketch showing application of the ΔZ formula to the general 3D planar problem.

the surface S_{inf}, as shown in Fig.5.4. With this choice for S_C and noting that the contribution from S_{inf} is negligible for induction problems, (5.38) becomes

$$\Delta Z = \frac{-j\omega}{\mu_0 I^2} \int\limits_{z=0} \mathbf{z}_0 \cdot \left(\frac{\partial W_a^{(0)}}{\partial z} \mathbf{B}^{(s)} - \frac{\partial W_a^{(s)}}{\partial z} \mathbf{B}^{(0)} \right) dxdy \tag{5.41}$$

which depends only on $W_a^{(0)}$ and $W_a^{(s)}$ if we substitute for $\mathbf{B}^{(s)}$ and $\mathbf{B}^{(0)}$ using

$$\mathbf{z}_0 \cdot \mathbf{B}^{(s)} = \frac{\partial^2 W_a^{(s)}}{\partial z^2} \tag{5.42}$$

$$\mathbf{z}_0 \cdot \mathbf{B}^{(0)} = \frac{\partial^2 W_a^{(0)}}{\partial z^2} \tag{5.43}$$

Noting also that $W_a^{(0)} = W_a^{(s)} + W_a^{(ec)}$, after some algebraic manipulation, (5.41) takes the form

$$\Delta Z = \frac{-j\omega}{\mu_0 I^2} \int\limits_{-\infty}^{\infty} \int\limits_{-\infty}^{\infty} \left(\frac{\partial W_a^{(ec)}}{\partial z} \frac{\partial^2 W_a^{(s)}}{\partial z^2} - \frac{\partial W_a^{(s)}}{\partial z} \frac{\partial^2 W_a^{(ec)}}{\partial z^2} \right)_{z=0} dxdy \tag{5.44}$$

Upon substituting for $W_a^{(s)}$ and $W_a^{(ec)}$ using (5.15) and (5.16) and applying Parseval's theorem for Fourier transforms, the impedance change reduces to

$$\Delta Z = \frac{j\omega}{2\pi^2 \mu_0 I^2} \int_{-\infty}^{\infty} \int_{-\infty}^{\infty} \kappa^3 C^{(s)}(-u,-v) D^{(ec)}(u,v) du dv \tag{5.45}$$

If we further use (5.28) and note that $W_a^{(s)}$ is a real function so that $C^{(s)}(-u,-v) = \left[C^{(s)}(u,v)\right]^*$ the above expression becomes

$$\Delta Z = \frac{j\omega}{2\pi^2 \mu_0 I^2} \int_{-\infty}^{\infty} \int_{-\infty}^{\infty} \kappa^3 \left|C^{(s)}(u,v)\right|^2 R(u,v) du dv \tag{5.46}$$

Note that the coefficient $1/2\pi^2$ in (5.46) has the form $8\pi^2$ in Theodoulidis (2002). This slight incompatibility has to do with the way we define the Fourier transform pair in (5.13)-(5.12) and specifically where we put the coefficient $1/4\pi^2$ in them. This is also true for the eddy current and magnetic field expressions.

Eq. (5.46) can also be written as

$$\Delta Z = \frac{j\omega 2}{\pi^2 \mu_0 I^2} \int_{0}^{\infty} \int_{0}^{\infty} \kappa^3 \left|C^{(s)}(u,v)\right|^2 R(u,v) du dv \tag{5.47}$$

This is a very general expression and is valid for any air-cored coil above a conductive half-space. It is made specific to a particular coil through the $C^{(s)}$ source coefficient. Note that the reflection coefficient in (5.28) and (5.46) is the same with the reflection coefficient $R(\kappa)$ that arose in axisymmetric configurations of Chapter 3, differing only in κ which is now $\sqrt{u^2+v^2}$. This similarity suggests that we can derive other forms of $R(u,v)$ simply by copying results from Chapter 3 and making the substitution $\kappa = \sqrt{u^2+v^2}$. For example, for a two-layer conductor with a top layer having σ_1, μ_{r1} and thickness d and a bottom layer having σ_2, μ_{r2} and extending infinitely in the z direction, the reflection coefficient in (5.28) and (5.46) should be as in (3.42)

$$R(u,v) = \frac{(\lambda_1\mu_{r2} + \lambda_2\mu_{r1})(\kappa\mu_{r1} - \lambda_1) + e^{-2\lambda_1 d}(\lambda_1\mu_{r2} - \lambda_2\mu_{r1})(\kappa\mu_{r1} + \lambda_1)}{(\lambda_1\mu_{r2} + \lambda_2\mu_{r1})(\kappa\mu_{r1} + \lambda_1) + e^{-2\lambda_1 d}(\lambda_1\mu_{r2} - \lambda_2\mu_{r1})(\kappa\mu_{r1} - \lambda_1)} \tag{5.48}$$

The extension of the SOVP formulation to a conductor with two layers was done by Clark (1990) for a perpendicular cylindrical coil and the results were verified experimentally. For a multi-layered conductor, we can just follow the matrix or recursive approaches presented in Chapter 3 where again κ in those equations is replaced by $\sqrt{u^2+v^2}$. More specifically the impedance change is given again by (5.46) with $R(u,v)$ replaced by $R(\kappa)$ that is used in (3.67) or by V_1/U_1 in (3.68).

5.2.3 *Alternative form of the source term and the numerical approach*

Up to now we have expressed both the electromagnetic field in all problem regions (with the exception of the electric field in air) and the coil impedance change in terms of a source term $C^{(s)}$. The rest of this chapter is devoted to techniques for calculating analytically $C^{(s)}$. However, there are always cases where such an analytical calculation is not possible, for example for complex coil shapes. The question then is what can we do when we cannot derive a closed-form expression for $C^{(s)}$ and the answer is that we can always resort to its numerical computation using 2D Fast Fourier transforms.

Ideally we would like to be able to compute numerically $W_a^{(s)}$ and then use a 2D-FFT routine to compute $\tilde{W}_a^{(s)}$, which is actually $C^{(s)}$. Unfortunately, there seems to be no numerical method in the literature for computing $W_a^{(s)}$ and therefore its Fourier transform $C^{(s)}$. In contrast, there are many methods to compute numerically the isolated coil magnetic flux density and in this respect the alternative form of the source term is invaluable. This can be derived by considering the connection of the potential $W_a^{(s)}$ with the free-space magnetic flux density $\mathbf{B}^{(s)}$. From (5.19)-(5.21) we have

$$\begin{aligned}\tilde{\mathbf{B}}^{(s)}|_{z=0} &= \left[\tilde{B}_x^{(s)}\mathbf{x}_0 + \tilde{B}_y^{(s)}\mathbf{y}_0 + \tilde{B}_z^{(s)}\mathbf{z}_0\right]_{z=0} \\ &= \kappa C^{(s)}(ju\mathbf{x}_0 + jv\mathbf{y}_0 + \kappa\mathbf{z}_0)\end{aligned} \tag{5.49}$$

and therefore

$$C^{(s)} = \frac{\tilde{B}_x^{(s)}|_{z=0}}{ju\kappa} = \frac{\tilde{B}_y^{(s)}|_{z=0}}{jv\kappa} = \frac{\tilde{B}_z^{(s)}|_{z=0}}{\kappa^2} \tag{5.50}$$

The close connection of the source term to the components of the transformed magnetic field makes possible the use of source terms that are based on the transformed magnetic field components. For example, Burke (1990)

uses a source term $h^s(u,v)$ which is actually $\tilde{B}_z^{(s)}/(\mu_0 I)$.

From the numerical point of view the idea is to compute numerically for example $\tilde{B}_z^{(s)}(u,v)$ and from that derive numerical values of $C^{(s)}(u,v)$. Thus, we need numerical values of $B_z^{(s)}(x,y,z=0)$ and we have to use a fast numerical computation scheme. In the Appendix we discuss how is this possible by using the Biot-Savart law. The numerical scheme is shown in Fig.5.5.

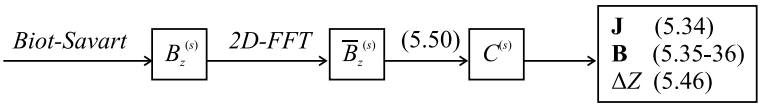

Fig. 5.5 Numerical computation scheme.

5.3 Analytical source term calculation

We will present now a number of methods to calculate the source term $C^{(s)}$ with the focus on the cylindrical coil. The same methods can be applied to other coil shapes and configurations such as rectangular coils with or without rounded corners, racetrack coils, D- and double-D coils, etc. We can follow two approaches. The first one involves a direct integration and the second one an indirect approach.

5.3.1 *The direct integration approach*

This approach is well suited to deriving source terms for filamentary loops. The derivation of the source term for the finite thickness coil is then performed by using superposition. Consider a filamentary current loop in free-space carrying a current I. The magnetic flux of this isolated current source can be derived from the Biot-Savart law:

$$\mathbf{B}^{(s)} = \frac{\mu_0 I}{4\pi} \nabla \times \oint_C \frac{d\mathbf{l}}{R} \tag{5.51}$$

where $d\mathbf{l}$ is the differential distance vector element tangential to the path of the source current C and $R = [(x-x_0)^2 + (y-y_0)^2 + (z-z_0)^2]^{1/2}$ is the distance between a source point (x_0, y_0, z_0) and a point where the field is calculated (x,y,z). Using the Stokes theorem the line integral is

transformed into a surface integral

$$\mathbf{B}^{(s)} = \frac{\mu_0 I}{4\pi} \nabla \times \iint\limits_S d\mathbf{s} \times \nabla_0 \left(\frac{1}{R} \right) \tag{5.52}$$

where the gradient operator ∇_0 acts with respect to the source coordinates and $d\mathbf{s}$ is the differential area vector normal to any surface S bounded by the path C. After some algebra (5.52) takes the following form

$$\mathbf{B}^{(s)} = \nabla \left[-\frac{\mu_0 I}{4\pi} \iint\limits_S d\mathbf{s} \cdot \nabla_0 \left(\frac{1}{R} \right) \right] \tag{5.53}$$

By comparing (5.53) and (5.9) the expression for $W_a^{(s)}$ becomes

$$W_a^{(s)} = -\frac{\mu_0 I}{4\pi} \iint\limits_S d\mathbf{s} \cdot \nabla_0 \left(\int \frac{dz}{R} \right) \tag{5.54}$$

where the expression for R^{-1}, in the Cartesian coordinate system, is found in see Morse and Feshbach (1953)

$$\frac{1}{R} = \frac{1}{2\pi} \int\limits_{-\infty}^{\infty} \int\limits_{-\infty}^{\infty} \frac{e^{\kappa(z-z_0)}}{\kappa} e^{ju(x-x_0)} e^{jv(y-y_0)} du dv \quad ; \quad z < z_0 \tag{5.55}$$

If (5.55) is replaced in (5.54) and the result compared to (5.13) and (5.15) we obtain the general expression for the source coefficient

$$C^{(s)} = -\frac{\mu_0 I}{2\kappa^2} \iint\limits_S d\mathbf{s} \cdot \nabla_0 e^{-[j(ux_0+vy_0)+\kappa z_0]} \tag{5.56}$$

We now apply (5.54) to a circular filamentary loop and examine two special cases: when this is parallel to the conducting half-space and when it is perpendicular to it. We then apply superposition to allow for respective finite thickness cylindrical coils of rectangular cross-section as shown in Fig.5.6.

5.3.1.1 *Parallel coil*

Consider a filamentary circular loop, with radius r_0, located at $z = z_0$ and driven by a current I. In this case we set $d\mathbf{s} = dx_0 dy_0 \mathbf{z}_0$ and (5.54) results

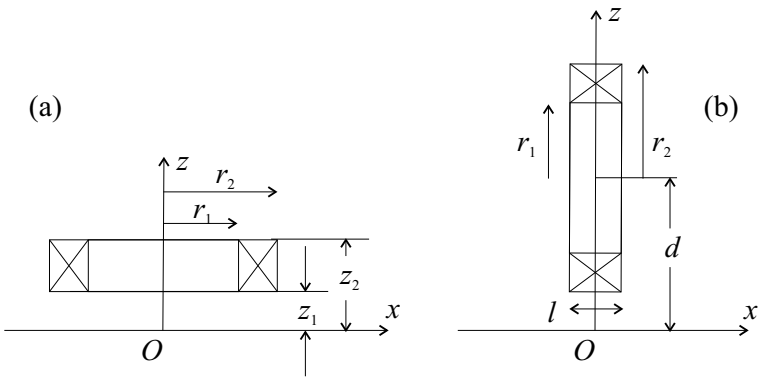

Fig. 5.6 (a) Parallel and (b) perpendicular isolated coil arrangement for calculation of $C^{(s)}$ with the direct integration approach.

in

$$W_a^{(s)} = \frac{\mu_0 I}{4\pi^2} \int_{-\infty}^{\infty} \int_{-\infty}^{\infty} \frac{e^{\kappa(z-z_0)}}{2\kappa} \left(\iint_S e^{-jux_0} e^{-jvy_0} dx_0 dy_0 \right) e^{jux} e^{jvy} du dv \tag{5.57}$$

hence

$$C^{(s)} = \mu_0 I \frac{e^{-\kappa z_0}}{2\kappa} \iint_S e^{-jux_0} e^{-jvy_0} dx_0 dy_0 \tag{5.58}$$

The double integration is carried over the circular surface of the loop and is facilitated by using a local polar coordinate transformation. Defining $x_0 = r_0 \cos\varphi_0$ and $y_0 = r_0 \sin\varphi_0$ the surface integral is written as

$$\int_{r=0}^{r_0} \int_{\varphi=0}^{2\pi} e^{-jr_0(u\cos\varphi_0 + v\sin\varphi_0)} r_0 dr_0 d\varphi_0 \tag{5.59}$$

The inner integral is evaluated using the following identity, see Eq.(3.937.2) in Gradshteyn (2000),

$$\int_0^{2\pi} e^{p\cos x + q\sin x} dx = 2\pi I_0 \left(\sqrt{p^2 + q^2} \right) \tag{5.60}$$

where $I_n(x)$ denotes the modified Bessel function of order n. Using also $I_0(jz) = J_0(z)$ and for the outer integral $\int x J_0(x) dx = x J_1(x)$ we derive

the result $r_0 J_1(\kappa r_0)/\kappa$ for (5.59). The final result for the source coefficient of the filamentary loop is

$$C^{(s)} = \mu_0 I \pi \frac{e^{-\kappa z_0}}{\kappa^2} r_0 J_1(\kappa r_0) \tag{5.61}$$

The coefficient for the rectangular cross-section coil is derived by superposition over this cross-section in the same manner as in the previous chapters. The final result is

$$C^{(s)} = \mu_0 \iota_0 \pi \frac{(e^{-\kappa z_1} - e^{-\kappa z_2})}{\kappa^5} \chi(\kappa r_1, \kappa r_2) \tag{5.62}$$

where $\iota_0 = NI/[(r_2 - r_1)(z_2 - z_1)]$ and $\chi(x_1, x_2)$ is defined in (3.27).

5.3.1.2 *Perpendicular coil*

Consider now a perpendicular filamentary circular loop, with radius r_0, lying on the plane $x = 0$ and driven by a current I. The center of the loop is located at $(x, y, z) = (0, 0, d)$. In this case we set $d\mathbf{s} = dy_0 dz_0 \mathbf{x}_0$ and (5.54) results in

$$W_a^{(s)} = \frac{\mu_0 I}{4\pi^2} \int_{-\infty}^{\infty} \int_{-\infty}^{\infty} ju \frac{e^{\kappa z}}{2\kappa^2} \left(\iint_S e^{\kappa z_0} e^{-jvy_0} dy_0 dz_0 \right) e^{jux} e^{jvy} du dv \tag{5.63}$$

hence

$$C^{(s)} = \mu_0 I \frac{ju}{2\kappa^2} \iint_S e^{-\kappa z_0} e^{-jvy_0} dy_0 dz_0 \tag{5.64}$$

The double integration is carried over the circular surface of the loop and is facilitated by using a local polar coordinate transformation. Defining $y_0 = r_0 \sin\varphi_0$ and $z_0 = d - r_0 \cos\varphi_0$ the surface integral is written as

$$e^{-\kappa d} \int_{r=0}^{r_0} \int_{\varphi=0}^{2\pi} e^{r_0(\kappa \cos\varphi_0 - jv \sin\varphi_0)} r_0 dr_0 d\varphi_0 \tag{5.65}$$

The inner integral is evaluated again using (5.60) to $2\pi I_0(\sqrt{\kappa^2 - v^2} r_0) = 2\pi I_0(u r_0)$. After also using $\int x I_0(x) dx = x I_1(x)$ we derive the result $2\pi r_0 I_1(u r_0)/u$ for the double integral in (5.65). The final result for the source coefficient of the filamentary loop is

$$C^{(s)} = \mu_0 I \pi \frac{\kappa e^{-\kappa d}}{u} r_0 I_1(u r_0) \tag{5.66}$$

The coefficient for the rectangular cross-section coil is derived by superposition over this cross-section in the same manner we did that in Chapter 3. This involves integration of the term $r_0 I_1(ur_0)$ from the inner radius r_1 to the outer radius r_2 and integration of the term $e^{ju\Delta l}$ from $-l/2$ to $l/2$, see Fig.5.6. The latter term is multiplied with the coefficient expression in 5.66 in order to represent a filamentary coil displaced by Δl. The final result is

$$C^{(s)} = j\mu_0 \iota_0 2\pi \frac{\mathrm{e}^{-\kappa d}}{u^3} \sin\left(\frac{ul}{2}\right) M(ur_1, ur_2) \tag{5.67}$$

where $\iota_0 = NI/[(r_2 - r_1)l]$ and the term $M(ur_1, ur_2)$ denotes a finite integral of the modified Bessel function that can be expressed as follows

$$M(x_1, x_2) = \int_{x_1}^{x_2} x I_1(x) dx = \frac{\pi}{2} x \left[I_0(x)\mathbf{L}_1(x) - I_1(x)\mathbf{L}_0(x) \right]_{x_1}^{x_2} \tag{5.68}$$

where $\mathbf{L}_n$ denotes the modified Struve function of order n. Later, when we comment on the computational aspects of the solution, we give some directions on computing $M(x_1, x_2)$ efficiently.

5.3.2 *The indirect approach*

We have chosen the term indirect to denote the approach of calculating the source term by utilizing already known integral expressions for the free-space magnetic field of a coil. We demonstrate this approach for the case of the parallel and the tilted cylindrical coil.

5.3.2.1 *Parallel coil*

From Chapter 3 where we studied this axisymmetric configuration we know such an expression for the magnetic flux density in the region below the coil. We can work with any of the two components, for example the expression for the z-component is:

$$B_z^{(s)} = \frac{\mu_0 \iota_0}{2} \int_0^{\infty} \frac{\chi(\kappa r_1, \kappa r_2)}{\kappa^2} \left(e^{-\kappa z_1} - e^{-\kappa z_2} \right) e^{\kappa z} J_0(\kappa r) d\kappa \tag{5.69}$$

Now we can transform this integral using the following identity which relates the inverse Hankel transform to the 2D inverse Fourier transform for a

function which exhibits axisymmetry, Papoulis (1968)

$$\int_0^\infty F(\kappa)J_0(\kappa r)\kappa d\kappa = \frac{1}{2\pi}\int_{-\infty}^{\infty}\int_{-\infty}^{\infty} F(u,v)e^{j(ux+vy)}dudv \tag{5.70}$$

where $\kappa = (u^2+v^2)^{1/2}$. Using (5.70) in (5.69) the magnetic flux becomes

$$B_z^{(s)} = \frac{\mu_0\iota_0}{4\pi}\int_{-\infty}^{\infty}\int_{-\infty}^{\infty}\frac{\chi(\kappa r_1,\kappa r_2)}{\kappa^3}\left(e^{-\kappa z_1}-e^{-\kappa z_2}\right)e^{\kappa z}e^{jux}e^{jvy}dudv \tag{5.71}$$

Now, from $B_z^{(s)} = \partial^2 W_a^{(s)}/\partial z^2$ we can write the expression for the source potential

$$W_a^{(s)} = \frac{\mu_0\iota_0}{4\pi}\int_{-\infty}^{\infty}\int_{-\infty}^{\infty}\frac{\chi(\kappa r_1,\kappa r_2)}{\kappa^5}\left(e^{-\kappa z_1}-e^{-\kappa z_2}\right)e^{\kappa z}e^{jux}e^{jvy}dudv \tag{5.72}$$

and therefore deduce the expression for the source term of the parallel coil

$$C^{(s)} = \mu_0\iota_0\pi\frac{\chi(\kappa r_1,\kappa r_2)}{\kappa^5}\left(e^{-\kappa z_1}-e^{-\kappa z_2}\right) \tag{5.73}$$

5.3.2.2 *The tilted coil*

We have said that the indirect approach is applied to existing expressions for magnetic field of the various coil designs. Consider the case of the tilted coil in Fig.5.7, which is also analyzed in Theodoulidis (2005d). This is actually the cylindrical coil oriented in such a way that its axis is still lying on the $y = 0$ plane, forming an angle φ with respect to the z axis and its center of rotation is at the coil center $(x, y, z) = (0, 0, d)$. We also identify the lift-off l_0 as the minimum distance between coil and conductor, which is kept constant during the coil rotation. Thus, when the coil is rotated, the coil center is kept on the z-axis but d is increased. This is a general arrangement and the parallel and perpendicular arrangements can be seen as the limiting cases $\varphi = 0$ and $\varphi = \pi/2$ respectively. In order to calculate $C^{(s)}$ we use the indirect approach to get an expression for the magnetic field of the relevant filamentary loop and then use superposition over the coil's cross-section. Consider Fig.5.8 where a loop of radius r_0 and current I is positioned so that it can be rotated around its center at $(x_0, y_0, z_0) = (0, 0, d)$.

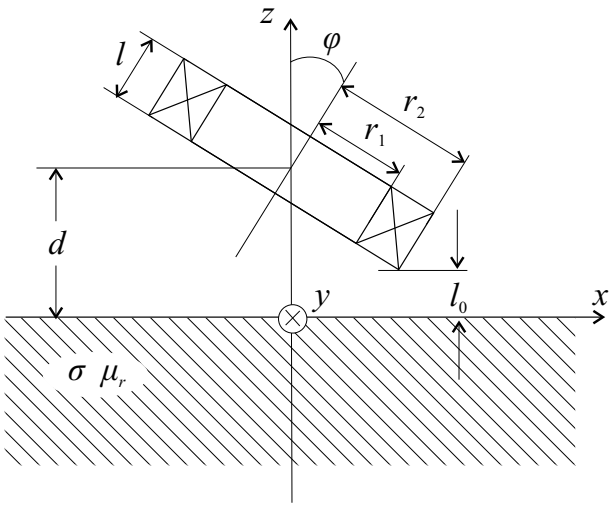

Fig. 5.7 Tilted cylindrical coil above a conductive half-space. The cross-sectional view shows the $y = 0$ plane.

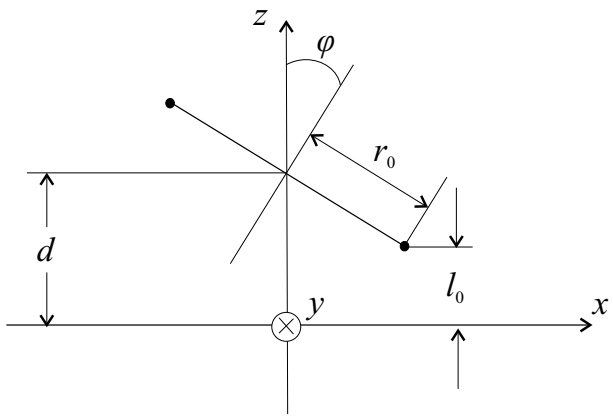

Fig. 5.8 Tilted filamentary circular loop in free-space. The cross-sectional view shows the $y = 0$ plane.

Following Tsaknakis (1985), where the isolated filamentary circular loop coil produces a magnetic flux density in the region below the coil $z < l_0$

$$B_z(x, y, z) = \frac{j\mu_0 r_0 I}{4\pi} \int_{-\infty}^{\infty} \int_{-\infty}^{\infty} I_1(\psi r_0) e^{\kappa(z-d)} e^{jux} e^{jvy} du dv \qquad (5.74)$$

where $d = l_0 + r_0 \sin|\varphi|$ and $\psi = u \sin\varphi + j\kappa \cos\varphi$ with angle φ taken positive for an anti-clockwise rotation and negative for a clockwise rotation. This result was obtained using the magnetic vector potential and a technique where the filamentary loop is considered as the intersection of two surfaces. A similar result was obtained by Beissner (1984) using coordinate transformations in Fourier space. From (5.74) and (5.36) the source term for the filamentary loop is

$$C^{(s)}(u,v) = j\mu_0 I \pi r_0 I_1(\psi r_0) e^{-\kappa d} \tag{5.75}$$

The procedure to find the source term for the rectangular cross-section coil of Fig.5.7 involves two superposition steps:

- Step 1: from filamentary to flat coil.

The first superposition is performed in terms of the filamentary coil radius r_0 in order to find the source term for the flat coil of Fig.5.9. This involves integration of the term $r_0 I_1(\psi r_0)$ from the inner to the outer radius of the flat coil and the result is

$$C^{(s)}(u,v) = j n_f I \mu_0 \pi \frac{M(\psi r_1, \psi r_2)}{\psi^2} e^{-\kappa d} \tag{5.76}$$

where now $d = l_0 + r_2 \sin|\varphi|$, n_f is the turns density of the flat coil and $M(x_1, x_2)$ is defined in (5.68).

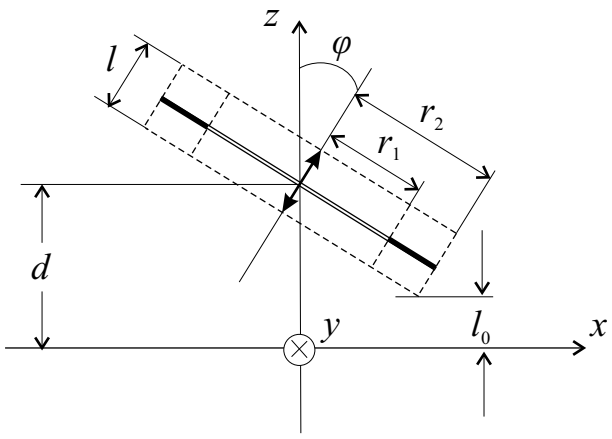

Fig. 5.9 Tilted flat coil in free-space. The cross-sectional view shows the $y = 0$ plane. The final coil cross-section after superposition is also shown as a dashed outline.

- Step 2: from flat to finite cross-section coil.

The second superposition is performed along the axis of the flat coil (the range of integration is depicted by the bold arrow in Fig.5.9). When a new flat coil is displaced by Δl along its axis, its center lies at the point $(x_0, y_0, z_0) = (\Delta l \sin\varphi, 0, d + \Delta l \cos\varphi)$ and therefore its source term is written as

$$C^{(s)}(u,v)e^{ju\Delta l \sin\varphi}e^{-\kappa\Delta l\cos\varphi} = C^{(s)}(u,v)e^{j\psi\Delta l} \tag{5.77}$$

where $C^{(s)}(u,v)$ is taken from (5.76). The source term for the coil of Fig.5.7 is obtained by integrating Δl from $-l/2$ to $+l/2$. The dashed outline in Fig.5.9 shows the final coil cross-section. The result is

$$C^{(s)}(u,v) = j2\pi\mu_0 nI\frac{M(\psi r_1, \psi r_2)}{\psi^3}e^{-\kappa d}\sin\left(\frac{\psi l}{2}\right) \tag{5.78}$$

After substituting (5.78) in (5.47), we get the expression for the impedance change

$$\Delta Z = j8\omega\mu_0 n^2 \int_0^\infty\int_0^\infty \frac{e^{-2\kappa d}}{\kappa}\left|\frac{M(\psi r_1,\psi r_2)}{\psi^3}\sin\left(\frac{\psi l}{2}\right)\right|^2 \frac{\mu_r\kappa-\lambda}{\mu_r\kappa+\lambda}dudv \tag{5.79}$$

where now $d = l_0 + r_2\sin|\varphi| + (l/2)\cos\varphi$.

A useful check is whether (5.78) reduces either to (5.62) or to (5.67) for the relevant tilt angles. In the perpendicular coil case when $\varphi = \pm\pi/2$ and $\psi = \pm u$ it is trivial and in the parallel coil case when $\varphi = 0$ and $\psi = ja$ it is easily shown after noting that $M(jar_1, jar_2) = j\chi(ar_1, ar_2)$.

Incidentally, the term $\sin(\psi l/2)$ in (5.79) may cause overflow if automatic integration routines are used and u and v take very large values. The problem is overcome by making the following substitution that results in a more stable numerical scheme

$$e^{-ad}\sin\left(\frac{\psi l}{2}\right) = \frac{e^{j\psi l/2-ad} - e^{-j\psi l/2-ad}}{2j} \tag{5.80}$$

5.3.2.3 *Arbitrary orientation coil*

Any other cylindrical coil arrangement can be modelled beginning with the basic configuration of the tilted coil and applying 2D Fourier identities for the skewed and shifted functions. Thus, if the coil is rotated around the

Table 5.1 Test parameters for the numerical computations in Figs 5.10-5.11.

Coil		Testpiece	
r_1	2 mm	σ	18.72 MS/m
r_2	4 mm	μ_r	1
l	2 mm		
l_0	1 mm		
N	400		

z-axis by an angle θ and shifted so that its center lies above (x_0, y_0) the new source term is calculated from the old one by

$$C^{(s)}(u\cos\theta + v\sin\theta, -u\sin\theta + v\cos\theta)e^{jux_0}e^{jvy_0} \tag{5.81}$$

5.3.3 *Numerical aspects and results*

Concerning the numerical aspects of the solution the reader should refer to the relevant section in Chapter 3. The additional aspects are now the computation of a double integral of infinite range and the computation of the finite integral $M(x_1, x_2)$ in (5.68) as well as the possible application of 2D-FFT routines. The infinite range integrals are computed using again the methods presented in Chapter 3, care should be taken to avoid recursion when using for example the Fortran routine `DQAGI`.

For the computation of $M(x_1, x_2)$, which is also present in (5.78) with a complex argument, we can avoid the calculation of the complex modified Struve function by using the identity

$$\int^z I_1(x)\,x\,dx = zI_0(z) - \int^z I_0(x)dx \tag{5.82}$$

and then compute the integral in (5.82) by the very fast converging series, Gradshteyn (2000)

$$\int^z I_0(x)dx = 2\sum_{k=0}^{\infty}(-1)^k I_{2k+1}(z) \tag{5.83}$$

Computation of the field quantities, eddy current density from (5.34) and magnetic flux density from (5.35)-(5.36), is facilitated by the use of 2D-Fast Fourier Transform routines. Thus, instead of computing a double integral at each space point we can just compute the integrand in a wide range and then apply an inverse 2D-FFT routine. The economy in

computational time is enormous. In order to decide on the spatial cut-off frequency we have to take into account the well known Fourier identity for the u and v range

$$\begin{aligned} ux &= 2\pi N_x \\ vy &= 2\pi N_y \end{aligned} \tag{5.84}$$

where u, v are the total range in the Fourier space and x, y are the total space to which the FFT will provide a solution.

Fig.5.10 shows amplitude contours and streamlines or surface eddy currents at three tilt angles for the test parameters of Table 5.1. The streamlines are contour plots of a scalar function ϕ where $\mathbf{J} = \nabla \times (\phi \mathbf{z}_0)$ and the expression for ϕ can be easily deduced from (5.34). For a parallel coil eddy currents flow on circular paths while for the perpendicular coil eddy current flow is uniform underneath the coil but tends to a circular pattern on either side of the coil faces. We note that the flow pattern for the $\varphi = 45^o$ tilt angle has an intermediate form compared to the parallel and perpendicular ones. As expected, eddy current density is stronger on the side where the coil is closer to the conductive half-space. Eq. (5.34) is also very useful in the assessment of the eddy current penetration depth. Previous numerical and experimental studies have shown that the perpendicular coil achieves greater penetration that the parallel one, Hoshikawa (1999) and Janousek (2005).

Fig.5.11 plots the normalized probe inductive reactance change vs normalized probe resistance change. Following the usual practice in eddy current NDE, the impedance is normalized to the reactance of the coil in free-space X_0. The arc-like curves are frequency curves and they are computed for zero lift-off (the coil touches the conductor surface) and for tilt angles of $\varphi = 0^o$, 10^o and 20^o. The straight lines, computed at four distinct frequencies, are tilt curves and we observe the decrease of impedance change with tilt angle due to the weaker electromagnetic coupling of the coil with the conductive half-space. We also observe that the tilt curves have a strong resemblance to lift-off curves, with which they share the same phase, see Fig.3.5 in Chapter 3. The constant phase signal is produced by any coil position or orientation change and it is characteristic of eddy current testing.

Together with lift-off, probe tilt is identified as the major source of noise in eddy current surface inspections. Conditions of tilt are met, for example,

when surface scanning manually or when using special probe designs comprising coils with a specific orientation. With the presented model there is no need to resort to computationally demanding numerical models such as 3D-FEM for the assessment of the tilt noise, Albanese (2004).

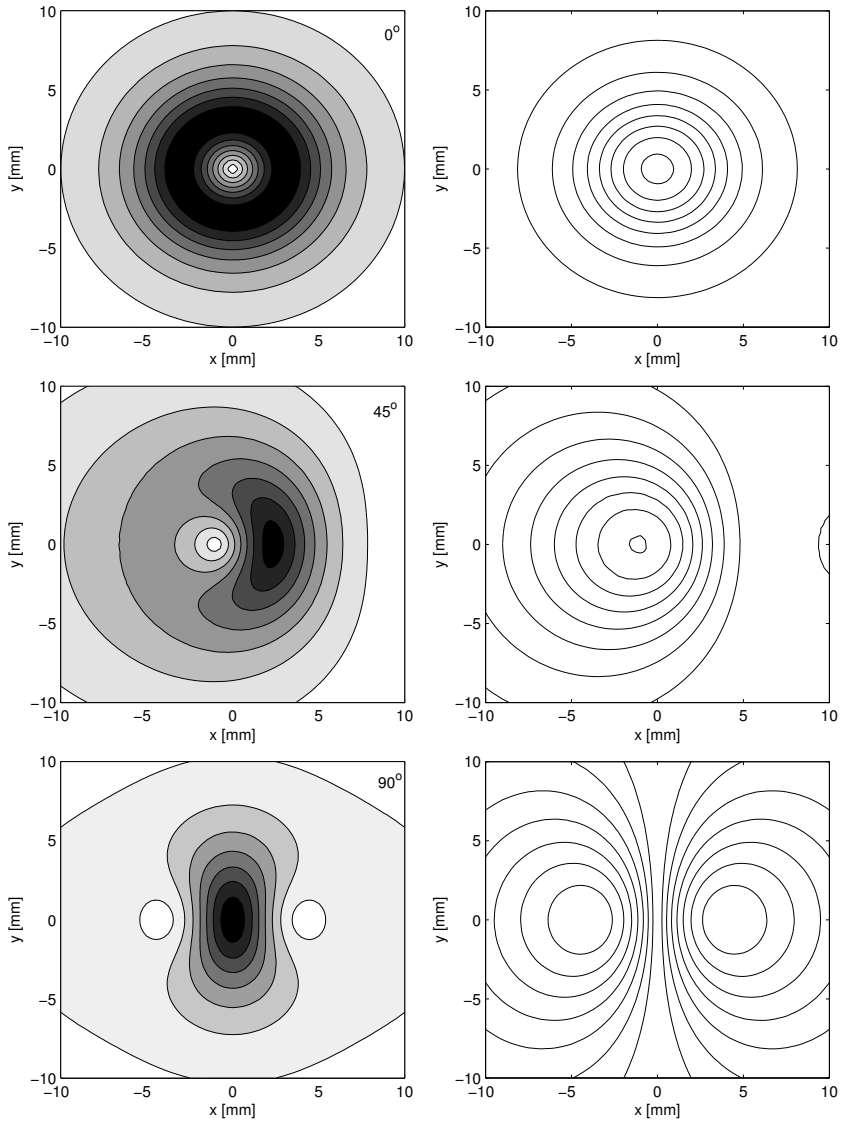

Fig. 5.10 Amplitude contours (left) and streamlines (right) of eddy currents induced on the surface of a conductive half-space by a cylindrical coil at various tilt angles. Coil rotation is clockwise.

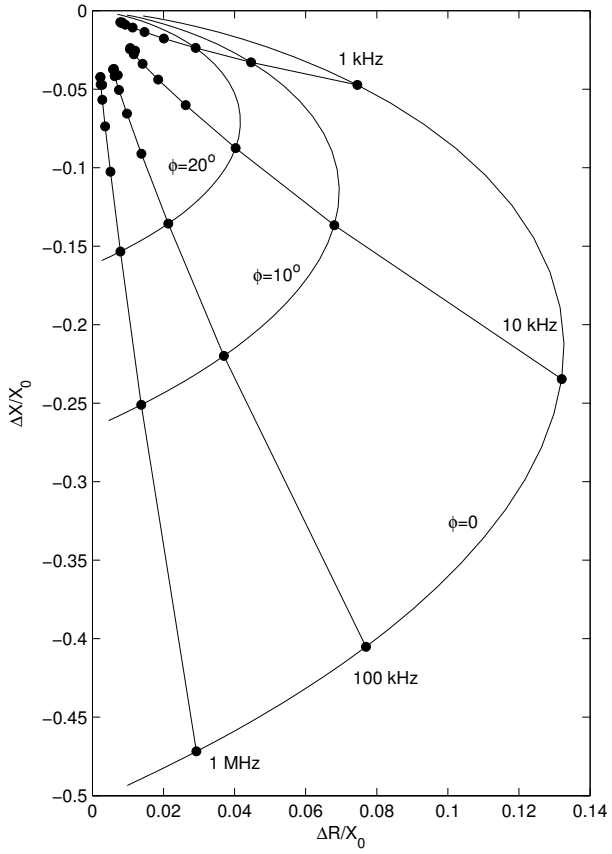

Fig. 5.11 Impedance change display showing tilt and frequency curves.

Chapter 6

Alternative Solutions for 3D Configurations

6.1 Introduction

In Chapter 5 we studied the problem of eddy current induction due to an arbitrarily shaped coil above a conductive half-space. The technique used was the SOVP formulation and the coordinate system was the Cartesian. The choice for the unit vector in the definition of $\mathbf{W}$ was $\mathbf{z}_0$ (z-preferred direction). This direction was perpendicular to the surface plane of the conductor and as a consequence the TM potential W_b vanished throughout the conductor volume and the whole problem reduced to the solution of a scalar one. In this chapter we show that solution of the problem is possible in the Cartesian coordinate system with an x or y preferred direction (tangential to the surface plane) and also in the cylindrical coordinate system. The alternative expressions provided for the electromagnetic field and the coil impedance can be more convenient depending on the specific configuration characteristics. For example, the x-preferred direction is reformulated in the next chapter to solve for the 3D edge problem while the solution in the cylindrical coordinate system facilitates the analysis of sources with cylindrical shape.

6.2 Cartesian coordinate system

With reference to the general 3D induction problem, which is shown again in Fig.6.1. we define the SOVP with an x-preferred direction

$$\mathbf{W} = W_a \mathbf{x}_0 + \mathbf{x}_0 \times \nabla W_b \tag{6.1}$$

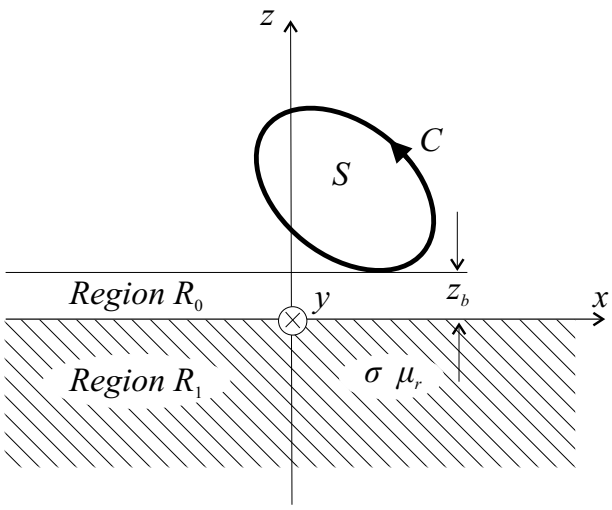

Fig. 6.1 General 3D coil arrangement above a planar conductor.

Now the equations connecting the components of **A** and **B** to W_a and W_b have a different form to the ones for the z-preferred direction (5.3)-(5.8)

$$A_x = \frac{\partial^2 W_b}{\partial y^2} + \frac{\partial^2 W_b}{\partial z^2} \tag{6.2}$$

$$A_y = \frac{\partial W_a}{\partial z} - \frac{\partial^2 W_b}{\partial x \partial y} \tag{6.3}$$

$$A_z = -\frac{\partial W_a}{\partial y} - \frac{\partial^2 W_b}{\partial x \partial z} \tag{6.4}$$

$$B_x = -k^2 W_a + \frac{\partial^2 W_a}{\partial x^2} \tag{6.5}$$

$$B_y = k^2 \frac{\partial W_b}{\partial z} + \frac{\partial^2 W_a}{\partial x \partial y} \tag{6.6}$$

$$B_z = -k^2 \frac{\partial W_b}{\partial y} + \frac{\partial^2 W_a}{\partial x \partial z} \tag{6.7}$$

As expected A_x depends only on W_b and B_x depends only on W_a. For the non-conductive region, the terms containing k^2 vanish and **B** can be written again as the gradient of a scalar quantity

$$\mathbf{B} = \nabla \left(\frac{\partial W_a}{\partial x} \right) \tag{6.8}$$

6.2.1 *Solution of the general problem*

Again we solve the general 3D problem without taking into account the TM potential in air. Thus, in region R_0 ($0 \leq z \leq z_b$) we have $W_a^{(0)} = W_a^{(s)} + W_a^{(ec)}$ while in region R_1 ($z \leq 0$) we have both potentials $W_a^{(1)}$ and $W_b^{(1)}$. Following (5.12)-(5.13) their 2D Fourier transforms are again written as in (5.15)-(5.18). $C^{(s)}$ is still the source coefficient and the other unknown coefficients $D^{(ec)}$, $C_a^{(1)}$, $C_b^{(1)}$ are determined in terms of it from the interface conditions at $z = 0$. The transformed magnetic field components are now written in terms of the transformed magnetic potentials from (6.5)-(6.7) as:

$$\tilde{B}_x = -k^2 \tilde{W}_a - u^2 \tilde{W}_a \tag{6.9}$$

$$\tilde{B}_y = k^2 \frac{\partial \tilde{W}_b}{\partial z} - uv\tilde{W}_a \tag{6.10}$$

$$\tilde{B}_z = -k^2 jv\tilde{W}_b + ju\frac{\partial \tilde{W}_a}{\partial z} \tag{6.11}$$

and the interface conditions now become

$$\tilde{H}_x^{(0)} = \tilde{H}_x^{(1)} \Rightarrow -\frac{1}{\mu_0} u^2 \left(\tilde{W}_a^{(s)} + \tilde{W}_a^{(ec)}\right) = \frac{1}{\mu_0 \mu_r} \left(-k^2 \tilde{W}_a^{(1)} - u^2 \tilde{W}_a^{(1)}\right) \tag{6.12}$$

$$\tilde{H}_y^{(0)} = \tilde{H}_y^{(1)} \Rightarrow -\frac{1}{\mu_0} uv \left(\tilde{W}_a^{(s)} + \tilde{W}_a^{(ec)}\right) = \frac{1}{\mu_0 \mu_r} \left(k^2 \frac{\partial \tilde{W}_b^{(1)}}{\partial z} - uv\tilde{W}_a^{(1)}\right) \tag{6.13}$$

$$\tilde{B}_z^{(0)} = \tilde{B}_z^{(1)} \Rightarrow ju\frac{\partial \left(\tilde{W}_a^{(s)} + \tilde{W}_a^{(ec)}\right)}{\partial z} = -k^2 jv\tilde{W}_b^{(1)} + ju\frac{\partial \tilde{W}_a^{(1)}}{\partial z} \tag{6.14}$$

These equations yield the following linear system of equations for the unknown coefficients

$$-u^2 \mu_r \left(C^{(s)} + D^{(ec)}\right) = -(k^2 + u^2) C_a^{(1)} \tag{6.15}$$

$$-uv\mu_r \left(C^{(s)} + D^{(ec)}\right) = k^2 \lambda C_b^{(1)} - uvC_a^{(1)} \tag{6.16}$$

$$ju\kappa \left(C^{(s)} - D^{(ec)}\right) = -k^2 jvC_b^{(1)} + ju\lambda C_a^{(1)} \tag{6.17}$$

The solution of the system in terms of $C^{(s)}$ is

$$D^{(ec)} = -\frac{\kappa\mu_r - \lambda}{\kappa\mu_r + \lambda} C^{(s)} = R(u,v) C^{(s)} \tag{6.18}$$

$$C_a^{(1)} = \frac{2u^2\lambda\mu_r}{(u^2+k^2)(\kappa\mu_r+\lambda)} C^{(s)} \tag{6.19}$$

$$C_b^{(1)} = \frac{2uv\mu_r}{(u^2+k^2)(\kappa\mu_r+\lambda)} C^{(s)} \tag{6.20}$$

As in Chapter 5, the term $R(u,v)$ is a reflection coefficient which determines the relationship of the eddy current secondary field to the incident free-space source field. But here we have the first difference with the z-preferred direction, the transverse magnetic potential W_b is not zero (does not vanish). Using (6.18)-(6.20) the final expressions for the potential in the two regions of interest are

$$W_a^{(0)}(x,y,z) = \frac{1}{4\pi^2} \int_{-\infty}^{\infty}\int_{-\infty}^{\infty} \left(e^{\kappa z} - \frac{\kappa\mu_r - \lambda}{\kappa\mu_r + \lambda} e^{-\kappa z} \right) C^{(s)} e^{jux} e^{jvy} du dv \tag{6.21}$$

$$W_a^{(1)}(x,y,z) = \frac{1}{4\pi^2} \int_{-\infty}^{\infty}\int_{-\infty}^{\infty} \frac{2u^2\lambda\mu_r}{(u^2+k^2)(\kappa\mu_r+\lambda)} e^{\lambda z} C^{(s)} e^{jux} e^{jvy} du dv \tag{6.22}$$

$$W_b^{(1)}(x,y,z) = \frac{1}{4\pi^2} \int_{-\infty}^{\infty}\int_{-\infty}^{\infty} \frac{2uv\mu_r}{(u^2+k^2)(\kappa\mu_r+\lambda)} e^{\lambda z} C^{(s)} e^{jux} e^{jvy} du dv \tag{6.23}$$

The left term in the parenthesis of (6.21) corresponds to the part of $W_a^{(0)}$ due to the source $W_a^{(s)}$ and the right term to the part due to the eddy currents $W_a^{(ec)}$. A good check of the results would be to see whether the z-component of the eddy current density is zero. Working with its Fourier transform and taking into account that $\tilde{J}_z = -j\omega\sigma\tilde{A}_z$ and

$$\begin{aligned} \tilde{A}_z &= -\frac{\partial \tilde{W}_a}{\partial y} - \frac{\partial^2 \tilde{W}_b}{\partial x \partial z} = -jv\tilde{W}_a - ju\frac{\partial \tilde{W}_b}{\partial z} \\ &= -jvC_a^{(1)} e^{\lambda z} - ju\lambda C_b^{(1)} e^{\lambda z} = -je^{\lambda z}\left(vC_a^{(1)} + u\lambda C_b^{(1)} \right) = 0 \end{aligned} \tag{6.24}$$

we deduce that it is indeed so. Thus, the eddy current density has only x and y components and in terms of the source coefficient is now written as follows

$$\mathbf{J} = \frac{-j\omega\sigma}{4\pi^2} \int_{-\infty}^{\infty} \int_{-\infty}^{\infty} C^{(s)} \frac{2u\mu_r}{\kappa\mu_r + \lambda} \left(v\mathbf{x}_0 - u\mathbf{y}_0\right) e^{\lambda z} e^{jux} e^{jvy} dadb \tag{6.25}$$

6.2.2 *The ΔZ formula*

Following again the analysis in Chapter 5, the impedance change is written as

$$\Delta Z = \frac{-j\omega}{\mu_0 I^2} \int_{z=0} \mathbf{z}_0 \cdot \left(\frac{\partial W_a^{(0)}}{\partial x} \mathbf{B}^{(s)} - \frac{\partial W_a^{(s)}}{\partial x} \mathbf{B}^{(0)} \right) dxdy \tag{6.26}$$

which again depends only on $W_a^{(0)}$ and $W_a^{(s)}$ if we substitute for $\mathbf{B}^{(s)}$ and $\mathbf{B}^{(0)}$ using

$$\mathbf{z}_0 \cdot \mathbf{B}^{(s)} = \frac{\partial^2 W_a^{(s)}}{\partial x \partial z} \tag{6.27}$$

$$\mathbf{z}_0 \cdot \mathbf{B}^{(0)} = \frac{\partial^2 W_a^{(0)}}{\partial x \partial z} \tag{6.28}$$

Noting also that $W_a^{(0)} = W_a^{(s)} + W_a^{(ec)}$ and after some algebraic manipulation, (6.26) takes the form

$$\Delta Z = \frac{-j\omega}{\mu_0 I^2} \int_{-\infty}^{\infty} \int_{-\infty}^{\infty} \left(\frac{\partial W_a^{(ec)}}{\partial x} \frac{\partial^2 W_a^{(s)}}{\partial x \partial z} - \frac{\partial W_a^{(s)}}{\partial x} \frac{\partial^2 W_a^{(ec)}}{\partial x \partial z} \right)_{z=0} dxdy \tag{6.29}$$

Upon substituting for $W_a^{(s)}$ and $W_a^{(ec)}$ from (6.21) and applying Parseval's theorem for Fourier transforms, the impedance change reduces to

$$\Delta Z = \frac{j\omega}{2\pi^2 \mu_0 I^2} \int_{-\infty}^{\infty} \int_{-\infty}^{\infty} \kappa u^2 C^{(s)}(-u, -v) D^{(ec)}(u, v) dudv \tag{6.30}$$

If we further use (6.18) and note that $W_a^{(s)}$ is a real function so that $C^{(s)}(-u,-v) = \left[C^{(s)}(u,v)\right]^*$ the above expression becomes

$$\Delta Z = \frac{j\omega}{2\pi^2\mu_0 I^2} \int_{-\infty}^{\infty}\int_{-\infty}^{\infty} \kappa u^2 \left|C^{(s)}(u,v)\right|^2 R(u,v)dudv \tag{6.31}$$

or equivalently

$$\Delta Z = \frac{j\omega 2}{\pi^2\mu_0 I^2} \int_{0}^{\infty}\int_{0}^{\infty} \kappa u^2 \left|C^{(s)}(u,v)\right|^2 R(u,v)dudv \tag{6.32}$$

This is the general expression for the impedance change when using the x-preferred direction. It is made specific to a particular coil through the $C^{(s)}$ source term. Incidentally, the general expression for ΔZ with a y-preferred direction is similar to (6.32) and is derived by replacing u^2 with v^2.

6.2.3 *Source term*

Again the key to the calculation of the electromagnetic field and coil impedance is the calculation of the source term $C^{(s)}$. This is of course different from $C^{(s)}$ calculated in Chapter 5 and has to be recalculated for the x-preferred direction. All the techniques presented with the z-preferred direction are also applicable with the x-preferred direction. Since for the latter we are not going into full detail, we just provide here the general expression for the direct integration technique for a filamentary coil and use the indirect technique for the cylindrical coil.

6.2.3.1 *The direct integration approach*

Comparing (5.53) to (6.8) we deduce the general expression for the TE potential of an isolated filamentary coil loop

$$W_a^{(s)} = -\frac{\mu_0 I}{4\pi} \iint_S d\mathbf{s} \cdot \nabla_0 \left(\int \frac{dx}{R}\right) \tag{6.33}$$

where R^{-1} is replaced by its expression in the Cartesian coordinate system (5.55). This approach of a direct integration with an x-preferred direction was favored by Xypteras (1978) and Kriezis (1979) in the analysis of the filamentary circular loop in a perpendicular position to the conductive half-space.

6.2.3.2 *The indirect integration approach*

Starting again from the axisymmetric configuration of the cylindrical coil and the expression for B_z in the region below the coil and transforming it to a double Fourier integral as in Chapter 5 we derive (5.71), which is repeated here for convenience

$$B_z^{(s)} = \frac{\mu_0 \iota_0}{4\pi} \int_{-\infty}^{\infty} \int_{-\infty}^{\infty} \frac{\chi(\kappa r_1, \kappa r_2)}{\kappa^3} \left(e^{-\kappa z_1} - e^{-\kappa z_2}\right) e^{\kappa z} e^{jux} e^{jvy} du dv \quad (6.34)$$

Now, from $B_z^{(s)} = \partial^2 W_a^{(s)} / \partial x \partial z$ we can write the expression for the source potential

$$W_a^{(s)} = \frac{\mu_0 \iota_0}{4\pi} \int_{-\infty}^{\infty} \int_{-\infty}^{\infty} \frac{\chi(\kappa r_1, \kappa r_2)}{\kappa^2 (ju)} \left(e^{-\kappa z_1} - e^{-\kappa z_2}\right) e^{\kappa z} e^{jux} e^{jvy} du dv \quad (6.35)$$

and therefore deduce the expression for the source term of the parallel coil

$$C^{(s)} = \mu_0 \iota_0 \frac{\chi(\kappa r_1, \kappa r_2)}{\kappa^2 (ju)} \left(e^{-\kappa z_1} - e^{-\kappa z_2}\right) \quad (6.36)$$

If we substitute (6.36) in (6.32) we derive the same expression for ΔZ that we derived by using the z-preferred direction, since the impedance change of the coil does not depend on the choice of the direction in the potential definition.

6.3 Cylindrical coordinate system

Apart from the Cartesian coordinate system the conductive half-space geometry can also be analyzed in the circular cylinder coordinate system, the general configuration is shown in Fig.6.2. In the cylindrical coordinate system, we have no other choice in the definition of $\mathbf{W}$ but to use the unit vector in the z-direction (see the discussion in Chapter 1), hence

$$\mathbf{W} = W_a \mathbf{z}_0 + \mathbf{z}_0 \times \nabla W_b \quad (6.37)$$

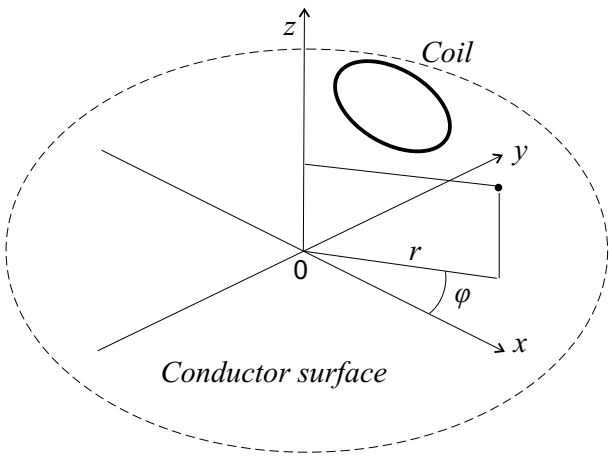

Fig. 6.2 General 3D coil arrangement above a planar conductor. The coordinate system used is the cylindrical one.

and the components of $\mathbf{A}$ and $\mathbf{B}$ are connected to W_a and W_b through (1.55)-(1.60) that are rewritten here for convenience

$$A_r = \frac{1}{r}\frac{\partial W_a}{\partial \varphi} - \frac{\partial^2 W_b}{\partial r \partial z} \tag{6.38}$$

$$A_\varphi = -\frac{\partial W_a}{\partial r} - \frac{1}{r}\frac{\partial^2 W_b}{\partial \varphi \partial z} \tag{6.39}$$

$$A_z = \frac{\partial^2 W_b}{\partial r^2} + \frac{1}{r}\frac{\partial W_b}{\partial r} + \frac{1}{r^2}\frac{\partial^2 W_b}{\partial \varphi^2} \tag{6.40}$$

$$B_r = \frac{k^2}{r}\frac{\partial W_b}{\partial \varphi} + \frac{\partial^2 W_a}{\partial r \partial z} \tag{6.41}$$

$$B_\varphi = -k^2\frac{\partial W_b}{\partial r} + \frac{1}{r}\frac{\partial^2 W_a}{\partial \varphi \partial z} \tag{6.42}$$

$$B_z = -k^2 W_a + \frac{\partial^2 W_a}{\partial z^2} \tag{6.43}$$

and again for the non-conductive region, the terms containing k^2 vanish and $\mathbf{B}$ can be written again as the gradient of a scalar quantity

$$\mathbf{B} = \nabla\left(\frac{\partial W_a}{\partial z}\right) \tag{6.44}$$

The potentials satisfy the scalar Helmholtz (or Laplace for $k = 0$) differential equation

$$\frac{1}{r}\frac{\partial}{\partial r}\left(r\frac{\partial W_{a,b}}{\partial r}\right) + \frac{1}{r^2}\frac{\partial^2 W_{a,b}}{\partial \varphi^2} + \frac{\partial^2 W_{a,b}}{\partial z^2} = k^2 W_{a,b} \tag{6.45}$$

After defining the forward and inverse exponential Fourier series transform

$$\tilde{W}_a^{(s)}(r, m, z) = \frac{1}{2\pi}\int_{-\pi}^{\pi} W_a^{(s)}(r, \varphi, z)e^{-jm\varphi}d\varphi \tag{6.46}$$

$$W_a^{(s)}(r, \varphi, z) = \sum_{m=-\infty}^{\infty} \tilde{W}_a^{(s)}(\kappa, m, z)e^{jm\varphi} \tag{6.47}$$

and subsequently transforming (6.45), it becomes

$$\frac{1}{r}\frac{\partial}{\partial r}\left(r\frac{\partial \tilde{W}_{a,b}}{\partial r}\right) - \frac{m^2}{r^2}\tilde{W}_{a,b} + \frac{\partial^2 \tilde{W}_{a,b}}{\partial z^2} = k^2 \tilde{W}_{a,b} \tag{6.48}$$

with a solution of the form $A(\kappa)J_m(\kappa r) + B(\kappa)Y_m(\kappa r)$. The r-dependence of the equation in the application of the method of separation of variables is a Bessel type equation. Taking into account only the J_m Bessel function since the problem region includes the origin $r = 0$, the general solution has the form

$$\tilde{W}_{a,b}(z) = \int_0^{\infty} \left[C(m)e^{\lambda z} + D(m)e^{-\lambda z}\right] J_m(\kappa r)d\kappa \tag{6.49}$$

where $\lambda = \sqrt{\kappa^2 + k^2}$.

6.3.1 *Solution of the general problem*

Since the potentials must remain finite, their expressions in the problem regions are written as

$$\tilde{W}_a^{(s)}(z) = \int_0^{\infty} C^{(s)}e^{\kappa z}J_m(\kappa r)d\kappa \tag{6.50}$$

$$\tilde{W}_a^{(ec)}(z) = \int_0^{\infty} D^{(ec)}e^{-\kappa z}J_m(\kappa r)d\kappa \tag{6.51}$$

$$\tilde{W}_a^{(1)}(z) = \int_0^\infty C_a^{(1)} e^{\lambda z} J_m(\kappa r) d\kappa \tag{6.52}$$

$$\tilde{W}_b^{(1)}(z) = \int_0^\infty C_b^{(1)} e^{\lambda z} J_m(\kappa r) d\kappa \tag{6.53}$$

and again the unknown coefficients $D^{(ec)}$, $C_a^{(1)}$, $C_b^{(1)}$ are expressed in terms of the source coefficient $C^{(s)}$ by applying the interface conditions at the interface $z = 0$. The transformed magnetic field components are written in terms of the transformed magnetic potentials as

$$\tilde{B}_r = k^2 \frac{jm}{r} \tilde{W}_b + \frac{\partial^2 \tilde{W}_a}{\partial r \partial z} \tag{6.54}$$

$$\tilde{B}_\varphi = -k^2 \frac{\partial \tilde{W}_b}{\partial r} + \frac{jm}{r} \frac{\partial \tilde{W}_a}{\partial z} \tag{6.55}$$

$$\tilde{B}_z = -k^2 \tilde{W}_a + \frac{\partial^2 \tilde{W}_a}{\partial z^2} \tag{6.56}$$

and the interface conditions become

$$\tilde{H}_r^{(0)} = \tilde{H}_r^{(1)} \Rightarrow \frac{1}{\mu_0} \frac{\partial^2 \left(\tilde{W}_a^{(s)} + \tilde{W}_a^{(ec)} \right)}{\partial r \partial z} = \frac{1}{\mu_0 \mu_r} \left(k^2 \frac{jm}{r} \tilde{W}_b^{(1)} + \frac{\partial^2 \tilde{W}_a^{(1)}}{\partial r \partial z} \right) \tag{6.57}$$

$$\tilde{H}_\varphi^{(0)} = \tilde{H}_\varphi^{(1)} \Rightarrow \tag{6.58}$$

$$\frac{1}{\mu_0} \frac{jm}{r} \frac{\partial \left(\tilde{W}_a^{(s)} + \tilde{W}_a^{(ec)} \right)}{\partial z} = \frac{1}{\mu_0 \mu_r} \left(-k^2 \frac{\partial \tilde{W}_b^{(1)}}{\partial r} + \frac{jm}{r} \frac{\partial \tilde{W}_a^{(1)}}{\partial z} \right)$$

$$\tilde{B}_z^{(0)} = \tilde{B}_z^{(1)} \Rightarrow \frac{\partial^2 \left(\tilde{W}_a^{(s)} + \tilde{W}_a^{(ec)} \right)}{\partial z^2} = -k^2 \tilde{W}_a^{(1)} + \frac{\partial^2 \tilde{W}_a^{(1)}}{\partial z^2} \tag{6.59}$$

These equations yield the following linear system of equations for the unknown coefficients

$$\mu_r \int_0^\infty \left(C^{(s)} - D^{(ec)}\right) \kappa^2 J'_m(\kappa r) d\kappa \tag{6.60}$$
$$= \int_0^\infty C_a^{(1)} \kappa\lambda J'_m(\kappa r) d\kappa + k^2 \frac{jm}{r} \int_0^\infty C_b^{(1)} J_m(\kappa r) d\kappa$$

$$\mu_r \frac{jm}{r} \int_0^\infty \left(C^{(s)} - D^{(ec)}\right) \kappa J_m(\kappa r) d\kappa \tag{6.61}$$
$$= \frac{jm}{r} \int_0^\infty C_a^{(1)} \lambda J_m(\kappa r) d\kappa - k^2 \int_0^\infty C_b^{(1)} \kappa J'_m(\kappa r) d\kappa$$

$$\int_0^\infty \left(C^{(s)} + D^{(ec)}\right) \kappa^2 J_m(\kappa r) d\kappa = \int_0^\infty C_a^{(1)} \kappa^2 J_m(\kappa r) d\kappa \tag{6.62}$$

Now the first two system equations (6.60) and (6.61) can be written as

$$\mu_r \int_0^\infty \left(C^{(s)} - D^{(ec)}\right) \kappa(\kappa r) J'_m(\kappa r) d\kappa \tag{6.63}$$
$$= \int_0^\infty C_a^{(1)} \lambda(\kappa r) J'_m(\kappa r) d\kappa + k^2 jm \int_0^\infty C_b^{(1)} J_m(\kappa r) d\kappa$$

$$-\mu_r \int_0^\infty \left(C^{(s)} - D^{(ec)}\right) \kappa m J_m(\kappa r) d\kappa \tag{6.64}$$
$$= -\int_0^\infty C_a^{(1)} \lambda m J_m(\kappa r) d\kappa - jk^2 \int_0^\infty C_b^{(1)} (\kappa r) J'_m(\kappa r) d\kappa$$

and after using the Bessel function identities

$$xJ'_m(x) = xJ_{m-1}(x) - mJ_m(x) \tag{6.65}$$
$$xJ'_m(x) = mJ_m(x) - xJ_{m+1}(x) \tag{6.66}$$

are finally written as

$$-\mu_r \int_0^\infty \left(C^{(s)} - D^{(ec)}\right) \kappa(\kappa r) J_{m+1}(\kappa r) d\kappa \tag{6.67}$$
$$= -\int_0^\infty C_a^{(1)} \lambda(\kappa r) J_{m+1}(\kappa r) d\kappa + jk^2 \int_0^\infty C_b^{(1)} (\kappa r) J_{m+1}(\kappa r) d\kappa$$

$$\mu_r \int_0^\infty \left(C^{(s)} - D^{(ec)}\right) \kappa(\kappa r) J_{m-1}(\kappa r) d\kappa \tag{6.68}$$
$$= \int_0^\infty C_a^{(1)} \lambda(\kappa r) J_{m-1}(\kappa r) d\kappa + jk^2 \int_0^\infty C_b^{(1)} (\kappa r) J_{m-1}(\kappa r) d\kappa$$

Now each equation has been written so that it has the same Bessel order in both sides. Following the definition of the Hankel transforms of order m in (3.6) we derive from (6.67), (6.68) and (6.62)

$$-\mu_r \kappa \left(C^{(s)} - D^{(ec)}\right) = -\lambda C_a^{(1)} + jk^2 C_b^{(1)} \tag{6.69}$$

$$\mu_r \kappa \left(C^{(s)} - D^{(ec)}\right) = \lambda C_a^{(1)} + jk^2 C_b^{(1)} \tag{6.70}$$

$$C^{(s)} + D^{(ec)} = C_a^{(1)} \tag{6.71}$$

which has a solution that is exactly the same with the one derived using the Cartesian coordinate system with a z-preferred direction.

$$D^{(ec)} = \frac{\kappa\mu_r - \lambda}{\kappa\mu_r + \lambda} C^{(s)} = R(u,v) C^{(s)} \tag{6.72}$$

$$C_a^{(1)} = \frac{2\kappa\mu_r}{\kappa\mu_r + \lambda} C^{(s)} \tag{6.73}$$

$$C_b^{(1)} = 0 \tag{6.74}$$

The final expressions for the potential in the two regions of interest are

$$W_a^{(0)} = \sum_{m=-\infty}^{\infty} e^{jm\varphi} \int_0^{\infty} \left(e^{\kappa z} + \frac{\kappa\mu_r - \lambda}{\kappa\mu_r + \lambda} e^{-\kappa z} \right) C^{(s)} J_m(\kappa r) d\kappa \tag{6.75}$$

$$W_a^{(1)} = \sum_{m=-\infty}^{\infty} e^{jm\varphi} \int_0^{\infty} \frac{2\kappa\mu_r}{\kappa\mu_r + \lambda} e^{\lambda z} C^{(s)} J_m(\kappa r) d\kappa \tag{6.76}$$

$$W_b^{(1)} = 0 \tag{6.77}$$

Again the left term in the parenthesis of (6.75) corresponds to the part of $W_a^{(0)}$ due to the source $W_a^{(s)}$ and the right term to the eddy currents $W_a^{(ec)}$. Eqs (6.74) and (6.77) were also derived when we solved the general 3D problem in the Cartesian coordinate system with a z-preferred direction. The fact that the TM potential vanishes throughout the conductor surface has to do with the preferred direction and not with the particular coordinate system. The eddy current density is written in terms of $C^{(s)}$ as

$$\mathbf{J} = -j\omega\sigma \sum_{m=-\infty}^{\infty} e^{jm\varphi} \int_0^{\infty} \frac{2\kappa\mu_r}{\kappa\mu_r + \lambda} \left(\frac{jm}{r} J_m(\kappa r)\mathbf{r}_0 - \kappa J_m'(\kappa r)\boldsymbol{\varphi}_0 \right) e^{\lambda z} C^{(s)} d\kappa \tag{6.78}$$

6.3.2 *The ΔZ formula*

Following again the analysis in Chapter 5, the impedance change is written as

$$\Delta Z = \frac{-j\omega}{\mu_0 I^2} \int_{z=0} \mathbf{z}_0 \cdot \left(\frac{\partial W_a^{(0)}}{\partial z} \mathbf{B}^{(s)} - \frac{\partial W_a^{(s)}}{\partial z} \mathbf{B}^{(0)} \right) r dr d\varphi \tag{6.79}$$

which again depends only on $W_a^{(0)}$ and $W_a^{(s)}$ if we substitute for $\mathbf{B}^{(s)}$ and $\mathbf{B}^{(0)}$ using

$$\mathbf{z}_0 \cdot \mathbf{B}^{(s)} = \frac{\partial^2 W_a^{(s)}}{\partial z^2} \tag{6.80}$$

$$\mathbf{z}_0 \cdot \mathbf{B}^{(0)} = \frac{\partial^2 W_a^{(0)}}{\partial z^2} \tag{6.81}$$

Noting also that $W_a^{(0)} = W_a^{(s)} + W_a^{(ec)}$ and after some algebraic manipulation, (6.26) takes the form

$$\Delta Z = \frac{-j\omega}{\mu_0 I^2} \int_{-\pi}^{\pi} \int_{0}^{\infty} \left(\frac{\partial W_a^{(ec)}}{\partial z} \frac{\partial^2 W_a^{(s)}}{\partial z^2} - \frac{\partial W_a^{(s)}}{\partial z} \frac{\partial^2 W_a^{(ec)}}{\partial z^2} \right)_{z=0} r dr d\varphi \quad (6.82)$$

Upon substituting for $W_a^{(s)}$ and $W_a^{(s)}$ from (6.75) and applying Parseval's theorem for the Fourier as well as for the Hankel transform:

$$\int_0^\infty r \left| f(r) \right|^2 dr = \int_0^\infty \kappa \left| F(\kappa) \right|^2 d\kappa \quad (6.83)$$

the impedance change reduces to

$$\begin{aligned} \Delta Z &= \frac{j\omega 4\pi}{\mu_0 I^2} \int_0^\infty \sum_{m=-\infty}^{\infty} \kappa^2 \left| C^{(s)}(\kappa, m) \right|^2 \frac{\kappa\mu_r - \lambda}{\kappa\mu_r + \lambda} d\kappa \\ &= \frac{j\omega 4\pi}{\mu_0 I^2} \int_0^\infty \sum_{m=0}^{\infty} (2 - \delta_m) \kappa^2 \left| C^{(s)}(\kappa, m) \right|^2 \frac{\kappa\mu_r - \lambda}{\kappa\mu_r + \lambda} d\kappa \end{aligned} \quad (6.84)$$

where δ_m is the Kronecker symbol. This general expression is made specific to a particular coil through the calculation of the $C^{(s)}$ coefficient, which has to be obtained for the cylindrical coordinate system.

6.3.3 *Source term*

The direct and indirect approaches can also be applied for calculating the source coefficient in the cylindrical coordinate system.

6.3.3.1 *Indirect approach: cylindrical coil*

Consider a cylindrical coil located in a parallel orientation with its axis at $(x, y) = (d, 0)$. We call this arrangement "an offset coil" since its axis does not coincide with the coordinate system's z-axis. If we define now a local cylindrical coordinate system (r_d, φ_d, z), where the z-axis does coincide with the coil axis, the magnetic flux density is given by (3.31). From $B_z = \partial^2 W_a^{(s)} / \partial z^2$ we deduce

$$W_a^{(s)} = \frac{\mu_0 \iota_0}{2} \int_0^\infty \frac{\chi(\kappa r_1, \kappa r_2)}{\kappa^4} \left(e^{-\kappa z_1} - e^{-\kappa z_2} \right) e^{\kappa z} J_0(\kappa r_d) d\kappa \quad (6.85)$$

where $\iota_0 = NI/[(r_2 - r_1)(z_2 - z_1)] = nI$ with n denoting the wire turns density. If we want to express the potential in the global cylindrical coordinate system (r, φ, z), we may use the addition theorem for Bessel functions, Abramowitz (1970)

$$J_n(\kappa r_d)\, e^{j\kappa\varphi_d} = \sum_{m=-\infty}^{\infty} J_{n-m}(\kappa d) J_m(\kappa r) e^{jm\varphi} \tag{6.86}$$

The final expression is

$$W_a^{(s)} = \sum_{m=-\infty}^{\infty} e^{jm\varphi} \int_0^{\infty} e^{\kappa z} J_m(\kappa r) \left[\frac{\mu_0 \iota_0}{2} \frac{\chi(\kappa r_1, \kappa r_2)}{\kappa^4} \left(e^{-\kappa z_1} - e^{-\kappa z_2} \right) J_m(\kappa d) \right] d\kappa \tag{6.87}$$

and the term in brackets is therefore $C^{(s)}$. This sort of transformation, by using the addition theorem, is very common in the cylindrical coordinate system.

The impedance change is now written as

$$\Delta Z = j\omega\mu_0\pi n^2 \sum_{m=0}^{\infty} (2 - \delta_m) \int_0^{\infty} \frac{\chi^2(\kappa r_1, \kappa r_2)}{\kappa^6} \left(e^{-\kappa z_1} - e^{-\kappa z_2} \right)^2 J_m^2(\kappa d) \frac{\kappa\mu_r - \lambda}{\kappa\mu_r + \lambda} d\kappa \tag{6.88}$$

This result can be further simplified by noting that only the term $J_m^2(\kappa d)$ depends on m and by using the identity, Gray (1931)

$$J_0^2(x) + 2 \sum_{m=1}^{\infty} J_m^2(x) = 1 \tag{6.89}$$

the impedance change is finally written as

$$\Delta Z = \frac{j\omega\mu_0\pi N^2}{(r_2 - r_1)^2 (z_2 - z_1)^2} \int_0^{\infty} \frac{\chi^2(\kappa r_1, \kappa r_2)}{\kappa^6} \left(e^{-\kappa z_1} - e^{-\kappa z_2} \right)^2 \frac{\kappa\mu_r - \lambda}{\kappa\mu_r + \lambda} d\kappa \tag{6.90}$$

which is the expression derived for the axisymmetric positioning of the coil. Needless to say that this should be the case because ΔZ does not change when moving the coil in x or y since in these directions the geometry is infinite.

6.3.3.2 *Direct integration approach: half cylindrical coil*

In the general expression for the potential with the z-preferred direction

$$W_a^{(s)} = -\frac{\mu_0 I}{4\pi} \iint\limits_S d\mathbf{s} \cdot \nabla_0 \left(\int \frac{dz}{R} \right) \tag{6.91}$$

we replace R^{-1} by its expression in the cylindrical coordinate system, Gray (1931)

$$\frac{1}{R} = \sum_{m=-\infty}^{\infty} e^{jm(\varphi-\varphi_0)} \int\limits_0^{\infty} e^{\kappa(z-z_0)} J_m(\kappa r) J_m(\kappa r_0) d\kappa \quad ; \quad z < z_0 \tag{6.92}$$

and becomes

$$W_a^{(s)} = \frac{\mu_0 I}{4\pi} \cdot \tag{6.93}$$
$$\cdot \sum_{m=-\infty}^{\infty} e^{jm\varphi} \int\limits_0^{\infty} e^{\kappa(z-z_0)} J_m(\kappa r) \left(\iint\limits_S J_m(\kappa r_0) e^{-jm\varphi_0} r_0 dr_0 d\varphi_0 \right) d\kappa$$

We will demonstrate the direct approach by (i) re-deriving the expression for the cylindrical coil and (ii) by deriving the expression for the half-cylindrical coil.

For the cylindrical coil the term in parenthesis becomes

$$\begin{aligned} \int\limits_{-\pi}^{\pi} e^{-jm\varphi_0} \left(\int\limits_0^{r_0} J_m(\kappa r_0) r_0 dr_0 \right) d\varphi_0 &= 2\pi\delta(m) \int\limits_0^{r_0} J_m(\kappa r_0) r_0 dr_0 \\ &= 2\pi r_0 \frac{J_1(\kappa r_0)}{\kappa} \end{aligned} \tag{6.94}$$

hence

$$W_a^{(s)} = \frac{\mu_0 I}{2} r_0 \int\limits_0^{\infty} e^{\kappa(z-z_0)} J_0(\kappa r) \frac{J_1(\kappa r_0)}{\kappa} d\kappa \tag{6.95}$$

Now applying superposition over the coil cross-section with respect to r_0 (from r_1 to r_2) and z_0 (from z_1 to z_2) we derive again (6.85) and from that the relevant source term $C^{(s)}$.

For the filamentary D-coil shown in Fig.6.3a, the term in parenthesis is

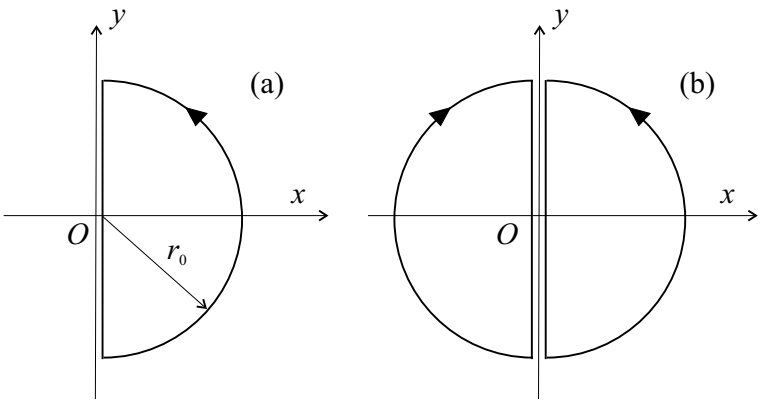

Fig. 6.3 Top view of half cylindrical filamentary coil arrangements (a) D-coil (b) double D-coil.

$$\int_{-\pi/2}^{\pi/2} e^{-jm\varphi_0} \left(\int_0^{r_0} J_m(\kappa r_0) r_0 dr_0 \right) d\varphi_0 = \frac{2\sin(m\pi/2)}{m} \int_0^{r_0} J_m(\kappa r_0) r_0 dr_0$$
$$= \frac{2\sin(m\pi/2)}{m} \frac{g_m(\kappa r_0)}{\kappa^2} \qquad (6.96)$$

The function $g_n(z)$ can be computed from the recursion relation, Abramowitz (1970)

$$(n-1)g_{n+1}(z) = -2nzJ_n(z) + (n+1)g_{n-1}(z) \quad n \geq 2 \qquad (6.97)$$

with the first three function computed from

$$g_0(z) = zJ_1(z)$$
$$g_1(z) = \int_0^z tJ_1(t)dt = \chi(z)$$
$$g_2(z) = -2J_0(z) - zJ_1(z) + 2$$

and $\chi(z)$ is defined in (3.27). In case we have a D-coil moved on the x-axis we may use the addition theorem. For a coil rotated around the z-axis by an angle θ, the new source term is just multiplied with $e^{jm\theta}$. Thus for the double-D coil of Fig.6.3b, the source term of the left coil is $-C^{(s)}e^{-jm\pi}$ with the minus sign added to invert the current flow. The total source term

of the double-D coil is

$$C^{(s)} - C^{(s)} e^{-jm\pi} = C^{(s)} - C^{(s)}(-1)^m \tag{6.98}$$

A similar result was derived previously by McKirdy (1995). The finite thickness coil can be modelled by applying superposition, see for example Bowler (2004). However, the current sheet approximation is not actually needed when the air-cored double-D coil arrangement is used with only a few turns, such as in SQUID systems. From the modelling point of view this is quite advantageous because we can perform only a discrete superposition over these turns.

Chapter 7

Edge Effects in 3D Configurations

7.1 Introduction

In this chapter we present a solution to the 3D eddy current induction problem where the excitation coil is the classical cylindrical one and the conductor is again the half-space but with an infinitely deep slot as shown in Fig.7.1. We can also visualize the deep slot geometry from a different perspective, that of two coplanar conductors each having the form of a right-angled wedge and separated by a gap $2c$. The coil lies parallel to the upper surface and it can be traversed across the gap. In the limiting case of a very large gap with the coil over one of the edges the geometry can simulate the edge effect produced by a coil approaching the edge of a planar conductor. In this case instead of a half-space we talk about a quarter-space. The deep slot and edge problems are of extreme interest in eddy current NDE and unfortunately they have no analytical solution, Maergoiz (1975). However, using again the TREE method we can provide an elegant quasi-analytical engineering solution. This is an excellent opportunity to demonstrate the ability of the TREE method to treat 3D canonical problems. It seems to be one of the most important (significant) contributions since it opens a new route for tackling a number of previously intractable problems in eddy current NDE.

7.2 Symmetry considerations

Using TREE means that we have to truncate the solution region in one of the coordinate directions and in this case it is the x-direction. The outer boundaries are set at $x = \pm h$ but we really need only solve for the region $0 \leq x \leq h$ by using symmetry. Consider the arrangement of Fig.7.2 where

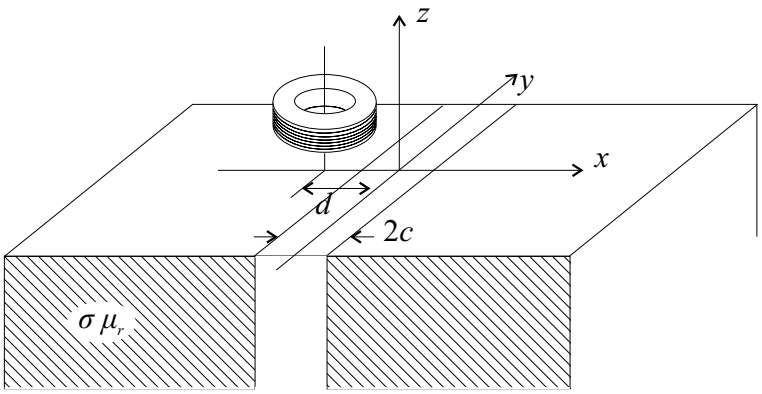

Fig. 7.1 Coil above a conductive half-space with an infinitely deep slot.

the original configuration is decomposed into even and odd configurations depending on the direction of current flow in the coil and image coil that mirrors the real coil in the slot mid-plane. The final solution for the electromagnetic field is the averaged sum of the even and odd solutions. This decomposition into odd and even symmetry simplifies the problem and requires a solution for only half of the original truncated region ($0 \leq x \leq h$) by keeping the boundary condition at $x = h$ and imposing an additional appropriate boundary condition at $x = 0$.

The symmetry plane $x = 0$ lies in air and since in air regions we use only W_a we need to impose a boundary condition there for W_a, as shown in Fig.7.2. For the even solution we have a vanishing potential on the symmetry plane while for the odd solution we have a vanishing x-derivative of the potential. These are physically consistent with the behavior of the magnetic field because when the potential vanishes at $x = 0$ it gives a vanishing B_x there (as required by the even solution) and when the derivative of the potential with respect to x vanishes at $x = 0$ it gives a vanishing B_y and B_z there (as required by the odd solution). In all cases we choose the $x = h$ plane to be a magnetic insulation boundary, that is $B_x(x = h) = 0$ as well as $J_y(x = h) = J_z(x = h) = 0$ in the conductive region, see discussion in Chapter 4 for the boundary condition in truncated regions. We could have chosen of course an electric insulation boundary, that is $B_y(x = h) = B_z(x = h) = 0$ and in addition $J_x(x = h) = 0$ in the conductive region.

For reasons that will be clarified later in the chapter we select the x-

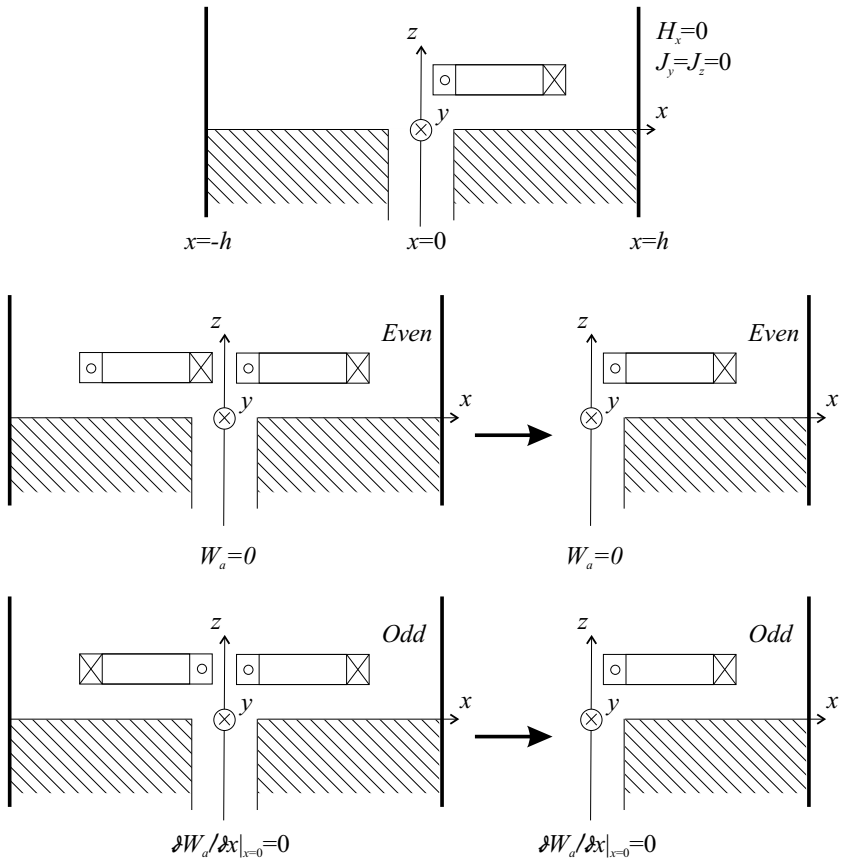

Fig. 7.2 Boundary conditions and decomposition of the original truncated configuration into even and odd symmetries.

preferred direction. Thus, the SOVP potential is defined by

$$\mathbf{W} = W_a \mathbf{x}_0 + \mathbf{x}_0 \times \nabla W_b \tag{7.1}$$

and the components of $\mathbf{A}$ and $\mathbf{B}$ are given in terms of W_a and W_b from

(6.2)-(6.7), rewritten here for convenience

$$A_x = \frac{\partial^2 W_b}{\partial y^2} + \frac{\partial^2 W_b}{\partial z^2} \tag{7.2}$$

$$A_y = \frac{\partial W_a}{\partial z} - \frac{\partial^2 W_b}{\partial x \partial y} \tag{7.3}$$

$$A_z = -\frac{\partial W_a}{\partial y} - \frac{\partial^2 W_b}{\partial x \partial z} \tag{7.4}$$

$$B_x = -k^2 W_a + \frac{\partial^2 W_a}{\partial x^2} \tag{7.5}$$

$$B_y = k^2 \frac{\partial W_b}{\partial z} + \frac{\partial^2 W_a}{\partial x \partial y} \tag{7.6}$$

$$B_z = -k^2 \frac{\partial W_b}{\partial y} + \frac{\partial^2 W_a}{\partial x \partial z} \tag{7.7}$$

The solution for the geometry of Fig.7.1 will be developed in three steps. First we find the expression for the source potential of the isolated coil, then we solve the problem for a conductive half-space and finally we derive the solution for the right-angled conductor. From the latter we can provide solutions for a number of special cases such as the edge effect and the infinitely deep ideal crack. In each step we analyze separately the even and odd configurations although the full analysis is presented only for the even.

7.3 Isolated coil

In order to accomplish the first task of calculating the potential produced by the isolated coil, we first find an expression for the filamentary circular loop of Fig.7.3 and then apply superposition for the finite thickness coil in Fig.7.4. We are dealing with a non-conductive region, therefore only W_a is considered. The differential equation for W_a is the Laplace equation is:

$$\frac{\partial^2 W_a}{\partial x^2} + \frac{\partial^2 W_a}{\partial y^2} + \frac{\partial^2 W_a}{\partial z^2} = 0 \tag{7.8}$$

We define the Fourier Transform (FT) and Inverse Fourier Transform (IFT) with respect to y as:

$$\tilde{W}_a(x,v,z) = \int_{-\infty}^{\infty} W_a(x,y,z)e^{-jvy}dy \tag{7.9}$$

$$W_a(x,y,z) = \frac{1}{2\pi}\int_{-\infty}^{\infty} \tilde{W}_a(x,v,z)e^{jvy}dv \tag{7.10}$$

and we obtain the relevant differential equation for $\tilde{W}_a(x,v,z)$:

$$\frac{\partial^2 \tilde{W}_a}{\partial x^2} + \frac{\partial^2 \tilde{W}_a}{\partial z^2} = v^2 \tilde{W}_a \tag{7.11}$$

The general solution of (7.11) is:

$$\begin{aligned}\tilde{W}_a(x,z) = {} & (A_0 + B_0 x)(C_0 e^{vz} + D_0 e^{-vz}) \\ & + \sum_{i=1}^{\infty} (A_i \sin u_i x + B_i \cos u_i x)(C_i e^{\kappa_i z} + D_i e^{-\kappa_i z})\end{aligned} \tag{7.12}$$

where $\kappa_i^2 = u_i^2 + v^2$ and the form of u_i will depend on whether we are dealing with an even or an odd solution.

7.3.1 *Even solution*

The isolated filamentary coil is a circular loop of radius r_0 in free-space at $z = z_0$ and its center at $x = d$ and $y = 0$ as shown in Fig.7.3. The solution region (free-space) is truncated at $x = h$ and a magnetic insulation boundary is set there $B_x(h,y,z) = 0$. The region above the loop is designated (1) while the region below the loop is designated (2).

The requirement that W_a vanishes at $x = 0$ while B_x vanishes at $x = h$ simplifies (7.12) to:

$$\tilde{W}_a^{(1)}(x,z) = D_0^{(1)} x e^{-vz} + \sum_{i=1}^{\infty} \sin u_i x \; e^{-\kappa_i z} D_i^{(1)} \tag{7.13}$$

for region (1), while for region (2)

$$\tilde{W}_a^{(2)}(x,z) = C_0^{(2)} x e^{vz} + \sum_{i=1}^{\infty} \sin u_i x \; e^{\kappa_i z} C_i^{(2)} \tag{7.14}$$

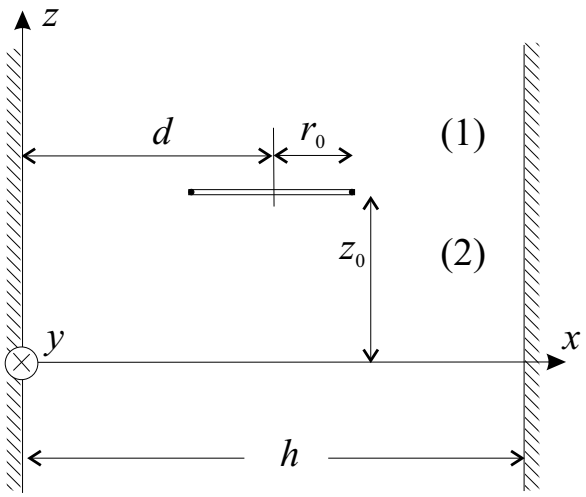

Fig. 7.3 Isolated filamentary coil in a truncated region.

where $u_i = i\pi/h$ and in each expression we have kept those exponential terms that ensure a finite potential for $z \to \pm\infty$. Hereafter, the various discrete coefficients in the solution will carry a superscript designating their region and a subscript showing their summation index. Moreover, the C coefficients correspond to exponential terms with a positive argument $e^{\kappa_i z}$, the D coefficients correspond to exponentials terms with a negative argument $e^{-\kappa_i z}$ and we occasionally refer to $D_0^{(1)}$, $C_0^{(2)}$ as dc coefficients.

Now in order to find these unknown coefficients, we apply the continuity of the normal magnetic flux component B_z and the discontinuity of the tangential components H_x and H_y at the surface containing the loop $z = z_0$, utilizing (7.5)-(7.7)

$$\tilde{B}_z^{(1)} = \tilde{B}_z^{(2)}\Big|_{z=z_0} \Rightarrow D_0^{(1)}(-v)e^{-vz_0} + \sum_{i=1}^{\infty} u_i \cos u_i x(-\kappa_i)e^{-\kappa_i z_0} D_i^{(1)}$$
$$= C_0^{(2)} v e^{vz_0} + \sum_{i=1}^{\infty} u_i \cos u_i x \; \kappa_i e^{\kappa_i z_0} C_i^{(2)} \qquad (7.15)$$

$$\tilde{H}_y^{(1)} - \tilde{H}_y^{(2)} = \tilde{J}_x\Big|_{z=z_0} \Rightarrow D_0^{(1)} e^{-vz_0} jv + \sum_{i=1}^{\infty} u_i \cos u_i x \; e^{-\kappa_i z_0} jv D_i^{(1)} \quad (7.16)$$
$$- \; C_0^{(2)} e^{vz_0} jv - \sum_{i=1}^{\infty} u_i \cos u_i x \; e^{\kappa_i z_0} jv C_i^{(2)} = \mu_0 \tilde{J}_x$$

$$\tilde{H}_x^{(1)} - \tilde{H}_x^{(2)} = -\tilde{J}_y\Big|_{z=z_0} \Rightarrow \sum_{i=1}^{\infty} -u_i^2 \sin u_i x \; e^{-\kappa_i z_0} D_i^{(1)} \quad (7.17)$$
$$- \sum_{i=1}^{\infty} -u_i^2 \sin u_i x \; e^{\kappa_i z_0} C_i^{(2)} = -\mu_0 \tilde{J}_y$$

where the Fourier transforms of the excitation current density components are defined by an expression similar to (7.9). These transforms can be calculated following Panas (1991) or by changing to cylindrical polar coordinates, see Theodoulidis (2005)

$$\tilde{J}_y = -2\pi I \delta(z - z_0) \sum_{i=1}^{\infty} \cos u_i d \; u_i r_0 \frac{J_1(\kappa_i r_0)}{\kappa_i} \sin u_i x \quad (7.18)$$

$$\tilde{J}_x = -2\pi I \delta(z - z_0) \sum_{i=0}^{\infty} jv \cos u_i d \; r_0 \frac{J_1(\kappa_i r_0)}{\kappa_i} \cos u_i x \quad (7.19)$$

If we multiply (7.15) by $\sum_{i=0}^{\infty} \cos u_i x$ and integrate from 0 to h, we get:

$$C_0^{(2)} = -D_0^{(1)} e^{-2vz_0} \quad (7.20)$$

$$C_i^{(2)} = -D_i^{(1)} e^{-2\kappa_i z_0} \quad (7.21)$$

Note that we get the same set of equations if first we just integrate (7.15) from 0 to h and get (7.20) and then multiply with $\sum_{i=1}^{\infty} \cos u_i x$ followed by an integration from 0 to h and get (7.21). For the integration we make use of the orthogonality relationship of the trigonometric function

$$\int_0^h \cos u_i x \cos u_j x \; dx = \delta_{ij} \frac{h}{2} \quad (7.22)$$

where δ_{ij} is the Kronecker symbol. Next, we multiply (7.16) with $\sum_{i=0}^{\infty} \cos u_i x$ and integrate from 0 to h:

$$C_0^{(2)} = D_0^{(1)} e^{-2vz_0} + 2\mu_0 I r_0 \frac{J_1(vr_0)}{vh} e^{-vz_0} \tag{7.23}$$

$$C_i^{(2)} = D_i^{(1)} e^{-2\kappa_i z_0} + 4\pi\mu_0 I \cos u_i d \; r_0 \frac{J_1(\kappa_i r_0)}{\kappa_i h u_i} e^{-\kappa_i z_0} \tag{7.24}$$

Finally, we multiply (7.17) with $\sum_{i=1}^{\infty} \sin u_i x$ and integrate from 0 to h:

$$C_i^{(2)} = D_i^{(1)} e^{-2\kappa_i z_0} + 4\pi\mu_0 I \cos u_i d \; r_0 \frac{J_1(\kappa_i r_0)}{\kappa_i h u_i} e^{-\kappa_i z_0} \tag{7.25}$$

We can see that (7.24) and (7.25) are the same, which means that we get the same information about the unknown coefficients from (7.16) and (7.17). The only difference is that (7.17) does not provide any information for the dc coefficients $D_0^{(1)}$, $C_0^{(2)}$. The solution to the systems (7.20)-(7.23), (7.21)-(7.24) for $C_0^{(2)}$ and $C_i^{(2)}$ gives:

$$C_0^{(2)} = \pi\mu_0 I \frac{e^{-vz_0} r_0 J_1(vr_0)}{vh} \tag{7.26}$$

$$C_i^{(2)} = 2\pi\mu_0 I \cos u_i d \frac{e^{-\kappa_i z_0} r_0 J_1(\kappa_i r_0)}{\kappa_i u_i h} \tag{7.27}$$

and $D_0^{(1)}$, $D_i^{(1)}$ are calculated from (7.20) and (7.21) respectively. Thus, in the regions above and below the loop:

$$\tilde{W}_a^{(s)}(x,z) = \frac{\mu_0 I 2\pi r_0}{h} \left[\frac{J_1(vr_0)}{2v} x \; e^{v|z-z_0|} + \sum_{i=1}^{\infty} \cos u_i d \frac{J_1(\kappa_i r_0)}{\kappa_i u_i} \sin u_i x \; e^{\kappa_i |z-z_0|} \right] \tag{7.28}$$

For the finite thickness coil of Fig.7.4, we apply superposition over the coil cross-section, as we have done in almost all preceding chapters, and derive:

$$\tilde{W}_a^{(s)}(x,z) = \frac{\mu_0 \iota_0 2\pi}{h} \left[\frac{\chi(vr_1, vr_2) F(vz, vz_1, vz_2)}{2v^4} x + \sum_{i=1}^{\infty} \cos u_i d \frac{F(\kappa_i z, \kappa_i z_1, \kappa_i z_2) \chi(\kappa_i r_1, \kappa_i r_2)}{\kappa_i^4 u_i} \sin u_i x \right] \tag{7.29}$$

where the z-dependence of the potential is described by the F function:

$$F(z, z_1, z_2) = \begin{cases} -e^{-z}\left(e^{z_2} - e^{z_1}\right) & z \geq z_2 \\ e^{-(z-z_1)} - e^{-(z_2-z)} & z_2 \geq z \geq z_1 \\ e^{z}\left(e^{-z_1} - e^{-z_2}\right) & z_1 \geq z \end{cases} \tag{7.30}$$

with $\iota_0 = NI/[(r_2 - r_1)(z_2 - z_1)]$ and $\chi(x_1, x_2)$ defined in (3.27). The source current density can also be written as $\iota_0 = nI$ where n stands for the wire-turns density.

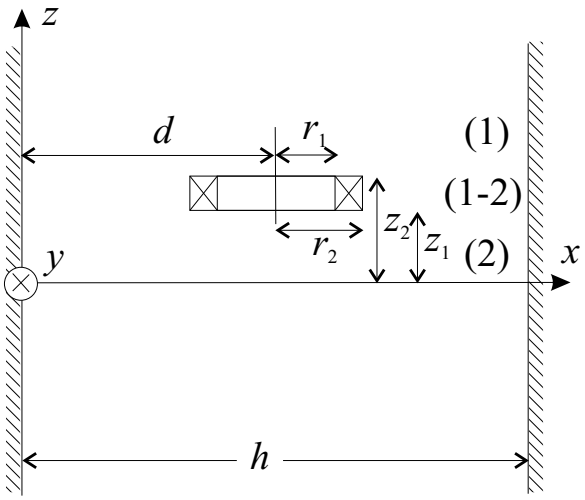

Fig. 7.4 Finite thickness coil in a truncated region.

For the solution of the conductive half-space and quarter-space cases we need the expression for region (2) below the coil since this is the region where the air-conductor interface will lie. If we write the source potential for $z \leq z_1$ in the form

$$\tilde{W}_a^{(s)}(x, z) = C_0^{(s)} x e^{vz} + \sum_{i=1}^{\infty} \sin u_i x \; e^{\kappa_i z} C_i^{(s)} \tag{7.31}$$

then from (7.29)

$$C_0^{(s)} = \frac{\pi \mu_0 nI}{h}\left(e^{-vz_1} - e^{-vz_2}\right)\frac{\chi(vr_1, vr_2)}{v^4} \tag{7.32}$$

and

$$C_i^{(s)} = \frac{2\pi\mu_0 nI}{h}\cos u_i d\left(e^{-\kappa_i z_1} - e^{-\kappa_i z_2}\right)\frac{\chi(\kappa_i r_1, \kappa_i r_2)}{\kappa_i^4 u_i} \tag{7.33}$$

7.3.2 *Odd solution*

The general solution is again given by (7.12). The requirement that the derivative of W_a with respect to x vanishes at $x = 0$ with the boundary condition at $x = h$ same as in the even solution, (7.12) simplifies to:

$$\tilde{W}_a^{(1)}(x,z) = D_0^{(1)} e^{-vz} + \sum_{i=1}^{\infty} \cos u_i x \; e^{-\kappa_i z} D_i^{(1)} \tag{7.34}$$

for region (1), while for region (2)

$$\tilde{W}_a^{(2)}(x,z) = C_0^{(2)} e^{vz} + \sum_{i=1}^{\infty} \cos u_i x \; e^{\kappa_i z} C_i^{(2)} \tag{7.35}$$

where now $u_i = (2i-1)\pi/(2h)$. The first term in (7.34)-(7.35) is independent of x and therefore it does not play any role in calculating the magnetic field; just remember that to take the magnetic field from W_a there is always an x derivative involved which makes this term vanish. Thus, the first term does not appear in the application of the interface conditions since these are based solely on the magnetic field. Every step in the derivation of the even solution is repeated and also we make use of the orthogonality relationship of the trigonometric function

$$\int_0^h \sin u_i x \sin u_j x \; dx = \delta_{ij}\frac{h}{2} \tag{7.36}$$

Ignoring the dc term, the final result for the potential produced by the rectangular cross-section coil of Fig.7.4 is

$$\tilde{W}_a^{(s)}(x,z) = \frac{\mu_0 \iota_0 2\pi}{h}\sum_{i=1}^{\infty} \sin u_i d \frac{F(\kappa_i z, \kappa_i z_1, \kappa_i z_2)\chi(\kappa_i r_1, \kappa_i r_2)}{\kappa_i^4 u_i}\cos u_i x \tag{7.37}$$

If we write the source potential for $z \leq z_1$ in the form

$$\tilde{W}_a^{(s)}(x,z) = \sum_{i=1}^{\infty} \cos u_i x \; e^{\kappa_i z} C_i^{(s)} \tag{7.38}$$

we get from (7.37)

$$C_i^{(s)} = \frac{2\pi\mu_0 nI}{h} \sin u_i d \left(e^{-\kappa_i z_1} - e^{-\kappa_i z_2}\right) \frac{\chi(\kappa_i r_1, \kappa_i r_2)}{\kappa_i^4 u_i} \tag{7.39}$$

The essential difference with the even solution is in the form of the eigenvalues u_i.

7.4 Coil above a conductive half-space

The second step in the analysis is to find the expression for the potential throughout space when the coil is located above a conductive half-space having conductivity σ and relative magnetic permeability μ_r, as shown in Fig.7.5. The solution domain is truncated again in the x-direction. In this

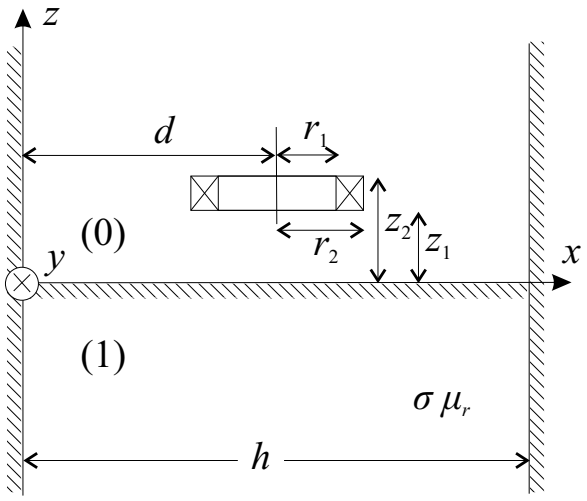

Fig. 7.5 Finite thickness coil above a conductive half-space in a truncated region.

case also we consider an x-preferred direction and a magnetic boundary at $x = h$; the latter meaning that the normal component of the magnetic flux density B_x should be zero as well as the tangential components of the eddy current density J_y and J_z in the conductive region (at $x = h$). The region $z \geq 0$ is designated (0) and the region $z \leq 0$ is designated (1).

The differential equation for the SOVP components W_a and W_b is:

$$\frac{\partial^2 W_{a,b}}{\partial x^2} + \frac{\partial^2 W_{a,b}}{\partial y^2} + \frac{\partial^2 W_{a,b}}{\partial z^2} = j\omega\mu_0\mu_r\sigma W_{a,b} = k^2 W_{a,b} \tag{7.40}$$

Using again the Fourier Transform (FT) and Inverse Fourier Transform (IFT) of $W_{a,b}$ with respect to y as in (7.9)-(7.10) we obtain the differential equation for the transformed potentials

$$\frac{\partial^2 \tilde{W}_{a,b}}{\partial x^2} + \frac{\partial^2 \tilde{W}_{a,b}}{\partial z^2} = (v^2 + k^2)\tilde{W}_{a,b} = w^2 \tilde{W}_{a,b} \tag{7.41}$$

The general solution of (7.41) has the form:

$$\begin{aligned} \tilde{W}_{a,b}(x,z) = {} & (A_0 + B_0 x)(C_0 e^{wz} + D_0 e^{-wz}) \\ & + \sum_{i=1}^{\infty} (A_i \sin u_i x + B_i \cos u_i x)(C_i e^{\lambda_i z} + D_i e^{-\lambda_i z}) \end{aligned} \tag{7.42}$$

where

$$\lambda_i^2 = u_i^2 + v^2 + k^2 = u_i^2 + w^2 = \kappa_i^2 + k^2 \tag{7.43}$$

7.4.1 *Even solution*

The potential in air $W_a^{(0)}$ is the sum of the source potential $W_a^{(s)}$ and the secondary potential produced by the eddy currents $W_a^{(ec)}$ while in the conductive space the potentials are $W_a^{(1)}$ and $W_b^{(1)}$. Taking into account the boundary conditions at $x = 0$ and $x = h$, their general expressions are written as follows:

$$\tilde{W}_a^{(s)}(x,z) = x\, e^{vz} C_0^{(s)} + \sum_{i=1}^{\infty} \sin u_i x\, e^{\kappa_i z} C_i^{(s)} \tag{7.44}$$

$$\tilde{W}_a^{(ec)}(x,z) = x\, e^{-vz} D_0^{(ec)} + \sum_{i=1}^{\infty} \sin u_i x\, e^{-\kappa_i z} D_i^{(ec)} \tag{7.45}$$

$$\tilde{W}_a^{(1)}(x,z) = \sum_{i=1}^{\infty} \sin u_i x\, e^{\lambda_i z} C_i^{(a)} \tag{7.46}$$

$$\tilde{W}_b^{(1)}(x,z) = C_0^{(b)} e^{wz} + \sum_{i=1}^{\infty} \cos u_i x\, e^{\lambda_i z} C_i^{(b)} \tag{7.47}$$

where $u_i = i\pi/h$ and we note that the TE and TM potentials share the same eigenvalues. For the even solution the source coefficients $C_0^{(s)}$ and $C_i^{(s)}$ in (7.44) are given in (7.32)-(7.33) and all other coefficients are to be determined from the usual interface conditions at $z = 0$:

$$\begin{aligned}
&\tilde{H}_x^{(0)}(x,z) = \tilde{H}_x^{(1)}(x,z)\Big|_{z=0} \qquad (7.48)\\
&\Rightarrow \mu_r \sum_{i=1}^{\infty} \sin u_i x(-u_i^2) C_i^{(s)} + \mu_r \sum_{i=1}^{\infty} \sin u_i x(-u_i^2) D_i^{(ec)}\\
&= \sum_{i=1}^{\infty} \sin u_i x(-u_i^2 - k^2) C_i^{(a)}
\end{aligned}$$

$$\begin{aligned}
&\tilde{H}_y^{(0)}(x,z) = \tilde{H}_y^{(1)}(x,z)\Big|_{z=0} \qquad (7.49)\\
&\Rightarrow \mu_r C_0^{(s)} jv + \mu_r \sum_{i=1}^{\infty} \cos u_i x\ u_i jv C_i^{(s)} + D_0^{(ec)} jv + \sum_{i=1}^{\infty} \cos u_i x\ u_i jv D_i^{(ec)}\\
&= \sum_{i=1}^{\infty} \cos u_i x\ u_i jv C_i^{(a)} + k^2 w C_0^{(b)} + k^2 \sum_{i=1}^{\infty} \cos u_i x\ \lambda_i C_i^{(b)}
\end{aligned}$$

$$\begin{aligned}
&\tilde{B}_z^{(0)}(x,z) = \tilde{B}_z^{(1)}(x,z)\Big|_{z=0} \qquad (7.50)\\
&\Rightarrow C_0^{(s)} v + \sum_{i=1}^{\infty} \cos u_i x\ u_i \kappa_i C_i^{(s)} - D_0^{(ec)} v + \sum_{i=1}^{\infty} \cos u_i x\ u_i(-\kappa_i) D_i^{(ec)}\\
&= \sum_{i=1}^{\infty} \cos u_i x\ u_i \lambda_i C_i^{(a)} - k^2 jv C_0^{(b)} - k^2 \sum_{i=1}^{\infty} \cos u_i x\ jv C_i^{(b)}
\end{aligned}$$

Following a similar procedure as in the isolated coil case, i.e. multiplying (7.48) with $\sum_{i=1}^{\infty} \sin u_i x$ and (7.49), (7.50) with $\sum_{i=0}^{\infty} \cos u_i x$, then integrating from 0 to h and finally using the orthogonality relations of trigonometric functions we end up with the following system for the unknown expansion coefficients:

For $i = 1, 2, 3, \ldots$

$$-u_i^2 \mu_r \left(C_i^{(s)} + D_i^{(ec)} \right) = \left(-u_i^2 - k^2 \right) C_i^{(a)} \qquad (7.51)$$

$$u_i jv \mu_r \left(C_i^{(s)} + D_i^{(ec)} \right) = u_i jv C_i^{(a)} + k^2 \lambda_i C_i^{(b)} \qquad (7.52)$$

$$u_i\kappa_i\left(C_i^{(s)}-D_i^{(ec)}\right)=u_i\lambda_i C_i^{(a)}-k^2 jvC_i^{(b)} \tag{7.53}$$

and for $i=0$

$$jv\mu_r\left(C_0^{(s)}+D_0^{(ec)}\right)=k^2 wC_0^{(b)} \tag{7.54}$$

$$v\mu_r\left(C_0^{(s)}-D_0^{(ec)}\right)=-k^2 jvC_0^{(b)}\Rightarrow jv\mu_r\left(C_0^{(s)}-D_0^{(ec)}\right)=k^2 vC_0^{(b)} \tag{7.55}$$

The solution of the systems (7.51)-(7.53) and (7.54)-(7.55) gives the unknown coefficients in terms of the source coefficients $C_0^{(s)}$ and $C_i^{(s)}$:

$$D_i^{(ec)}=C_i^{(s)}\frac{\lambda_i-\kappa_i\mu_r}{\lambda_i+\kappa_i\mu_r} \tag{7.56}$$

$$C_i^{(a)}=C_i^{(s)}\frac{u_i^2 2\lambda_i\mu_r}{(u_i^2+k^2)(\lambda_i+\kappa_i\mu_r)} \tag{7.57}$$

$$C_i^{(b)}=C_i^{(s)}\frac{u_i 2jv\mu_r}{(u_i^2+k^2)(\lambda_i+\kappa_i\mu_r)} \tag{7.58}$$

and

$$D_0^{(ec)}=C_0^{(s)}\frac{w-v\mu_r}{w+v\mu_r} \tag{7.59}$$

$$C_0^{(b)}=C_0^{(s)}\frac{2jv\mu_r}{k^2(w+v\mu_r)} \tag{7.60}$$

Note the similarity of (7.56)-(7.58) to (6.18)-(6.20) in Chapter 6 where the same problem is solved in an unbounded region with the same x-preferred direction.

The normal component of the magnetic vector potential and hence of the eddy current density is expected to be zero:

$$\begin{aligned}\tilde{A}_z&=-\frac{\partial\tilde{W}_a^{(1)}}{\partial y}-\frac{\partial^2\tilde{W}_b^{(1)}}{\partial x\partial z}\\&=\left[-jv\frac{u_i^2 2\lambda_i\mu_r}{(u_i^2+k^2)(\lambda_i+\kappa_i\mu_r)}-\frac{2u_i\lambda_i(-u_i)jv\mu_r}{(u_i^2+k^2)(\lambda_i+\kappa_i\mu_r)}\right]=0\end{aligned} \tag{7.61}$$

Now, using (7.56), (7.59) and (7.7), we can derive the final expression for the change of the z-component of the magnetic flux density produced by

the conductive half-space. This change is due to $W_a^{(ec)}$ only:

$$\Delta B_z = B_z^{(ec)} = \frac{\mu_0 \iota_0}{2h} \int\limits_{-\infty}^{\infty} \frac{(e^{-vz_1} - e^{-vz_2})}{v^3} \chi(vr_1, vr_2) e^{-vz} \frac{v\mu_r - w}{v\mu_r + w} e^{jvy} dv$$

$$+ \frac{\mu_0 \iota_0}{h} \int\limits_{-\infty}^{\infty} \sum_{i=1}^{\infty} \frac{(e^{-\kappa_i z_1} - e^{-\kappa_i z_2})}{\kappa_i^3} \chi(\kappa_i r_1, \kappa_i r_2) \cos u_i d \tag{7.62}$$

$$\cos u_i x e^{-\kappa_i z} \frac{\kappa_i \mu_r - \lambda_i}{\kappa_i \mu_r + \lambda_i} e^{jvy} dv$$

where $\iota_0 = nI = NI/[(r_2 - r_1)(z_2 - z_1)]$, n is the wire-turns density and $\chi(x_1, x_2)$ is defined in (3.27). The voltage change to a filamentary loop of radius r_0, at $z = z_0$, centered at $x = d$ is computed from:

$$\Delta V = j\omega \int\limits_S \Delta \mathbf{B} \cdot d\mathbf{s} = j\omega \iint\limits_S \Delta B_z dx dy \tag{7.63}$$

The surface integration in (7.63) results in evaluating the following integral over the area enclosed by the loop and the derived result follows from the analysis in Panas (1991)

$$\int\limits_{-r_0}^{r_0} \int\limits_{d-\sqrt{r_0^2-y^2}}^{d+\sqrt{r_0^2-y^2}} \cos u_i x \; e^{jvy} dx dy$$

$$= \frac{1}{u_i} \int\limits_{-r_0}^{r_0} \left[\sin u_i \left(d + \sqrt{r_0^2 - y^2} \right) - \sin u_i \left(d + \sqrt{r_0^2 - y^2} \right) \right] e^{jvy} dx =$$

$$= ... = 2\pi \cos u_i d \; r_0 \frac{J_1(\kappa_i r_0)}{\kappa_i} \tag{7.64}$$

Putting $u_i = 0$ in (7.64) we obtain also the result for the integral required in the surface integration of the first term in (7.62)

$$\int\limits_{-r_0}^{r_0} \int\limits_{d-\sqrt{r_0^2-y^2}}^{d+\sqrt{r_0^2-y^2}} e^{jvy} dx dy = ... = 2\pi \; r_0 \frac{J_1(vr_0)}{v} \tag{7.65}$$

After applying superposition, we can calculate the voltage change and hence

the impedance change of the coil in Fig.7.5:

$$\Delta Z = \frac{j\omega\pi\mu_0 n^2}{h} \int_{-\infty}^{\infty} \frac{(e^{-vz_1} - e^{-vz_2})^2}{v^7} \chi(vr_1, vr_2)^2 \frac{v\mu_r - w}{v\mu_r + w} dv \tag{7.66}$$

$$+\frac{j\omega 2\pi\mu_0 n^2}{h} \int_{-\infty}^{\infty} \sum_{i=1}^{\infty} \frac{(e^{-\kappa_i z_1} - e^{-\kappa_i z_2})^2}{\kappa_i^7} \chi(\kappa_i r_1, \kappa_i r_2)^2 \cos^2(u_i d) \frac{\kappa_i\mu_r - \lambda_i}{\kappa_i\mu_r + \lambda_i} dv$$

which can be written in a more compact form:

$$\Delta Z = \frac{j\omega\pi\mu_0 n^2}{h} \tag{7.67}$$

$$\int_{-\infty}^{\infty} \sum_{i=0}^{\infty} (2 - \delta_i) \frac{(e^{-\kappa_i z_1} - e^{-\kappa_i z_2})^2}{\kappa_i^7} \chi(\kappa_i r_1, \kappa_i r_2)^2 \cos^2(u_i d) \frac{\kappa_i\mu_r - \lambda_i}{\kappa_i\mu_r + \lambda_i} dv$$

Numerical results that validate (7.67) are given later in the chapter.

7.4.2 *Odd solution*

The potential in air $W_a^{(0)}$ is again the sum of the source potential $W_a^{(s)}$ and the secondary potential produced by the eddy currents $W_a^{(ec)}$ while in the conductive space, the potentials are $W_a^{(1)}$ and $W_b^{(1)}$. Taking into account the boundary conditions at $x = 0$ and $x = h$, their general expressions are now written as follows:

$$\tilde{W}_a^{(s)}(x, z) = \sum_{i=1}^{\infty} \cos u_i x \; e^{\kappa_i z} C_i^{(s)} \tag{7.68}$$

$$\tilde{W}_a^{(ec)}(x, z) = \sum_{i=1}^{\infty} \cos u_i x \; e^{-\kappa_i z} D_i^{(ec)} \tag{7.69}$$

$$\tilde{W}_a^{(1)}(x, z) = \sum_{i=1}^{\infty} \cos u_i x \; e^{\lambda_i z} C_i^{(a)} \tag{7.70}$$

$$\tilde{W}_b^{(1)}(x, z) = \sum_{i=1}^{\infty} \sin u_i x \; e^{\lambda_i z} C_i^{(b)} \tag{7.71}$$

where $u_i = (2i - 1)\pi/(2h)$. For the odd solution the source coefficient $C_i^{(s)}$ in (7.68) is taken from (7.39) and all other coefficients are to be determined

from the usual interface conditions at $z = 0$. Repeating all the steps followed in the development of the even solution we end up with the following expressions for the magnetic field change due to the conductive half-space

$$\Delta B_z = \frac{\mu_0 \iota_0}{h} \int_{-\infty}^{\infty} \sum_{i=1}^{\infty} \frac{(e^{-\kappa_i z_1} - e^{-\kappa_i z_2})}{\kappa_i^3} \chi(\kappa_i r_1, \kappa_i r_2) \sin u_i d \ \sin u_i x \ e^{-\kappa_i z} \frac{\kappa_i \mu_r - \lambda_i}{\kappa_i \mu_r + \lambda_i} e^{jvy} dv \tag{7.72}$$

and the impedance change

$$\Delta Z = \frac{j\omega\pi\mu_0 n^2}{h} \int_{-\infty}^{\infty} \sum_{i=1}^{\infty} \frac{(e^{-\kappa_i z_1} - e^{-\kappa_i z_2})^2}{\kappa_i^7} \chi(\kappa_i r_1, \kappa_i r_2)^2 \sin^2(u_i d) \frac{\kappa_i \mu_r - \lambda_i}{\kappa_i \mu_r + \lambda_i} dv \tag{7.73}$$

7.5 Coil above a right-angled conductor

The final step in the analysis is to find the expression for the potential throughout space when the coil is located above a right-angled conductive space having conductivity σ and relative magnetic permeability μ_r, as shown in Fig.7.6. Here, however, we will simplify somewhat the analysis by considering a nonmagnetic conductor, i.e. $\mu_r = 1$. The solution domain is truncated again in the x-direction. In this case also we consider an x-preferred direction and a magnetic insulation boundary at $x = h$; the latter meaning that the normal component of the magnetic flux density B_x should be zero as well as the tangential components of the eddy current density J_y and J_z in the conductive region (at $x = h$). The region $z \geq 0$ is designated (0) and region $z \leq 0$ is designated (1).

The differential equation for the transformed SOVP components W_a and W_b is again (7.41). The general solutions of (7.41) for W_a and W_b have the form

$$\tilde{W}_a(x, z) = (A_0 + B_0 x)(C_0 e^{wz} + D_0 e^{-wz}) + \sum_{i=1}^{\infty} (A_i \sin q_i x + B_i \cos q_i x)(C_i e^{\gamma_i z} + D_i e^{-\gamma_i z}) \tag{7.74}$$

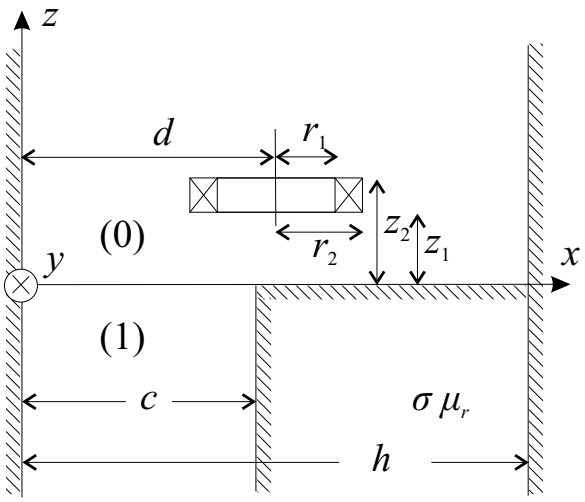

Fig. 7.6 Finite thickness coil above a right-angled conductor in a truncated region.

where

$$\gamma_i^2 = u_i^2 + v^2 + k^2 = u_i^2 + w^2 \tag{7.75}$$

and

$$\begin{aligned}\tilde{W}_b(x,z) &= (A_0 + B_0 x)(C_0 e^{wz} + D_0 e^{-wz}) \\ &+ \sum_{i=1}^{\infty} (A_i \sin r_i x + B_i \cos r_i x)(C_i e^{s_i z} + D_i e^{-s_i z})\end{aligned} \tag{7.76}$$

where

$$s_i^2 = r_i^2 + v^2 + k^2 = r_i^2 + w^2 \tag{7.77}$$

and we note a first difference with the conductive half-space solution: The TE and TM potentials do not share the same eigenvalues any more.

7.5.1 *Even solution*

The potential in air $W_a^{(0)}$ is the sum of the source potential $W_a^{(s)}$ and the secondary potential produced by the eddy currents $W_a^{(ec)}$ while in the conductive space the potentials are $W_a^{(1)}$ and $W_b^{(1)}$. Taking into account the boundary conditions at $x = 0$, $x = c$ and $x = h$, their general expressions are written as follows:

$$\tilde{W}_a^{(s)}(x,z) = C_0^{(s)} x\, e^{vz} + \sum_{i=1}^{\infty} \sin u_i x\, e^{\kappa_i z} C_i^{(s)} \tag{7.78}$$

$$\tilde{W}_a^{(ec)}(x,z) = D_0^{(ec)} x\, e^{-vz} + \sum_{i=1}^{\infty} \sin u_i x\, e^{-\kappa_i z} D_i^{(ec)} \tag{7.79}$$

$$\tilde{W}_a^{(1)}(x,z) = C_0^{(a)} x\, e^{vz} + \sum_{i=1}^{\infty} \sin p_i x\, e^{\gamma_i z} C_i^{(a)air} \quad ; \quad 0 \le x \le c \tag{7.80}$$

$$= \sum_{i=1}^{\infty} \sin q_i (h-x)\, e^{\gamma_i z} C_i^{(a)con} \quad ; \quad c \le x \le h \tag{7.81}$$

$$\tilde{W}_b^{(1)}(x,z) = C_0^{(b)} \cosh k(h-x)\, e^{vz} + \sum_{i=1}^{\infty} \cos r_i (h-x)\, e^{s_i z} C_i^{(b)} \tag{7.82}$$

where $u_i = i\pi/h$, $\kappa_i^2 = u_i^2 + v^2$, $k^2 = j\omega\mu_0\sigma$, $\gamma_i^2 = q_i^2 + v^2 + k^2$, $p_i^2 = \gamma_i^2 - v^2 = q_i^2 + k^2$, $r_i = (2i-1)\pi/[2(h-c)]$, $s_i^2 = r_i^2 + v^2 + k^2$.

Let us comment a bit more on (7.80)-(7.82) since these expressions describe the potentials in region (1) where the interface $x = c$ lies. We have already mentioned that on this interface the matching of the potential expressions (and therefore the fulfilment of the interface conditions) will be done on a term by term basis.

Taking into account the boundary condition at $x = h$ the general expression of $\tilde{W}_b$ is in the form $\cos r_i(h-x)\, e^{s_i z}$ where the specific x-dependence ensures a vanishing electric field at $x = h$ (at least its part owing to the W_b potential). In addition, this term must obey the Laplace equation at $x = c$ because of (7.2) and the requirement that the eddy current density component perpendicular to this interface has to vanish

$$\frac{\partial^2 \tilde{W}_b}{\partial y^2} + \frac{\partial^2 \tilde{W}_b}{\partial z^2} = 0 \tag{7.83}$$

Putting the general term in (7.83) means that the term $(-v^2 + s_i^2)\cos r_i(h-c)\, e^{s_i z}$ must vanish. This is possible if we select the eigenvalues $r_i = (2i-1)\pi/[2(h-c)]$ or $s_i = v$. The latter provides the additional eigenvalues $r = \pm jk$. If in the form $\cos r_i(h-x)\, e^{s_i z}$ we replace r_i with $\pm jk$ and s_i with v, we get the extra term of (7.82). This is actually a transverse electromagnetic (TEM) term and has been identified in the solution of 3D

eddy current problems in Flitz (1990, 1993). It arises only in the case of the right-angled geometry and as we will see later only for the even symmetry solution.

The vanishing W_b on the interface $x = c$ means that W_a and W_b are decoupled there and this is the reason for selecting the x-preferred direction. We can now work only with W_a and apply the interface conditions (continuity of B_x, $H_{y,z}$), again on a term by term basis.

Note that the eigenfunctions and eigenvalues of $W_a^{(1)}$ in the air and conductor subregions are chosen so as to make matching possible, lets explain: Separation of variables for the transformed potential W_a implies that a solution is sought in the form of a product of two functions, which are conveniently written for the field in the conductor as

$$X(x) = a(q)\sin(qx) + b(q)\cos(qx) \tag{7.84}$$

and

$$Z(z) = c(q)\exp(\gamma z) + d(q)\exp(-\gamma z), \tag{7.85}$$

where $\gamma = \sqrt{q^2 + v^2 + k^2}$. One of the functions $a(q)$ $b(q)$ $c(q)$ and $d(q)$ is redundant and the other three are determined by interface conditions ensuring that the tangential electric and magnetic fields are continuous at the surface of the conductor.

In order to construct a solution for the nonconductive region, one can either replace γ in the exponential function arguments of (7.85) with $\sqrt{q^2 + v^2}$ or replace q in the trigonometric function arguments of (7.84) with $\sqrt{q^2 + k^2}$. In either case, (7.41) is satisfied for $k = 0$. The latter option is non-conventional but it has been adopted for the air subregion of region (1), allowing the z-dependence of the solution for the non-conductive region to conform to that used for the conductive region. A similar "trick" was used in Chapter 4 when we solved the 2D problem of a coil above a conductive half-space with a cylindrical hole.

From the continuity of B_x on the $x = c$ interface

$$\sin p_i c \; C_i^{(a)air} = \sin q_i(h - c) \; C_i^{(a)con} \tag{7.86}$$

and from the continuity of $H_{y,z}$

$$p_i \cos p_i c \; C_i^{(a)air} = -q_i \cos q_i(h - c) \; C_i^{(a)con} \tag{7.87}$$

and

$$\begin{aligned} C_0^{(a)} &= -jk^2 C_0^{(b)} \cosh k(h-c) \\ &= a_0 C_0^{(b)} \end{aligned} \tag{7.88}$$

While (7.88) connects $C_0^{(a)}$ and $C_0^{(b)}$ we can also write from (7.86) and (7.87) the connection between $C_i^{(a)air}$ and $C_i^{(a)con}$. Hence,

$$C_i^{(a)air} = a_i C_i^{(a)con} \tag{7.89}$$

where

$$a_i = \frac{\sin q_i(h-c)}{\sin p_i c} = -\frac{q_i \cos q_i(h-c)}{p_i \cos p_i c} \tag{7.90}$$

From (7.90) the values of q_i and hence p_i are sought, with $p_i = \sqrt{q_i^2 + k^2}$, which satisfy

$$q_i \tan p_i c + p_i \tan q_i(h-c) = 0 \tag{7.91}$$

the roots of which give the eigenvalues for the even parity solution. It has to be emphasized that the eigenvalues do not depend on the Fourier transform variable v, which means that their numerical computation needs to be carried out only once.

In the above equations we have the unknown coefficients are $D_0^{(ec)}$, $C_0^{(b)}$ $D_i^{(ec)}$, $C_i^{(a)}$ and $C_i^{(b)}$. These are calculated in terms of the source coefficients $C_0^{(s)}$ and $C_i^{(s)}$ that are given in (7.32) and (7.33) respectively. Writing in (7.80) $C_i^{(a)air}$ in terms of $C_i^{(a)con}$ and $C_0^{(a)}$ in terms of $C_0^{(b)}$, the final expressions in both algebraic and matrix form are:

$$\begin{aligned} \tilde{W}_a^{(s)}(x,z) &= C_0^{(s)} x\, e^{vz} + \sum_{i=1}^{\infty} \sin u_i x\, e^{\kappa_i z} C_i^{(s)} \\ &= C_0^{(s)} x\, e^{vz} + S_u^{\mathbf{T}}(x) e^{\boldsymbol{\kappa} z} \mathbf{C}^{(s)} \end{aligned} \tag{7.92}$$

$$\begin{aligned} \tilde{W}_a^{(ec)}(x,z) &= D_0^{(ec)} x\, e^{-vz} + \sum_{i=1}^{\infty} \sin u_i x\, e^{-\kappa_i z} D_i^{(ec)} \\ &= D_0^{(ec)} x\, e^{-vz} + S_u^{\mathbf{T}}(x) e^{-\boldsymbol{\kappa} z} \mathbf{D}^{(ec)} \end{aligned} \tag{7.93}$$

$$\tilde{W}_a^{(1)}(x,z) = a_0 C_0^{(b)} x\ e^{vz} + \sum_{i=1}^{\infty} \sin p_i x\ e^{\gamma_i z} a_i C_i^{(a)}$$
$$= a_0 C_0^{(b)} x\ e^{vz} + S_p^{\mathbf{T}}(x) e^{\boldsymbol{\gamma} z} \mathbf{a}\mathbf{C}^{(a)} \quad ; \quad 0 \le x \le c \tag{7.94}$$
$$= \sum_{i=1}^{\infty} \sin q_i(h-x)\ e^{\gamma_i z} C_i^{(a)}$$
$$= S_q^{\mathbf{T}}(h-x) e^{\boldsymbol{\gamma} z} \mathbf{C}^{(a)} \quad ; \quad c \le x \le h \tag{7.95}$$

$$\tilde{W}_b^{(1)}(x,z) = C_0^{(b)} \cosh k(h-x)\ e^{vz} + \sum_{i=1}^{\infty} \cos r_i(h-x)\ e^{s_i z} C_i^{(b)}$$
$$= C_0^{(b)} \cosh k(h-x)\ e^{vz} + C_r^{\mathbf{T}}(h-x) e^{\mathbf{s}z} \mathbf{C}^{(b)} \tag{7.96}$$

where a_0, a_i are given in (7.88) and (7.90) respectively and the superscript $\mathbf{T}$ designates a row vector. For these row vectors we use the notation S or C to indicate sines or cosines respectively and a subscript to indicate the eigenvalue. It has to be noted that we truncate the series to a number N_s which means that all vectors have N_s elements and all matrices are $N_s \times N_s$.

We can identify the unknown coefficients $D_0^{(ec)}$, $C_0^{(b)}$ as scalars and $\mathbf{D}^{(ec)}$, $\mathbf{C}^{(a)}$ and $\mathbf{C}^{(b)}$ as vectors. The next step in the analysis is the computation of the unknown coefficients by applying the continuity of the magnetic field components on the $z = 0$ plane. First let's write down these components in regions (0) and (1) in matrix notation:

Source generated $\mathbf{B}$ in region (0)

$$\tilde{B}_x^{(s)}(x,z) = S_u^{\mathbf{T}}(x) \left(-\mathbf{u}^2\right) e^{\boldsymbol{\kappa} z} \mathbf{C}^{(s)} \tag{7.97}$$

$$\tilde{B}_y^{(s)}(x,z) = C_0^{(s)} jv\ e^{vz} + C_u^{\mathbf{T}}(x) \mathbf{u}\ jv\ e^{\boldsymbol{\kappa} z} \mathbf{C}^{(s)} \tag{7.98}$$

$$\tilde{B}_z^{(s)}(x,z) = C_0^{(s)} v\ e^{vz} + C_u^{\mathbf{T}}(x) \mathbf{u}\ \boldsymbol{\kappa}\ e^{\boldsymbol{\kappa} z} \mathbf{C}^{(s)} \tag{7.99}$$

Eddy current generated $\mathbf{B}$ in region (0)

$$\tilde{B}_x^{(ec)}(x,z) = S_u^{\mathbf{T}}(x) \left(-\mathbf{u}^2\right) e^{-\boldsymbol{\kappa} z} \mathbf{D}^{(ec)} \tag{7.100}$$

$$\tilde{B}_y^{(ec)}(x,z) = D_0^{(ec)} jv\, e^{-vz} + C_u^{\mathbf{T}}(x)\mathbf{u}\, jv\, e^{-\boldsymbol{\kappa} z}\mathbf{D}^{(ec)} \tag{7.101}$$

$$\tilde{B}_z^{(ec)}(x,z) = D_0^{(ec)}(-v)\, e^{-vz} + C_u^{\mathbf{T}}(x)\mathbf{u}\, (-\boldsymbol{\kappa})\, e^{-\boldsymbol{\kappa} z}\mathbf{D}^{(ec)} \tag{7.102}$$

B in region (1)

$$\begin{aligned}\tilde{B}_x^{(1)}(x,z) &= S_p^{\mathbf{T}}(x)\left(-\mathbf{p}^2\right) e^{\boldsymbol{\gamma} z}\mathbf{a}\mathbf{C}^{(a)} \quad ; \quad 0 \le x \le c \\ &= S_q^{\mathbf{T}}(h-x)\left(-\mathbf{q}^2 - k^2\right) e^{\boldsymbol{\gamma} z}\mathbf{C}^{(a)} \quad ; \quad c \le x \le h\end{aligned} \tag{7.103}$$

$$\begin{aligned}\tilde{B}_y^{(1)}(x,z) &= jva_0 C_0^{(b)} e^{vz} + C_p^{\mathbf{T}}(x)\mathbf{p} jv\, e^{\boldsymbol{\gamma} z}\mathbf{a}\mathbf{C}^{(a)} \quad ; \quad 0 \le x \le c \\ &= C_q^{\mathbf{T}}(h-x)(-\mathbf{q}) jv e^{\boldsymbol{\gamma} z}\mathbf{C}^{(a)} + k^2 v\, C_0^{(b)} \cosh k(h-x) e^{vz} \\ &+ k^2 C_r^{\mathbf{T}}(h-x)\mathbf{s} e^{\mathbf{s} z}\mathbf{C}^{(b)} \quad ; \quad c \le x \le h\end{aligned} \tag{7.104}$$

$$\begin{aligned}\tilde{B}_z^{(1)}(x,z) &= va_0 C_0^{(b)} e^{vz} + C_p^{\mathbf{T}}(x)\mathbf{p}\boldsymbol{\gamma} e^{\boldsymbol{\gamma} z}\mathbf{a}\mathbf{C}^{(b)} \quad ; \quad 0 \le x \le c \\ &= C_q^{\mathbf{T}}(h-x)(-\mathbf{q})\boldsymbol{\gamma} e^{\boldsymbol{\gamma} z}\mathbf{C}^{(a)} - k^2 jv C_0^{(b)} \cosh k(h-x) e^{vz} \\ &- k^2 C_r^{\mathbf{T}}(h-x) jv e^{\mathbf{s} z}\mathbf{C}^{(b)} \quad ; \quad c \le x \le h\end{aligned} \tag{7.105}$$

The interface conditions will be satisfied following a similar procedure as in the case of the conductive half-space: multiply the continuity equations with $\sum_{i=0}^{\infty} \cos u_i x$ for y, z components and $\sum_{i=1}^{\infty} \sin u_i x$ for the x component, and integrate them from 0 to h. The multiplication with $\sum_{i=0}^{\infty} \cos u_i x$ can be done in two steps: first for $i = 0$ and then for $\sum_{i=1}^{\infty} \cos u_i x$. The first step (for $i = 0$) is actually an integration of the continuity equations and provides information for the unknown coefficients of the dc terms:

$$\int_0^h \left(\tilde{H}_y^{(s)} + \tilde{H}_y^{(ec)}\right) dx = \int_0^h \tilde{H}_y^{(1)} dx = \int_0^c \tilde{H}_y^{(1)air} dx + \int_c^h \tilde{H}_y^{(1)con} dx \tag{7.106}$$

$$\int_0^h \left(\tilde{B}_z^{(s)} + \tilde{B}_z^{(ec)}\right) dx = \int_0^h \tilde{B}_z^{(1)} dx = \int_0^c \tilde{B}_z^{(1)air} dx + \int_c^h \tilde{B}_z^{(1)con} dx \tag{7.107}$$

From (7.106) and (7.107) we derive the following equations, which are written in algebraic form:

$$\left(C_0^{(s)} + D_0^{(ec)}\right) jvh = C_0^{(b)} \left[k^2 \cosh k(h-c)\ vc + k \sinh k(h-c)\ v\right] + k^2 \sum_{i=1}^{\infty} (-1)^{i+1} \frac{s_i}{r_i} C_i^{(b)} \tag{7.108}$$

$$\left(C_0^{(s)} - D_0^{(ec)}\right) jvh = C_0^{(b)} \left[k^2 \cosh k(h-c)\ vc + k \sinh k(h-c)\ v\right] + k^2 \sum_{i=1}^{\infty} (-1)^{i+1} \frac{v}{r_i} C_i^{(b)} \tag{7.109}$$

and we have used the fact that $\sin r_i(h-c) = \sin(2i-1)\pi/2 = (-1)^{i+1}$. The solution to the system (7.108)-(7.109) is

$$\begin{aligned} D_0^{(ec)} &= \frac{k^2}{2jvh} \sum_{i=1}^{\infty} (s_i - v) \frac{(-1)^{i+1}}{r_i} C_i^{(b)} \\ &= \mathbf{R}_{ec}^{\mathbf{T}} \mathbf{C}^{(b)} \end{aligned} \tag{7.110}$$

$$\begin{aligned} C_0^{(b)} &= \frac{1}{2\left[k^2 \cosh k(h-c)\ vc + k \sinh k(h-c)\ v\right]} \times \\ &\times \left[C_0^{(s)} 2jvh - k^2 \sum_{i=1}^{\infty} (s_i + v) \frac{(-1)^{i+1}}{r_i} C_i^{(b)}\right] \\ &= \lambda_b C_0^{(s)} + \mathbf{R}_b^{\mathbf{T}} \mathbf{C}^{(b)} \end{aligned} \tag{7.111}$$

where we use vector multiplication form to simplify expressions. Note that the dc coefficients $D_0^{(ec)}$ and $C_0^{(b)}$ depend not only on the dc source coefficient $C_0^{(s)}$ but also on the TM potential coefficients $C_i^{(b)}$. This sort of term inter-coupling does not appear in the half-space solution and is characteristic of the right-angled conductor solution.

Next we take the second step, which is to multiply the continuity equations with $\sum_{i=1}^{\infty} \sin u_i x$ (x-component) and $\sum_{i=1}^{\infty} \cos u_i x$ (y, z-components), and integrate from 0 to h. Apart from the unknown vector coefficients, the resulting expressions will also contain $D_0^{(ec)}$ and $C_0^{(b)}$, which will have to be replaced from (7.110) and (7.111) respectively.

$$\tilde{H}_x^{(0)} = \tilde{H}_x^{(1)} \Rightarrow$$
$$S_u^{\mathbf{T}}(x)\left(-\mathbf{u}^2\right)\left(\mathbf{C}^{(s)} + \mathbf{D}^{(ec)}\right) = S_p^{\mathbf{T}}(x)\left(-\mathbf{p}^2\right)\mathbf{a}\mathbf{C}^{(a)}; \quad 0 \le x \le c \quad (7.112)$$
$$S_u^{\mathbf{T}}(x)\left(-\mathbf{u}^2\right)\left(\mathbf{C}^{(s)} + \mathbf{D}^{(ec)}\right) = S_q^{\mathbf{T}}(h-x)\left(-\mathbf{q}^2 - k^2\right)\mathbf{C}^{(a)}; \quad c \le x \le h$$

Multiply both sides with $S_u(x)$ and integrate from 0 to h:

$$\frac{h}{2}\mathbf{u}^2\left(\mathbf{C}^{(s)} + \mathbf{D}^{(ec)}\right) = \mathbf{M}_s\mathbf{C}^{(a)} \quad (7.113)$$

$$\tilde{H}_y^{(0)} = \tilde{H}_y^{(1)} \Rightarrow$$
$$C_u^{\mathbf{T}}(x)\mathbf{u}jv\left(\mathbf{C}^{(s)} + \mathbf{D}^{(ec)}\right) = a_0 C_0^{(b)} + C_p^{\mathbf{T}}(x)\mathbf{p}jv\mathbf{a}\mathbf{C}^{(a)} \quad ; \quad 0 \le x \le c$$
$$C_u^{\mathbf{T}}(x)\mathbf{u}jv\left(\mathbf{C}^{(s)} + \mathbf{D}^{(ec)}\right) = C_q^{\mathbf{T}}(h-x)(-\mathbf{q})jv\mathbf{C}^{(a)} \quad (7.114)$$
$$+k^2 C_0^{(b)}\cosh k(h-x)\, v + k^2 C_r^{\mathbf{T}}(h-x)\mathbf{s}\mathbf{C}^{(b)} \quad ; \quad c \le x \le h$$

Multiply both sides with $C_u(x)$ and integrate from 0 to h:

$$\frac{h}{2}\mathbf{u}jv\left(\mathbf{C}^{(s)} + \mathbf{D}^{(ec)}\right) = \mathbf{M}_c jv\mathbf{C}^{(a)} + k^2\mathbf{M}_r\mathbf{s}\mathbf{C}^{(b)} + vk^2\lambda_b C_0^{(s)}\mathbf{L} + vk^2\mathbf{L}\mathbf{R}_b^{\mathbf{T}}\mathbf{C}^{(b)} \quad (7.115)$$

$$\tilde{B}_z^{(0)} = \tilde{B}_z^{(1)} \Rightarrow$$
$$C_u^{\mathbf{T}}(x)\mathbf{u}\boldsymbol{\kappa}\left(\mathbf{C}^{(s)} - \mathbf{D}^{(ec)}\right) = -a_0 C_0^{(b)} + C_p^{\mathbf{T}}(x)\mathbf{p}\boldsymbol{\gamma}\mathbf{a}\mathbf{C}^{(a)} \quad ; \quad 0 \le x \le c$$
$$C_u^{\mathbf{T}}(x)\mathbf{u}\boldsymbol{\kappa}\left(\mathbf{C}^{(s)} - \mathbf{D}^{(ec)}\right) = C_q^{\mathbf{T}}(h-x)(-\mathbf{q})\boldsymbol{\gamma}\mathbf{C}^{(a)} \quad (7.116)$$
$$-k^2 C_0^{(b)}\cosh k(h-x)\, jv - k^2 C_r^{\mathbf{T}}(h-x)jv\mathbf{C}^{(b)} \quad ; \quad c \le x \le h$$

Multiply both sides with $C_u(x)$ and integrate from 0 to h:

$$\frac{h}{2}\mathbf{u}\boldsymbol{\kappa}\left(\mathbf{C}^{(s)} - \mathbf{D}^{(ec)}\right) = \mathbf{M}_c\boldsymbol{\gamma}\mathbf{C}^{(a)} - k^2\mathbf{M}_r jv\mathbf{C}^{(b)} - jvk^2\lambda_b C_0^{(s)}\mathbf{L} - vk^2\mathbf{L}\mathbf{R}_b^{\mathbf{T}}\mathbf{C}^{(b)} \quad (7.117)$$

where the matrices $\mathbf{M}_s$, $\mathbf{M}_c$, $\mathbf{M}_r$, $\mathbf{L}$ are defined next.

7.5.1.1 *Definition of matrices*

All the various matrices elements have closed-form expressions. Consider $\mathbf{M}_s$:

$$\mathbf{M}_s[i,j] = p_j^2 \left[a_j \int_0^c \sin(u_i x) \sin(p_j x)\ dx + \int_c^h \sin(u_i x) \sin[q_j(h-x)]\ dx \right] \tag{7.118}$$

The first integral in (7.118) is calculated from

$$\int_0^c \sin(u_i x) \sin(p_j x) dx = \frac{\sin[(p_j - u_i)c]}{2(p_j - u_i)} - \frac{\sin[(p_j + u_i)c]}{2(p_j + u_i)} \tag{7.119}$$

and the second one from

$$\int_c^h \sin(u_i x) \sin[q_j(h-x)] dx = \tag{7.120}$$

$$= \frac{u_i \cos(u_i c) \sin[q_j(c-h)] - q_j \sin(u_i c) \cos[q_j(c-h)]}{q_j^2 - u_i^2}$$

The elements of matrix $\mathbf{M}_c$ are defined by

$$\mathbf{M}_c[i,j] = a_j p_j \int_0^c \cos(u_i x) \cos(p_j x)\ dx - q_j \int_c^h \cos(u_i x) \cos q_j[(h-x)]\ dx \tag{7.121}$$

with the first integral calculated from

$$\int_0^c \cos(u_i x) \cos(p_j x) dx = \frac{\sin[(p_j - u_i)c]}{2(p_j - u_i)} + \frac{\sin[(p_j + u_i)c]}{2(p_j + u_i)} \tag{7.122}$$

and the second one from

$$\int_c^h \cos(u_i x) \cos[q_j(h-x)] dx = \tag{7.123}$$

$$\frac{-q_j \cos(u_i c) \sin[q_j(c-h)] + u_i \sin(u_i c) \cos[q_j(c-h)]}{q_j^2 - u_i^2}$$

Finally we have matrix $\mathbf{M}_r$

$$\mathbf{M}_r[i,j] = \int_c^h \cos(u_i x)\cos[r_j(h-x)]\,dx \tag{7.124}$$
$$= \frac{r_j\cos(u_i c)(-1)^{j+1}}{r_j^2 - u_i^2}$$

and matrix $\mathbf{L}$

$$\mathbf{L}[i] = \cosh[k(h-c)]\int_0^c \cos(u_i x)\,dx + \int_c^h \cos(u_i x)\cosh[k(h-x)]\,dx \tag{7.125}$$

The first integral in (7.125) gives $\sin(u_i c)/u_i$ while the second one is calculated from

$$\int_c^h \cos(u_i x)\cosh[k(h-x)]\,dx = \tag{7.126}$$
$$= \frac{-u_i\sin(u_i c)\cosh[k(h-c)] + k\cos(u_i c)\sinh[k(h-c)]}{k^2 + u_i^2}$$

Note that all of the above matrices have a common characteristic: they are independent of the integration variable v and therefore they need to be formed just once. Now, let's rewrite the system: (7.113), (7.115), (7.117):

$$\frac{h}{2}\mathbf{u}^2\left(\mathbf{C}^{(s)} + \mathbf{D}^{(ec)}\right) = \mathbf{M}_s\mathbf{C}^{(a)} \tag{7.127}$$

$$\frac{h}{2}\mathbf{u}jv\left(\mathbf{C}^{(s)} + \mathbf{D}^{(ec)}\right) = \mathbf{M}_c jv\mathbf{C}^{(a)} + k^2\left(\mathbf{M}_r\mathbf{s} + v\mathbf{L}\mathbf{R}_b^{\mathbf{T}}\right)\mathbf{C}^{(b)}$$
$$+ vk^2\lambda_b C_0^{(s)}\mathbf{L} \tag{7.128}$$

$$\frac{h}{2}\mathbf{u}\boldsymbol{\kappa}\left(\mathbf{C}^{(s)} - \mathbf{D}^{(ec)}\right) = \mathbf{M}_c\boldsymbol{\gamma}\mathbf{C}^{(a)} - jvk^2\left(\mathbf{M}_r + \mathbf{L}\mathbf{R}_b^{\mathbf{T}}\right)\mathbf{C}^{(b)} - jvk^2\lambda_b C_0^{(s)}\mathbf{L} \tag{7.129}$$

From (7.127) and (7.128) we have

$$0 = \left(\mathbf{u}\mathbf{M}_c jv - jv\mathbf{M}_s\right)\mathbf{C}^{(a)} + k^2\mathbf{u}\left(\mathbf{M}_r\mathbf{s} + v\mathbf{L}\mathbf{R}_b^{\mathbf{T}}\right)\mathbf{C}^{(b)} + vk^2\lambda_b C_0^{(s)}\mathbf{u}\mathbf{L} \tag{7.130}$$

and from (7.127) and (7.129) we have

$$h\mathbf{u}^2\boldsymbol{\kappa}\mathbf{C}^{(s)} = (\boldsymbol{\kappa}\mathbf{M}_s + \mathbf{u}\mathbf{M}_c\boldsymbol{\gamma})\,\mathbf{C}^{(a)} - jvk^2\mathbf{u}\left(\mathbf{M}_r + \mathbf{L}\mathbf{R}_b^{\mathbf{T}}\right)\mathbf{C}^{(b)} - jvk^2\lambda_b C_0^{(s)}\mathbf{u}\mathbf{L} \tag{7.131}$$

These two equations can be written in the form:

$$\mathbf{A}_1\mathbf{C}^{(a)} + \mathbf{B}_1\mathbf{C}^{(b)} = \mathbf{C}_1\mathbf{C}^{(s)} + \mathbf{D}_1 C_0^{(s)} \tag{7.132}$$

$$\mathbf{A}_2\mathbf{C}^{(a)} + \mathbf{B}_2\mathbf{C}^{(b)} = \mathbf{C}_2\mathbf{C}^{(s)} + \mathbf{D}_2 C_0^{(s)} \tag{7.133}$$

where

$$\mathbf{A}_1 = jv\left(\mathbf{u}\mathbf{M}_c - \mathbf{M}_s\right) \tag{7.134}$$
$$\mathbf{A}_2 = \boldsymbol{\kappa}\mathbf{M}_s + \mathbf{u}\mathbf{M}_c\boldsymbol{\gamma} \tag{7.135}$$
$$\mathbf{B}_1 = k^2\mathbf{u}\left(\mathbf{M}_r\mathbf{s} + v\mathbf{L}\mathbf{R}_b^{\mathbf{T}}\right) \tag{7.136}$$
$$\mathbf{B}_2 = -k^2 jv\mathbf{u}\left(\mathbf{M}_r + \mathbf{L}\mathbf{R}_b^{\mathbf{T}}\right) \tag{7.137}$$
$$\mathbf{C}_1 = 0 \tag{7.138}$$
$$\mathbf{C}_2 = h\mathbf{u}^2\boldsymbol{\kappa} \tag{7.139}$$
$$\mathbf{D}_1 = -vk^2\lambda_b\mathbf{u}\mathbf{L} \tag{7.140}$$
$$\mathbf{D}_2 = jvk^2\lambda_b\mathbf{u}\mathbf{L} \tag{7.141}$$

The solution to the system (7.132)-(7.133) is:

$$\mathbf{C}^{(b)} = \left(\mathbf{B}_1 - \mathbf{A}_1\mathbf{A}_2^{-1}\mathbf{B}_2\right)^{-1} \cdot \cdot \left[\left(\mathbf{C}_1 - \mathbf{A}_1\mathbf{A}_2^{-1}\mathbf{C}_2\right)\mathbf{C}^{(s)} + \left(\mathbf{D}_1 - \mathbf{A}_1\mathbf{A}_2^{-1}\mathbf{D}_2\right)C_0^{(s)}\right] \tag{7.142}$$

$$\mathbf{C}^{(a)} = \mathbf{A}_2^{-1}\left(-\mathbf{B}_2\mathbf{C}^{(b)} + \mathbf{C}_2\mathbf{C}^{(s)} + \mathbf{D}_2 C_0^{(s)}\right) \tag{7.143}$$

$$\mathbf{D}^{(ec)} = \frac{2}{h}\mathbf{u}^{-2}\mathbf{M}_s\mathbf{C}^{(a)} - \mathbf{C}^{(s)} \tag{7.144}$$

and also $D_0^{(ec)}$ and $C_0^{(b)}$ are calculated from (7.110) and (7.111) respectively. The unknown coefficients are derived in terms of the source coefficients $C_0^{(s)}$ and $C_i^{(s)}$ from (7.32) and (7.33).

The eddy current density components are calculated from $\mathbf{J} = -j\omega\sigma\mathbf{A}$ and (7.2)-(7.4). Thus, for $c \leq x \leq h$:

$$J_x = \frac{j\omega\sigma}{2\pi} \int\limits_{-\infty}^{\infty} \left[\sum_{i=1}^{\infty} \cos r_i(h-x) \left(s_i^2 - v^2\right)\ e^{s_i z} C_i^{(b)} \right] e^{jvy} dv \tag{7.145}$$

$$J_y = \frac{-j\omega\sigma}{2\pi} \int\limits_{-\infty}^{\infty} \left[\sum_{i=1}^{\infty} \sin q_i(h-x)\ \gamma_i e^{\gamma_i z} C_i^{(a)} \right. \tag{7.146}$$
$$\left. -kjvC_0^{(b)} \sinh k(h-x)\ e^{vz} + \sum_{i=1}^{\infty} \sin r_i(h-x)\ r_i jv e^{s_i z} C_i^{(b)} \right] e^{jvy} dv$$

$$J_z = \frac{-j\omega\sigma}{2\pi} \int\limits_{-\infty}^{\infty} \left[\sum_{i=1}^{\infty} \sin q_i x\ (-jv)\gamma_i e^{\gamma_i z} C_i^{(a)} \right. \tag{7.147}$$
$$\left. -kvC_0^{(b)} \sinh k(h-x)\ e^{vz} + \sum_{i=1}^{\infty} \sin r_i(h-x)\ r_i s_i e^{s_i z} C_i^{(b)} \right] e^{jvy} dv$$

Next, we use (7.102) and calculate the z-component of the magnetic flux density in air $B_z^{(ec)}$, which is produced by the conductive quarter-space. This is actually the magnetic flux density change ΔB_z. The knowledge of $D_0^{(ec)}$ and $D_i^{(ec)}$ provides an expression for $W_a^{(ec)}$ and therefore ΔB_z.

$$\Delta B_z = B_z^{(ec)} = \frac{1}{2\pi} \int\limits_{-\infty}^{\infty} (-v) D_0^{(ec)} e^{-vz} e^{jvy} dv$$
$$+ \frac{1}{2\pi} \int\limits_{-\infty}^{\infty} \sum_{i=1}^{\infty} u_i(-\kappa_i) D_i^{(ec)} \cos u_i x\ e^{-\kappa_i z} e^{jvy} dv \tag{7.148}$$

The voltage change to a filamentary loop of radius r_0, at $z = z_0$, centered at $x = d$ is computed from:

$$\Delta V = j\omega \int\limits_S \Delta\mathbf{B} \cdot d\mathbf{s} = j\omega \iint\limits_S \Delta B_z dx dy \tag{7.149}$$

and the surface integration in (7.149) is evaluated as in the conductive half-space case, see (7.64). The final result for the impedance change after

applying superposition is:

$$\Delta Z = -j\omega n \left[\int_{-\infty}^{\infty} \frac{(e^{-vz_1} - e^{-vz_2})}{v^3} \chi(vr_1, vr_2) D_0^{(ec)} dv \right. \tag{7.150}$$
$$\left. + \int_{-\infty}^{\infty} \sum_{i=1}^{\infty} \frac{(e^{-\kappa_i z_1} - e^{-\kappa_i z_2})}{\kappa_i^3} u_i \chi(\kappa_i r_1, \kappa_i r_2) \cos(u_i d) D_i^{(ec)} dv \right]$$

It has to be noted that although the sums in the coil impedance and field expressions are shown to have an infinite upper limit, this limit is actually N_s, which is the number of terms after the series truncation.

7.5.2 *Odd solution*

The potential in air $W_a^{(0)}$ is the sum of the source potential $W_a^{(s)}$ and the secondary potential produced by the eddy currents $W_a^{(ec)}$ while in the conductive space the potentials are $W_a^{(1)}$ and $W_b^{(1)}$. Taking into account the boundary conditions at $x = 0$, $x = c$ and $x = h$, their general expressions are written as follows:

$$\tilde{W}_a^{(s)}(x, z) = \sum_{i=1}^{\infty} \cos u_i x \; e^{\kappa_i z} C_i^{(s)} \tag{7.151}$$

$$\tilde{W}_a^{(ec)}(x, z) = \sum_{i=1}^{\infty} \cos u_i x \; e^{-\kappa_i z} D_i^{(ec)} \tag{7.152}$$

$$\tilde{W}_a^{(1)}(x, z) = \sum_{i=1}^{\infty} \cos p_i x \; e^{\gamma_i z} a_i C_i^{(a)} \quad ; \quad 0 \le x \le c \tag{7.153}$$
$$= \sum_{i=1}^{\infty} \sin q_i (h - x) \; e^{\gamma_i z} C_i^{(a)} \quad ; \quad c \le x \le h \tag{7.154}$$

$$\tilde{W}_b^{(1)}(x, z) = \sum_{i=1}^{\infty} \sin r_i (x - c) \; e^{s_i z} C_i^{(b)} \tag{7.155}$$

where $u_i = (2i-1)\pi/(2h)$, $\kappa_i^2 = u_i^2 + v^2$, $k^2 = j\omega\mu_0\mu_r\sigma$, $\gamma_i^2 = q_i^2 + v^2 + k^2$, $p_i^2 = \gamma_i^2 - v^2 = q_i^2 + k^2$, $r_i = (2i-1)\pi/2[(h-c)]$, $s_i^2 = r_i^2 + v^2 + k^2$. Note

also that an alternative expression for the TM potential which satisfies also the required boundary conditions is

$$\tilde{W}_b^{(1)}(x,z) = \sum_{i=1}^{\infty} \sin r_i(h-x)\; e^{s_i z} C_i^{(b)} \tag{7.156}$$

with the same r_i. In (7.153) the coefficient a_i is

$$a_i = \frac{\sin q_i(h-c)}{\cos p_i c} = \frac{q_i \cos q_i(h-c)}{p_i \sin p_i c} \tag{7.157}$$

From (7.157) the values of q_i and hence p_i, with $p_i = \sqrt{q_i^2 + k^2}$, are sought that satisfy

$$p_i \tan p_i c - q_i \cot q_i(h-c) = 0 \tag{7.158}$$

the roots of which give the eigenvalues for the odd parity solution.

The new system of unknown vector coefficients is

$$\frac{h}{2}\mathbf{u}^2 \left(\mathbf{C}^{(s)} + \mathbf{D}^{(ec)}\right) = \mathbf{M}_s \mathbf{C}^{(a)} \tag{7.159}$$

$$\frac{h}{2}\mathbf{u} jv \left(\mathbf{C}^{(s)} + \mathbf{D}^{(ec)}\right) = \mathbf{M}_c jv \mathbf{C}^{(a)} + k^2 \mathbf{M}_r \mathbf{s} \mathbf{C}^{(b)} \tag{7.160}$$

$$\frac{h}{2}\mathbf{u}\kappa \left(\mathbf{C}^{(s)} - \mathbf{D}^{(ec)}\right) = \mathbf{M}_c \gamma \mathbf{C}^{(a)} - jvk^2 \mathbf{M}_r \mathbf{C}^{(b)} \tag{7.161}$$

where the various matrices are now defined as follows

$$\mathbf{M}_s[i,j] = p_j^2 \left[a_j \int_0^c \cos(u_i x)\cos(p_j x)\; dx + \int_c^h \cos(u_i x)\sin[q_j(h-x)]\; dx \right] \tag{7.162}$$

The first integral in (7.162) is calculated from

$$\int_0^c \cos(u_i x)\cos(p_j x) dx = \frac{\sin[(p_j - u_i)c]}{2(p_j - u_i)} + \frac{\sin[(p_j + u_i)c]}{2(p_j + u_i)} \tag{7.163}$$

and the second one from

$$\int_c^h \cos(u_i x)\sin[q_j(h-x)]dx = \tag{7.164}$$

$$= \frac{-q_j\cos(u_i c)\cos[q_j(c-h)] - u_i\sin(u_i c)\sin[q_j(c-h)]}{q_j^2 - u_i^2}$$

The elements of matrix $\mathbf{M}_c$ are defined by

$$\mathbf{M}_c[i,j] = a_j p_j \int_0^c \sin(u_i x)\sin(p_j x)\ dx + q_j \int_c^h \sin(u_i x)\cos[q_j(h-x)]\ dx \tag{7.165}$$

with the first integral calculated from

$$\int_0^c \sin(u_i x)\sin(p_j x)dx = \frac{\sin[(p_j-u_i)c]}{2(p_j-u_i)} - \frac{\sin[(p_j+u_i)c]}{2(p_j+u_i)} \tag{7.166}$$

and the second one from

$$\int_c^h \sin(u_i x)\cos[q_j(h-x)]dx = \tag{7.167}$$

$$= \frac{-u_i\cos(u_i c)\cos[q_j(c-h)] - q_j\sin(u_i c)\sin[q_j(c-h)]}{q_j^2 - u_i^2}$$

Finally we have matrix $\mathbf{M}_r$

$$\mathbf{M}_r[i,j] = \int_c^h \sin(u_i x)\sin[r_j(x-c)]\ dx \tag{7.168}$$

$$= \frac{r_j\sin(u_i c)}{r_j^2 - u_i^2} \tag{7.169}$$

The solution to the system (7.159)-(7.161) is again (7.142)-(7.144) where

now

$$\mathbf{A}_1 = jv\left(\mathbf{u}\mathbf{M}_c - \mathbf{M}_s\right) \tag{7.170}$$

$$\mathbf{A}_2 = \kappa\mathbf{M}_s + \mathbf{u}\mathbf{M}_c\gamma \tag{7.171}$$

$$\mathbf{B}_1 = k^2\mathbf{u}\mathbf{M}_r\mathbf{s} \tag{7.172}$$

$$\mathbf{B}_2 = -k^2 jv\mathbf{u}\mathbf{M}_r \tag{7.173}$$

$$\mathbf{C}_1 = 0 \tag{7.174}$$

$$\mathbf{C}_2 = h\mathbf{u}^2\kappa \tag{7.175}$$

$$\mathbf{D}_1 = 0 \tag{7.176}$$

$$\mathbf{D}_2 = 0 \tag{7.177}$$

The eddy current density components are calculated from $\mathbf{J} = -j\omega\sigma\mathbf{A}$ and (7.2)-(7.4). Thus, for $c \le x \le h$:

$$J_x = \frac{j\omega\sigma}{2\pi}\int\limits_{-\infty}^{\infty}\left[\sum_{i=1}^{\infty}\sin r_i(x-c)\left(s_i^2 - v^2\right)\ e^{s_i z}C_i^{(b)}\right]e^{jvy}dv \tag{7.178}$$

$$J_y = \frac{-j\omega\sigma}{2\pi}\int\limits_{-\infty}^{\infty}\left[\sum_{i=1}^{\infty}\sin q_i(h-x)\ \gamma_i e^{\gamma_i z}C_i^{(a)} + \sum_{i=1}^{\infty}\cos r_i(x-c)\ r_i jv e^{s_i z}C_i^{(b)}\right]e^{jvy}dv \tag{7.179}$$

$$J_z = \frac{-j\omega\sigma}{2\pi}\int\limits_{-\infty}^{\infty}\left[\sum_{i=1}^{\infty}\sin q_i x\ (-jv)\gamma_i e^{\gamma_i z}C_i^{(a)} + \sum_{i=1}^{\infty}\cos r_i(x-c)\ r_i s_i e^{s_i z}C_i^{(b)}\right]e^{jvy}dv \tag{7.180}$$

Next, we use (7.102) and calculate the z-component of the magnetic flux density in air $B_z^{(ec)}$, which is produced by the conductive quarter-space. This is actually the magnetic flux density change ΔB_z. The knowledge of $D_0^{(ec)}$ and $D_i^{(ec)}$ provides an expression for $W_a^{(ec)}$ and therefore ΔB_z.

$$\Delta B_z = B_z^{(ec)} = \frac{1}{2\pi}\int\limits_{-\infty}^{\infty}\sum_{i=1}^{\infty}u_i(-\kappa_i)D_i^{(ec)}\sin u_i x\ e^{-\kappa_i z}e^{jvy}dv \tag{7.181}$$

The voltage change to a filamentary loop of radius r_0, at $z = z_0$, centered at $x = d$ is computed from:

$$\Delta V = j\omega \int_S \Delta \mathbf{B} \cdot d\mathbf{s} = j\omega \iint_S \Delta B_z dx dy \tag{7.182}$$

and the surface integration in (7.182) is evaluated as in the conductive half-space case, see (7.64). The final result for the impedance change after applying superposition is:

$$\Delta Z = -j\omega n \int_{-\infty}^{\infty} \sum_{i=1}^{\infty} \frac{(e^{-\kappa_i z_1} - e^{-\kappa_i z_2})}{\kappa_i^3} u_i \chi(\kappa_i r_1, \kappa_i r_2) \sin(u_i d) D_i^{(ec)} dv \tag{7.183}$$

7.6 Possible extensions to the solution

After solving the basic 3D problem of Fig.7.1 we can analyze a number of special cases with minimum effort. These are the following:

7.6.1 *Other coil and material characteristics*

Both even and odd solutions depend on the isolated coil incident field through the source coefficients $C_i^{(s)}$ and $C_0^{(s)}$. These coefficients can be found for the truncated configuration for other coils as well. In addition, the conductor can also be magnetic $\mu_r > 1$ and furthermore the gap can be filled with a conductive and/or magnetic medium. In this case, however, the solution will be somewhat more complicated since we will have to use a TM potential for the "gap" region as well.

7.6.2 *The quarter-space edge effect*

In order to simulate the edge effect due to a coil from a wedge in the form of a quarter-space, we can employ either the odd or even parity solutions. In either case, the slot is very wide and the coil lying above the edge very far from its image coil, therefore the latter does not interact with the edge. While the impedance change calculation should, in principle, be based again on calculating the average of the odd and even parity, we can get an approximate solution by taking into account only one of them. This case is

analyzed in Theodoulidis (2005c) for a nonmagnetic quarter-space and the theoretical results are in excellent agreement with experimental ones.

7.6.3 *The plate*

The model can also be extended to a conductive plate of finite thickness to simulate the plate edge effect as well as the effect of a long through-thickness slot in the plate. This can be done either by following the solution method in the previous paragraphs by adding another air-conductor interface at the bottom of the plate or by the following approach: Imagine a horizontal plane (located at $z = 0$) dividing the plate into two equal parts and treated as a plane of symmetry about which solutions are created that are either odd or even with respect now to z. Then the desired field is expressed as a superposition of these solutions. We choose the even solution to be half the field generated by two coaxial coils in which the current flows in the same direction, one coil above the plane $z = 0$ and an image coil equidistant below the plane, as shown in Fig.7.7. For the odd solution, we choose half the field produced with these currents in the opposite direction. Taking the sum of odd and even solutions or the difference, gives the field due to a single coil either above or below the plate. This approach is followed in Bowler (2005) and again the theoretical results are in excellent agreement with experimental ones.

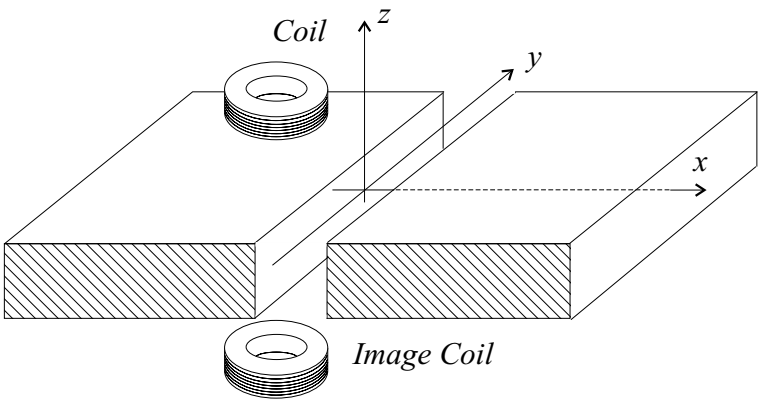

Fig. 7.7 Coil above a conductive plate with a through-thickness slot.

7.6.4 *The finite depth slot*

The model can be extended to the case of a slot having finite depth. This

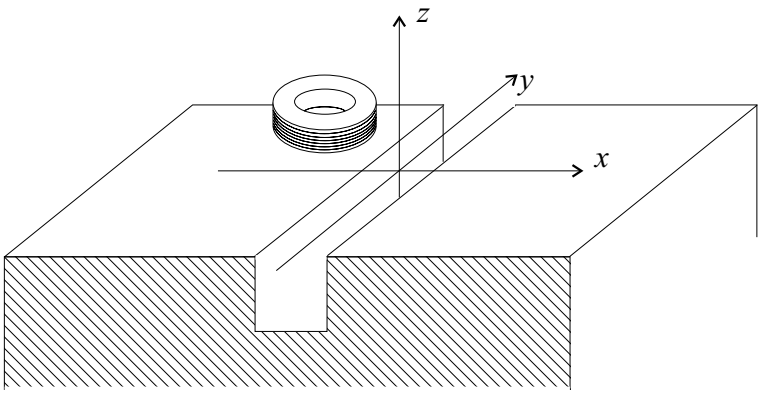

Fig. 7.8 Coil above a conductive half-space with a long and finite-depth slot.

will provide for the first time an exact semi-analytical solution in the important long crack problem for any excitation frequency. A relevant approximating model does exist in the thin-skin limit for cracks with a small opening and it is presented in Chapter 8. The proposed model could be used in cases that cannot be handled by the thin-skin model such as cracks with a wide opening, low frequency inspections and magnetic media. In addition, the successful completion of the proposed model extension will provide us with a tool for assessing the thin-skin model presented in Chapter 8 although this can also be done by comparing results from the two models in the case of the deep slot. The relevant 2D problem involving a 2D long coil and a finite depth slot is solved in Theodoulidis (2005a). Although the 2D problem is straightforward it is expected that the derivation of the solution for the 3D one will be more laborious. What is really interesting though, is that the eigenvalues for both the 2D and 3D problems are the same (both for the even and odd solutions) since they do not depend on the coil details but rather on the electromagnetic and dimensional properties of the slotted conductor.

7.6.5 *The Green's function*

Further benefits are available when the presented model is used in conjunction with a numerical method since the TREE method can be used to get a

solution for a singular source in the metal and thereby determine a Green's function for the right-angled conductor. This is a crucial step in the utilization of an integral method for the simulation of a crack near the edge. Such a simulation can be computationally very demanding but by using a kernel that accounts for the plate edge, the computation time should be greatly reduced.

7.6.6 *The ideal deep crack*

In the limit of $c \to 0$ the configuration in Fig.7.1 simulates the case of a conductive half-space with an infinitely long and infinitely deep ideal crack. Although the case of an infinitely deep crack is not representative of any practical situation, it provides insight to the behavior of eddy currents and the form of the acquired signals in surface eddy current inspections. Moreover, in this case the expressions for the various matrices elements are greatly simplified and also the eigenvalues are all real since $q_i = u_i$. Furthermore, only the even solution provides an impedance change due to the crack. The odd solution reduces to the odd solution for the impedance change due to the conductive half-space and thus it does not contribute to the impedance change due to the crack.

7.6.7 *Reversing of the air and conductor regions*

If we put a conductive material in the gap and replace the conductor with air, then we get another special case of the basic configuration, as shown in Fig.7.9. This can simulate the coil traversed vertically from the edge of a plate. Combining it with other coil types or other cylindrical coil orientations we can model a large number of eddy current inspection configurations.

7.6.8 *Truncation in the y-direction*

Finally, the numerical computations can be facilitated by replacing the integral with a series. This would be possible by truncating the solution region also in the y-direction and taking initially a Fourier series transform instead of a Fourier integral transform. Such a truncation is necessary not only for the right-angled conductor geometry but also for the isolated coil and the coil above the conductive half-space case.

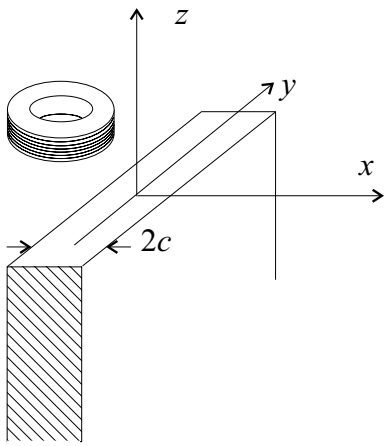

Fig. 7.9 Coil traversed across the edge of a plate.

7.7 Numerical aspects and results

The numerical aspects of the 3D edge solution are the computation of eigenvalues, infinite range integration and matrix inversion. Since these were also discussed in Chapters 3 and 4, we focus on the computation of eigenvalues and particularly on computing the complex roots of (7.91) and (7.158).

7.7.1 *Computation of eigenvalues*

An important numerical requirement is the precise computation of the eigenvalues q_i (or p_i) in both the even and odd parity solutions, which requires an efficient method of finding complex roots of the equations (7.91) and (7.158). We can try automatic root finding routines as in Chapter 4, but the following approach that uses an iteration scheme is a more robust technique.

For small c, we start by considering the case of $c = 0$. In this case, for the even parity solution, the starting value for each eigenvalue is $p_i = \lambda_i^{\text{even}}$, which is the eigenvalue for the unslotted half-space. We then increase the slot width step by step in small increments Δc until it acquires the value for which the calculations are performed. In each step we use the Newton-Raphson iteration scheme to compute the eigenvalue for that particular c until p_i^{m+1} differs from p_i^m by a specified, very small amount. The iterative

change in the eigenvalue is written

$$p_i^{m+1} = p_i^m - \frac{f(p_i)^m}{\left.\frac{df(p_i)}{dp_i}\right|^m}, \tag{7.184}$$

where

$$f^{\text{even}}(p_i) = q_i \tan(p_i c) + p_i \tan[q_i(h-c)]. \tag{7.185}$$

$$\begin{aligned}\frac{df^{\text{even}}(p_i)}{dp_i} &= cq_i \sec(p_i c)^2 + \frac{(h-c)p_i^2 \sec[q_i(h-c)]^2}{q_i} \\ &+ \frac{p_i \tan(p_i c)}{q_i} + \tan[q_i(h-c)]\end{aligned} \tag{7.186}$$

and m is the iteration number. Next, c is incremented by Δc, and the starting eigenvalue for the new crack width, $c+\Delta c$, is the one that was computed for c in the previous step. With this method an accurate computation of eigenvalues is performed.

In the odd solution the procedure is similar, differing only in the starting eigenvalues for $c = 0$, which are $p_i = \lambda_i^{\text{odd}}$ and in the functions that appear in (7.184), which are:

$$f^{\text{odd}}(p_i) = p_i \tan(p_i c) - q_i \cot[q_i(h-c)] \tag{7.187}$$

$$\begin{aligned}\frac{df^{\text{odd}}(p_i)}{dp_i} &= \frac{-p_i \cot[q_i(h-c)]}{q_i} + (h-c)p_i \csc[q_i(h-c)]^2 \\ &+ cp_i \sec(p_i c)^2 + \tan(p_i c)\end{aligned} \tag{7.188}$$

For large c as in the edge case when $c = h/2$, we perform two eigenvalue calculations. The first involves incrementing the slot width from $c = 0$ to $c = h/2$ and the second decrementing the slot width from $c = h$ to $c = h/2$. These calculations, which we have earlier called "incrementing" and "decrementing" provide two different sets of eigenvalues. Both of these sets are necessary in the calculations, so the final set is formed by merging them. In Fig.7.10 we depict even and odd eigenvalues p_i for the cases of $c = h/2 = 50$mm and $c = 2.1$mm, the later meaning that the slot width is 4.2mm. The rest of the data are given in Table 7.1.

For $c = h/2$ all p_i are complex and we can see that they comprise two sets. The set with the larger imaginary part is the result of the incrementing calculation while the set with the smaller imaginary part is the result of

Table 7.1 Coil and half-space parameters used for Figs 7.10, 7.11 and 7.12.

Coil		Testpiece	
r_1 [mm]	7.04	σ [MS/m]	25.51
r_2 [mm]	12.4	μ_r	1
$z_2 - z_1$ [mm]	5.04	c [mm]	2.1
z_1 [mm]	2.0	h [mm]	100
N	556	N_s	100

the decrementing calculation. The $c = h/2$ case is symmetrical and both calculations result in the same number of eigenvalues. Incidentally, for example when $c = 0$ all even solution p_i are complex given by $[(i\pi/h)^2 + j\omega\mu_0\mu_r\sigma]^{1/2}$ and when $c = h$ all p_i are real given by $i\pi/h$.

The situation is a little different when $c \ll h/2$. We can see that almost all eigenvalues come from the incrementing calculation except one eigenvalue for the odd solution that comes from the decrementing calculation. The relative number of eigenvalues produced from the two calculations depends on the slot width, see discussion in Theodoulidis (2005a). In all cases, for large index i the two sets start to converge and produce the same eigenvalues. The eigenvalues that we use in the various computations are the ones having real part smaller that a specific number. In Fig.7.10 we depict those with $\mathrm{Re}[p_i] \leq 1000$.

7.7.2 *Results*

First we test the case of a coil above a conductive half-space in a truncated region, which means that we test the validity of (7.67) and (7.73), by comparing numerical results to results calculated from the expression in Dodd (1968) and to experimental ones. The experimental results were provided by Burke (2003) and were produced for coil C5 at 1kHz and for coil C27 at 20kHz, all other data are given in Table 7.2. Table 7.3 shows the excellent agreement.

Next we test the case of the coil above a 4.2mm wide slot by comparing theoretical results from (7.150) and (7.183) to experimental impedance change measurements, Burke (2004). These were recorded (i) as a function of position, in 1mm steps, while the coil was traversed above the slot and (ii) as a function of frequency with the coil centered above the slot. Again the agreement is very good as shown in Figs 7.11 and 7.12, where we depict the resistance change ΔR and inductance change ΔL (instead of reactance

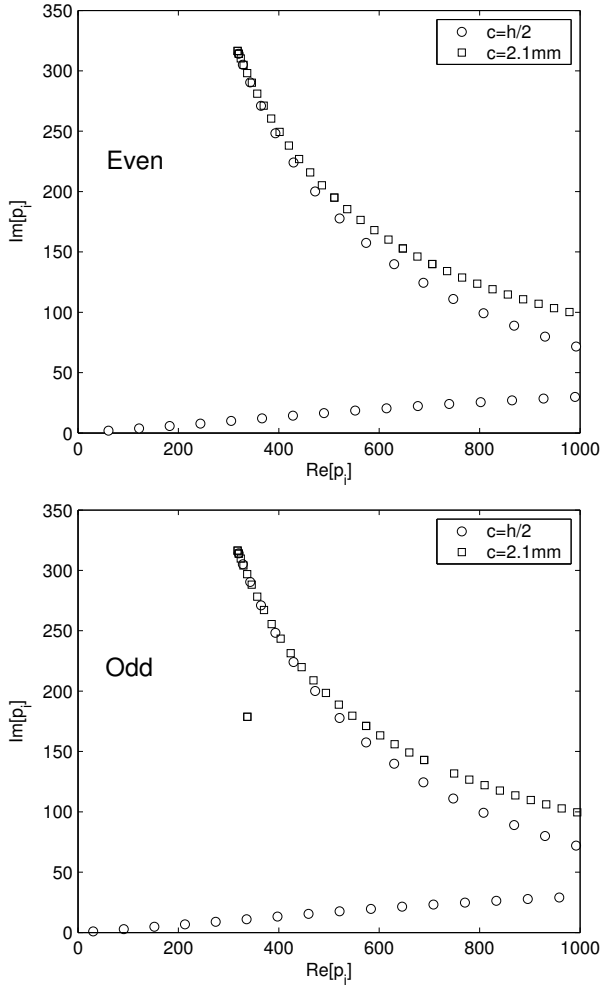

Fig. 7.10 Even and odd solution eigenvalues (in units of m^{-1}) for a quarter-space and a 4.2mm slot (c=2.1mm). The frequency is 1kHz.

$\Delta X = \omega \Delta L$). In all cases we used Mathematica and computed the infinite integral by truncating at the empirical value $10/r_2$ and using 150 terms in Gauss-Legendre integration.

Table 7.2 Coil and half-space parameters used for Table 7.3.

Coil	C5	C27	Test	
r_1 [mm]	6.88	7.04	σ [MS/m]	21.83
r_2 [mm]	10.7	12.4	μ_r	1
$z_2 - z_1$ [mm]	5.0	5.04	f [KHz]	1
z_1 [mm]	2.02	3.43	h	$20r_2$
N	410	556	N_s	100

Table 7.3 Impedance change results in Ohm for comparison of results.

Coil	C5	C27
Experiment	26.400-j84.006	12.650-j125.098
Dodd and Deeds	26.117-j82.927	12.801-j125.388
TREE	26.117-82.883	12.801-j125.329

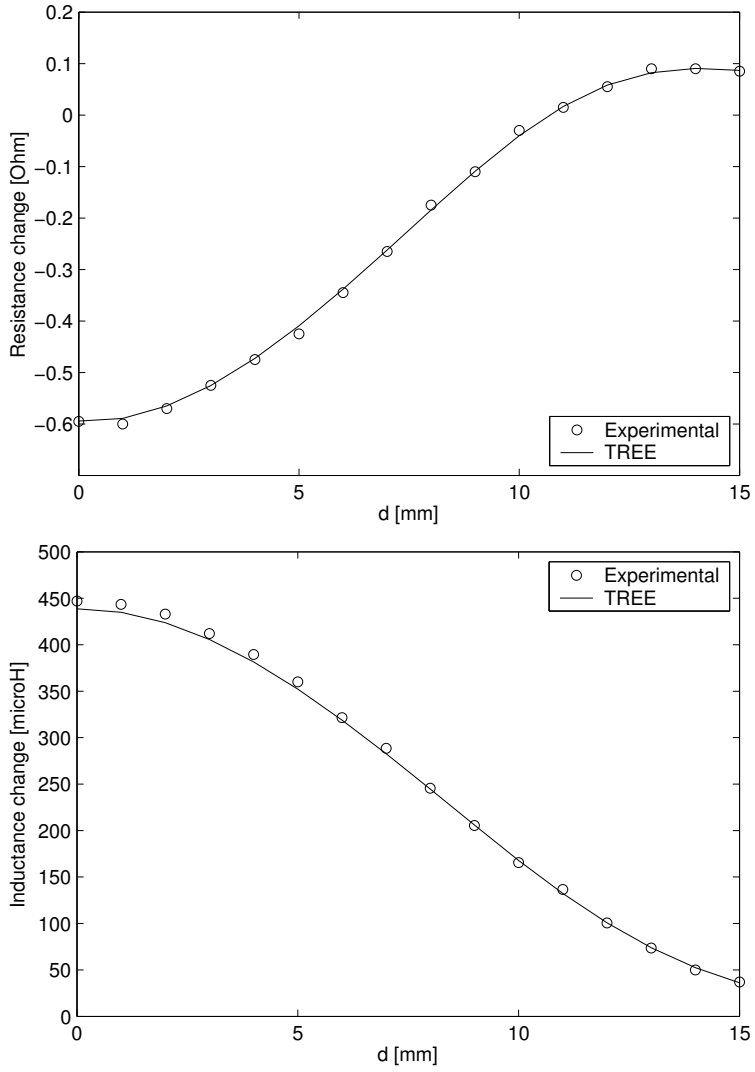

Fig. 7.11 Variation of the resistive and inductive parts of the impedance change with coil position at a frequency of 1kHz. At zero offset the coil is centered above the gap.

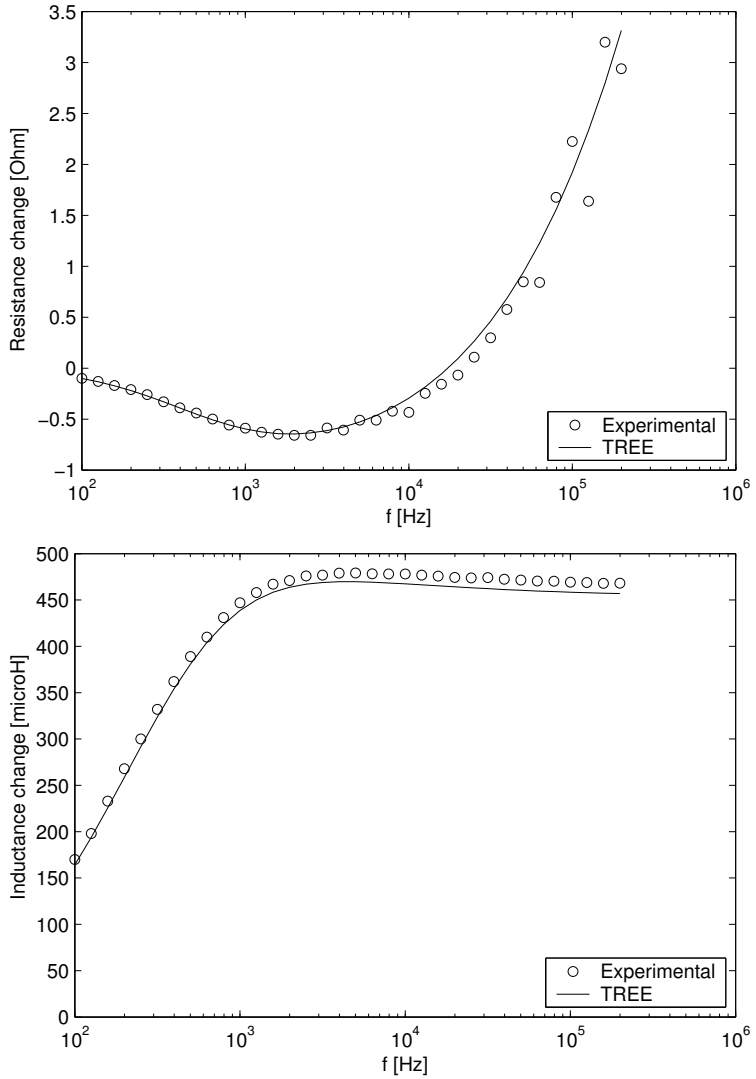

Fig. 7.12 Variation of the resistive and inductive parts of the impedance change with frequency. The coil is centered above the gap.

Chapter 8

Modelling of Surface Cracks in Planar Media

8.1 Introduction

While modelling of discontinuities that simulate flaws, defects, cracks, etc. is not the subject of this monograph, the analytical results derived so far can be used in the modelling of these discontinuities in order to simulate such eddy current inspections. We have mentioned in Chapter 1 that analytical results are particularly useful in the application of integral methods since they can be used to compute the incident field and the required Green's functions. Although we do not implement such methods here, we demonstrate how the results derived so far can be used for surface crack inspections. In order to do that we use an existing thin-skin model (valid in the high frequency regime) that has been shown from previous studies to agree well with experiment, Harfield *et al* (1997) and Ditchburn *et al* (2003, 2005). By combining it with analytical results for the incident field we have a fast and reasonably accurate analytical tool that can assist in understanding the acquired eddy current test signals and assist in the design optimization of eddy current probe coils.

A detailed presentation of analytical and integral models for simulating flaws can be found in Bowler (2004). The development of models for high frequency inspections and lists of references can be found in Harfield (1997), Auld (1999) and Salemi (2004).

8.2 The Harfield-Bowler thin-skin model

A major advance in analytical modelling of eddy current surface crack inspections was the thin-skin model by Harfield and Bowler (1997) who presented an expression for the impedance change produced by a crack, accu-

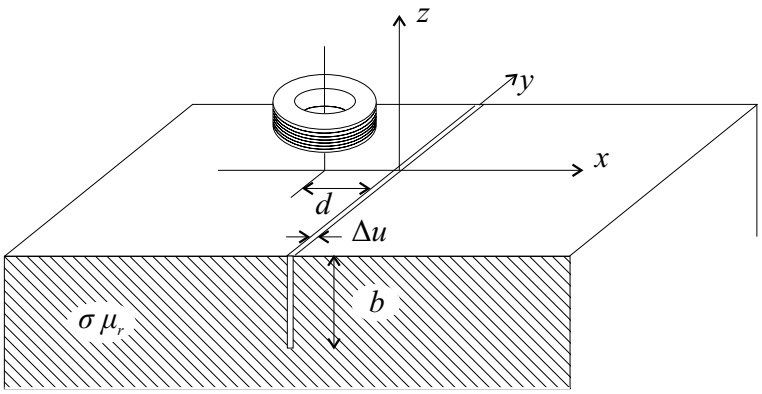

Fig. 8.1 Inspection of a long surface crack by a cylindrical coil traversed across the x-axis.

rate to a second-order expansion. This crack model is valid in the limit of small skin depth (high frequency regime) and it is successful in predicting the impedance change in cases such as (i) closed cracks (zero opening) in both magnetic and non-magnetic half-space for all coil configurations, (ii) open cracks (small opening) in non-magnetic half-space again for all coil configurations and (iii) open cracks in magnetic half-space only for symmetric coils and coil positions; see discussion in Harfield (1997). Although here we implement the simplest version of a long crack, the model is also valid for cracks with finite length and rectangular shape, Bowler (1998), semielliptical and epicyclic cracks, Bowler (2000), and ultimately using a numerical approach involving conformal mapping, it is valid for cracks of arbitrary shape, Bowler (2002). The model is indeed applicable to most surface crack inspections since these are operated at high frequencies and the cracks do have a negligible opening.

8.2.1 *Problem description and symmetry considerations*

Consider a probe coil above a conductive half-space of conductivity σ and relative magnetic permeability μ_r. Using a Cartesian coordinate system, the infinitely long crack lies at $x = 0$ and has a uniform depth b. The crack can have a small opening Δu and in addition it can be filled with a magnetic but non-conductive material with relative magnetic permeability μ_c. If the coil is offset from the crack plane $x = 0$ or the coil has a non-symmetric shape, the solution can be found as the averaged sum of odd

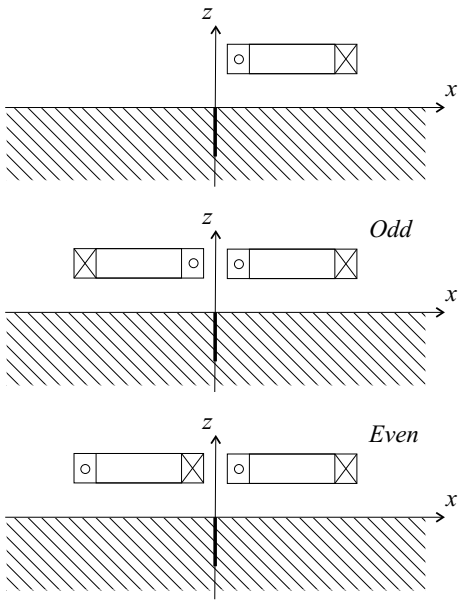

Fig. 8.2 Odd-even decomposition for simulating a coil in an offset position with respect to the crack line. In the odd configuration the interaction is mainly magnetic while in the even configuration the interaction is mainly electric.

and even configurations as shown in Fig.8.2. In the odd configuration, the electromagnetic field interaction is mainly magnetic since the component of the unperturbed electric field normal to the crack plane is zero. In the even configuration the interaction is mainly electric since the component of the unperturbed magnetic field normal to the crack plane is zero. For cracks with zero opening (ideal eddy current barriers) and for cracks with small opening (especially in non-magnetic media) the interaction is mainly electric (the magnetic field is continuous across the crack line) and thus the solution can be given only in terms of the even configuration. We should emphasize here that the odd-even decomposition and thus the model itself are valid for any coil configuration and not only for the cylindrical coil of Fig.8.1.

In conclusion, the model is valid in the limit of small skin depth (high frequency regime) and for (i) closed cracks (zero opening) in both magnetic and non-magnetic half-space for all coil configurations, (ii) open cracks (small opening) in non-magnetic half-space again for all coil configurations and (iii) open cracks (small opening) in magnetic half-space only for sym-

metric coils and coil orientations with respect to the crack line.

8.2.2 *General formulae*

For small skin depth, the change in coil impedance caused by the surface-breaking crack can be regarded as the sum of three terms:

$$\Delta Z^c = \Delta Z_s + \Delta Z_f + \Delta Z_k \tag{8.1}$$

where ΔZ_s arises from the removal of the surface of the metal when the crack is introduced, ΔZ_f is the dominant term and contains information about the shape and depth of the crack, and ΔZ_k (the "Kahn effect" term) takes into account deviations from the surface-impedance boundary conditions assumed in deriving the first two terms. The lengthy analysis in the derivation of the final formulae will not be repeated here. These will be given in a compact form following Ditchburn *et al* (2003), who provided a solution for a long slot in a compact form. Referring to Fig.8.1 the impedance change of the coil due to the crack is:

$$\Delta Z^c = \frac{\mu_0 \omega}{2\pi} \int_{-\infty}^{\infty} \frac{g}{1 + 2\,(v/jk)\,\tilde{U}\tanh(vb)} \tilde{\phi}^{(i)}(-v)\,\tilde{\phi}^{(i)}(v) dv \tag{8.2}$$

where

$$g = j\mu_c g_f \Delta u + (1+j)\mu_r \delta \left(g_f - \frac{1}{2} g_s \Delta u \right) + \frac{1}{2} g_k \mu_r \delta^2 \tag{8.3}$$

and

$$g_s = g_{s0} - g_{s1} \tag{8.4}$$

$$g_k = -\frac{4}{\pi}\left(g_{s0} + g_{s2}\right) + g_{s1} \tag{8.5}$$

$$g_{s0} = \left[1 + 2\,(v/jk)\left(\tilde{U} + \tilde{V}\right)\tanh(vb)\right] v^2 \tag{8.6}$$

$$g_f = v\tanh(vb) \tag{8.7}$$

$$g_{s1} = v^2 \operatorname{sec} h(vb) \tag{8.8}$$

$$g_{s2} = v^2 \tag{8.9}$$

For a magnetic half-space material the functions $\tilde{U}(v)$ and $\tilde{V}(v)$ are computed from:

$$\tilde{U}(v) = \frac{\mu_r}{2\pi\left[\left(\mu_r^2-1\right)w^2+\mu_r^2\right]} \left[\frac{\mu_r}{w}\ln\left(\frac{1+w}{1-w}\right) - \frac{1}{\sqrt{1+w^2}}\ln\left(\frac{1+\sqrt{1+w^2}}{1-\sqrt{1+w^2}}\right) + \frac{\mu_r^2-1}{\sqrt{\left(\mu_r^2-1\right)w^2+1}}\ln\left(\frac{\sqrt{\left(\mu_r^2-1\right)w^2+1}+\mu_r}{\sqrt{\left(\mu_r^2-1\right)w^2+1}-\mu_r} \times \frac{\sqrt{\left(\mu_r^2-1\right)w^2+1}-1}{\sqrt{\left(\mu_r^2-1\right)w^2+1}+1}\right)\right]$$

$$\tilde{V}(v) = -\frac{\mu_r}{2\pi\sqrt{\left(\mu_r^2-1\right)w^2+1}} \tag{8.10}$$

$$\cdot\ \ln\left(\frac{\sqrt{\left(\mu_r^2-1\right)w^2+1}+\mu_r}{\sqrt{\left(\mu_r^2-1\right)w^2+1}-\mu_r} \times \frac{\sqrt{\left(\mu_r^2-1\right)w^2+1}-1}{\sqrt{\left(\mu_r^2-1\right)w^2+1}+1}\right) \tag{8.11}$$

where $w = v/k$ and $k = (-1+i)/\delta$ with $\delta = \sqrt{2/(\omega\mu_0\mu_r\sigma)}$ denoting the electromagnetic skin depth. For non-magnetic half-space material, (8.10) and (8.10) should reduce to:

$$\tilde{U}(v) = \frac{1}{2\pi}\left[\frac{1}{w}\ln\left(\frac{1+w}{1-w}\right) - \frac{1}{\sqrt{1+w^2}}\ln\left(\frac{1+\sqrt{1+w^2}}{1-\sqrt{1+w^2}}\right)\right] \tag{8.12}$$

$$\tilde{V}(v) = -\frac{\mu_r}{2\pi}\ln\left(\frac{w^2}{\sqrt{w^2-1}}\right) \tag{8.13}$$

Eq. (8.2) is a general expression valid for any coil. The coil characteristics enter the calculations through the Fourier transform (with respect to y) of the magnetic potential $\phi^{(i)}$

$$\tilde{\phi}^{(i)} = \int_{-\infty}^{\infty} \phi^{(i)} e^{-jvy} dy \tag{8.14}$$

This potential is defined by

$$\begin{aligned}\mathbf{H}^{(i)} &= \nabla\phi^{(i)} \quad z \geq 0 \\ &= \frac{\partial\phi}{\partial x}\mathbf{x}_0 + \frac{\partial\phi}{\partial y}\mathbf{y}_0 + \frac{\partial\phi}{\partial z}\mathbf{z}_0\end{aligned} \tag{8.15}$$

where $\mathbf{H}^{(i)}$ is the unperturbed magnetic field at the crack line ($x = 0, y, z = 0$) in the absence of the crack. Eq. (8.15) implies that the impedance

change expression can also be written in terms of the components of the unperturbed magnetic field. For example using $\tilde{H}_y^{(i)}(v) = jv\tilde{\phi}^{(i)}$, (8.2) can be rewritten as

$$\Delta Z^c = \frac{\mu_0 \omega}{2\pi} \int_{-\infty}^{\infty} \frac{g}{1 + 2\,(v/ik)\,\tilde{U}\tanh(vb)} \frac{\tilde{H}_y^{(i)}(-v)\tilde{H}_y^{(i)}(v)}{v^2} \mathrm{d}v \tag{8.16}$$

Although in the next section we provide a general expression for air-cored coils of arbitrary offset and tilt let us provide here a specific for the cylindrical coil of Fig.8.1. From (3.53) and $H_z = B_z/\mu_0 = \partial\phi/\partial z$ we derive the expression for the magnetic potential at the surface of the conductor when the coil is centered above the crack.

$$\phi(r,z) = nI \int_0^{\infty} \frac{\chi(\kappa r_1, \kappa r_2)}{\kappa^3} J_0(\kappa r)(e^{-\kappa z_1} - e^{-\kappa z_2}) \frac{\lambda}{\kappa\mu_r + \lambda} d\kappa \tag{8.17}$$

where n is the wire turns density. Here we can replace r with y and the Fourier transform with respect to y reduces to the Fourier transform of the Bessel function term $J_0(\kappa y)$. Now using the identity

$$\begin{aligned} \int_{-\infty}^{\infty} e^{-j\omega t} J_n(t) dt &= \frac{2(-i)^n T_n(\omega)}{\sqrt{1-\omega^2}} \quad \left(\omega^2 < 1\right) \\ &= 0 \quad \left(\omega^2 > 1\right) \end{aligned} \tag{8.18}$$

where $T_n(\omega)$ is the Chebyshev polynomial of the first kind, with $T_0(\omega) = 1$, and the following identity for the Fourier pair f, F

$$f(t) \leftrightarrow F(\omega) \Rightarrow f(at) \leftrightarrow \frac{1}{|a|} F\left(\frac{\omega}{a}\right) \tag{8.19}$$

we obtain the relation

$$\tilde{\phi}^{(i)}(v) = 2n \int_{|v|}^{\infty} \frac{\chi(\kappa r_1, \kappa r_2)}{\kappa^3 \sqrt{\kappa^2 - v^2}} (e^{-\kappa z_1} - e^{-\kappa z_2}) \frac{\lambda}{\kappa\mu_r + \lambda} d\kappa \tag{8.20}$$

where $\chi(x_1, x_2)$ is defined in (3.27). A similar result was derived by Ditchburn (2003). By comparing experimental measurements to theoretical results derived using (8.2) and (8.20), Burke (2004) showed that the thin-skin model can be used in the case of an offset coil also. The offset coil was modelled, using Fourier identities, by multiplying the integrand with $\cos\left(d\sqrt{\kappa^2 - v^2}\right)$. Comparison of theory with experiment is shown in Fig.8.3

Table 8.1 Coil and half-space parameters used for Fig.8.3

Coil C26		Testpiece	
r_1	6.88 mm	σ	28.5%IACS
r_2	10.7 mm	μ_r	1
$z_2 - z_1$	5.0 mm	b	5.96 mm
z_1	2.02 mm	Δu	0.43 mm
N	410	μ_c	1
L_0 (expt)	3.008 mH	f	10 kHz
Coil C27		Testpiece	
r_1	7.04 mm	σ	28.4%IACS
r_2	12.4 mm	μ_r	1
$z_2 - z_1$	5.04 mm	b	11.99 mm
z_1	2.01 mm	Δu	0.41 mm
N	556	μ_c	1
L_0 (expt)	5.859 mH	f	10 kHz

for two coil-testpiece combinations with data given in Table 8.1 Note that the theoretical value of isolated coil inductance for coil C26 is 2.997 mH, for coil C27 it is 5.862 mH and the conductivities are given in %IACS. [1]

8.3 Analytical approach

The details of the particular coil enter the model via the magnetic potential $\phi^{(i)}$ and in this respect the general expressions of Chapter 5 will be very useful. From (5.35) or (5.36) the y-component of the incident magnetic field on the conductor surface in terms of the source coefficient $C^{(s)}$ is

$$B_y^{(i)}(x, y, z = 0) = \frac{1}{4\pi^2} \int_{-\infty}^{\infty} \int_{-\infty}^{\infty} C^{(s)}(u, v) \frac{2\kappa\mu_r\lambda}{(\kappa\mu_r + \lambda)} jv e^{jux} e^{jvy} du dv \quad (8.21)$$

and therefore its Fourier transform with respect to y at the crack line $x = 0$ is

$$\tilde{B}_y^{(i)}(x = 0, v, z = 0) = \frac{1}{2\pi} \int_{-\infty}^{\infty} C^{(s)}(u, v) \frac{2\kappa\mu_r\lambda}{(\kappa\mu_r + \lambda)} jv du \quad (8.22)$$

[1]The conductivity unit %IACS stands for the International Annealed Copper Standard and is defined by equating 100%IACS to a conductor made of copper with 58 MSiemens/m and 0%IACS to an insulator.

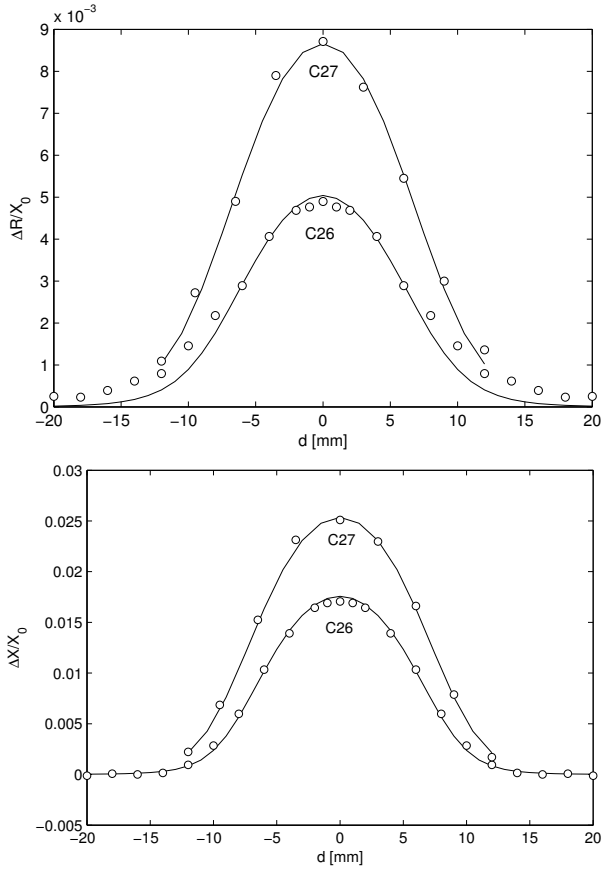

Fig. 8.3 Variation of the normalized impedance change due to the crack as the coil is traversed across the crack. Solid curves are theoretical results and circles are experimental ones. The latter are courtesy of S.K. Burke, DSTO, Australia.

The Fourier transform of the magnetic potential is thus

$$\tilde{\phi}^{(i)}(v) = \frac{1}{2\pi\mu_0} \int_{-\infty}^{\infty} C^{(s)}(u,v) \frac{2\kappa\lambda}{(\kappa\mu_r + \lambda)} du \tag{8.23}$$

This is also a general expression that depends on the source coefficient. In Chapter 5 we saw that the solution of the general 3D induction problem in a conductive half-space by an arbitrarily shaped coil depends on the source coefficient. Here we see that this is also true when the conductive half-space

has a surface crack.

Now for the general case of a tilted cylindrical coil $C^{(s)}$ is given by (5.78) and if needed also by using (5.81). Here however we will give explicitly the form of the source coefficient for the offset parallel coil and the offset perpendicular coil, the latter rotated by an angle θ around its axis, as shown in Fig.8.4. For the parallel coil it is

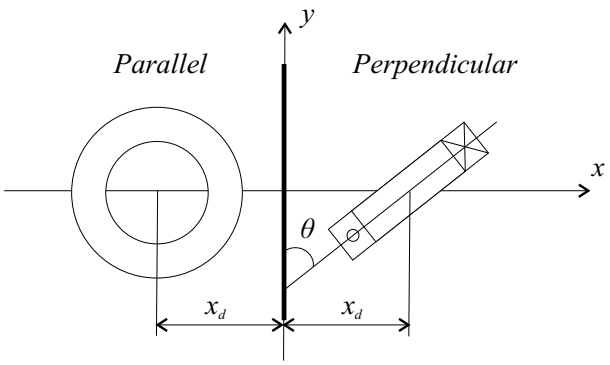

Fig. 8.4 Top view of an offset parallel and an offset rotated perpendicular coil in the vicinity of a crack.

$$C^{(s)} = \frac{\mu_0 n I \pi}{\kappa^5} \left(e^{-\kappa z_1} - e^{-\kappa z_2} \right) \chi \left(\kappa r_1, \kappa r_2 \right) e^{-jux_d} \tag{8.24}$$

and for the perpendicular coil it is

$$C^{(s)} = \frac{j\mu_0 n I 2\pi e^{-\kappa d}}{w^3} \sin\left(\frac{wl}{2}\right) M \left(w r_1, w r_2 \right) e^{jux_d} \tag{8.25}$$

where $w = u\cos\theta + v\sin\theta$ and the functions χ and M are defined in (3.27) and (5.68) respectively. Provided the crack opening is zero, the perpendicular coil expressions are useful for example in simulating the so called WeldScan probe which is used extensively in weld inspections, Theodoulidis (2000). Numerical results and a discussion on the tilted coil inspecting a long crack can be found in Theodoulidis (2005).

8.4 Numerical approach

If it is not possible to find an analytical expression for the coefficient $C^{(s)}$ we have to resort to its numerical computation, which means a numerical

computation of the potential $\tilde{\phi}^{(i)}(v)$. We have seen in Chapter 5 that a numerical computation of the source coefficient is based on the numerical calculation of the incident free-space magnetic field from the Biot-Savart law and the use of 2D-FFT routines. If we use the z-component of the magnetic field, (8.23) can be re-written as

$$\tilde{\phi}^{(i)}(x=0,v,z=0)=\frac{1}{2\pi}\int_{-\infty}^{\infty}\frac{\tilde{B}_z^{(s)}(u,v)}{\kappa^2}\frac{2\kappa\mu_r\lambda}{(\kappa\mu_r+\lambda)}du \tag{8.26}$$

with

$$\tilde{B}_z^{(s)}(u,v)=\int_{-\infty}^{\infty}\int_{-\infty}^{\infty}B_z^{(s)}(x,y,z=0)e^{-jux}e^{-jvy}dxdy \tag{8.27}$$

The expressions involving the source coefficient are valid in the case of an air-cored probe coil. There are however cases when we should not evaluate numerically the source coefficient but rather the incident potential or magnetic field. These cases are (i) when we use the reformulated expressions developed in Chapter 4 and (ii) when the magnetic field or potential cannot be written in terms of the potential $C^{(s)}$ as in the case of the ferrite-cored coil. In this case we compute the magnetic field or potential along the crack line and then perform a numerical Fourier transform by using an FFT routine. The result is a list of numbers describing the transformed magnetic field or potential. This can be used as is or further interpolated to provide $\tilde{\phi}^{(i)}(v)$ at arbitrary v.

From Chapter 5, for the ferrite-cored coil with a semi-infinite core

$$H_y(0,y,z)=\iota_0 J_1(\boldsymbol{\kappa}^{\mathbf{T}}y)\mathbf{M}^{-1}(e^{-\mathbf{q}z_2}-e^{-\mathbf{q}z_1})\mathbf{q}^{-3}\mathbf{D}^{-1}\chi_R(\mathbf{q}r_1,\mathbf{q}r_2) \tag{8.28}$$

while for the air-cored coil centered above the crack

$$H_y(0,y,z)=2\iota_0\sum_{i=1}^{\infty}\lambda_i J_1(\kappa_i y)\frac{(e^{-\kappa_i z_1}-e^{-\kappa_i z_2})}{\kappa_i\mu_r+\lambda_i}\frac{\chi(\kappa_i r_1,\kappa_i r_1)}{\kappa_i^3\left[hJ_0\left(\kappa_i h\right)\right]^2} \tag{8.29}$$

In any case this is a much faster technique (short calculation time) compared with the required double integration especially when multiple ΔZ^c values are needed at various frequencies or coil positions. This is due to the fact that many terms in the expressions are pre-computed (for example only the first order Bessel term has to be recomputed for a different y).

Table 8.2 Coil and half-space parameters used for Figs 8.5-8.7

Coil		Testpiece	
r_1	2 mm	Al	
r_2	4 mm	σ	35.4 MS/m
$z_2 - z_1$	2 mm	μ_r	1
z_1	1 mm	St	
N	400	σ	5.0 MS/m
f	500 kHz	μ_r	80

8.5 Practical implementation

The thin-skin model is very useful for simulating surface crack inspections. Consider Figs 8.5, 8.6 which depict typical crack signals produced by the cylindrical coil with data shown in Table 8.2. The main characteristic of these crack signals, which are obtained here for both nonmagnetic and magnetic conductors, are their phase difference (phase separation) from the lift-off signal, which is considered as noise. This is actually what the display of an eddyscope will show while the surface coil is traversed across the crack line. In fact, the display is rotated so that the lift-off signal is set horizontal so that the crack signals are upright deflections.

Fig.8.5 shows that for nonmagnetic conductors the larger phase separation between lift-off and crack signals is obtained for tight cracks but on the other hand cracks with finite opening produce a somewhat larger signal due to the volume of conductive material that is absent.

In contrast to nonmagnetic conductors, crack signals in magnetic ones have larger phase separation from the lift-off signal, see Fig.8.6. Moreover, they are much stronger signals because the surface eddy current density is higher in magnetic conductors for the same excitation frequency.

Using the thin-skin model we can study the inspection of deep cracks since the model is particularly suited for this application as it requires a high ratio of crack depth to skin depth. A known disadvantage of the ECT method is that the surface crack signal gets saturated from the increasing depth of the crack due to skin depth. Therefore, evaluation of a crack is quite difficult when it is deeper than a certain value. This behavior can easily be shown by the presented thin-skin model, see Fig.8.7 which depicts the variation of the impedance change maximum amplitude with crack depth for surface cracks in an aluminum half-space.

In general, a lower frequency excitation provides deeper penetration of eddy currents but at the same time it causes other problems such as reduced

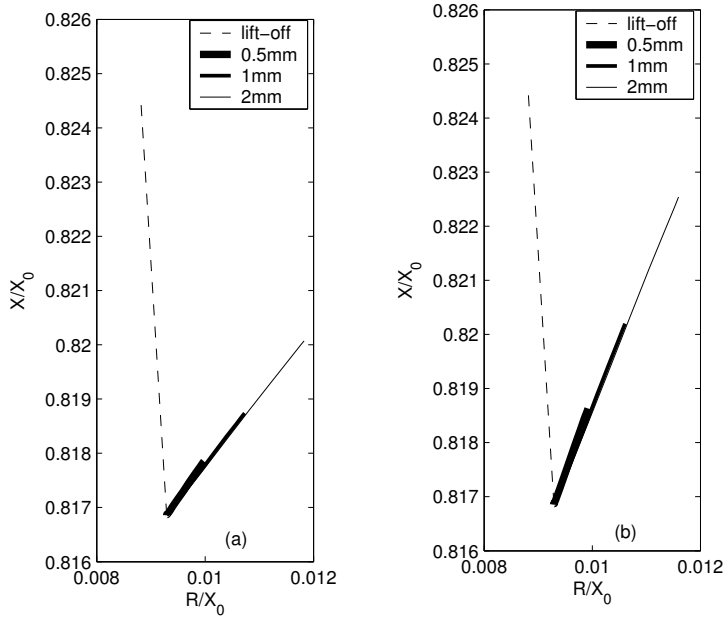

Fig. 8.5 Impedance signals produced by three surface cracks of varying depth in an aluminum half-space (a) zero opening (b) 0.1mm opening. The lift-off signal is produced by an increase of 0.05mm.

sensitivity (decreased signal to noise ratio) and smaller phase separation of the crack signal. Since, as already mentioned in Chapter 3, the true penetration is also affected by the coil dimensions, some improvement can be obtained by optimizing the excitation coils, for example with an excitation system using phase-shifted driving as in Janousek (2005). In this respect, the thin-skin model is a valuable tool since it requires only the knowledge of the incident magnetic field and thus allows the designer to concentrate of the probe characteristics.

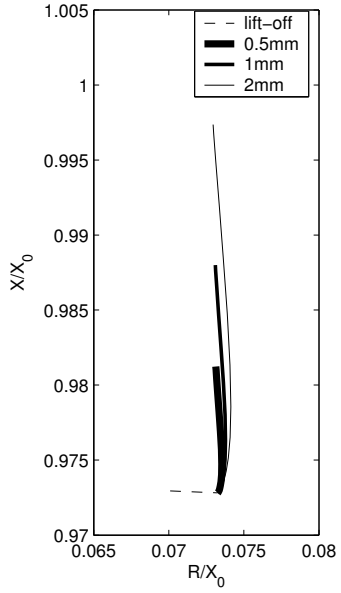

Fig. 8.6 Impedance signals produced by three surface cracks of varying depth and zero opening in a steel half-space. The lift-off signal is produced by an increase of 0.05mm.

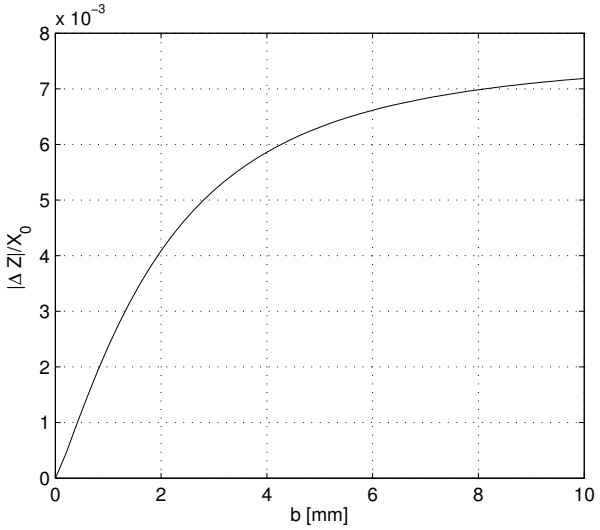

Fig. 8.7 Variation of the impedance change maximum amplitude with crack depth for surface cracks in an aluminum half-space.

Appendix A

Magnetic Field Calculation of Isolated Coils

In many cases we may need a fast and accurate calculation of the magnetic field of an isolated coil, that is a coil in free-space. Such a calculation can be performed using the Biot-Savart law in its integral form, as follows:

$$\mathbf{B}(\mathbf{r}) = \frac{\mu_0}{4\pi} \int_{\Omega_s} \mathbf{J} \times \frac{\mathbf{r} - \mathbf{r}'}{|\mathbf{r} - \mathbf{r}'|^3} d\mathbf{r}' \tag{A.1}$$

where Ω_s is the source region, $\mathbf{J}$ the volume distribution of source current density and $\mathbf{r}$, $\mathbf{r}'$ define the position vectors of the field point and source point respectively.

A.1 General coil

The required integration in (A.1) can be performed analytically, providing thus a closed-form expression for $\mathbf{B}$, only for a very limited number of canonical coil shapes. In cases of more complex shapes or in cases where coils with simple forms are positioned with respect to the coordinate system in such a way that a closed-form expression cannot be derived, we resort to numerical methods.

Bacause a direct numerical calculation of the volume integral in (A.1) is time consuming what we usually do is divide the coil volume into a number of current blocks. The magnetic field for each block is calculated analytically and the total magnetic field is acquired from the addition of each block's field, Azzerboni (1989), (1993), Ciric (1991), Urankar (1982), Lei (2002). Consider for example the various coil shapes in Fig.A.1.

It may even be desirable to approximate the curved portion of the coil

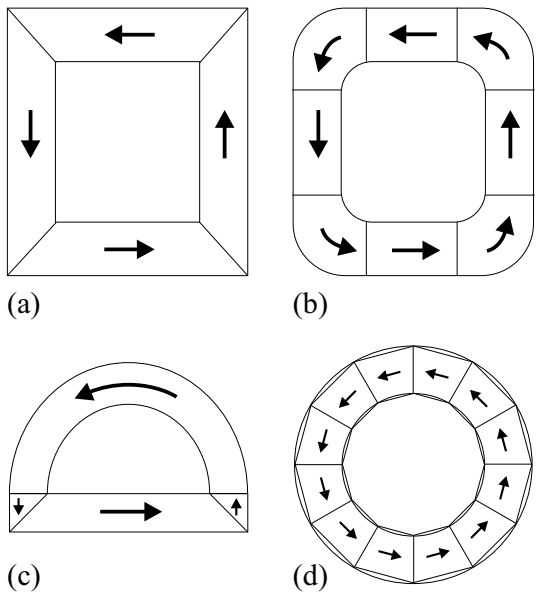

Fig. A.1 Top view of four coil shapes used in eddy current testing (a) rectangular (b) rounded-corner rectangular (c) D-coil (d) cylindrical. Arrows show the uniform source current density vector in the respective segment

body with a number of straight currents of trapezoidal shape. Some researchers even propose this technique for the cylindrical coil although this would increase the computation time considerably. Since the main interest of this book is the cylindrical coil, we proceed to the presentation of it.

A.2 Cylindrical coil

In this section we provide analytical expressions for the magnetic field of the cylindrical coil. This particular coil design has only an azimuthal current density $\mathbf{J} = \iota_0 \boldsymbol{\varphi}_0$ if the geometry is described in a cylindrical coordinate system (r, φ, z). A bibliographic search has shown a number of approaches in computing the radial and axial components of $\mathbf{B}$. The coil consists of N wire turns and in each turn flows a current I, therefore the current density is $\iota_0 = NI(r_2 - r_1)^{-1}(z_2 - z_1)^{-1}$. Because in every wire turn the current has the same amplitude and phase, the coil region is assumed to have zero conductivity, ie no eddy current effects are taken into account. Such coils are sometimes referred in the bibliography as stranded in contrast to solid

ones where there is only one turn and eddy currents have to be taken into account since the coil region is assumed solid and having the conductivity of copper.

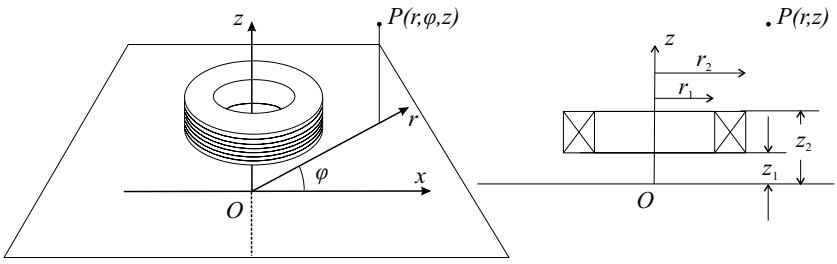

Fig. A.2 The multi-turn cylindrical coil.

There are two possibilities for a rapid calculation: Urankar (1982) presented analytical expressions that involved Elliptic integrals of the first, second and third kind as well as an integral expression that evades analytical treatment. Similarly treating the Biot-Savart law, Babic (1988) derived expressions in terms of incomplete Jacobi elliptic functions and the lambda function. On the other hand, Forbes (1997) provided expressions in terms of two single integrals, each of which has the form of a periodic function integrated over its period. These integrals can be evaluated numerically with high accuracy since an attempt to express them in terms of special functions would not offer any numerical advantage. Throughout this book we use the Forbes formulae since they are easily programmed, they avoid the likelihood of errors in the implementation of complicated formulas, see for example Fontana (2001) who addresses a number of issues regarding the Unrankar formulae, and they are overall faster than the two other approaches by a factor of about two, from personal experience. Moreover, these formulas that are reproduced here, do not suffer from singularities in the resulting expressions. Referring to dimensions depicted in Fig.A.2

$$B_r = \frac{\mu_0 \iota_0}{2\pi} \left[N(r_2, z_2; r, z) - N(r_1, z_2; r, z) - N(r_2, z_1; r, z) + N(r_1, z_1; r, z) \right] \tag{A.2}$$

$$B_z = \frac{\mu_0 \iota_0}{2\pi} \left[L(r_2, z_2; r, z) - L(r_1, z_2; r, z) - L(r_2, z_1; r, z) + L(r_1, z_1; r, z) \right] \tag{A.3}$$

where the N and L functions are defined as:

$$N(r_0, z_0; r, z) = \int_0^{\pi} \cos\beta \left[\sqrt{\xi^2 + Q^2} + U \ln\left(\xi + \sqrt{\xi^2 + Q^2} \right) \right] d\beta \quad \text{(A.4)}$$

$$L(r_0, z_0; r, z) = \frac{1}{r} \int_0^{\pi} \cos\beta \left[F + UVG + \frac{1}{2} W \sqrt{\xi^2 + Q^2} \right] d\beta \quad \text{(A.5)}$$

and the various terms that appear in (A.4) and (A.5) are

$$\begin{aligned} F = {} & 2UW \ln\left(\xi + \sqrt{\xi^2 + Q^2} \right) \\ & + \frac{1}{4} \left[3\left(U^2 - V^2\right) - (\xi + U)^2 \right] \ln\left(\frac{\sqrt{\xi^2 + Q^2} - W}{\sqrt{\xi^2 + Q^2} + W} \right) \end{aligned} \quad \text{(A.6)}$$

$$\begin{aligned} G = {} & -2 \arctan\left[\frac{\xi\left(\xi + \sqrt{\xi^2 + Q^2} \right) + V^2}{VW} \right] + \arctan\left[\frac{W + \xi + \sqrt{\xi^2 + Q^2}}{V} \right] \\ & - \arctan\left[\frac{-W + \xi + \sqrt{\xi^2 + Q^2}}{V} \right] \end{aligned} \quad \text{(A.7)}$$

$$V = r \sin\beta \quad \text{(A.8)}$$

$$W = z_0 - z \quad \text{(A.9)}$$

$$\xi = r_0 - r \cos\beta \quad \text{(A.10)}$$

$$Q^2 = (r \sin\beta)^2 + (z_0 - z)^2 \quad \text{(A.11)}$$

$$U = r \cos\beta \quad \text{(A.12)}$$

In the special case of $r = 0$ the radial component of $\mathbf{B}$ vanishes and the axial component is again calculated from (A.3), this time with the L function given by

$$L(r_0, z_0; 0, z) = \pi (z_0 - z) \ln\left[r_0 + \sqrt{r_0^2 + (z_0 - z)^2} \right] \quad \text{(A.13)}$$

The above formulae are easily programmed with a higher programming language such as Fortran or a general mathematical package such as Mathematica.

Bibliography

Abramowitz M. and Stegun I. A. (1970), *Handbook of Mathematical Functions (with formulas, graphs and mathematical tables)*, Dover, New York.

Albach M. and Hannakam L. (1981) "Induzierte wirbelstrome in einer Kreischeibe und in einem Rechteckzylinder endlicher Hohe", *Archiv fur Elektrotechnik* **64**, 127–134.

Albanese R., Baresi R., Carbone M. and Gasparics A. (2004) "Tools for the design of fluxset probes addressed to the detection of deep defects", *Electromagnetic Nondestructive Evaluation (VIII)*, T. Sollier *et al* eds, IOS Press, 2–57.

American Society for Nondestructive Testing, NDT Handbook, 2nd edition, Vol.4 Electromagnetic Testing, 1986.

American Society for Nondestructive Testing, NDT Handbook, 3rd edition, Vol.5 Electromagnetic Testing, S.S.Udpa and P.O.Moore eds, 2004.

Anisimov S.D., Voloshina A.G., Vinogradova I.Yu and Golubova G.S. (1985) "Approximate equations for electromagnetic transducers with ferromagnetic cores", *The Soviet Journal of Nondestructive Testing* **21**, (2), 86–92.

Antimirov M. Ya, Kolyshkin A. A. and Vaillancourt R. (1997), *Mathematical Models for Eddy Current Testing*, Les Publications CRM, Montreal.

Auld B. A., Muennemann F. and Winslow D. K. (1981) "Eddy current probe response to open and closed surface flaws", *Journal of Nondestructive Evaluation* **2**, (1), 1–21.

Auld B. A., (1981) "Theoretical characterization and comparison of resonant-probe microwave eddy current methods", *Eddy-Current Characterization of Materials and Structures*, Birnbaum/Free eds, American Society for Testing and Materials, STP-722, 332–347.

Auld B. A. and Riaziat M. (1983) "Spatial frequency analysis and matched filtering in electromagnetic nondestructive evaluation", *Journal of Applied Physics* **54**, (6), 3509–3517.

Auld B. A., Muennemann F. G. and Riaziat R. (1984) "Quantitative modelling of flaw responses in eddy current testing", *Nondestructive Testing* **7**, 37–76.

Auld B. A. and Moulder J.C. (1999) "Review of advances in quantitative eddy current nondestructive evaluation", *Journal of Nondestructive Evaluation*

18, (1), 3–36.

Auld B. A. (1999) "John Moulder and the evolution of model-based quantitative eddy current NDE", *Review of Progress in Quantitative Nondestructive Evaluation* **18**, 441–448.

Azzerboni B., Cardelli E. and Tellini A. (1989) "Computation of the magnetic field in massive conductor systems", *IEEE Transactions on Magnetics* **25**, (6), 4462–4473.

Azzerboni B., Cardelli E., Raugi M., Tellini A. and Tina G. (1993) "Magnetic field evaluation for thick annular conductors", *IEEE Transactions on Magnetics* **29**, (3), 2090–2094.

Babic S., Andjelic Z., Krstajic B. and Salon S. (1988) "Analytical calculation of the 3D magnetostatic field of a toroidal conductor with rectangular cross-section", *IEEE Transactions on Magnetics* **24**, (6), 3162–3164.

Bae B.-H., Choi J.-M. and Kim S.-Y. (2002) "Eddy current testing probe with dual half-cylindrical coils", *Review of Scientific Intstruments* **71**, (2), 567–570.

Bahr A. J., (1981) "Theoretical characterization and comparison of resonant-probe microwave eddy current methods", *Eddy-Current Characterization of Materials and Structures*, Birnbaum/Free eds, American Society for Testing and Materials, STP-722, 311–331.

Bahr A. J. and Auld B. A. (1988) "An electromagnetic model for eddy-current imaging", *Journal of Nondestructive Evaluation* **7**, (1/2), 71–77.

Bavall L. (2002) "Determination of the thickness of copper coatings on steel by measuring the impedance of a thin elliptic coil", *Measurement Science and Technology* **13**, (4), 510–519.

Becker R., Betzold K., Boness K. D., Collins R., Holt C. C. and Simkin J. (1986) "The modeling of electrical current NDT methods. Its application to weld testing (Part 1)", *British Journal of NDT*, 286–294.

Becker R., Betzold K., Boness K. D., Collins R., Holt C. C. and Simkin J. (1986) "The modeling of electrical current NDT methods. Its application to weld testing (Part 2)", *British Journal of NDT*, 361–370.

Beissner R. E. and Sablik M. J. (1984) "Theory of eddy currents induced by a nonsymmetric coil above a conducting half-space", *Journal of Applied Physics* **56**, (2), 448–454.

Beissner R. E. (1986) "Analytic Green's dyads for an electrically conducting half-space", *Journal of Applied Physics* **60**, (3), 855–858.

Beissner R. E. (1988) "Approximate model of eddy current probe impedance for surface breaking flaws", *Journal of Nondestructive Evaluation* **7**, (1/2), 25–34.

Beissner R. E. and Temple J. A. G. (1990) "Calculation of eddy current fields for coils of arbitrary shape", *Review of Progress in Quantitative Nondestructive Evaluation*, D.O.Thompson and D.E.Chimenti (Eds.), Plenum Press, **9**, 257–265.

Bihan Y. L. (2004) "Analytical model of a shielded U-core sensor", *International Journal of Applied Electromagnetics and Mechanics* **19**, 99–102.

Blitz J., Williams D. J. A. and Tilson J. (1981) "Calibration of eddy-current test

equipment", *NDT International* **14**, 119–123.

Blitz J. (1991), *Electrical and Magnetic Methods of Nondestructive Testing*, Adam Hilger, New York.

Bowler J. R. (1987) "Calculations using half-space Green's functions", *Journal of Applied Physics* **61**, (3), 833–839.

Bowler J. R., Sabbagh H. A. and Sabbagh L. D. (1989) "The reduced impedance function for cup-core eddy-current probes", *IEEE Transactions on Magnetics* **25**, (3), 2646–2649.

Bowler J. R. and Harfield N. (1998) "Evaluation of probe impedance due to thin-skin eddy-current interaction with surface cracks", *IEEE Transactions on Magnetics* **34**, (2), 515–523.

Bowler J. R. and Harfield N. (2000) "Thin-skin eddy-current interaction with semielliptical and epicyclic cracks", *IEEE Transactions on Magnetics* **36**, (1), 281–291.

Bowler J. R. (2002) "Thin-skin eddy-current inversion for the determination of crack shapes", *Inverse Problems* **18**, 1891–1905.

Bowler J. R. and Katyal V. (2004) "Magnetic sensor array for eddy current field measurement with a racetrack coil excitation", *Electromagnetic Nondestructive Evaluation (VIII)*, T. Sollier *et al* eds, IOS Press, 36–43.

Bowler J. R. (2004) "Analytical and integral models for simulating cracks", *Electromagnetic Testing. Nondestructive Testing Handbook.*, S.S.Udpa and P.O.Moore eds, 3rd edn, **5**, 74–92.

Bowler J. R. and Theodoulidis T. P. (2005) "Eddy currents induced in a conducting rod of finite length by a coaxial encircling coil", *Journal of Physics D: Applied Physics* **38**, 2861–2868.

Bowler J. R., Fu F. and Theodoulidis T. P. (2005) "The effect of opening on eddy current response for an idealized through crack", presented in *Review of Progress in Quantitative Nondestructive Evaluation*, Maine, USA.

Burke S. K. (1986) "Impedance of a horizontal coil above a conducting half-space", *Journal of Physics D: Applied Physics* **19**, 1159–1173.

Burke S. K. (1990) "Eddy-current induction in a uniaxially anisotropic plate", *Journal of Applied Physics* **68**, (7), 3080–3090.

Burke S. K. (1992) "A semi-empirical model for eddy-current NDE using ferrite-cored probes", *Nondestructive Testing and Evaluation* **6**, 267–277.

Burke S. K. (2002) "Experimental data: air-cored coil outside a conducting cylinder", Private communication.

Burke S.K. (2003) "3D edge effect in eddy-current NDE: Experimental data for a cylindrical air-cored coil and an Al alloy quarter space", Private communication.

Burke S. K. (2004) "Inductance change due to a 2D slot in a perfectly conducting plate. II. Experimental data for a cylindrical air-cored coil offset from the slot", Private communication.

Burke S. K. (2004) "Inductance change due to a 2D slot in a conductive half-space III. Experimental results for a wide slot with infinite depth in an Al alloy half space", Private communication.

Burke S. K. and Theodoulidis T. P. (2004) "Impedance of a horizontal coil in a

borehole: a model for eddy-current bolthole probes", *Journal of Physics D: Applied Physics* **37**, (3), 485–494.

Burke S. K. and Ibrahim M. E. (2004) "Mutual impedance of air-cored coils above a conducting plate", *Journal of Physics D: Applied Physics* **37**, 1857–1868.

Buvat F., Pichenot G., Lesselier D., Lambert M. and Voillaume H. (2004) "A fast model of eddy current ferrite-cored probes for NDE", *Electromagnetic Nondestructive Evaluation (VIII)*, T. Sollier *et al* eds, IOS Press, 44–51.

Capobianco T. E., Splett J. D. and Capobianco T. E. (1990) "Eddy current probe sensitivity as a function of coil construction parameters", *Research in Nondestructive Evaluation* **2**, 169–186.

Cecco V. S. and Van Drunen G. (1985) "Recognizing the scope of eddy current testing", *Nondestructive Testing* **8**, Chapter 6, 269–301.

Cecco V. S., Van Drunen G. and Sharp F. L. (1987), *Eddy current testing. Volume One*, GP Courseware, Columbia.

Cheng C. C., Dodd C. V. and Deeds W. E. (1971) "General analysis of probe coils near stratified conductors", *International Journal of NDT* **3**, 109–130.

Ciric I. R. (1991) "Simple analytical expressions for the magnetic field of current coils", *IEEE Transactions on Magnetics* **27**, (1), 669–673.

Clark R. and Bond L. J. (1990) "Response of horizontal axis eddy current coils to layered media: a theoretical and experimental study", *IEE Proceedings Pt A* **137**, (3), 141–146.

Claycomb J. R., Tralshawala N. and Miller Jr J. H. (2000) "Theoretical investigation of eddy-current induction for nondestructive evaluation by superconducting quantum interference devices", *IEEE Transactions on Magnetics* **36**, (1), 292–298.

Coffey M. W. (2001) "Theory for coil impedance of a conducting half space: Analytic results for eddy current analysis", *Journal of Applied Physics* **89**, (4), 2473–2481.

Ditchburn R. J., Burke S. K. and Posada M. (2003) "Eddy current nondestructive inspection with thin spiral coils: long cracks in steel", *Journal of Nondestructive Evaluation* **22**, (2), 63–77.

Ditchburn R. J. and Burke S. K. (2005) "Planar rectangular spiral coils in eddy-current nondestructive inspection", *NDT&E International* **38**, (8), 690–700.

Dodd C. V. and Deeds W. E. (1968) "Analytical solutions to eddy current probe coil problems", *Journal of Applied Physics* **39**, (6), 2829–2838.

Dodd C. V., Deeds W. E. and Luquire J. W. (1969) "Integral solutions to some eddy current problems", *International Journal of NDT* **1**, 29–90.

Dodd C. V. and Deeds W. E., Luquire J. W. and Spoeri W. G. (1969) "Analysis of eddy current problems with a time-sharing computer", *Materials Evaluation*, 165–168.

Dodd C. V. and Simpson W. A. (1971a) "Measurement of small magnetic permeability changes by eddy current techniques", *Materials Evaluation*, 217–221.

Dodd C. V. (1971b) "Optimizing defect detection in eddy current testing", *Materials Evaluation*, 59–63.

Dodd C. V. and Simpson W. A. (1973) "Thickness measurements using eddy current techniques", *Materials Evaluation*, 73–79.

Dodd C. V., Cheng C. C. and Deeds W. E. (1974a) "Induction coils coaxial with an arbitrary number of cylindrical conductors", *Journal of Applied Physics*, **45**, (2), 638–647.

Dodd C. V., Smith J. H. and Simpson W. A. (1974b) "Eddy current evaluation of nuclear control rods", *Materials Evaluation*, 93–99.

Dodd C. V. (1980) "The use of computer modeling for eddy-current testing", *Research Techniques in NDT*, Volume III, 429–479.

Dodd C. V. (1982) "Absolute eddy-current measurement of electrical conductivity", *Review of Progress in Quantitative Nondestructive Evaluation* **1**, 387–392.

Dunbar W. S. (1988) "The volume integral method of eddy-current modeling: verification", *Journal of Nondestructive Evaluation* **7**, (1/2), 43–54.

Elsberry R. T. and Bailey D. M. (1986) "Characterization of shielded eddy current probes", *Materials Evaluation* **44**, (7), 984–988.

Fawzi T. H. (1995) "Analytical solutions of transverse electric eddy current problems with rotational symmetry", *IEEE Transactions on Magnetics* **31**, (3), 1396–1399.

Flitz M. and Nethe A. (1990) "Anregung dreidimensionaler Wirbelstrome in massiven Kreiszylindern endlicher Lange durch ein homogenes magnetisches Wechselfeld beliebiger Ausrichtung", *Archiv fur Elektrotechnik* **73**, 227–237.

Flitz M. and Nethe A. (1993) "Bemerkungen zur Losung des dreidimensional Wirbelstromproblems in Kreiszylindern endlicher Lange", *Archiv fur Elektrotechnik* **76**, 195–200.

Fontana M. (2001) "Integration methods for the calculation of the magnetostatic field due to coils", *Chalmers Finite Element Center*, Preprint 2001-07.

Forbes L. K., Cozier S. and Doddrell D. M. (1997) "Rapid computation of static fields produced by thick circular solenoids", *IEEE Transactions on Magnetics* **33**, (5), 4405–4410.

Gradshteyn I. S. and Ryzhik I. M. (2000), *Table of Integrals Series and Products*, Academic Press, 6th edn.

Gray A., Mathews G. B. and MacRobert T. M. (1931), *A Treatise on Bessel Functions and Their Applications to Physics*, 2nd edn, MacMillan, London.

Grimberg R., Savin A., Radu E. and Mihalache O. (2000) "Nondestructive evaluation of the severity of discontinuities in flat conductive materials by an eddy current transducer with orthogonal coils", *IEEE Transactions on Magnetics* **36**, (1), 299–307.

Grover F. W. (1973), *Inductance Calculations*, Dover Phoenix Editions, New York.

Hagemaier D. J. (1983) "Eddy current impedance plane analysis", *Materials Evaluation* **41**, 211–218.

Hagemaier D. J. (1984) "Application of eddy current impedance plane testing", *Materials Evaluation* **42**, 1035–1040.

Hajian N. T., Blitz J. and Hall R. B., (1982) "Impedance changes for air-cored probe coils of finite lengths used for eddy current testing", *NDT International* **15**, 3–8.

Hammond P. (1982) "Use of potentials in calculation of electromagnetic fields",

IEE Proceedings Part A **129**, (2), 106–112.

Hannakam L. (1972) "Wirbelstrome in leitenden Halbraum be beliebiger Form der erregenden Leiterschleife", *Archiv fur Elektrotechnik* **54**, 251–261.

Hannakam L. and Kost A. (1982) "Leitender Rechteckkeil im Felde einer Doppelleitung", *Archiv fur Elektrotechnik* **65**, 363–368.

Harfield N. and Bowler J. R. (1994) "Analysis of eddy current interaction with a surface breaking crack", *Journal of Applied Physics* **76**, (8), 4853–4856.

Harfield N. and Bowler J. R. (1995) "Solution of the two-dimensional problem of a crack in a uniform field in eddy current nondestructive evaluation", *Journal of Physics D: Applied Physics* **28**, 2197–2205.

Harfield N., Yoshida Y. and Bowler J. R. (1996) "Low frequency perturbation theory in eddy-current non-destructive evaluation", *Journal of Applied Physics* **80**, (7), 4090–4100.

Harfield N. and Bowler J. R. (1997) "Theory of thin-skin eddy-current interaction with surface cracks", *Journal of Applied Physics* **82**, (9), 4590–4603.

Harfield N. and Bowler J. R. (1997) "A geometrical theory for eddy current nondestructive evaluation", *Proceedings of the Royal Society of London A* **453**, 1121–1152.

Harrison D. J., Jones L. D. and Burke S. K. (1996) "Benchmark problems for defect size and shape determination in eddy-current nondestructive evaluation", *Journal of Nondestructive Evaluation* **15**, (1), 21–34.

Harrison D. J. (2001) "Characterization of cylindrical eddy current probes in terms of their spatial frequency spectra", *IEE Proceedings - Science Measurement Technology* **148**, (4), 183–186.

Hill D. A. and Wait J. R. (1977) "Analysis of alternating current excitation of a wire rope by a toroidal coil", *Journal of Applied Physics* **48**, (12), 4893–4897.

Hower G. L., Philipp L. D., Abtahi A. and Rupe R. W. (1984) "Some computational considerations in eddy-current NDE", *Journal of Nondestructive Evaluation* **4**, (1), 39–42.

Hower G. L. (1987) "Stationary formulas for computing the response in eddy-current NDE", *Journal of Nondestructive Evaluation* **6**, (4), 177–180.

Hoshikawa H. and Koyama K. (1998) "Eddy current distribution using parameters normalized by standard penetration depth", *Materials Evaluation* **57**, (6), 587–593.

Ida N. (1995), *Numerical modeling for electromagnetic non-destructive evaluation*, Chapman & Hall, London.

Janousek L., Chen Z., Yusa N. and Miya K. (2005) "Excitation with phase shifted fields-enhancing evaluation of deep cracks in eddy-current testing", *NDT&E International* **38**, (6), 508–515.

Juillard J., Barmon B. and Berthiau G. (2000) "Simple analytical three-dimensional eddy current model", *IEEE Transactions on Magnetics* **36**, (1), 258–266.

Kahn A. H., Spal R. and Feldman A. (1977) "Eddy current losses due to a surface crack in conducting material", *Journal of Applied Physics* **48**, (11), 4454–4459.

Kahn A. H. (1988) "Boundary integral equation methods for two-dimensional models of crack-field interactions", *Journal of Applied Physics* **48**, (11), 4454–4459.

Kriezis E. E. and Xypteras I. E. (1979) "Eddy current distribution and loss in a semi-infinite conducting space due to a vertical current loop", *ETZ Archiv* **7**, 201–207.

Kriezis E. E., Tsiboukis T. D., Panas S. M. and Tegopoulos J. A. (1992) "Eddy currents: Theory and applications", *Proceedings of the IEEE* **80**, (10), 1559–1589.

Kolyshkin A. A., Smolyakov A. P. and Vaillancourt R. (1991) "Analytical solution in eddy-current testing double-layer media with depth-varying magnetic properties", *IEEE Transactions on Magnetics* **27**, (5), 4360–4365.

Kolyshkin A. A. and Vaillancourt R. (1995) "Method of solution of forward problems in eddy-current testing", *Journal of Applied Physics* **77**, (10), 4903–4913.

Kolyshkin A. A. and Vaillancourt R. (1997) "Analytical solutions to eddy-current testing problems for a layered medium with varying properties", *IEEE Transactions Magnetics* **33**, (4), 2473–2477.

Lei H., Wang L. Z. and Wu Z. N. (2002) "Integral analysis of a magnetic field for an arbitrary geometry coil with rectangular cross section", *IEEE Transactions on Magnetics* **38**, (6), 3589–3593.

Lepine B. A. and Moulder J. C. (1995) "Calibration of commercial eddy current instruments for quantitative NDE", *Review of Progress in Quantitative Nondestructive Evaluation* **14B**, 2301–2308.

Libby H. L. (1979), *Introduction to Electromagnetic Nondestructive Test Methods*, Robert E. Krieger Publishing Company, Malabar, Florida.

Luke Y. L. (1962), *Integrals of Bessel functions*, McGraw-Hill, New York.

Luquire J. W., Deeds W. E. and Dodd C. V. (1970) "Axially symmetric eddy currents in a spherical conductor", *Journal of Applied Physics* **41**, (10), 3976–3982.

Luquire J. W., Dodd C. V. and Deeds W. E. (1970) "Alternating current distribution between planar conductors", *Journal of Applied Physics* **41**, (10), 3983–3991.

MacLeod A. J. (1996) "Algorithm 757: MISCFUN, a software package to compute uncommon special functions", *ACM Transactions on Mathematical Software* **22**, (3), 288–301.

Maergoiz I. D. and Nizhnik L. P. (1975) "Rectangular conducting wedge in a moving electromagnetic field", *Soviet Physics: Technical Physics* **19**, (10), 1281–1286.

McKirdy D. McA., Cochran A., Donaldson G. B. and McNab A. (1996) "Forward and inverse processing in electromagnetic NDE using SQUIDs", *Review of Progress in Quantitative Nondestructive Evaluation*, D.O.Thompson and D.E.Chimenti eds, Plenum Press, **15**, 347–354.

McKirdy D. McA., Cochran S., Donaldson G. B. and McNab A. (1995), "Theoretical consideration of fatigue crack detection and characterization using SQUID sensors", *Nondestructive Testing of Materials*, IOS Press, Amster-

dam, p.185.

McLachlan N. W. (1947), *Theory and Application of Mathieu Functions*, Oxford University Press, Oxford.

McNab A. (1988) "A review of eddy current system technology", *British Journal of Nondestructive Testing* **30**, (7), 249–255.

Michael D. H., Waechter R. T. and Collins R. (1982) "The measurement of surface cracks in metals by using a.c. electric fields", *Proceedings of the Royal Society of London A* **381**, 139–157.

Mirshekar-Syahkal D., Collins R. and Michael D. H. (1982) "The influence of skin depth on crack measurement by the ac field technique", *Journal of Nondestructive Evaluation* **3**, 65–76.

Moon P. and Spencer D. E. (1971), *Field Theory Handbook*, 2nd edition, Springer-Verlag.

Morse P. M. and Feshbach H. (1953), *Methods of Theoretical Physics*, McGraw-Hill Book Company, New York.

Mottl Z. (1990) "The quantitative relations between true and standard depth of penetration for air-cored probe coils in eddy current testing", *NDT International* **23**, (1), 11–18.

Mukhopadhyay S. C., Yamada S. and Iwahara M. (2002) "Experimental determination of optimum coil pitch for a planar mesh-type micromagnetic sensor", *IEEE Transactions on Magnetics* **38**, (5), 3380–3382.

Mullin C. J. (1953) "Solution of the wave equation near an extremum of the potential", *Physical Review* **92**, (5), 1323–1324.

Nethe A. (1991) "Einschaltstrome in Spulen mit leitendem permeablem Kern bei Berucksichtigung der induzierten Wirbelstrome", *Archiv fur Elektrotechnik* **74**, 389–401.

Nikitin A. I. (1980) "Interaction of eddy-current transducers with layer construction shells of curved form and instruments for measuring the dimensions of these shells (Review)", *Soviet Journal of Nondestructive Testing* **16**, (11), 775–792.

Nondestructive Testing: Eddy current, Classroom Training Handbook, Second Edition, General Dynamics, Convair Division, 1979.

Onoe M. (1968) "An analysis of a finite solenoid coil near a conductor (in Japanese)", *Journal of IEE Japan* **88-10**, (961), 1894–1902.

Palanisamy R. and Lord W. (1980) "Prediction of eddy current probe signal trajectories", *IEEE Transactions on Magnetics* **16**, (5), 1083–1085.

Palanisamy R. and Lord W. (1983) "Prediction of eddy current signals for nondestructive testing of condenser tubing", *IEEE Transactions on Magnetics* **19**, (5), 2213–2215.

Panas S. M. and Papayiannakis A. G. (1991) "Eddy currents in an infinite slab due to an elliptic current excitation", *IEEE Transactions on Magnetics* **27**, (5), 4328–4337.

Papoulis A. (1968), *Systems and transforms with applications in optics*, McGraw-Hill Book Company, USA.

Popov V. K. and Kabasheva A. A. (1973) "Effect of ferrite cores on the electrical circuit parameters of eddy current inductive probes", *The Soviet Journal*

of Nondestructive Testing **9**, (4), 448–452.

Press W. H., Flannery B. P., Teukolsky S. A. and Vetterling W. T. (2001), *Numerical Recipes in Fortran 77. The Art of Scientific Computing.*, Cambridge University Press, Cambridge.

Sabbagh H. A. and Vernon S. N. (1985) "Ferrite core eddy current probe model: description and verification", *Materials Evaluation* **43**, (2), 184–187.

Sabbagh H. A. (1987) "A model of eddy-current probes with ferrite cores", *IEEE Transactions on Magnetics* **23**, (2), 1988–1904.

Sadeghi S. H. H. and Salemi A. H. (2001) "Electromagnetic field distributions around conducting slabs produced by eddy current probes with arbitrary shape current carrying excitation loops", *IEE Proceedings: Science, Measurement and Technology* **148**, (4), 187–192.

Salemi A. H., Sadeghi S. H. H. and Moini R. (2004) "Thin-skin analysis technique for interaction of arbitrary-shape inducer field with long cracks in ferromagnetic metals", *NDT&E International* **37**, (6), 471–479.

Sandovskii V. A. (1974) "Calculations on a flat coil above a ferromagnetic halfspace", *The Soviet Journal of Nondestructive Testing* **10**, (6), 660–663.

Sandovskii V. A. and Barabashkin V. M. (1977) "Approximate calculation of the impedance introduced by a nonmagnetic plate in a superposed transducer", *The Soviet Journal of Nondestructive Testing* **13**, (1), 13–17.

Sandovskii V. A. (1980) "Design of eddy current transducer with shell-type ferrite core", *The Soviet Journal of Nondestructive Testing* **16**, (3), 225–229.

Satveli R., Moulder J. C., Wang B. and Rose J. H. (1996) "Impedance of a coil near an imperfectly layered metal structure: The layer approximation", *Journal of Applied Physics.* **79**, (6), 2811–2821.

Smythe W. R. (1968), *Static and Dynamic Electricity*, McGraw-Hill, New York.

Spal R. and Kahn A. H. (1979) "Eddy currents in a conducting cylinder with a crack", *Journal of Applied Physics* **50**, 6135–6138.

Stoll R. L. (1974), *The Analysis of Eddy Currents*, Clarendon Press, Oxford.

Sun H., Bowler J. R. and Theodoulidis T. P. (2005) "Eddy currents induced in a finite length layered rod of a coaxial coil", *IEEE Transactions on Magnetics* **41**, (9), 2455–2461.

Tegopoulos J. A. and Kriezis E. E. (1985), *Eddy Currents in Linear Conducting Media*, Elsevier Science publishers, Amsterdam.

Theodoulidis T. P., Panas S. M. and Kriezis E. E. (1994) "Eddy current detection of crack orientation using elliptical excitation", *IEE Proceedings: Science, Measurement and Technology* **141**, (1), 41–47.

Theodoulidis T. P., Tsiboukis T. D. and Kriezis E. E. (1995) "Analytical solutions in eddy current testing of layered metals with continuous conductivity profiles", *IEEE Transactions on Magnetics* **31**, (3), 2254–2260.

Theodoulidis T. P., Kantartzis N. V., Tsiboukis T. D. and Kriezis E. E. (1997) "Analytical and numerical solution of the eddy current problem in spherical coordinates based on the second order vector potential", *IEEE Transactions on Magnetics* **33**, (4), 2461–2472.

Theodoulidis T. P. and Kotouzas M. K. (2000) "Application of the eddy current method in ferritic weld inspection", *Emerging Technologies in NDT*,

Balkema, Rotterdam, 357–361.

Theodoulidis T. P. and Kriezis E. E. (2002a) "Impedance evaluation of rectangular coils for eddy current testing of planar media", *NDT&E International* **35**, 407–414.

Theodoulidis T. P. (2002b) "Application of the eigenvalues method in eddy current NDE: a model of eddy current ferrite-cored probes", *Proceedings eNDE 2002 Workshop*, Saarbruecken, Germany.

Theodoulidis T. P. and Kriezis E.E. (2002c) "Coil impedance due to a sphere of arbitrary radial conductivity and permeability profiles", *IEEE Transactions on Magnetics*, **38**, (3), 1452–1460.

Theodoulidis T. P. (2002d) "Analytical modeling of wobble in eddy current tube testing with bobbin coils", *Research in Nondestructive Evaluation*, **14**, 111–126.

Theodoulidis T. P. (2003) "Model for ferrite-cored probes for eddy current nondestructive evaluation", *Journal of Applied Physics* **93**, 3071–3078.

Theodoulidis T. P. (2004a) "End effect modelling in eddy current tube testing with bobbin coils", *International Journal of Applied Electromagnetics and Mechanics* **19**, (1-4), 207–212.

Theodoulidis T. P. and Bowler J. R. (2004b) "Field and impedance analysis for a long crack in a conductive slab excited by a uniform field at arbitrary frequency", *Proceedings of eNDE 2004 Workshop*, Michigan, USA.

Theodoulidis T. P. and Bowler J.R. (2004c) "The truncated region eigenfunction expansion method for the solution of boundary value problems in eddy current nondestructive evaluation", *Review of Progress in Quantitative Nondestructive Evaluation* **24A**, 403–408.

Theodoulidis T. and Bowler J. (2005a) "Eddy-current interaction of a long coil with a slot in a conductive plate", *IEEE Transactions on Magnetics* **41**, (4), 1238–1247.

Theodoulidis T. P. and Kriezis E. E. (2005b) "Series expansions in eddy current nondestructive evaluation", *Journal of Materials Processing Technology* **161**, (1-2), 343–347.

Theodoulidis T. P. and Bowler J. R. (2005c) "Eddy current interaction with a right-angled conductive wedge", *Proceedings of the Royal Society A* **461**, 3123–3139.

Theodoulidis T. (2005d) "Analytical model for tilted coils in eddy current nondestructive inspection", *IEEE Transactions on Magnetics* **41**, (9), 2447–2454.

Timmerberg J. (1983) "Kraftwirkung auf eine raeumliche zylindrische Spule infolge eines hochpermeablen Zylinders", *Archiv fur Elektrotechnik* **66**, 289–293.

Ton Tran-Cong (1984) "Eddy current solutions applicable to the problem of nondestructive inspection of flat and cylindrical surface layer", *Journal of Nondestructive Evaluation* **4**, (1), 29–38.

Treece J. C. (1991) "The z-current phenomenon in anisotropic (composite) materials", *Review of Progress in Quantitative Nondestructive Eevaluation*, D.O.Thompson and D.E.Chimenti eds, Plenum Press, **10A**, 341–346.

Treece J. C. (1994) "The value of modelling in understanding eddy-current probe-

flaw experiments", *Review of Progress in Quantitative Nondestructive Evaluation* D.O.Thompson and D.E.Chimenti eds, Plenum Press, **13**, 319–326.

Tsaknakis H. J. and Kriezis, E. E. (1985) "Field distribution due to a circular current loop placed in an arbitrary position above a conducting plate", *IEEE Transactions on Geoscience and Remote Sensing* **23**, (4), 834–840.

Udpa S. S. and Udpa L. (1999) "Eddy current nondestructive evaluation", *Wiley Encyclopedia of Electrical and Electronics Engineering*, John Wiley and Sons, New York, 149–163.

Udpa S. S. and Udpa L. (2004) "Eddy current testing - are we at the limits?", *World Conference in NDT*, presentation No.776, available at: www.ndt.net

Urankar L. K. (1982) "Vector potential and magnetic field of current carrying finite arc segment in analytical form, Part III: Exact computation for rectangular cross-section", *IEEE Transactions on Magnetics* **18**, (6), 1860–1867.

Uzal E., Moulder J. C., Mitra S. and Rose J. H. (1993) "Impedance of coils over layered metals with continuously variable conductivity and permeability: Theory and experiment", *Journal of Applied Physics* **74**, (3), 2076–2089.

Uzal E., Moulder J. C., Mitra S. and Rose J. H. (1994) "Experimental determination of the near-surface conductivity profiles of metals from electromagnetic induction (eddy current) measurements", *Inverse Problems* **10**, 753–764.

Van Drunen G. and Cecco C.V. (1984) "Recognizing limitations in eddy-current testing", *NDT International* **17**, (1), 9–17.

Vernon S. N. (1989) "The universal impedance diagram of the ferrite pot core eddy current transducer", *IEEE Transactions on Magnetics* **25**, (3), 2639–2645.

Weaver J. T. (1970) "The general theory of electromagnetic induction in a conducting half-space", *Geophysical Journal of the Royal Astronomical Society* **22**, 83–100.

Weider T. (1999) "Algorithm 794: numerical Hankel transform by the Fortran program HANKEL", *ACM Transactions on Mathematical Software* **25**, (2), 240–250.

Weigelt K. (1990) "Solution of complex eignevalue equations as used in the analytical solution of eddy-current problems of coupled regions", *Journal of Magnetism and Magnetic Materials* **83**, 501–505.

Xypteras I. E. (1978), *Eddy-current distribution in a conducting slab due to a circular current-loop placed vertically to the dividing surface*, PhD Thesis, Thessaloniki.

Zaman A. J. M., Long S. A. and Gardner C. G. (1980) "The impedance of a single-turn coil near a conducting half space", *Journal of Nondestructive Evaluation* **1**, (3), 183–189.

Zaman A. J. M., Gardner C. G. and Long S. A. (1982) "Change in impedance of a single-turn coil due to a flaw in a conducting half-space", *Journal of Nondestructive Evaluation* **3**, (1), 37–43.

Zhou J., Collins R. and Michael D. H. (1994) "Half-space induction by a rectangular coil with rounded corners: local uniformity and ACFM", *Review of Progress in Quantitative Nondestructive Evaluation*, D.O.Thompson and D.E.Chimenti eds, Plenum Press, **13**, 36–43.